

**INVOLVEMENT OF MYOSIN V IN ORGANELLE TRANSPORT
AND ITS UNCONVENTIONAL INTERACTION WITH
MICROTUBULES**

**Dissertation zur Erlangung
des Doktorgrades der Naturwissenschaften**

**an der Fakultät für Biologie der
Ludwig-Maximilians-Universität München**

Angefertigt am
Institut für Zellbiologie
der Ludwig-Maximilians-Universität München
unter der Betreuung von Hr. Prof. Dr. Schliwa

vorgelegt von
Dennis Zimmermann

1. Gutachter: Hr. Prof. Dr. Manfred Schliwa
2. Gutachter: Fr. Prof. Dr. Barbara Conradt

Dissertation eingereicht am: 6. Juni 2012

Tag der mündlichen Prüfung: 27. Juli 2012

Für meine Eltern, Corinna, Dan und Steffi

Table of Contents

Zusammenfassung

Summary

1. Introduction	18
1.1. The cytoskeleton and its motor proteins	18
1.2. The myosin superfamily	19
1.3. Myosin V-Overview	20
1.3.1. Myosin V structure and function	20
1.3.2. Myosin V processivity and ATPase activity	22
1.3.3. Regulation of Myosin V	24
1.4. <i>In vitro</i> motility assays and TIRF-Microscopy	26
1.5. Melanophores: A model system to study intracellular organelle transport	28
1.5.1. Cytoskeletal components of melanosome transport	29
1.5.2. Regulation of intracellular melanosome transport	30
1.6. Networking of the cytoskeleton	32
1.7. One-dimensional diffusive search of Myosin V on microtubules	34
2. Project Aims of this Thesis	35
2.1. One-dimensional diffusive motility of Myosin Va on microtubules	35
2.2. Calcium-/Calmodulin-dependent Kinase II- α and its role in Myosin V release from pigment organelles	36
2.3. MACS [®] bead-assisted purification of pigment organelles – A novel approach	37
2.4. Determining the sequence of the full-length Myosin Va from <i>Xenopus laevis</i>	38
3. Materials	39
3.1. Laboratory utensils and consumption items	39
3.2. Cell culture accessories	40
3.3. Plasmids and vectors	41
3.4. Oligonucleotides (Primers)	41
3.4.1. Cloning primers	41
3.4.2. Sequencing primers	43

Table of Contents

3.5. Microorganisms	44
3.6. Mediums and agars for microorganisms	44
3.7. Antibodies and peptides	45
3.8. Chemicals and ready-to-use solutions	45
3.9. Buffers and ready-to-use solutions	47
3.10. Enzymes and kits for biochemistry & molecular biology	60
3.11. Software for data acquisition and analysis	60
4. Methods	61
4.1. Cell culturing	61
4.1.1. Culturing of immortalized <i>Xenopus l.</i> melanophores	61
4.1.2. Preparation of cryo-cultures from <i>Xenopus l.</i> melanophores	61
4.1.3. Thawing and propagating melanophore cryo-cultures	62
4.1.4. Protocol for MACS-bead assisted melanosome purification	62
4.1.5. Culturing of Sf9 insect cells	63
4.2. Molecular biological methods	64
4.2.1. RNA	64
4.2.1.1. Isolation of cellular total RNA	64
4.2.1.2. cDNA synthesis via reverse transcriptase (RT)-PCR	65
4.2.1.3. RACE-PCR on isolated RNA	66
4.2.2. DNA	69
4.2.2.1. Polymerase chain reaction (PCR)	69
4.2.2.2. PCR protocols	69
4.2.2.2.1. PCR for the cloning of HMM-like Myosin Va and CaMKII- α	69
4.2.2.2.2. PCR for determining the full-length <i>Xenopus l.</i> Myosin Va	70
4.2.2.2.3. PCR-mediated preparation of the full-length <i>Xenopus l.</i> Myosin Va gene for vector cloning	72
4.2.2.3. DNA analysis by agarose gel electrophoresis	73
4.2.2.4. Gel-extraction of DNA fragments	73
4.2.2.5. Purification of PCR and restriction-digest products	73
4.2.2.6. DNA Sequencing	73

Table of Contents

4.2.2.6.1. Sequencing reactions of full-length <i>Xenopus l.</i> Myosin Va _____	74
4.2.2.7. Determination of DNA concentration _____	75
4.2.2.8. DNA sequence synthesis of HMM-like Myosin Va loop 2 constructs _____	76
4.2.3. Cloning techniques _____	76
4.2.3.1. Restriction enzyme-mediated DNA digest _____	76
4.2.3.2. Dephosphorylation of linearized DNA _____	77
4.2.3.3. Ligation of DNA fragments into linearized vector _____	77
4.2.3.4. Transformation of chemically competent <i>E. coli</i> XL1-Blue cells _____	78
4.2.3.5. Selection and expansion of transformed <i>E. coli</i> _____	78
4.2.3.6. Plasmid-DNA extraction from transformed bacteria _____	79
4.3. Protein Biochemistry _____	79
4.3.1. Analytical methods _____	79
4.3.1.1. Protein analysis by SDS-polyacryl amide gel electrophoresis (SDS-PAGE) _____	79
4.3.1.2. Protein identification and conformation by mass spectrometry _____	79
4.3.1.3. Determination of protein concentration _____	80
4.3.1.4. Determination of tubulin concentration _____	81
4.3.1.5. Western-blot analysis _____	81
4.3.2. Isolation, purification and handling of cytoskeletal Proteins _____	82
4.3.2.1. G-actin purification from rabbit muscle tissue _____	82
4.3.2.2. G-actin polymerization _____	83
4.3.2.3. Isolation and purification of porcine tubulin _____	84
4.3.2.3.1. Tubulin polymerization _____	85
4.3.2.3.2. Polymerization of fluorescently labeled tubulin for <i>in vitro</i> motility assays _____	85
4.3.2.3.3. Polymerization of unlabeled tubulin for ATPase activity assays _____	86
4.3.2.4. Microtubule E-hook removal via Subtilisin digest _____	86
4.3.3. Protein expression using the baculovirus expression system _____	88

Table of Contents

4.3.3.1. Construction of the recombinant transfer vector for protein expression_____	89
4.3.3.2. Generation of the recombinant bacmid_____	90
4.3.3.3. Isolation of the recombinant bacmid DNA_____	91
4.3.3.4. Transfection of Sf9 insect cells with recombinant bacmid_____	92
4.3.3.5. Amplification of baculovirus V ₀ generation_____	93
4.3.3.6. Protein expression in Sf9 insect cells_____	94
4.3.4. FLAG-tag affinity protein purification_____	95
4.3.4.1. General FLAG-tag affinity purification protocol_____	97
4.3.4.2. Optimized protocol for FLAG-tag affinity purification of full-length <i>Xenopus l.</i> Myosin Va_____	98
4.3.5. Methods for functional protein analysis_____	99
4.3.5.1. <i>In vitro</i> motility assays_____	99
4.3.5.1.1. Flow cell preparation_____	99
4.3.5.1.2. Fluorescent labeling of motor proteins_____	100
4.3.5.1.3. Single-molecule motility assays on microtubules and F-actin_____	100
4.3.5.1.4. Gliding filament assays_____	102
4.3.5.2. TIRF and epi-fluorescence microscopy_____	102
4.3.5.3. ATPase activity assays_____	103
4.3.5.4. Microtubule-affinity co-sedimentation assays_____	105
4.3.5.5. CaMKII- α autophosphorylation assays_____	107
4.3.5.6. Assays to monitor CaMKII- α -mediated Myosin V release from melanosomes_____	108
4.4. Data Analysis_____	109
4.4.1. Fluorescence microscopy data analysis: Single-molecule motility measurements_____	109
4.4.2. Fluorescence microscopy data analysis: Gliding-filament motility measurements_____	111
4.4.3. Fluorophore measurement and statistical analysis_____	111
4.4.4. Quantitation of data obtained from microtubule-affinity co-sedimentation_____	111
4.4.5. Analysis of data obtained from ATPase assays on actin and microtubules_____	112

Table of Contents

4.4.6. Sequence alignment	112
5. Results	113
5.1. One-dimensional diffusion of Myosin Va on microtubules	113
5.1.1. Strategy	113
5.1.1.1. Generating HMM-like Myosin Va loop 2 mutants	113
5.1.1.2. Designing and cloning of HMM-like Myosin Va loop 2 mutants	113
5.1.1.3. Actin- and microtubule-activated ATPase activity of HMM-like Myosin Va constructs	115
5.1.1.4. Microtubule-affinity co-sedimentation assays with HMM-like Myosin Va constructs	116
5.1.2. Results	117
5.1.2.1. Purification of HMM-like Myosin Va loop 2 constructs	117
5.1.2.2. Loop 2 is not the prime determinant of the interaction between Myosin V and microtubules	117
5.1.2.3. All Myosin Va loop 2 charge mutants show unperturbed diffusion on microtubules	122
5.1.2.4. Myosin Va diffusion takes place without the help of E-hooks	127
5.1.2.5. Non-electrostatic attraction forces contribute to the interaction of Myosin Va with microtubules	131
5.1.2.6. A negative charge on loop 2 impairs the Myosin Va interaction with actin filaments whereas Myosin Va carrying a Kinesin-loop is functional on F-actin	131
5.2. Studying the effects of Calcium-/Calmodulin-dependent Kinase II- α on melanosome-associated Myosin V	136
5.2.1. Results	136
5.2.1.1. Cloning and purification of baculovirus-expressed CaMKII- α	136
5.2.1.2. Autophosphorylation of CaMKII- α	138
5.2.1.3. Initial structural analysis of CaMKII- α by cryo-electron tomography	140
5.2.1.4. Assaying the interaction of CaMKII- α and melanosomes	142
5.3. Purification of isolated melanosomes via MACS technology	145
5.3.1. Results	146

Table of Contents

5.3.1.1. Comparative analysis of the different purification methods	146
5.3.1.2. Qualitative analysis of the purity of MACS-purified melanosomes	147
5.3.1.3. Analysis of the MACS-purification protocol by FACS	148
5.4. Determining the full-length sequence of <i>Xenopus l.</i> Myosin Va	150
5.4.1. Strategy	150
5.4.1.1. Step-by-step PCR on cDNA from <i>Xenopus l.</i> melanophores	150
5.4.1.1.1. Overview on Phases A, B and C	151
5.4.1.2. Cloning of full-length <i>Xenopus l.</i> Myosin Va for baculovirus expression in Sf9 cells	152
5.4.2. Results	153
5.4.2.1. Cloning of full-length <i>Xenopus l.</i> Myosin Va	153
5.4.2.2. Domain analysis and comparative alignment	156
5.4.2.3. FLAG-affinity purification of full-length <i>Xenopus l.</i> Myosin Va	160
5.4.2.4. <i>In vitro</i> gliding motility of full-length <i>Xenopus l.</i> Myosin Va on F-actin	161
5.4.2.5. <i>In vitro</i> single-molecule motility of full-length <i>Xenopus l.</i> Myosin Va on F-actin	165
6. Discussion	169
6.1. Movement of Myosin Va loop 2 mutants on F-actin and microtubules	169
6.1.1. Myosin Va loop 2 mutant behavior on F-actin	169
6.1.2. Role of the loop 2 net charge for its interaction behavior with microtubules	173
6.1.3. Role of the microtubule E-hooks for the interaction of Myosin Va with microtubules	174
6.1.4. Conclusion and Outlook	176
6.2. Studying the effects of Calcium-/Calmodulin-dependent Kinase II- α on melanosome-associated Myosin Va	180
6.2.1. Expression and purification of functional recombinant CaMKII- α	180
6.2.2. Functional analyses of FLAG-tag affinity-purified CaMKII- α	181
6.2.2.1. Biochemical analysis	181
6.2.2.2. Structural analysis by cryo-electron tomography	182
6.2.3. Studying the interaction between CaMKII- α and melanosomes	184

Table of Contents

6.2.4. Conclusion and Outlook_____	187
6.3. Purification of isolated melanosomes via MACS technology_____	188
6.3.1. Efficiency of MACS-based melanosome isolation_____	189
6.3.2. Summary and Outlook_____	192
6.4. Determining the full-length sequence of <i>Xenopus l.</i> Myosin Va_____	193
6.4.1. Comparative Sequence-analysis_____	193
6.4.2. Expression and purification of full-length <i>Xenopus l.</i> Myosin Va_____	196
6.4.3. <i>In vitro</i> motility of full-length <i>Xenopus l.</i> Myosin Va_____	197
6.4.4. Summary and Outlook_____	201
7. Supporting Information_____	204
8. Literature_____	227
9. Abbreviations_____	245
Eidesstattliche Versicherung	248
Curriculum Vitae	249
Acknowledgments	253

Zusammenfassung

Das Zytoskelett, mitsamt seinen Motorproteinen spielt bei der Bewältigung so essentieller biologischer Prozesse wie der Zellbewegung, der Muskelkontraktion, der Chromosomen-Segregation und dem intrazellulären Transport eine Hauptrolle. So ist z. B. während der Tarnung bei Fischen und Amphibien der rasche Farbwechsel in der Haut überhaupt erst durch den Transport von pigmenthaltigen Organellen (Melanosomen) von der Zellmitte zur Peripherie und zurück möglich. Dieser Vorgang, bei dem abertausende Organellen im Zytoplasma verteilt werden, bedarf einer streng regulierten Zusammenarbeit der verschiedenen Transportsysteme einer Zelle. Hierbei wird der Langstreckentransport zur Zellperipherie entlang der Mikrotubuli vom Motorprotein Kinesin-2 bestimmt, während im Aktin-reichen Zellkortex Myosin V den Kurzstreckentransport steuert. Es wird daher angenommen, dass eine Art Frachtübergabe vom einen zum anderen Transportsystem vonnöten ist.

Bis zum heutigen Tage ist sowohl der Mechanismus als auch die Regulation der Interaktion zwischen den beiden Transportsystemen noch weitestgehend unklar. Durch neuere *in vitro*-Studien wurde gezeigt, dass an Aktin-Mikrotubuli-Kreuzungen Myosin V die "Schiene" wechseln kann und entlang des Mikrotubulus auf Diffusion basierende Bewegungen ausführt (Ali *et al.*, 2007).

Ein Hauptziel dieser Arbeit war es, die molekularen Faktoren dieser unerwarteten Interaktion zwischen Myosin V und dem Mikrotubuli-basierten Transportsystem zu untersuchen. Mit Hilfe von *Total Internal Reflection Fluorescence-Microscopy* sowie Mikrotubuli-Affinitäts- und Cosedimentations-Experimenten, konnte in diesem Teil der Arbeit gezeigt werden, dass für die elektrostatische Interaktion zwischen Myosin V und Mikrotubuli, anders als ursprünglich vermutet, die positiv geladene Myosin-Oberflächenstruktur Loop 2 und die negativ geladenen Carboxy-terminalen Mikrotubuli-Enden (E-hooks) wider Erwarten entbehrlich sind. Des Weiteren zeigten Ali *et al.*, dass *in vitro* der Myosin V-Motor dem Kinesin-gesteuerten Transport unter die Arme greifen kann. Dazu passend zeigen die hier präsentierten Ergebnisse für das Binden von Myosin V an den Mikrotubulus eine neue und unkonventionelle Art auf, welche den E-hook-abhängigen Langstreckentransport durch Kinesin nicht behindert.

Zusammenfassung

Ob Zellen tatsächlich den hier vorgeschlagenen biophysikalischen Trick anwenden, um die Transporteffizienz *in vivo* zu steigern, bleibt nach wie vor zu klären. Um dies zu beantworten bedarf es eines biologisch relevanten Systems, mit dem das Transportverhalten einer natürlichen Cargos (z.B. Organellen), welches entweder beide Motoren (d.h. Myosin V und Kinesin-2) oder Kinesin-2 allein besitzt, *in vitro* untersucht werden kann. Hierfür sind Melanosomen von Pigmentzellen (Melanophoren) ideal geeignet, da sie als funktionell intakte Organellen isoliert werden können. Aber wie kann nun der Cargo so manipuliert werden, dass das am Cargo gebundene Kinesin-2 haften bleibt, während Myosin V abgelöst wird? Um mich dieser Frage anzunehmen, nutze ich das Ergebnis einer früheren Studie, in der gezeigt wurde, dass die Phosphorylierung von Myosin V, die durch Calcium-/Calmodulin-abhängige Kinase II- α (CaMKII- α) vermittelt wird, den Motor selektiv von Melanosomen löst. Die hier präsentierten Daten zeigen, dass schon allein die in den Pigmentzellen vorkommende endogene CaMKII- α das Ablösen von Myosin V vom Melanosom auslöst, und dass die Aktivierung der Kinase ausschließlich von ihrer Rekrutierung an das Melanosom abhängt. Hingegen war für die hier generierte und *in vitro*-aktivierte exogene Kinase kein signifikanter Effekt auf Melanosom-gebundenes Myosin V erkennbar. Daraus lässt sich schließen, dass womöglich weitere Cofaktoren am Ablösen des Myosin V-Motors vom Melanosom beteiligt sind. Der hier vorgestellte „CaMKII- α Release Assay“ wirft wichtige Fragen nach den regulatorischen Mechanismen während des Bindens von Motorproteinen an Organellen auf. Des Weiteren bildet der „CaMKII- α Release Assay“ nun eine Grundlage für das Etablieren eines Protokolls, mit dem es möglich sein sollte, die Rolle von Myosin V bei der Unterstützung des Kinesin-gesteuerten Transports zu ergründen.

Wie ist die Regulation des intrazellulären Organellentransports zeitlich und räumlich organisiert? Und wie reagiert das Melanosomen-assoziierte Proteom auf extrazelluläre Einflüsse? Um diesen Fragen sowohl qualitativ als auch quantitativ auf den Grund zu gehen, bieten hochentwickelte Technologien wie die Massenspektrometrie vielversprechende Möglichkeiten. Bis jetzt wurden eventuell auftretende Proteommodifikationen am Melanosom noch nicht experimentell hinterfragt. Beim Anwenden so sensibler Techniken wie der Massenspektrometrie stellt die Probenreinheit die größte Herausforderung dar. Obgleich zum

Zusammenfassung

Aufreinigen von Mitochondrien oder Lipoproteinen die Sucrosegradienten-Ultrazentrifugation standardmäßig verwendet wird, birgt die harsche Behandlung der Probe die Gefahr, Teile des auf dem Organell sich befindenden Proteoms zu verlieren. Daher war es mein Ziel eine Technik zu etablieren, mit der es möglich ist, Melanosomen von kontaminierenden zytoplasmatischen Bestandteilen zu reinigen. Dabei sollten keine harschen Zentrifugationsschritte oder später eventuell störende Zusätze (z. B. Sucrose) verwendet werden. Mit der hier präsentierten Methode werden mittels eines Magneten sowie paramagnetischer Nanokügelchen, welche gegen Melanosomen-spezifische Oberflächenmarker gerichtet sind, intakte Organellen aufgereinigt. Zusätzlich zur der Tatsache, dass diese Technik eine alternative Aufreinigungsmethode von Melanosomen darstellt, bietet sie auch die Möglichkeit, anhand von spezifischen Oberflächenmarkern Melanosomenpopulationen aus unterschiedlichen Zellstadien (Aggregation oder Dispersion) zu gewinnen.

Obwohl bereits vor über drei Jahrzehnten gezeigt werden konnte, dass Myosin V für die vollständige Pigmentverteilung in Melanophoren von *Xenopus l.* unentbehrlich ist, ist die vollständige Sequenz dieses Motors erstaunlicherweise noch immer nicht bekannt. Im letzten Teil dieser Arbeit wird nun die vollständige Sequenz des Myosin V aus *Xenopus l.* präsentiert. Mit Hilfe von Einzelmolekül-Motilitätsversuchen wurde rekombinantes *Xenopus l.* Myosin V erstmals biophysikalisch untersucht. Die Bewegungsgeschwindigkeit des überexprimierten Myosin V-Motorproteins stimmt mit *in vivo*-bestimmten Melanosomen-Transportgeschwindigkeiten überein.

Zusammenfassend kann gesagt werden, dass diese Arbeit sowohl neue Einblicke in das komplexe Zusammenspiel zwischen dem Aktin- und Mikrotubuli-basierten Transportsystem eröffnet, als auch alternative Wege aufzeigt, um bislang ungelöste Probleme des Organelltransports besser erforschen zu können.

Summary

The cytoskeleton along with its motor proteins plays a central role in the accomplishment of essential biological processes such as cell motility, muscle contraction, chromosome segregation and intracellular transport of entire organelles. For instance, the rapid color change of the skin during camouflage in fish and amphibians is achieved by the transport of pigment-filled organelles (melanosomes) from the cell center to the periphery and vice versa. This highly concerted distribution of thousands of organelles throughout the cytoplasmic microcosm of a cell requires a strictly regulated networking between the different transport systems.

The long-range transport of melanosomes along microtubules towards the cell periphery is powered by the Kinesin-2 motor, while Myosin V accomplishes the short-range transport in the actin-rich cell cortex. Therefore, some form of hand-off mechanism is believed to be required. However, to date the mechanistic nature and regulation of the crosstalk between the two transport systems remains elusive.

Recently, *in vitro* Myosin V was shown to switch tracks at actin-microtubule intersections, followed by diffuse movements on the microtubule (Ali *et al.*, 2007). To dissect the molecular determinants of this unexpected interaction between Myosin V and the microtubule transport system was a major goal of this thesis. By means of single-molecule Total Internal Reflection Fluorescence microscopy as well as microtubule-affinity co-sedimentation assays, in this study the originally suggested electrostatic tethering between the positively charged myosin loop 2 and the negatively charged C-terminal E-hooks of microtubules was proven to be dispensable. Consistent with the observation by Ali *et al.*, who showed that Myosin V is able to assist kinesin-driven transport *in vitro*, the findings presented in this work provide evidence for a novel and unconventional way of Myosin V tethering to microtubules that does not interfere with other E-hook-dependent processes such as kinesin-driven long-range transport.

However, a still open question is whether cells indeed employ this proposed biophysical trick to enhance the transport efficiency *in vivo*. Answering this question requires a biologically relevant system, in which the transport behavior of

Summary

a native cargo (e.g., organelles) containing either both sets of motors (i.e., Myosin V and Kinesin-2) or Kinesin-2 alone, can be assessed *in vitro*. For this, melanosomes from pigment cells are ideally suited, as they can be isolated as functionally intact organelles. But how can the cargo be manipulated in such a way that bound Kinesin-2 remains attached, while the Myosin V motor is depleted from the cargo? To address this question I made use of a previous finding, where Myosin V was shown to be released upon phosphorylation by the Calcium-/Calmodulin-dependent Kinase II- α (CaMKII- α). The data presented in this work demonstrate that endogenous kinase alone is capable of triggering Myosin V release and the activation of the kinase is dependent on the recruitment onto the melanosome. In contrast, activated exogenous kinase had no significant effect on the melanosome-bound Myosin V, indicating that additional co-factors might be involved. The CaMKII- α release assay presented here raises important questions about the regulatory mechanisms involved in binding of motor proteins to organelles. It further provides important clues for the establishment of an experimental setup by which it will be possible to test Myosin V's potential role in assisting kinesin-driven cargo transport.

Inside cells, how is spatio-temporal regulation of organelle transport orchestrated? And how does the proteome of an organelle respond to extracellular clues? Advanced technologies such as mass-spectrometry hold the promise of qualitatively and quantitatively addressing those questions. So far, potential cell state-dependent proteomic modifications on the melanosome have not been experimentally scrutinized. When applying sensitive techniques like mass-spectrometry, the greatest challenge is to obtain highly pure samples. While sucrose density gradient ultra-centrifugation has been successfully used to obtain pure mitochondria, lipoproteins etc., the harsh sample treatment often leads to loss of parts of the associated proteome. Therefore, I established a novel technique to obtain pure melanosomes free of cytoplasmic contaminants. This technique does neither involve harsh ultra-centrifugation steps, nor does it include any potential contaminating additives (e.g., sucrose). Instead, by applying paramagnetic beads directed against unique melanosome-specific markers, pure fractions of intact organelles are retrieved. The technique presented here not only represents an alternative way to purify melanosomes, but by exploiting unique cell-state-dependent surface markers, it will also allow for the sorting of different

Summary

melanosome populations from distinct cellular states.

Even though over three decades ago on specialized pigment cells (melanophores) from *Xenopus l.* it has been elegantly demonstrated that for the successful distribution of pigments into the distal tips of a cell, Myosin V-powered organelle transport is indispensable, the full-length *Xenopus l.* Myosin V sequence remained unresolved. Therefore, in the final part of this thesis, the full-length Myosin V sequence from *Xenopus l.* melanophores is presented. Furthermore, by means of gliding filament as well as single-molecule motility approaches, recombinant full-length Myosin V from *Xenopus l.* was subjected to initial biophysical characterization. The reconstituted velocity of the overexpressed Myosin V motor protein from *Xenopus l.* is in remarkable agreement with *in vivo* melanosome transport velocities inside pigment cells.

To conclude, this work not only provides novel insights into the intricate interplay between the actin- and microtubule-based transport system, it also presents new and alternative ways to approach the yet unsolved problems in the field of cytoskeletal organelle transport.

1 Introduction

1.1 The cytoskeleton and its motor proteins

Cellular motility becomes essential with the progression past the single-cell state and is required for nearly all the cellular processes that accomplish life itself. Motile immune cells are able to accumulate at sites of infection, active movements within a cell realize the nourishment of distal parts in nerve or plant cells and for animals to respond physically to dangerous situations, muscle contraction is indispensable. Those and many more examples in biology have been driving scientists to unravel the secrets of cellular motility, a process accomplished through the intricate work of the cytoskeleton along with its molecular motors.

The cytoskeleton itself consists of a complex network of protein polymers that resist deformation and transmit mechanical forces. The three polymer classes are referred to as actin filaments, microtubules and intermediate filaments and are composed of specific protein subunits. In this thesis, actin filaments and microtubules took the center stage and are thus described in more detail. Microtubules are hollow, cylindrical polymers (approx. 25 nm in diameter) that sustain both compression and tension. This feature makes them useful for supporting asymmetrical cellular processes as well as for bidirectional traffic that is generated by the respective motor proteins ^{2,3}. Filamentous actin (F-actin; approx. 8 nm in diameter) is much more flexible and builds up a cytoskeletal transport as well as motility system, which is present in all eukaryotes. The actin cytoskeleton complements and interacts physically with cytoskeletal structures composed of microtubules and intermediate filaments ⁴.

Inside cells, most biological movements are accomplished by motor proteins – small nano-scale machines, which move along two different types of polarized cytoskeletal tracks (i.e., actin filaments and microtubules). These motor proteins take nanometer steps along their track to transport cargo from one location inside the cell to another. To do so, motor proteins convert chemical energy (adenosine triphosphate, ATP) into mechanical energy. The thereby generated force is then used to propel cargoes along their specific tracks.

Altogether three different classes of motor proteins transport cargo molecules along two different types of cytoskeletal tracks. Kinesins and dyneins move along microtubules, whereas myosins move on actin filaments.

In addition, these molecular motors are specialized regarding their directional movement along their appropriate track. While the majority of kinesin motors moves toward the plus-end of microtubules, all dyneins exhibit minus end-directed movements on the microtubule. With the exception of Myosin VI, which moves towards the minus-end, all myosins perform barbed end (also referred to as plus end) -directed movements on actin filaments ².

Microtubule-based motors are used not only for the transport of particles through the cytoplasm or chromosomal movement during cell division, but they also carry out more specialized roles. One of these roles is for instance flagellar motility, for which microtubules and dynein are crucial components ^{5,6}. Many types of cellular movements, including muscle contraction, cytokinesis, cytoplasmic streaming and amoeboid motion are accomplished by the actin-myosin system ⁴.

As large parts of this work focus on characterizing the behavior of the class V myosin, an overview on the superfamily of myosins is presented in the following section.

1.2 The myosin superfamily

Myosins as a large family of actin-based mechano-enzymes bind and hydrolyze ATP to generate force and movement along actin filaments, which is necessary to assist in a variety of cellular tasks. Besides the classic example of skeletal muscle contraction, many other cellular events such as cell motility, cell adhesion, cytokinesis, endocytosis, exocytosis, membrane trafficking, movement of mRNA and organelle transport are controlled by the joint action of myosin and actin filaments ⁷. Mutations within myosin genes often result in severe phenotypes such as cardiomyopathy, deafness, blindness, sterility and neurological seizures ^{8,9}. To date 35 different classes have been officially designated as classes Myosin I to XXXV, of which at least 12 are present in vertebrates ¹⁰. Myosins are further divided into conventional and unconventional myosins. Due to historical reasons, all class II myosins are denoted conventional myosins, whereas all the other members of the myosin superfamily are referred to as unconventional myosins.

1.3 Myosin V-Overview

Initially described as an unusual calmodulin-binding protein from brain with a number of myosin-like biochemical properties, today Myosin V is known to provide continuous transport of membranous cargo, lipids, mRNA, secretory as well as protein vesicles and organelles on actin ¹¹.

Myosin V is found in a wide variety of eukaryotic cells (excluding plant cells) including organisms as primitive as yeast, which contain two class V myosins. Interestingly, plants contain the class XI Myosins, which almost certainly derived from an ancient class V myosin ^{10,12}.

Three class V myosins (Va, Vb, Vc) are found in mammalian cells, each one associated with different tissue specificity and with a specific set of membrane trafficking events ¹³. For example, mutations in the human ortholog of the *dilute* Myosin V (class Va) gene cause Griscelli syndrome, a rare recessive disease characterized by pigmentary dilution of the skin, neurological disorders and in some cases even immunodeficiency ^{14,15}. Myosin Va is known to associate with diverse organelles, for example pigment granules (melanosomes) in pigment cells of the skin and secretory vesicles in neurons of the brain ^{16,17}. Very recently, Myosin Va was shown to move endoplasmatic reticulum into the spines of Purkinje cells ¹⁸. Myosins Vb and Vc are mainly expressed in epithelial cells where they have been implicated as motors involved in recycling endosomes ^{13,19,20}.

1.3.1 Myosin V structure and function

As all other myosins, class V myosins are composed of three functional domains: a) the motor or head domain; b) the neck domain or lever arm; and c) the tail domain (Figure 1). *In vivo* two Myosin V heavy chains dimerize along their tail domains to form a double-headed homodimer ²¹. The N-terminal motor domain (catalytic domain) shares conserved sequence homology with other members of the myosin superfamily and contains both the nucleotide and actin binding sites ²². The ATP binding site is located near the so-called loop 1 region, which was shown to be involved in the catalytic ATPase cycle ²³.

The actin-binding interface is part of a surface loop, referred to as loop 2 region and is involved in the initial weak electrostatic interaction of myosin with actin ²⁴.

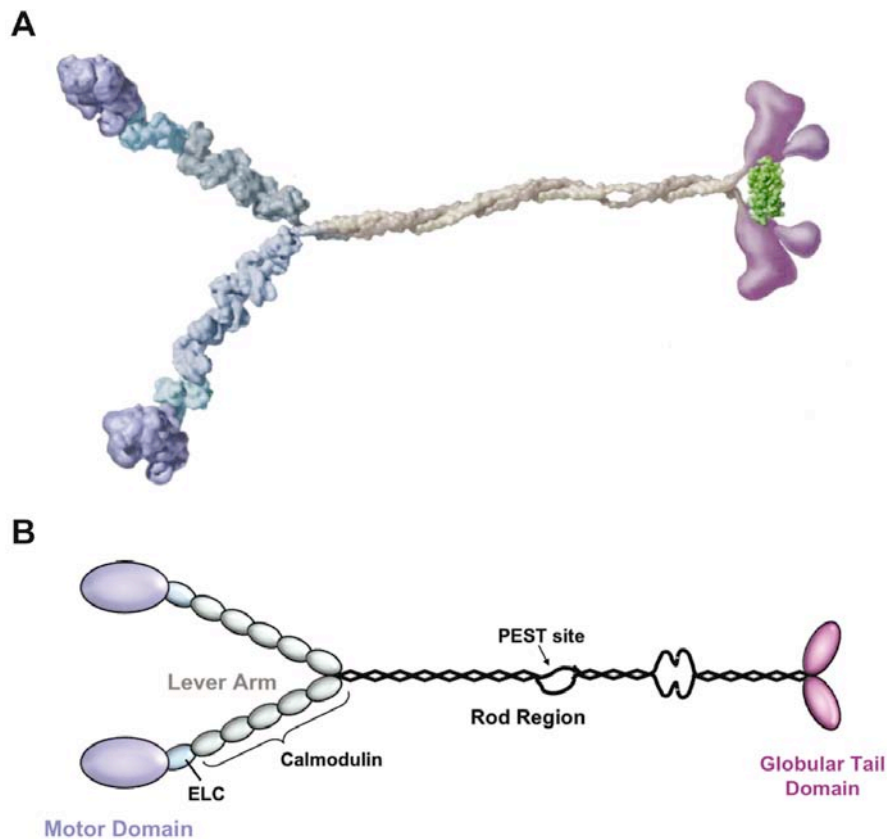


Figure 1. Atomic resolution and schematic domain structure of the full-length Myosin Va.

(A) Surface features were rendered based upon atomic resolution structures and appear as smooth images for domains of unknown structure (adapted from Vale, R., *Cell*, Vol. 112, 2003). (B) Schematic domain structure of the full-length Myosin Va. At the N'-terminus, the motor catalytic domains (*light purple*) contain the actin-binding site and nucleotide-binding site, followed by an approx. 24-nm-long lever arm (*grey*) that binds six calmodulin-like light chains. The rod region (*black*) of the tail domain contains three stretches of α -helical coiled-coil, which are interrupted by two major regions of non-coiled-coil. At the very C'-terminus, the globular tail domain (*magenta*, GTD) binds to adaptor proteins that link the GTD to cargo molecules.

The long (24 nm) neck domain contains six light chain-binding consensus repeats (IQ motifs) and fulfills two major functions: i) regulating the activity of Myosin V via calcium-dependent binding of calmodulin-like light chains to its IQ motifs and thereby affecting the ATPase cycle and processivity; and ii) enabling the Myosin V dimer to bind to actin with a 36 nm pitch, which in turn allows for taking 36 nm steps along the actin filament^{25,26,27}. Myosin V's step size on actin is the longest among all yet identified myosin family members²⁸.

In contrast to the catalytic domains, the tail domains are the most diverse in their primary sequence and structure among the different myosin classes. The tail domain of Myosin V is divided into two functional regions, i.e. the rod region and the globular tail domain (GTD).

The N-terminal rod region with its three major stretches of α -helical coiled-coil is responsible for dimerization of the two heavy chains, whereas the C-terminal GTD has two distinct major functions: i) linking the motor protein to cargo molecules; and ii) stabilizing the auto-inhibited folded conformation of Myosin V via interactions with portions of the motor domain. In addition, the GTD was shown to be important for the motor's cellular localization^{29,30,31}.

1.3.2 Myosin V processivity and ATPase activity

To generate motility, Myosin V converts chemical energy into mechanical work by coupling the hydrolysis of ATP to conformational changes. All myosins characterized to date show a characteristic cyclic interaction with actin (actomyosin ATPase cycle).

The kinetic cycle of class V myosins is characterized by the following four major steps: i) the rapid binding of ATP to actin-bound myosin; ii) the hydrolysis of ATP; iii) the rapid release of phosphate (P_i) but slow release of ADP; and iv) the rebinding of ATP to myosin^{32,33} (reviewed in³⁴). By progressing through these four states, myosin alternates between the actin-detached and actin-attached (strong-binding) state. Importantly, only the strong-binding state allows myosin to generate mechanical force (power stroke), and thus directed movement on actin^{32,35} (**Figure 2**).

Belonging to the class of cytoplasmic transport motors, *in vivo* Myosin V typically works in isolation under conditions where it must move its cargo long distances without dissociating from its track^{36,37}. The ability to take multiple steps along the actin filament without detaching is thus a mechanical prerequisite to Myosin V function. Vertebrate Myosin V was the first myosin shown *in vitro* to be capable of exhibiting this so-called processive walking behavior^{38,39}. It should be mentioned that some of the details regarding processivity of Myosin V are still under debate. Therefore, in **Figure 2** only a consensus mechanism is shown³⁴.

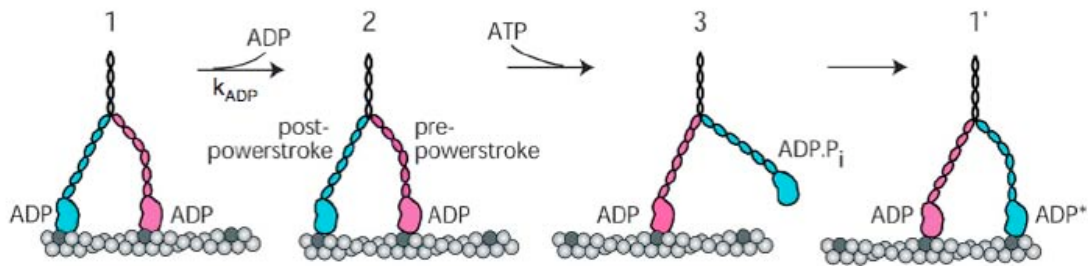


Figure 2. Consensus model for the processive movement of Myosin Va on F-actin.

(*State 1*) Both heads are strongly bound to actin with ADP bound at the active site of the motor domain (“waiting state”). The trailing head is in a post-powerstroke conformation, and the leading head is in a strained, pre-powerstroke state. The trailing head releases ADP at approx. 12 s^{-1} , thereby representing the rate-limiting state of the ATPase cycle (*state 2*). ATP binding to the trailing head causes it to dissociate from actin, thereby allowing the actin-bound leading head to complete its powerstroke. Simultaneously, the detached head is thrust forward, hydrolyzes ATP, and becomes the new leading head in a pre-powerstroke conformation (*state 3*). While detached from the filament, the head undergoes a diffusive search for the next actin binding site, P_i release follows and the detached head undergoes a transition to the strong binding state. The lead-head may pass through an isomerized ADP^* state before returning to state 1 (*state 1'*). The half-helical actin repeats (approx. 36 nm apart from each other) to which Myosin Va binds, is illustrated by darker grey actin filament-subunits. Figure was adapted from Trybus, K., *Cell. Mol. Life Sci.*, Vol. 65, 2008.

The kinetic cycle starts with the two-heads-bound intermediate state (also referred to as “waiting state”), which the motor adopts in between steps⁴⁰. Being tethered by the actin-bound trailing head, the leading head cannot swing its lever arm forward. ADP-release from the trailing head is required for a step to occur (*state 2*). The release of ADP is the rate-limiting step and triggers the following sequence of events³². ATP binds to the vacant site on the trailing head and makes it dissociate from the actin track leading to a transient one-head bound intermediate. This allows the lead head to release stored elastic energy and to throw the trailing head in front (*state 3*). The detached “new” leading head hydrolyzes ATP and undergoes a diffusional search to interact weakly with the next binding-site on actin. The weak-binding state is in rapid equilibrium with the dissociated state, so that phosphate release must be fast for the motor to eventually interact strongly with actin^{38,41}.

Unique structural and kinetic adaptations allow Myosin V to be an efficient processive motor. The slow release (12 s^{-1}) of ADP leaves the ADP-bound head strongly attached and thus the predominant steady-state intermediate of the cycle. This way a Myosin V molecule spends most (70%) of its ATPase cycle attached to the filament, making it a high duty ratio motor (i.e., time that one head

spends attached to the filament during one kinetic cycle). Not only does the high duty ratio ensure that one head always remains strongly bound to the filament, but it also provides enough time for the detached head to hydrolyze ATP and to search for the next binding site.

The characteristic 36-nm step-size of Myosin V matches exactly the length of one half-helical repeat on the actin filament, suggesting that Myosin V can walk straight along the intrinsically twisted actin filament and must not spiral around it²⁵. Strain-dependent changes in the kinetics of the two heads accomplished through the long lever arm, account for further enhancement of the processive run length⁴². In addition, Myosin V with its highly positively charged loop 2 possesses a relatively high affinity for actin in the weak-binding states. Hence there is an increased likelihood for the new leading head to find its next binding site^{43,44}.

All of the above allow Myosin V to walk processively on actin in a hand-over-hand fashion^{45,46}, which has been demonstrated not only *in vitro* but also *in vivo*^{47,48}.

1.3.3 Regulation of Myosin V

With the exemption of the mammalian skeletal muscle myosin whose ATPase activity is inherently unregulated⁴⁹, in essentially all myosins characterized so far, regulation almost always targets the myosin's enzymatic activity. However, the form of regulation varies from case to case.

The study of myosin regulation *in vitro* has been greatly aided by the development of ATPase activity as well as gliding filament or single-motor molecule motility assays (see Section 1.4). With those assays at hand, enzymatic and/or mechanical properties of a given myosin can be elegantly defined.

For the full-length Myosin Va to be active *in vitro*, micromolar levels of Calcium (Ca^{2+}) must be present^{21,50,51,52}. In the absence of Ca^{2+} Myosin Va was shown to interact only weakly with actin, resulting in low or no actin-stimulated ATPase activity⁵³. However, Myosin Va versions that lack the GTD along with parts of the distal coiled-coil, have been shown to be constitutively active *in vitro*⁵⁴. This finding indicated that most likely the tail domain mediates the inhibition of the full-length Myosin Va. Via studies using ultracentrifugation and electron-microscopy, the final proof that at zero Ca^{2+} the full-length Myosin Va adopts a closed conformation, was provided. For this folded inhibited conformation, the two motor domains fold back to the GTD, while low concentrations of Ca^{2+} induce the

Introduction

unfolding of the molecule (**Figure 3**)^{31,52,55,56}. Importantly, additional studies could show that upon GTD-binding to the motor's head domain solely the ATP-binding pocket but not the nearby actin-binding site is blocked, making the auto-inhibited Myosin Va likely to stay strongly attached to the filament⁵⁵.

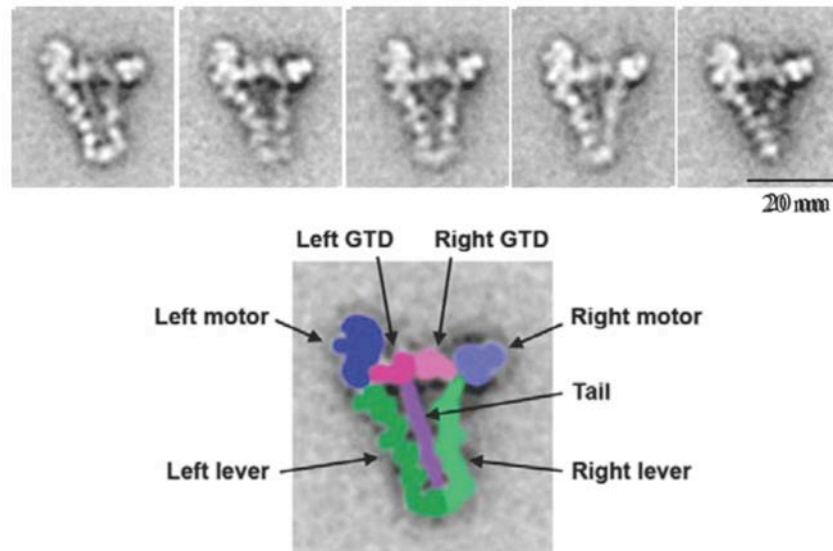


Figure 3. Structure of switched-off Myosin Va.

Upper panels: averaged images of negative-stained, folded whole Myosin V molecules; scale bar is 20 nm. *Lower panel:* superimposition of the left-most image in the upper panel; colored and labeled to show domains within folded Myosin Va. Data taken from Thirumurugan, K. et al., *Nature*, Vol. 442, 2006.

It should be mentioned, however, that activation of the auto-inhibited full-length Myosin Va by low Ca^{2+} concentrations entails a dramatic decrease in the motor's affinity for actin^{21,50}. Therefore, *in vivo* Ca^{2+} seems unlikely to be the physiological regulator of Myosin Va.

At present the only known cytoplasmic regulator that has been shown to directly unfold auto-inhibited Myosin Va (even at zero Ca^{2+}), is the cargo receptor molecule melanophilin, which in pigment cells is responsible for linking Myosin Va to pigment-containing organelles. Further support came from studies, which showed that melanophilin is essential for the Myosin Va-dependent transport of melanosomes on actin^{57,58,59}.

At this point it seems that auto-inhibition via head-to-tail folding is a common way to regulate the activity of various motor proteins.

1.4 *In vitro* motility assays and TIRF-Microscopy

For a long time the interaction between myosins and actin was studied mainly by ultracentrifugation, chemical cross-linking and ATPase activity-measuring methods. However, with the development of the so-called *in vitro* sliding filament assay by Kron and Spudich (1986)⁶⁰ the study of motor proteins was revolutionized. This assay elegantly takes advantage of the ability to image fluorescently labeled actin filaments via fluorescence microscopy as they interact with, and are transported by, myosins attached to a coverslip (Figure 4).

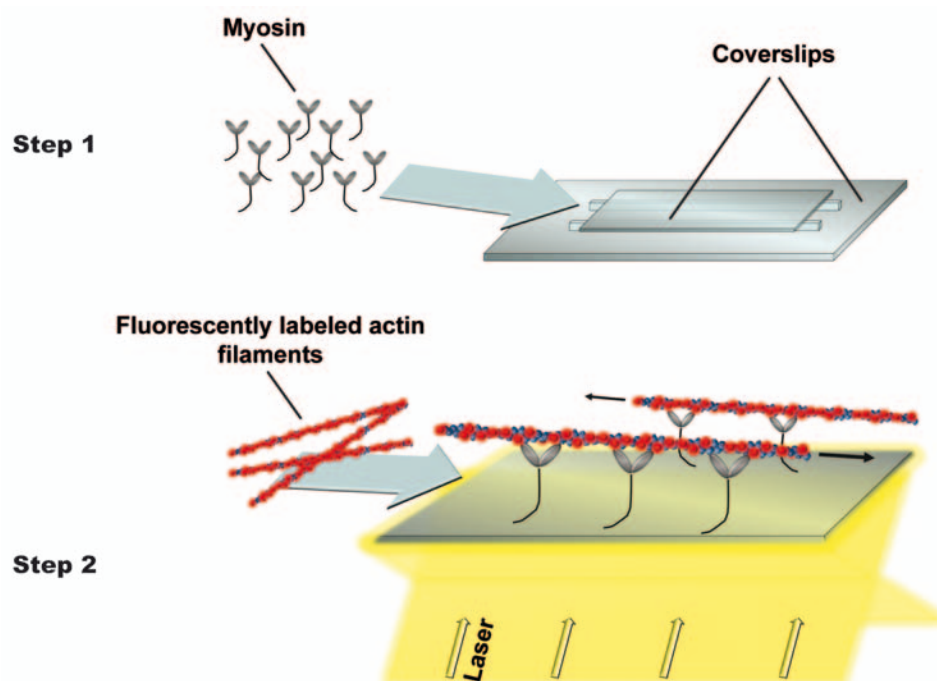


Figure 4. Gliding filament assay setup.

Step one: purified myosin is attached to the surface of a coverslip, either unspecifically or by using a myosin tail-specific surface-adhered antibody. *Step two:* perfusion of fluorescently labeled actin filaments into the flow-cell with surface-attached myosin molecules. *In vitro* filament gliding motility is followed by fluorescence microscopy (optimally by TIRFM) and movements are imaged onto a CCD camera. The arrow indicates the direction of filament movement.

Thereby it has become possible to reconstitute the motility of purified motor proteins along purified cytoskeletal filaments under cell-free conditions. With the advent of higher resolution fluorescence microscopy, the so-called single-molecule motility assay, resembling an advanced version of the sliding filament assay, was developed. Via total internal reflection fluorescence (TIRF) microscopy, by this assay the movement of fluorescently labeled single motor

Introduction

molecules along surface-bound filaments can be measured, allowing for highly accurate determination of parameters such as motor velocity, runlength and runtime (Figure 5).

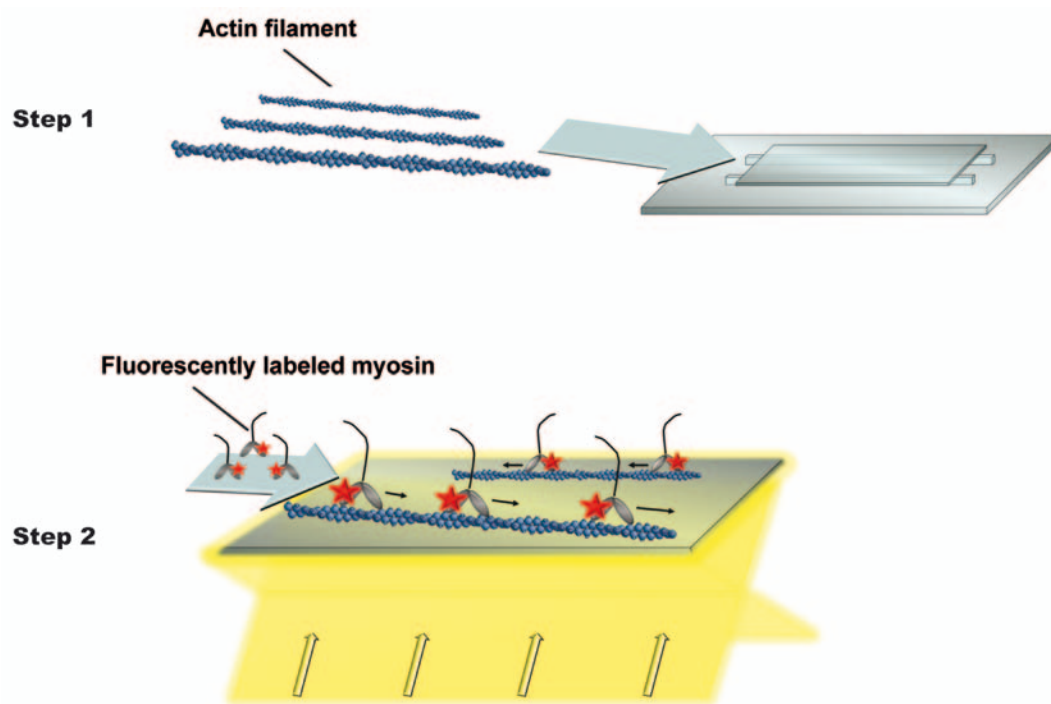


Figure 5. Single-molecule motility assay setup.

Step one: attachment of *in vitro* polymerized actin filaments to the surface of a coverslip is typically achieved by using a catalytically inactive and immobilized heavy-meromyosin. *Step two:* fluorescently labeled (on head or tail) Myosin V is perfused into the flow-cell with surface-attached F-actin. *In vitro* motility of single Myosin V molecules on F-actin is followed by TIRF microscopy and movements are imaged onto a CCD camera. The arrow indicates into which the direction the individual motors are walking.

This movement can be imaged onto an intensified charge-coupled device (CCD) camera and the motion can be acquired on a computer. With standard epifluorescence microscopes it has always been a challenge to distinguish between filaments that are bound by surface-attached motor proteins and unbound filaments that are still in solution. However with the development of TIRF microscopy, it is nowadays possible to study objects that are very close (100 to 200 nm) to the surface because TIRF microscopy makes use of the evanescent field that via total internal reflection of the incoming laser-beam is formed at the glass-water interface⁶¹. Therefore fluorophores that are close to the surface are excited, whereas molecules in the bulk of the sample are not excited, yielding

much higher signal-to-noise ratios than with conventional epi-fluorescence microscopy (Figure 6).

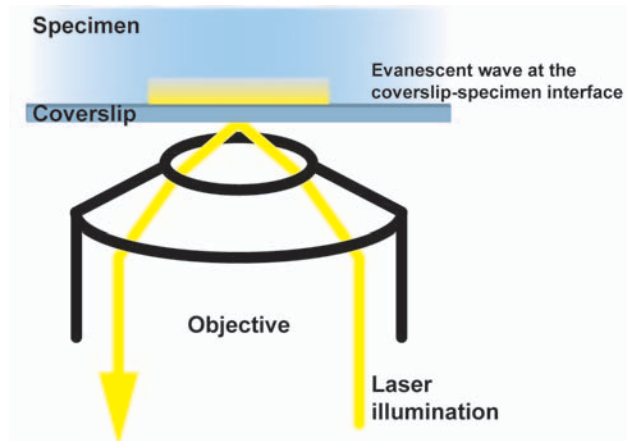


Figure 6. Total internal reflection fluorescence microscopy (TIRFM).

The laser beam is focused to propagate along the objective edge, so that total internal reflection of the beam into the slide occurs. As the electrical field cannot vanish abruptly, an oscillating electromagnetic field, termed evanescent wave, is produced. This evanescent wave penetrates 100 to 200 nm into the aqueous solution where it excites fluorescently labeled filaments that are close to the surface.

1.5 Melanophores: A model system to study intracellular organelle transport

In mammalian pigment cells (melanocytes) skin darkening is induced by UV-radiation, which is caused by either rapid oxidation of melanin, or dispersion-mediated transfer of melanosomes into the keratinocyte-containing layer of the epidermis⁶².

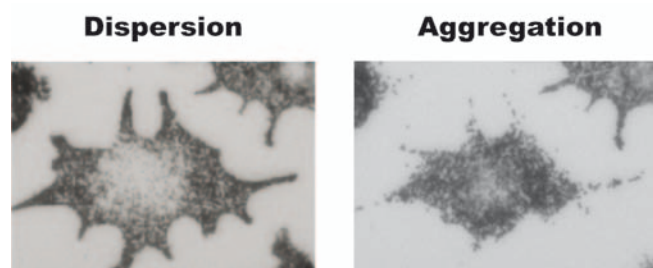


Figure 7. Pigment dispersion and aggregation in melanophores from *Xenopus I*.

Pigment dispersion (*left image*) and aggregation (*right image*) was induced by stimulation of cultured *Xenopus* melanophores with 100 nM α -melanocyte stimulating hormone (MSH) and 50 nM melatonin, respectively. Images were acquired by brightfield-light microscopy (objective, 20 \times). The left and right image sections show the same cell after complete pigment dispersion and aggregation, respectively.

In fish and amphibians, the main physiological role of pigment cells (melanophores) is to rapidly change color in response to variations in the environment. This is accomplished by a synchronous and bidirectional transport of pigment organelles (melanosomes). In response to extracellular stimuli (hormones or light) melanosomes from lower vertebrates are reversibly transported throughout the cytoplasm⁶³. Upon anterograde melanosome transport (dispersion) animals appear darker, whereas retrograde transport (aggregation) makes the skin appear lighter (**Figure 7**)^{64,65}.

To study pigment dispersion and aggregation on physiological as well as molecular level, in 1990 Lerner *et al.* established an immortalized melanophore cell line from *Xenopus laevis* (African clawed frog), which has been used also for the purpose of this work⁶⁶. These cells are easily maintained and large quantities of cells can be obtained and used for subsequent studies⁶⁴. Most importantly, intact melanosomes can be isolated from these cells and subjected to *in vitro* studies. Therefore, melanophores have become a central model system to address the issues of intracellular organelle transport and motor regulation^{67,68,69}.

1.5.1 Cytoskeletal components of melanosome transport

Melanosomes are large (approx. 500 nm in diameter) tissue-specific organelles that are specialized in the biosynthesis and storage of the black pigment, melanin⁷⁰. Because of their dark appearance, melanosomes can be easily imaged and discriminated from other cellular components using bright field transmission microscopy^{71,72}.

By means of *in vitro* motility assays, transport of purified melanosomes can be reconstituted, demonstrating that all factors needed to drive melanosome transport are present on these organelles^{65,73,74}. This way, purified melanosomes readily display bidirectional movement on microtubules, where Kinesin-2 drives organelles towards the plus- and dynein toward the minus-ends of surface-attached microtubules, while frequently switching the direction of movement⁶⁵. *In vivo* this bidirectional melanosome transport is tightly regulated, favoring Kinesin-2-dependent transport towards the cell periphery during dispersion and dynein-dependent transport towards the cell center during aggregation, respectively.

In vivo, the dispersion of melanosomes additionally requires the actin-based motor protein Myosin Va^{75,76}, which has been shown to be responsible for the

local transport and efficient tethering of melanosomes within the dense cortical actin meshwork to support efficient dispersion⁷⁷. The presence of an actin-based motor together with two oppositely directed microtubule-based motors on the same cargo requires a tight spatio-temporal regulation of the three motor protein families^{78,79,80}.

It has been shown that during dispersion, with Myosin Va helping Kinesin-2 to dominate over cytoplasmic dynein and thereby leading to a net plus-end directed transport of the melanosomes, there is continuous competition between both transport systems. During aggregation, on the other hand, Myosin Va appears to be unable to compete with dynein-driven movement, resulting in an inward-biased transport on microtubules⁶³.

1.5.2 Regulation of intracellular melanosome transport

To date several mechanisms have been proposed for governing melanosome aggregation and dispersion: i) modifications of the filamentous network itself might be involved, therefore favoring one state over the other; ii) extracellular hormone-mediated regulation; iii) alterations in the number of melanosome-bound motors; iv) adaptor molecule complex-mediated regulation; and v) signaling-mediated off- and on-switching of specific motors to tip the balance of the movement. Most likely all of these mechanisms intertwine to achieve proper melanosome transport⁶⁷.

In order to efficiently regulate the transport of melanosomes, extracellular binding of specific hormones to cell-surface receptors must occur, which then initiates intracellular signaling cascades⁸¹. Aggregation is induced by the receptor-specific binding of melatonin or noradrenalin^{82,83}, while dispersion is induced by the binding of α -melanocyte stimulating hormone (MSH) to its specific receptor (**Figure 7**)^{84,85,86}.

It is still not clear whether variations of the total amount of melanosome-associated motors or rather the motor's state of activity change during melanosome transport. While the motor number on melanosomes for both the microtubule-based motors, dynein and Kinesin-2, remains unaltered, during aggregation more dynein molecules are tuned active than during dispersion^{63,87}. The fact that Kinesin-2 activity remains unaffected, supports the notion that only the minus-end component of microtubule-dependent transport is regulated,

Introduction

whereas the plus-end component is continuously active^{63,88}. Interestingly, for the Myosin Va-driven melanosome transport during dispersion an increase in the total number of melanosome-bound Myosin Va molecules has been reported⁶³.

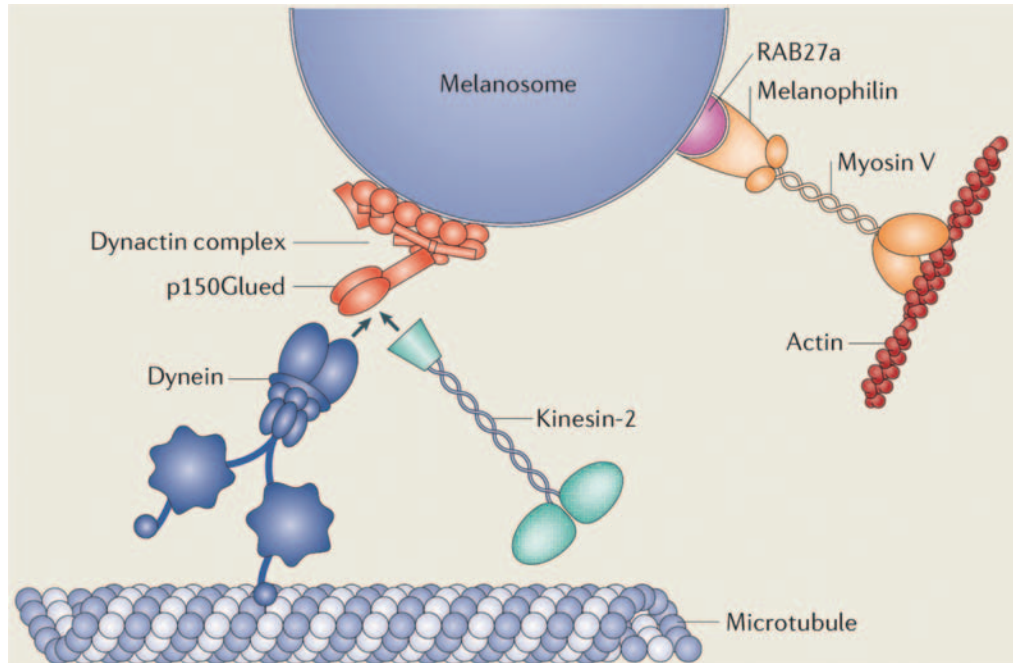


Figure 8. The transport machinery of melanosomes.

In pigment cells, the tripartite complex consisting of Rab27a, melanophilin and Myosin Va on melanosomes, enables cargo transport on F-actin. Cytoplasmic dynein and Kinesin-2 are recruited to the melanosome via the Dynactin-p150Glued complex, thereby enabling the long-range cargo transport to the plus- and/or minus- ends of the microtubules.

All three motor protein families that are involved in melanosome transport require motor-specific adaptor-molecules by which they are linked to their cargo. The dynactin protein complex on melanosomes from fish and frog has been shown to mediate the anchoring of both dynein and Kinesin-2 to the melanosome (Figure 8)^{87,89,90}. For Myosin V to bind to melanosomes it first has to bind melanophilin, which then physically links the motor to its cargo. The recruitment of Myosin Va onto the organelle is G-protein (Rab27a-GTP)-dependent and thus a tripartite Rab27a-Melanophilin-Myosin Va complex is formed on the melanosome (Figure 8), allowing the melanosome to move along actin filaments and to become retained in the actin-rich cell periphery^{58,59,91,92}. Taken together, adaptor molecules represent important potential regulators during actin- and microtubule-based transport⁹⁰.

Recently, protein kinase A (PKA) has been shown to bind to a dynein-containing aggregation as well as to a Kinesin-2-/Myosin V-containing dispersion complex. The interaction of those signaling pathway components with the melanosome surface was proposed to take place via scaffolding molecules⁹³. However, it seems likely that additional signaling cascades act downstream of PKA⁹⁴. For instance, only recently Rab32 was shown to mediate the positioning of PKA on melanosomes⁹⁵. Therefore, it is very likely that Rab-GTPases constitute an additional switch in the regulation of melanosome transport^{96,97}.

Even though each of the established hypotheses might explain certain aspects of melanosome transport regulation, there are still important questions that have remained unanswered: How do molecular motors interact with each other on melanosomes? What are the exact functions of scaffolding molecules? How are molecular motors activated and regulated via G-protein coupled receptors as well as downstream signaling cascades? Does the proteomic composition on melanosomes change during aggregation and dispersion?

1.6 Networking of the cytoskeleton

Even though at first, the actin-myosin and kinesin-/dynein-microtubule systems seem to constitute two fundamentally different and separate transport systems, in most recent years the picture has significantly changed. For example, in neurons Myosin Va colocalizes with both the microtubule and actin cytoskeleton⁹⁸, and was observed to even localize to the centrosome of interphase and dividing cells of various types^{30,99}. Furthermore, it has been observed that *in vivo*, individual cargo molecules often carry both actin- and microtubule-based motors so that a cargo might be able to move along either filament when encountering an intersection of both filament types^{79,80}.

While in cultured *Xenopus* melanophores, the removal of microtubules results in shuttling movements of pigment granules and a slow movement of melanosomes towards the cell periphery, the disruption of the actin cytoskeleton induces aggregation of melanosomes. Therefore, it has been suggested that the integrity of the actin cytoskeleton is a crucial requirement for the maintenance of the dispersed state^{73,100}. The microtubule- and actin-transport systems seem to

Introduction

highly depend on each other as removing either component dramatically changes the organization of the other ^{101,102}.

Furthermore, for melanophores to aggregate and disperse pigment properly, switching of the melanosomes between cytoskeletal tracks in both directions is required ⁶³. In fish and amphibian melanophores, long-range melanosome transport from the cell center to the cell periphery and back takes place on microtubules and is driven by Kinesin-2 and cytoplasmic dynein, respectively. In the actin-rich cell cortex, Myosin Va drives the short-range transport along actin filaments (Figure 9) ^{103,104,105,106}.

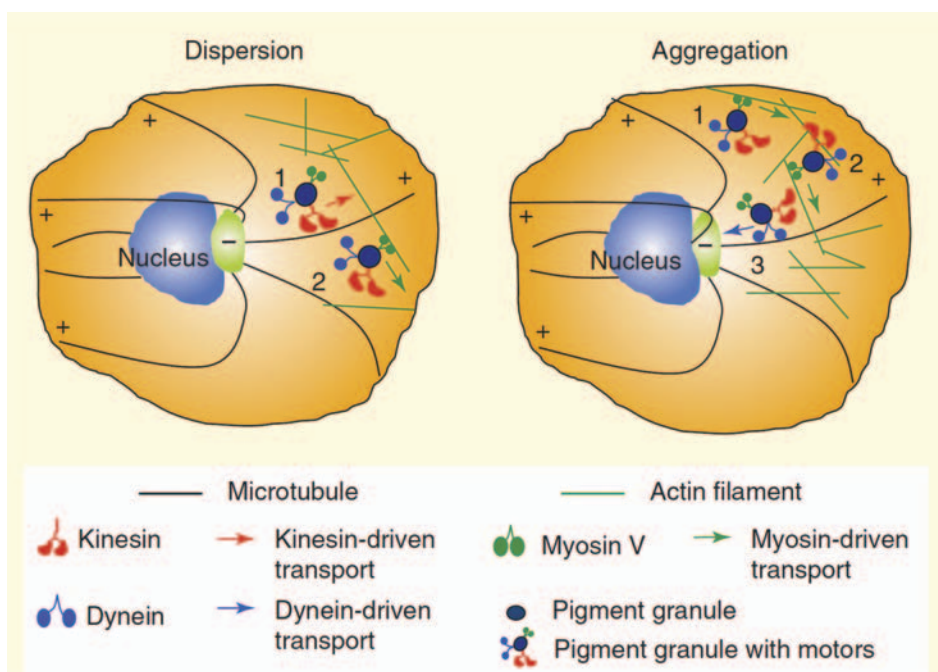


Figure 9. Co-active working of two different transport systems during pigment dispersion and aggregation.

Left: dispersing pigment granules move out on microtubules (1), then switch to actin filaments (2); *Right:* aggregating granules are transported on actin filaments (1 and 2) and switch eventually to microtubules, which transport them towards the cell center (3). + and - denote the plus- and minus- ends of microtubules. *Figure adapted from Gross, S., Curr. Biol., Vol. 17, 2007.*

All of this implies that for efficient transport of cellular components a coordinated interplay between actin- and microtubule-based motor systems is required. Though in various studies a number of different hypotheses to explain this coordinated hand-off mechanism at intersections between actin and microtubules have been presented, to date the regulation of this crosstalk remains elusive.

1.7 One-dimensional diffusive search of Myosin V on microtubules

A further facet to the yet unclear interaction between actin- and microtubule motor systems was added by a recent study, where Myosin V was found to switch from an actin filament onto an intersecting microtubule. Furthermore, following microtubule binding, Myosin Va even exhibited one-dimensional diffusive motion over large distances *in vitro*¹⁰⁷. The authors further hypothesized that the observed diffusion events of Myosin Va might result from an electrostatic interaction with the negatively charged tubulin E-hook. So far, E-hooks have been shown to be important for the binding to microtubules by some members of the kinesin superfamily^{25,31,108,109}. In a follow-up publication Ali *et al.* provide evidence that *in vitro* the interaction of Myosin Va with microtubules enhances the processivity of kinesin-based cargo transport on microtubules¹¹⁰. One possible explanation for this would be that on microtubules Myosin Va might act as a tether and thereby prevent diffusion of the cargo away from the track.

To study the events that occur at intersecting filaments is crucial for the understanding of how intracellular organelle transport is coordinated. With this in mind, part of this work focused on the investigation and characterization of the nature of this intriguing interaction between Myosin V and microtubules and its biological relevance emerging from it.

2 Project Aims of this Thesis

2.1 One-dimensional diffusive motility of Myosin Va on microtubules

In pigment cells from fish and amphibians, the long-range transport of pigment granules towards the cell periphery takes place on microtubules and is driven by Kinesin-2. However, within the actin-rich cell cortex short-range movement is carried out by the actin-based motor Myosin V ^{103,104,105,106}.

Therefore, some kind of handoff mechanism between Kinesin-2 and Myosin V has been proposed, but to date the regulation and molecular basis of this crosstalk has remained elusive.

Studies by Ali *et al.* ¹⁰⁷ demonstrated that *in vitro* Myosin V is capable of switching from an actin filament to an intersecting microtubule, followed by long-distance one-dimensional diffusive movements. Furthermore, Ali *et al.* ¹¹⁰ suggested that Myosin V's ability to interact with microtubules might even enhance the processivity of Kinesin-2-powered cargo transport on microtubules. This biophysical trick could enable cells to exploit both tracks for the same transport process without switching motors. Based on previous studies dealing with the binding of myosins to F-actin and kinesins to microtubules, the authors proposed that this novel and unconventional interaction between the heads of Myosin V and microtubules results from an electrostatic interaction between the positively charged myosin loop 2 and the negatively charged microtubule E-hooks ^{35,44,111,112,113,114,115,116,117,118,119,120}.

The aim of this project was to understand the underlying basis of this intriguing interaction between Myosin V and microtubules. Therefore, three major questions were addressed in this study: Does indeed the charge of loop 2 contribute to microtubule binding? If E-hooks are at all required for the interaction between Myosin V and microtubules, do they aid during the initial binding or rather during the diffusive movement? If E-hooks are dispensable, then what biophysical feature enables Myosin V to start diffusing along the filament?

For this, via single-molecule TIRF microscopy as well as different biochemical assays, I set out to characterize the behavior of three Myosin V mutants

containing differently charged (positive and negative) loop 2 motifs, on microtubules and also on F-actin.

2.2 Calcium-/Calmodulin-dependent Kinase II- α and its role in Myosin V release from pigment organelles

As detailed in Section 2.1, Myosin V was proposed to assist Kinesin-2-driven cargo transport on microtubules by enhancing kinesin's runlength *in vivo* (i.e., processivity)¹¹⁰. However, this hypothesis derives from *in vitro* experiments and awaits further clarification in a biologically relevant setup.

An ideal set up would involve the transport of a native cargo that employs both Kinesin-2 and Myosin V motor proteins. As intact melanosomes can be isolated from melanophores and involve both Kinesin-2 as well as Myosin V to achieve pigment dispersion, once again the pigment cells from lower vertebrates offer the most suitable system to study the interplay between these distinct transport systems. To dissect the effects of Myosin V on the Kinesin-2-powered cargo transport, the composition of the melanosome transport machinery would need to be manipulated. How would one obtain melanosomes that lack Myosin V and have Kinesin-2 still attached? To solve this problem as well as to pave the way for testing whether Myosin V is indeed capable of assisting the Kinesin-2-powered cargo transport on microtubules, was the main motivation of this project.

Rogers *et al.* (1999)¹⁰³ reported that Myosin V undergoes motor-specific release from melanosomes when incubated with mitotic *Xenopus* egg-cell extract. In very elegant assays using biochemical as well as mass-spectrometry analysis, Karcher *et al.* provided evidence that Calcium-/Calmodulin-dependent kinase II- α (CaMKII- α) induces the release of Myosin V from melanosomes by phosphorylating a specific Serine in the tail of Myosin V¹²¹.

These findings formed the two major goals of this project: i) to establish the baculoviral expression and subsequent purification of recombinant CaMKII- α , and ii) to build-up an assay, by which Myosin V release from melanosomes can be induced and monitored biochemically *in vitro*. With this assay, the following questions were addressed: Without egg-cell extract, is there endogenous CaMKII- α from melanophores that might also interact with melanosome-associated

Myosin V? If that is the case, then to which extent can it induce the release of Myosin V? And thirdly, can the recombinant exogenous kinase trigger the complete release of Myosin V from melanosomes?

In collaboration with Z. Kochovski and V. Lucic from the Baumeister-laboratory (MPI for Biochemistry, Martinsried, Germany) one additional goal of this work was to analyze the structure of the stimulated as well as unstimulated form of CaMKII- α via cryo-electron tomography. This is particularly interesting as CaMKII- α *in vivo* and in solution forms a dodecameric holoenzyme structure^{122,123,124}, which to date constitutes the most complex and unique structure among all kinases identified so far.

2.3 MACS[®] bead-assisted purification of pigment organelles – A novel approach

Although melanosomes were central to study organelle transport *in vivo* and *in vitro*, the methodology used so far has been limited to inhibitor studies, microinjection and electron as well as fluorescence or differential interference contrast microscopy. However, with the rapid progress of proteomic analysis techniques, as a next step it would be important to perform a “bottom-up” approach, which bears the great potential to reveal novel interaction partners involved in spatial and temporal regulation of melanosome transport. To date just a couple of studies approached the melanosome via proteomics, targeting melanosomes from human melanoma skin cells^{125,126}, not those from melanophores with rapid intracellular transport. Undoubtedly, the greatest challenge of mass-spectrometry, representing a very sensitive analytical method, pose the crude purification techniques that are used to isolate organelles for *in vitro* functional analyses. Even though mass-spectrometry on fractions of other types of organelles (e.g., mitochondria) that had been obtained by sucrose density ultra-centrifugation has been successfully carried out^{127,128,129,130}, melanosomes tend to lose their transport machinery upon such harsh treatments. Therefore, the ultimate goal would be to establish a method, by which functionally intact but at the same time, pure melanosome fractions are obtained. For this, the established, conventional crude melanosome isolation protocol was combined

with a technique that uses paramagnetic beads functionalized with antibodies against organelle-specific surface markers. This way, neither harsh centrifugation nor contaminating additives (e.g., sucrose) were applied. This feat allows for the analysis of functional organelles without having any contaminating cytosolic components present, which might overwhelm the signals from any melanosome-specific candidate.

2.4 Determining the sequence of the full-length Myosin Va from *Xenopus laevis*

Over the past three to four decades, great efforts have been undertaken to understand the mechanisms that drive intracellular organelle transport. In addition to studies on murine melanocytes, a large portion of today's knowledge on cytoplasmic organelle transport derives from studies on melanosomes from pigment cells of the African clawed frog *Xenopus laevis*. By using immunohisto- as well as immuno-biochemistry along with drug-dependent disruption of the actin cytoskeleton, the motor responsible for melanosome transport on actin in the outer margins of the cell was identified as Myosin Va^{63,121,131,132}. However, the full-length sequence of the *Xenopus l.* Myosin Va has remained unknown. Instead, mutated or truncated versions of the mouse Myosin Va version were used to manipulate melanosome transport (even in frog cells) *in vivo*. The aim of this project was to obtain the full-length sequence of Myosin Va from *Xenopus l.* melanophores, and to express it in insect cells.

I approached this problem by retrieving the full-length coding sequence of the Myosin Va gene using conventional step-by-step PCR and RACE (Rapid Amplification of cDNA Ends) PCR from melanophore cDNA. An additional aim was the initial biophysical characterization of the recombinantly expressed full-length Myosin Va protein via fluorescence microscopy on F-actin as a first step towards a more complete characterization of this motor.

3 Materials

3.1 Laboratory utensils and consumption items

Name of Item	Company, Location
Amersham Hyperfilm ECL	GE Healthcare, Munich
Amicon Ultra-4 Centrifugal Filter Unit with Ultracel-50 membrane	Millipore, Munich
Analytical Scale Analytic AC210P	Sartorius, Göttingen
Balch cell homogenizer with 0.6 μ tungsten-carbide ball	Isobiotec, Heidelberg
Centrifuge 5415 D	Eppendorf, Hamburg
Centrifuge GS-15R	Beckman-Coulter, Fullerton (U.S.A.)
Centrifuge J2-21M/E	Beckman-Coulter, Fullerton (U.S.A.)
Centrifuge Rotanta 460R	Hettich, Tuttlingen
Centrifuge Rotina 420	Hettich, Tuttlingen
Centrifuge Rotor JA-14	Beckman-Coulter, Fullerton (U.S.A.)
Centrifuge Tube with Sealing Cap, 250 ml	Nalgene Labware, Rochester (U.S.A.)
Developing machine Curix 60	(formerly) Agfa, Germany
DVS1000 Video Processor	Hamamatsu Photonics, Herrsching
ELISA 96-Well Plate for Biotek Reader	Greiner, Frickenhausen
FluoArc 01.26 Hg Lamp	Jena GmbH
FPLC Device Pharmacia	GMI, Ramsey (U.S.A.)
Front-illuminated Coupled Charge Device (CCD) C9100 Camera	Hamamatsu Photonics, Herrsching
Glass Homogenizer	Fisher Scientific, Schwerte
Hemocytometer Neubauer-improved	Blaubrand, Wertheim
Ice Machine AF20	Scotsman, Herborn
Incubator B5060	Heraeus, Hanau
Incubator-Shaker Device Certomat BS-T	Sartorius, Göttingen
Incubator-Shaker Device HT	Infors, Bottmingen (Switzerland)
Laboratory Film "M"	American National Can™, Chicago (U.S.A.)
MACS LS separation column	Miltenyi Biotec, B. Gladbach
Microcentrifuge (max. Speed 6,000 rpm)	Roth, Karlsruhe
Microwave Intellrowave	LG, Willich
Milli-Q®, Water Purifier	Millipore, Schwalbach
Minifuge RF	Heraeus, Hanau
MonoQ® Pharmacia Column	GMI, Ramsey (U.S.A.)
Newicon C2400 Camera	Hamamatsu Photonics, Herrsching
Nitrocellulose Membrane	Protran-Whatman, Dassel
PCR-Thermocycler Primus 96	PeqLab, Erlangen
pH-Meter	Knick, Berlin
Pipetman Gilson (10, 20, 100 and 1000 μ l)	Gilson, Middleton (U.S.A.)
Pipettips (with/without sterile filter)	Sarstedt, Nürmbrecht
PolyPrep® Chromatography Column	Bio-Rad, Hercules (U.S.A.)
Power Supplier Powerpack P21	Biometra, Göttingen
PowerWave™ Microplate Spectrophotometer	Biotek, Winooski, (U.S.A.)
Purple Nitrile Powder-free Exam Gloves	Kimberly Clark, Roswell (U.S.A.)
QuadroMACS™ Separator magnet	Miltenyi Biotec, B. Gladbach
Reaction tubes, 1.5 ml	Sarstedt, Nürmbrecht
Reaction Tubes, 13 ml	Sarstedt, Nürmbrecht
Reaction Tubes, 15 ml	Sarstedt, Nürmbrecht
Reaction tubes, 50 ml	Sarstedt, Nürmbrecht

Materials

Rotator Labquake	Barnstead, Dubuque (U.S.A.)
SDS-PAGE Electrophoresis Module	Biorad, Hercules (U.S.A.)
Semi-dry Elektrobloetter SEDEC M	PeqLab, Erlangen
Sephadex® G300 Pharmacia Column Material	GMI, Ramsey (U.S.A.)
Serological Pipettes (5, 10, 25 and 50 ml)	Sarstedt, Nürmbrecht
Silica Cuvette QS (10.00 mm)	Hellma Optika, Jena
Slide-A-Lyzer® 10K MWCO 0.1-0.5 ml capacity	Pierce, Rockford (U.S.A.)
Dialysis Cassette	
Slide-A-Lyzer® 10K MWCO 0.5-3 ml capacity Dialysis Cassette	Pierce, Rockford (U.S.A.)
Solid-phase Laser Device λ 532 nm	Hamamatsu Photonics, Herrsching
Solid-phase Laser device λ 488 nm	Hamamatsu Photonics, Herrsching
Sonifier 250	Branson, Danbury (U.S.A.)
Sorvall GSA Rotor	Thermo Fisher Scientific, Waltham (U.S.A.)
Spectrometer Uvikon 930	Kontron Instruments, Groß-Zimmern
Sterile Work Bench Infinity	Envair, Emmendingen
Surgical Disposable Scalpels	Braun, Tuttlingen
Table-top Centrifuge 5415D	Eppendorf, Hamburg
Thermomixer Comfort	Eppendorf, Hamburg
Total Internal Reflection Fluorescence (TIRF) Microscope X71	Olympus Biosystems, Planegg
(Plan objective lens 100 \times , N.A. 1.65 Oil)	
Ultra-Centrifuge L8-70M	Beckman-Coulter, Fullerton (U.S.A.)
Ultra-Centrifuge Optima-TL	Beckman-Coulter, Fullerton (U.S.A.)
Ultra-Centrifuge Rotor 35 Ti	Beckman-Coulter, Fullerton (U.S.A.)
Ultra-Centrifuge Rotor 42.1	Beckman-Coulter, Fullerton (U.S.A.)
Ultra-Centrifuge Rotor 45Ti	Beckman-Coulter, Fullerton (U.S.A.)
Ultra-Centrifuge Rotor TLA 100	Beckman-Coulter, Fullerton (U.S.A.)
Ultra-Centrifuge Rotor TLA 120	Beckman-Coulter, Fullerton (U.S.A.)
Ultra-Centrifuge Tubes for 42.1-Rotor	Beckman-Coulter, Fullerton (U.S.A.)
Vinyl Powder-free Exam Gloves	Med Comfort, Stelle
Vortex Mixer 72020	Neo-Lab, Heidelberg
Zeiss Axiophot Microscope (Plan-Apochromatic Objective lens 63 \times , N.A. 1.4 Oil, DIC prisms and Oil-immersion Condenser for N.A. 1.4)	Zeiss, Oberkochen
Zeiss Axiovert 200M	Zeiss, Jena
Zeiss CCD AxioCam MRm camera	Zeiss, Jena

3.2 Cell culture accessories

Name of Item	Company, Location
Corning® 500 ml Polycarbonate Erlenmeyer Flask with Plug Seal Cap	Corning Inc., Lowell (U.S.A.)
Cell Scraper	Greiner Bio-one, Munich
Cellfectin® Reagent	Invitrogen, Karlsruhe
Centrifugation Tube (250 ml) with Plug Seal Cap	Nalgene Labware, Rochester (U.S.A.)
Corning® 2 L Polycarbonate Erlenmeyer Flask with Plug Seal Cap	Corning Inc., Lowell (U.S.A.)
Corning® 250 ml Polycarbonate Erlenmeyer Flask with Plug Seal Cap	Corning Inc., Lowell (U.S.A.)
Electrical Vacuum Pump BVC21 NT	Vacuubrand, Wertheim
Fetal Bovine Serum (FBS) USA origin, sterile-filtered, Cell Culture- and Hybridoma-tested	Sigma-Aldrich, St. Louis (U.S.A.)
Filter Syringe 0.22 μ m Millex® GP (sterile)	Millipore, Schwalbach

Materials

Gentamicin (10 mg/ml)	c.c. Pro, Oberdorla
Glass Erlenmeyer Flasks (0.2 L to 6L)	Fisher Scientific, Schwerte
Insulin (bovine)	Sigma-Aldrich, St. Louis (U.S.A.)
Leibovitz's L-15 Medium	Invitrogen, Karlsruhe
Light-Microscope Labovert	Leitz, Wetzlar
Medium Sf-900 II SFM	Gibco-Invitrogen, Karlsruhe
Melanophores (<i>Xenopus laevis</i>), immortalized	kind gift from V. Gelfand, Chicago (U.S.A.)
Melatonin	Sigma-Aldrich, St. Louis (U.S.A.)
Penicilin-Streptomycin	Invitrogen, Karlsruhe
Sf9 Cells, SFM Adapted	Invitrogen, Karlsruhe
Six-Well Plate Multiwell™	Becton-Dickinson, Franklin (U.S.A.)
Syringes 2 ml (sterile)	Braun, Melsungen
Trypsin/EDTA	Promega, Mannheim
Vent-cap Cell Culture Flasks, 25-175 cm ² , PS	Greiner, Munich
Water Bath Preservative	Roth, Karlsruhe
α-Melanocyte Stimulating Hormone (α-MSH)	Sigma-Aldrich, St. Louis (U.S.A.)

3.3 Plasmids and vectors

Description	Distributor, Location
p2bac/pfastbac (containing HMM-like Myosin Va+CaM)	J. Spudich, Stanford (U.S.A.)
pBluescript SK (-) (containing CaMKII-α coding sequence)	Y. Hayashi, Saitama (Japan)
pFastBac™Dual	Invitrogen, Karlsruhe
pFastBac™ 1	Invitrogen, Karlsruhe

3.4 Oligonucleotides (Primers)

3.4.1 Cloning primers

Primer ID	Primer Sequence	Rest. site
HMM-like Myosin Va (N' FLAG-tag)		
HMM-M5_Fw01	5'-atagcggccgcatggactacaaggacgacgatgacaagggc-3'	NotI
HMM-M5_Rv01	5'-atagtcgactcgactcactccccgacaagcttctaagt-3'	Sall
Calmodulin (no tag)		
CaM_Fw01	5'-atagctagcatggcagatcaactgacagaagagc -3'	NheI
CaM_Rv01	5'-atagcggctactcacttcgctgcatcatctg -3'	KpnI
CaMKII-α (N' FLAG-tag)		
CaMKII-FLAG_Fw1	5'-cgataactagtaggactacaaggacgacgatgacaagggcgcacctgctaccatcacctgcacc-3'	SpeI
CaMKII_Rv1	5'-cgcttgcggccgctcaatggggcaggacggagg-3'	NotI

Materials

CaMKII-α (C' FLAG-tag)		
CaMKII_Fw2	5'-cgataactagtagtggtaccatcacctgcacccg-3'	SpeI
CaMKII-FLAG_Rv2	5'-cgcttgcggccgctcactgtcatcgtcgtcctttagtcagggtgcgcatggggcaggacggagggc-3'	NotI
CaMKII-α (No FLAG-tag)		
CaMKII_Fw2	5'-cgataactagtagtggtaccatcacctgcacccg-3'	SpeI
CaMKII_Rv1	5'-cgcttgcggccgctcaatggggcaggacggagg-3'	NotI
Full-length <i>Xenopus I.</i> Myosin Va (N' FLAG-tag)		
FLXM5_NheIFL AG-Fw	5'-gcgctagcatggactacaaggacgacgatgacaagggcgacacctgaaaacaatttagattttgc-3'	NheI
FLXM5_SphI-Rv	5'-gttgcagctcagacgctgtgaggaacc-3'	SphI
Full-length <i>Xenopus I.</i> Myosin Va (C' FLAG-tag)		
FLXM5_Nhe- Fw2	5'-gcgctagcatggaaaacaatttagattttgc-3'	NheI
FLXM5_SphIFL AG-Rv	5'-gttgcagctcactgtcatcgtcgtcctttagtcagggtgcgccgacgctgtgaggaacc-3'	SphI
Full-length <i>Xenopus I.</i> Myosin Va (No FLAG-tag)		
FLXM5_NheI- Fw2	5'-gcgctagcatggaaaacaatttagattttgc-3'	NheI
FLXM5_SphI-Rv	5'-gttgcagctcagacgctgtgaggaacc-3'	SphI
Full-length <i>Xenopus I.</i> Myosin Va (intermediate products)		
Phase A		
FLXM5_Fw#1	5'-atggaaaacaatttagattttgc-3'	–
FLXM5_Rv5	5'-atgtttctgcctgctcctg-3'	–
Phase B		
FLXM5_Fw#5	5'-atgtatgtttcgacagaagtaccg-3'	–
FLGgM5_Rv412 6	5'-agccgggtgatctcatgctg-3'	–
Phase C		
FLXM5_Fw#7	5'-gaggaaactgacgtgcgtaaggaag-3'	–
UPM (long)	5'-ctaatacgaactactatagggcaagcagtggtatcaacgcagagt-3'	–
UPM (short)	5'-ctaatacgaactactatagggc-3'	–

Materials

3.4.2 Sequencing primers

Primer ID	Primer Sequence
Full-length Xenopus I. Myosin Va-specific	
FLXM5_Seq#1	5'-atggaaaacaatttagatttgc-3'
#2	5'-atacattgaaattggcttgataaac-3'
#3	5'-gctttgaacagtttgtatcaactatg-3'
#4	5'-agaaattcccttcaccttctgatg-3'
#5	5'-atgtatgttgttcgacagaagtaccg-3'
#6	5'-ttaatccaggagcaggcaag-3'
#7	5'-gaggaactgacgtgcgtaaggaag-3'
#8	5'-gccacctgaagcaagaattg-3'
#9	5'-agctggaagtgggtcaaatg-3'
#10	5'-ttgtcatgttttgcgtca-3'
#11	5'-actgtcagtgttctgccagtg-3'
#12	5'-attccagattacaagccaccaatgc-3'
#13	5'-gttgccgagctgagagaaacagaatgc-3'
#14	5'-ccataccgaaatgaggagcctgctg-3'
#15	5'-agctggaagtgggtcaaatg-3'
#16	5'-accgatgaagatgcagaagc-3'
HMM-like Myosin Va-specific	
HMM-M5_Seq#1	5'-ggggcaggaaagacggttctgcc-3'
#2	5'-gggcaacgtggagttgcatctcggg-3'
#3	5'-ggatctgtagatgaggaaatgcaagatgcc-3'
#4	5'-ggacataccaagattctcagccg-3'
#5	5'-ggctggctggctcgagtgc-3'
CaMKII-α-specific	
CaMKII_Seq#1	5'-cgacctgaagcctgagaatc-3'
#2	5'-aaactgaaggagccatcct-3'
Calmodulin-specific	
CaM_Seq#1	5'-ggatcagctgaccgaagaac-3'
Baculovirus transfer vector-specific	
pPolyhedrin_Seq	5'-cctataaatattccgg-3'
pP10_Seq	5'-cggaccttaattcaacc-3'
M13_Seq (reverse)	5'-caggaacagctatgac-3'

Materials

3.5 Microorganisms

Description of Cells	Company, Location
MAX Efficiency [®] DH10Bac [™] Competent <i>E. coli</i> XL1-Blue Subcloning-Grade Competent Cells	Invitrogen, Karlsruhe Stratagene, La Jolla (U.S.A.)

3.6 Mediums and agars for microorganisms

LB-Ampicillin Agar

- 1.5 % (w/v) Agar
- 1 % (w/v) Tryptone
- 0.5 % (w/v) Yeast Extract
- 1 % (w/v) NaCl
- 0.1 % (v/v) Ampicillin-Solution (100mg/ml)

LB-Ampicillin Medium

- 1 % (w/v) Tryptone
- 0.5 % (w/v) Yeast Extract
- 1 % (w/v) NaCl
- 0.1 % (v/v) Ampicillin-Solution (100mg/ml)

S.O.C Medium

- 2 % (w/v) Tryptone
- 0.5 % (w/v) Yeast Extract
- 10 mM NaCl
- 2.5 mM KCl
- 10 mM MgCl₂
- 10 mM MgSO₄
- 2 % (v/v) 1 M Glucose

3.7 Antibodies and peptides

	Antibody Name	Isotype/host	Company, Location
Primary	Anti-FLAG [®] M2 affinity gel	IgG1/Mouse	Sigma-Aldrich, St. Louis (U.S.A.)
	Anti-FLAG [®] Biotinylated M5, monoclonal	IgG1/Mouse	Sigma-Aldrich, St. Louis (U.S.A.)
	Anti-Myosin Va (LF-18), polyclonal	IgG/Rabbit	Sigma-Aldrich, St. Louis (U.S.A.)
	Anti-FLAG [®] M2-Cy3 [™] , monoclonal	IgG1/Mouse	Sigma-Aldrich, St. Louis (U.S.A.)
	Anti- α -Tubulin (YL 1/2), monoclonal	IgG/Rat	R. Gräf, Postdam
	Anti- β -Tubulin (SAP.4G5), monoclonal	IgG1/Mouse	Santa Cruz Biotech., Heidelberg
	Anti-total CaMKII (6G9), monoclonal	IgG1/Mouse	Thermo Scientific, Bonn
	Anti-Phospho (Thr286)-CaMKII (22B1), monoclonal	IgG1/Mouse	Thermo Scientific, Bonn
	Anti-Kinesin-2 (K2.4), monoclonal	IgG1/Mouse	Covance, Princeton (U.S.A.)
	Anti-GAPDH (6C5), monoclonal	IgG1/Mouse	Merck-Millipore, Darmstadt
	Anti-Trp1 (TA99), monoclonal	IgG2a/Mouse	Abcam, Cambridge (U.K.)
Secondary	Anti-Mouse IgG Microbeads	IgG/Goat	Miltenyi Biotec, B. Gladbach
	Anti-Rat IgG (Whole Molecule)- Peroxidase	IgG/Rabbit	Sigma-Aldrich, St. Louis (U.S.A.)
	Anti-Mouse IgG (Fc-specific) Peroxidase Conjugate	IgG/Goat	Sigma-Aldrich, St. Louis (U.S.A.)
	Anti-Rabbit IgG (Whole Molecule) Peroxidase Conjugate	IgG/Goat	Sigma-Aldrich, St. Louis (U.S.A.)
	FLAG [®] peptides		Sigma-Aldrich, St. Louis (U.S.A.)

3.8 Chemicals and ready-to-use solutions

Name of Chemical/Solution	Company, Location
1-Brom-3-Chloropropane	Merck, Darmstadt
Acetic Acid (99.5% p. A.)	Roth, Karlsruhe
Acteone	Sigma-Aldrich, St. Louis (U.S.A.)
Agarose NEEQ Ultra-Quality	Roth, Karlsruhe
AMP-PNP (Adenosine 5'-(β,γ -imido) triphosphate lithium salt hydrate)	Sigma-Aldrich, St. Louis (U.S.A.)
Ampicillin (No Salt)	Roth, Karlsruhe
APS	Biorad, Hercules (U.S.A.)
Apyrase from Potato grade IV	Sigma-Aldrich, St. Louis (U.S.A.)
Betaine	Sigma-Aldrich, St. Louis (U.S.A.)
Bio-Rad Protein Assay Dye Reagent Concentrate	Biorad, Hercules (U.S.A.)
Biotin Bovine Serum Albumin	Sigma-Aldrich, St. Louis (U.S.A.)
Bovine Serum Albumin 99% purity	Sigma-Aldrich, St. Louis (U.S.A.)
Bromophenol Blue	Sigma-Aldrich, St. Louis (U.S.A.)
CaCl ₂ x 2H ₂ O	Merck, Darmstadt
Calmodulin from Bovine Brain, High Purity	Merck-Millipore, Darmstadt

Materials

Casein from Bovine Milk	Sigma-Aldrich, St. Louis (U.S.A.)
Collodion solution, 2% in amyl acetate	Sigma-Aldrich, St. Louis (U.S.A.)
Coomassie Brilliant Blue R-250	Sigma-Aldrich, St. Louis (U.S.A.)
complete, Mini Protease Inhibitor (EDTA-free)	Roche Applied Science, Penzberg
DEPC (Diethyl pyrocarbonate)	Sigma-Aldrich, St. Louis (U.S.A.)
DMSO	Roth, Karlsruhe
dNTPs (100 mM)	PeqLab, Erlangen
DTT	Sigma-Aldrich, St. Louis (U.S.A.)
EDTA	Sigma-Aldrich, St. Louis (U.S.A.)
EGTA	Sigma-Aldrich, St. Louis (U.S.A.)
Ethanol (99.8% p.a.)	Roth, Karlsruhe
Ethidium Bromide	Roth, Karlsruhe
Gelsolin from Bovine Plasma	Sigma-Aldrich, St. Louis (U.S.A.)
Gene Ruler™ 100 bp Plus DNA Ladder (0.1 µg/µl) #SM0328	Fermentas, St. Leon Roth
Gentamicin Sulfate	Sigma-Aldrich, St. Louis (U.S.A.)
Glacial Acetic Acid (99%)	Roth, Karlsruhe
Glucose	Roth, Karlsruhe
Glycerol Rotipuran® (99.5% p.a.)	Sigma-Aldrich, St. Louis (U.S.A.)
Goat Anti-Mouse IgG Microbeads	Miltenyi Biotec, B. Gladbach
GTP	Sigma-Aldrich, St. Louis (U.S.A.)
Guanidinium-HCl Solution (8 M in H ₂ O, filtered)	Sigma-Aldrich, St. Louis (U.S.A.)
HCl	Merck, Darmstadt
Hepes	Merck, Darmstadt
High Molecular Weight Protein Ladder	Sigma-Aldrich, St. Louis (U.S.A.)
Imidazole	Sigma-Aldrich, St. Louis (U.S.A.)
Isoamylalcohol (99.8% p.a.)	Sigma-Aldrich, St. Louis (U.S.A.)
Isopropanol (99% p.a.)	Roth, Karlsruhe
K-Acetate	Merck, Darmstadt
Kanamycin Monosulfate	Sigma-Aldrich, St. Louis (U.S.A.)
KCl	Merck, Darmstadt
KH ₂ PO ₄	Merck, Darmstadt
KOH	Merck, Darmstadt
Luminol (3-Aminophtalhydrazide)	Sigma-Aldrich, St. Louis (U.S.A.)
Methanol (99.5% p.a.)	Roth, Karlsruhe
Mg-Acetate x 4 H ₂ O	Merck, Darmstadt
MgCl ₂ x 6 H ₂ O	Merck, Darmstadt
MgSO ₄ x 7 H ₂ O	Merck, Darmstadt
Milkpowder	Roth, Karlsruhe
N-Phenylthiourea (PTU)	Sigma-Aldrich, St. Louis (U.S.A.)
Na ₂ ATP	Sigma-Aldrich, St. Louis (U.S.A.)
Na ₂ HPO ₄	Merck, Darmstadt
NaCl	Sigma-Aldrich, St. Louis (U.S.A.)
NaHCO ₃	Merck, Darmstadt
NaN ₃	Merck, Darmstadt
p-Coumaric Acid	Sigma-Aldrich, St. Louis (U.S.A.)
P11 Cellulose Phosphate Material	Merck, Darmstadt
Paclitaxel from <i>Taxus brevifolia</i>	Sigma-Aldrich, St. Louis (U.S.A.)
Page Ruler™ Prestained Protein Ladder #SM0671	Fermentas, St. Leon Roth
Phalloidin from <i>Amanita phalloidies</i>	Sigma-Aldrich, St. Louis (U.S.A.)
Phalloidin-Atto 488	Sigma-Aldrich, St. Louis (U.S.A.)

Materials

Phalloidin-TRITC	Invitrogen, Karlsruhe
Phenylmethanesulfonyl fluoride (PMSF) Premium	Sigma-Aldrich, St. Louis (U.S.A.)
Phospho(enol)pyruvic acid trisodium sulfohydate	Sigma-Aldrich, St. Louis (U.S.A.)
PIPES	Sigma-Aldrich, St. Louis (U.S.A.)
Ponceau Red S	Sigma-Aldrich, St. Louis (U.S.A.)
Protector RNase-inhibitor	Roche Applied Science, Penzberg
QDot [®] 525 Streptavidin Conjugate	Life Technologies, Grand Island (U.S.A.)
Rotiphorese Gel 30	Roth, Karlsruhe
SDS	Sigma-Aldrich, St. Louis (U.S.A.)
Streptavidin from <i>Streptomyces avidinii</i>	Sigma-Aldrich, St. Louis (U.S.A.)
Sucrose	Merck, Darmstadt
Taq Polymerase Reaction Buffer (10X)	PeqLab, Erlangen
Temed	Sigma-Aldrich, St. Louis (U.S.A.)
Tetracyclin	Sigma-Aldrich, St. Louis (U.S.A.)
TRI-reagent [®]	Molecular Research Center, Cincinnati (U.S.A.)
Triton-X 100	Fluka, Buchs (Switzerland)
Trizma Base	Sigma-Aldrich, St. Louis (U.S.A.)
Trypan Blue Solution	Invitrogen, Karlsruhe
Tryptic Soy Broth (Tryptone, microbiologically tested)	Sigma-Aldrich, St. Louis (U.S.A.)
Tween [®] 20 Premium	Sigma-Aldrich, St. Louis (U.S.A.)
Yeast Extract Agar	Sigma-Aldrich, St. Louis (U.S.A.)
β-Mercaptoethanol	Sigma-Aldrich, St. Louis (U.S.A.)
β-Nicotinamide-adenine-dinucleotide (NADH), reduced disodium salt	Sigma-Aldrich, St. Louis (U.S.A.)

3.9 Buffers and ready-to-use solutions

12A25 Buffer (1X):

12.5 mM KOH (pH 6.8)

2 mM Mg-Acetat

25 mM K-Acetat

1 mM EGTA

ABSA Buffer (1X, 10 ml):

1 ml BSA (10 mg/ml)

9 ml AB Buffer (1X)

Materials

Agarose Gel Loading Buffer:

20% Glycerol

0.1 M EDTA

1% SDS

0.25% Bromophenol Blue

APS Solution (100X):

10% (w/v) APS in Water

Assay Buffer AB (1X):

25 mM Imidazole, pH 7.4

25 mM KCl

4 mM MgCl₂

1 mM EGTA

10 mM DTT

ATP Solution (0.1 M, pH 7.0):

100 mM Na₂ATP in Water

BBSA Solution (10 ml):

10 mg BBSA

10 ml PBS

BRB80 Buffer (1X):

80 mM Pipes

2 mM MgCl₂

1 mM EGTA

1 mM DTT

BRB80-Tx (1X):

+5 μM Paclitaxel (4 mM in DMSO)

Materials

Brickey Buffer (1X):

10 mM TrisCl, pH 7.5

1 mM EGTA

1 mM EDTA

2.5% (v/v) Betaine

1 Tablet/50 ml c0mplete, Mini Protease Inhibitor (EDTA-free, Roche)

BSA Solution (10 ml):

100 mg BSA

10 ml Water

Buffer A (pH 6.9):

0.1 mM Pipes

2 mM EGTA

1 mM MgSO₄

0.1 mM Na₂ATP

1 mM DTT

Buffer B (pH 6.94):

0.5 M Pipes

2 mM EGTA

1 mM MgSO₄

Buffer C:

0.1 M Pipes

1 mM EGTA

1 mM MgSO₄

1 mM Na₂ATP

1 mM DTT

Materials

Buffer D:

0.1 M Pipes (pH 6.94)

1 mM EGTA

1 mM MgSO₄

0.05 mM Na₂ATP

0.022 mM GTP (pH 7.0)

1 mM DTT

Catalase Solution (100X):

170000 U/ml Catalase in O₂ Quench Buffer (1X)

50% (v/v) Glycerol

Coomassie Brilliant Blue Solution:

0.25% (w/v) Brilliant Blue R-250

50% (v/v) Methanol

10% (v/v) Glacial Acetic acid

DB-CK (1X):

150 mM KCl

10 mM Hepes, pH 7.4

0.1 mM EGTA

10% (v/v) Glycerol

DB-HMM-M5 (1X):

Assay Buffer (1X)

50% (v/v) Glycerol

EB-CK (1X):

500 mM NaCl

40 mM Hepes, pH 7.4

1 mM EGTA

+ 400 µg/ml FLAG peptides (in TBS)

Materials

EB-HMM-M5 (1 ml):

300 µg FLAG[®] Peptides in TBS

940 µl Wash Buffer (1X)

EB-XM5 (1X):

1.25 mg FLAG[®] Peptides (in TBS)

750 µl Wash Buffer (1X)

ECL- Solution (1 ml):

0.5 ml Solution A

0.5 ml Solution B

0.01% H₂O₂

EDTA Solution (pH 7.0):

200 mM EDTA in TAE (50X)

EGTA Solution (pH 7.0):

200 mM EGTA in TAE (50X)

Electrophoresis Buffer (10X, pH 8.8):

3% (w/v) Tris Base

1% (w/v) SDS

14% (w/v) Glycine

Ethanol (1 L, 70% Vol.):

700 ml Ethanol (99.9%)

300 ml Water

FLAG[®] Peptides (1 ml of 5 µg/µl Aliquots):

5 mg FLAG[®] Peptides

1 ml TBS (1X)

Materials

G Buffer:

2 mM TrisHCl

0.2 mM CaCl₂

0.2 mM ATP

0.2 mM DTT

0.005% (v/v) NaN₃ (20% Stock Solution)

Gentamicin Solution (100 ml):

50 mg Gentamicin Sulfate

100 ml Water

Glucose Oxidase Solution (100X):

2600 U/ml Glucose Oxidase in O₂ Quench Buffer (1X)

50% (v/v) Glycerol

Glucose Solution (100X, 1 ml):

500 mg Glucose

1 ml Water

GTP Solution (pH 7.0):

0.1 M GTP in Water

Guanidine Hydrochloride (6.6 M):

6.6 M Guanidinium Hydrochloride Solution (8 M)

Water

Hepes Buffer (1X):

100 mM Hepes (pH 7.0)

1 mM MgCl₂

0.5 mM EGTA

Materials

High Ca²⁺ Reaction Mix (2.5X):

125 mM Tris Base, pH 7.1

>2.5 mM MgCl₂ (included in 0.5 M TrisCl / 0.01 MgCl₂)

1 mM EGTA

1.75 mM CaCl₂

1 mg/ml BSA (in H₂O)

High Molecular Weight (HMW) Protein Ladder-Aliquots:

3 mg HMW

1.5 ml SDS Sample Buffer (1X)

High Salt Buffer (pH 8.5):

10 mM Tris Base (pH 8.0)

0.25 mM CaCl₂

0.1 mM EGTA

0.2 mM DTT

2 M NaCl

Kanamycin Solution (100 ml):

50 mg Kanamycin Monosulfate

100 ml Water

KMg50 Buffer (1X):

50 mM KCl

1 mM EGTA

1 mM MgCl₂

1 mM DTT

10 mM Imidazole (HCl, pH 7.0)

Materials

LB-HMM-M5 (1X):

200 mM NaCl

4 mM MgCl₂

20 mM Imidazole, pH 7.5

0.5 mM EDTA

7% (w/v) Sucrose

5 mM DTT

2 mM ATP

0.5% (v/v) Triton-X 100

1 Tablet/50 ml c0mplete, Mini Protease Inhibitor (EDTA-free)

LB-XM5 (1X):

200 mM NaCl

20 mM Imidazole, pH 7.5

mM MgCl₂

1 mM EGTA

1 mM EDTA

7% (w/v) Sucrose

1 mM PMSF (in Isopropanol)

3 mM ATP

1 Tablet/50 ml c0mplete, Mini Protease Inhibitor (EDTA-free, Roche)

Low Ca²⁺ Reaction Mix (2.5X):

125 mM Tris Base, pH 7.1

>2.5 mM MgCl₂ (included in 0.5 M TrisCl / 0.01 MgCl₂)

1 mM EGTA

1 mM CaCl₂

1 mg/ml BSA (in H₂O)

MgATP Solution (90 mM):

90 mM ATP

9 mM MgCl₂

Materials

Na₂ATP Solution (0.1 M for Tubulin-Prep, pH 6.9):

100 mM Na₂ATP in Buffer A (no DTT)

NHB 1X:

300 mM KCl

25 mM Imidazole, pH 7.0

1 mM EGTA

1 mM MgCl₂

1 mM DTT

Nitrocellulose solution (0.1%):

0.1% (final concentration) Collodion solution (2% in Amyl Acetate)
dilute into Isoamylalcohol (99.8% p.a.)

No Salt Buffer (pH 8.5):

10 mM Tris Base (pH 8.0)

0.25 mM CaCl₂

0.1 mM EGTA

0.2 mM DTT

O₂ Quench Buffer (1X):

24 mM Pipes

4 mM MgCl₂

4 mM EGTA

Oxygen-scavenging system (25X), 20 µl:

10 µl Catalase Solution (100X)

10 µl Glucose-oxidase Solution (100X)

(Glucose (100X in H₂O) is added directly to assay)

Paclitaxel (4 mM in DMSO):

25 mg Paclitaxel

7.3 ml DMSO

Materials

PBS (1X, pH 7.4):

140 mM NaCl

2.7 mM KCl

1.8 mM KH₂PO₄

10 mM Na₂HPO₄

PBS for MACS (1X, pH 7.4):

75 mM NaCl

16.2 mM Na₂HPO₄

3.8 mM NaH₂PO₄

PEB (1X):

PBS for MACS (1X)

2 mM EDTA

1 Tablet/50 ml c0mplete, Mini Protease Inhibitor (EDTA-free, Roche)

SDS Protein Sample Buffer (6X):

300 mM Tris Base (pH 6.8)

15 mM EDTA

12% (w/v) SDS

30% (v/v) Glycerol

0.06% (v/v) Bromophenol blue

15% (v/v) β-Mercaptoethanol

Separating Gel (10%, 10 ml):

3.3 ml Rotiphorese Gel 30

2.5 ml Separating Gel Buffer

4.2 ml Water

10 μl Temed

100 μl APS

Materials

Separating Gel Buffer (10X):

0.5 M Tris Base (pH 6.8)

0.4% (w/v) SDS

Solution A (100 ml):

9 ml Tris Base (1 M), pH 8.5

1 ml Luminol (0.25 M)

90 ml H₂O

Solution B (100 ml):

9.6 ml Tris Base (1 M), pH 8.5

440 µl Coumaric Acid (90 mM)

90 ml H₂O

Solution I (1X, pH 6.5):

100 mM KCl

150 mM KH₂PO₄

Solution II (1X, pH 7.4):

50 mM NaHCO₃

Solution III (1X, pH 7.0):

1 mM EDTA

Stacking Gel (10%, 10 ml):

1.3 ml Rotiphorese Gel 30

2.5 ml Stacking Gel Buffer

6.2 ml Water

10 µl Temed

100 µl APS

Stacking Gel Buffer (10X):

1.5 M Tris Base (pH 8.8)

0.4% (w/v) SDS

Materials

Streptavidin Solution (10 ml):

10 mg Streptavidin

10 ml PBS

Sucrose Solution (20%):

20% (w/v) Sucrose in Water

TAE Buffer (50X):

24.2% (w/v) Tris Base

5.7% (v/v) Glacial Acetic acid

50 mM EDTA, pH 7.0

TBS Buffer (1X, pH 7.2):

20 mM Tris Base

150 mM NaCl

TBST (1X):

TBS (1X)

0.05% (v/v) Tween-20

TE Buffer (pH 8.0):

10 mM Tris Base

1 mM EDTA

Tetracycline Solution (100 ml):

50 mg Tetracycline

100 ml Water

TrisCl (0.5 M / 0.01 M MgCl₂), 50 ml:

5 ml 0.5 M Tris Base / 0.1 M MgCl₂

45 ml 0.5 M Tris Base, pH 7.1

Materials

WB-CK (1X):

100 mM NaCl

40 mM Hepes, pH 7.4

1 mM EGTA

1 Tablet/50 ml c0mplete, Mini Protease Inhibitor (EDTA-free, Roche)

WB-HMM-M5 (1X):

150 mM KCl

20 mM Imidazole, pH 7.5

5 mM MgCl₂

1 mM EGTA

1 mM EDTA

10 mM DTT

3 mM ATP

1 Tablet/50 ml c0mplete, Mini Protease Inhibitor (EDTA-free, Roche)

WB-XM5 (1X):

150 mM KCl

20 mM Imidazole, pH 7.5

5 mM MgCl₂

1 mM EGTA

1 mM EDTA

2 mM DTT

1 mM PMSF (in Isopropanol)

3 mM ATP

1 Tablet/50 ml c0mplete, Mini Protease Inhibitor (EDTA-free, Roche)

Zero Ca²⁺ Reaction Mix (2.5X):

125 mM Tris Base, pH 7.1

>2.5 mM MgCl₂ (included in 0.5 M TrisCl / 0.01 MgCl₂) 1 mM EGTA

1 mg/ml BSA (in H₂O)

3.10 Enzymes and kits for biochemistry & molecular biology

Name of Item	Company, Location
Antarctic Phosphatase (Kit)	New England Biolabs, Frankfurt a. Main
Bac-to-Bac [®] Baculovirus Expression System	Invitrogen, Karlsruhe
Catalase from Bovine Liver	Sigma-Aldrich, St. Louis (U.S.A.)
First Strand cDNA Synthesis Kit for RT-PCR (AMV)	Roche Applied Science, Penzberg
Glucose Oxidase Type VII from <i>Aspergillus Niger</i>	Sigma-Aldrich, St. Louis (U.S.A.)
Peq Gold DNA Taq DNA Polymerase (5 U/μl)	PeqLab, Erlangen
Platinum [®] Pfx Polymerase (Kit)	Invitrogen, Karlsruhe
Platinum [®] Taq HF Polymerase (Kit)	Invitrogen, Karlsruhe
Pyruvate Kinase/Lactic Dehydrogenase from Rabbit Muscle; PK (700 U/ml) and LDH (1000 U/ml)	Sigma-Aldrich, St. Louis (U.S.A.)
Qiaprep [®] Midiprep Kit	Qiagen, Hilden
Qiaprep [®] Miniprep Kit	Qiagen, Hilden
Qiaquick [®] Purification Kit	Qiagen, Hilden
Restriction Enzymes	New England Biolabs, Frankfurt/Main
SMARTer [™] RACE-PCR Kit	BD-Clontech, Heidelberg
SubtilisinA, bacterial, Type VIII from <i>Bacillus licheniformis</i>	Sigma-Aldrich, St. Louis (U.S.A.)
T4 DNA Ligase (Kit)	New England Biolabs, Frankfurt a. Main

3.11 Software for data acquisition and analysis

Software Name	Company, Location
CellR	Olympus Biosystems, Planegg
ImageJ Plugins + Macros	NIH, Bethesda (U.S.A.)
ImageJ Plugins MTrackJ and MultipleKymograph	NIH, Bethesda (U.S.A.)
ImageJ Version 1.46j	NIH, Bethesda (U.S.A.)
ImageQuant, Version TL 7.0	GE Healthcare, Munich
Igor Pro Version 6.1.2	WaveMetrics, Inc., Lake Oswego (U.S.A.)
Megalign Version 2.1.0.97	DNASStar, Madison, (U.S.A.)
Kaleidagraph Version 4.0.3	Synergy, Pittsburgh, (U.S.A.)

4 Methods

4.1 Cell culturing

4.1.1 Culturing of immortalized *Xenopus l. melanophores*

Immortalized *Xenopus laevis* melanophores (kind gift of Prof. V. Gelfand, Northwestern University, Chicago, U.S.A.) were cultured as previously described⁶⁶ at 28°C in 0.7X Leibovitz-15 (L-15) medium supplemented with 10% fetal bovine serum, 5 µg/ml insulin, 100 U/ml penicillin/streptomycin. Depending on the experiment to be performed, cells were cultured in small (25 cm²), medium (75 cm²) or large (175 cm²) sterile tissue culture-treated flasks with vent-cap. Typically, the cells were split by trypsinization once a week when confluency was reached.

To hormone-induce pigment aggregation or dispersion, first the cells had to be transferred into serum-free medium 24 hours prior to hormone stimulation. One hour prior melanosome purification, aggregation or dispersion of pigment granules was stimulated by adding 50 nM melatonin or 100 nM α-melanocyte stimulating hormone α-MSH to the serum-free culture medium, respectively.

4.1.2 Preparation of cryo-cultures from *Xenopus l. melanophores*

For the preparation of melanophore cryo-cultures, at first melanosomes had to be eliminated by the tyrosinase inhibitor phenylthiourea (PTU). That is because upon freezing melanin, as the main component of melanosomes, is released from accidentally freeze-ruptured cells, leading to low efficiency in the successful re-culturing of the frozen cell stocks.

For the actual elimination, the medium was supplemented with PTU at a final concentration of 1 mM and was maintained in this medium for about 4 weeks. The effect of PTU is completely reversible and non-toxic for the cells⁶³.

Once the melanophores were made devoid of melanosomes, cells from one confluent grown medium-size (75 cm²) flask were trypsinized into 0.7X L-15 medium (containing additives and 10% serum) and pelleted at 150 × g for 5 minutes at room temperature (Rotina 420, Hettich). The cell pellet was resuspended in 1.5 ml 0.6X L-15 Medium (containing 40% serum) and incubated

Methods

for 5 minutes on ice. As a next step, in total 1.5 ml of 0.5X L-15 medium (containing 30% serum, 20% DMSO) were added drop-wise to the cell suspension while gently stirring. The suspension was kept on ice for an additional 15 minutes. This way a final concentration of 10% DMSO, 35% FBS was reached. At last, 0.5 ml aliquots were prepared and kept overnight at -70°C before storage in liquid nitrogen.

4.1.3 Thawing and propagating melanophore cryo-cultures

To take cryo-cultures of melanophores back into culture, the cells were thawed quickly, mixed with 10 ml of 0.7X L-15 medium (containing additives and 10% serum) and pelleted at 150 × g for 5 minutes at room temperature (Rotina 420, Hettich) to remove the DMSO. The cell pellet was resuspended gently in 10 ml of 0.7X L-15 medium (containing additives and 10% serum), followed by transfer into a small (25 cm²) culturing flask for subsequent propagation at 28°C.

4.1.4 Protocol for MACS-bead assisted melanosome purification

The first part of the melanosome isolation procedure was performed as described previously by Rogers *et al.* (1997)⁶¹ and Kashina *et al.* (2004)^{65,93}, except that PBS 0.7X instead of AB 1X was used. In brief, before harvesting of the cells with a cell-scraper, 5 flasks of confluent melanophores were rinsed once with an appropriate amount of PBS 0.7X. Typically, cells were scraped into 2 ml PBS 0.7X (containing protease inhibitor) before cell lysis via Balch-homogenization (1 ml-syringes and 0.6 micron ball diameter). It was important not to lyse for more than 10 up-and-down cycles and to keep the Balch device on ice at all times. Membrane fractions and cell debris were pelleted at 750 × g for 7 minutes and 4°C (Hettich Rotanta 460R), with the melanosomes remaining in the supernatant. After pelleting the melanosomes at 3,000 × g for 5 minutes and 4°C (Hettich Rotanta 460R), pellets were resuspended in 800 µl of PBS 0.7X (plus protease inhibitor).

For the subsequent purification by MACS bead technology, 400 µl of the melanosome solution was incubated rolling with 1 to 2 µg anti-Tyrosinase related protein Trp1 (mouse monoclonal, clone TA99) or anti-Kinesin-2 antibody (mouse monoclonal, clone K2.4) (in PBS 1X) at 4°C for 20 minutes. Subsequently, 35 µl

Methods

of anti-mouse IgG conjugated MACS[®] beads (Miltenyi Biotec) were added. Following an incubation of 40 minutes at 4°C, the reaction volume was expanded by adding 500 µl PBS 1X (containing protease inhibitors), while incubating for additional 20 minutes at 4°C.

The melanosome-MACS bead mixture was applied dropwise onto a MACS LS-column, equilibrated with 3 ml PEB 1X (containing protease inhibitors). Still attached to the magnet, the column to which the melanosomes are now bound was washed three times with 3 ml of PEB 1X (containing protease inhibitors) each. Then the column was detached from the magnet and elution was carried out twice with 3 ml PEB 1X (containing protease inhibitors) each. To yield a more concentrated solution of purified melanosomes, an additional pelleting step of the sample at 3,000 × g for 5 minutes and 4°C (Hettich Rotanta 460R) with subsequent resuspension in 100 to 200 µl PBS 1X (containing protease inhibitors) was included. For Western-blot analysis, samples were run on a 10% SDS-PAGE.

4.1.5 Culturing of Sf9 insect cells

For the expression of recombinant proteins from the baculovirus-expression system, the Sf9 insect cell line (Invitrogen) was used. This cell line is a clonal isolate derived from the parental *Spodoptera frugiperda* (fall armyworm) cell line IPLB-Sf-21-AE^{133,134,135}, that itself originated from a population of cells that was isolated from *S. frugiperda* ovarian tissue¹²⁶. Sf9 cells are adapted to serum-free suspension growth in Sf-900 II SFM (Invitrogen), which is a serum-free medium that is optimized for growth of Sf9 but also other invertebrate cell lines.

Sf9 cells were suspension-cultured in Sf-900 II SFM medium (supplemented with 10% vol. FBS and 0.5 mg/ml Gentamicin). The actual culturing took place at 28°C and 110 rpm in spinner flasks that contained a final volume of 100 to 500 ml cell suspension at a cell density of 0.5 to 6*10⁶ cells/ml. Typically, cells were split every other day. For the purpose of protein expression with subsequent purification, cells were brought to a density of 2*10⁶ cells/ml, while for virus amplification cells were diluted to a density of 0.5*10⁶ cells/ml.

In general, cells were propagated up to 30 passages. To start a new round of Sf9 cell propagation, liquid nitrogen-stored cell stocks were thawed and expanded

Methods

according to the manufacturer's protocol (Invitrogen). Aliquots of cells to be stored in liquid nitrogen were prepared and handled as proposed by the manufacturer.

4.2 Molecular biological methods

4.2.1 RNA

4.2.1.1 Isolation of cellular total RNA

RNA was isolated via Total RNA Isolation (TRI)-reagent-mediated cell lysis. TRI-reagent (same as TRIzol) contains phenol and thiocyanate and reacts strongly with chloroform, thus is used for RNA isolation.

Typically, RNA from approx. 10^6 melanophores was isolated. For this, cells were harvested by trypsinization as described in Section 4.1.1, collected in 10 ml 0.7X L-15 medium (no additives) and pelleted twice at $800 \times g$ for 5 minutes at room temperature (Swinging-bucket centrifuge Rotina 420, Hettich). Between centrifugation steps, one washing step of the pellet with 1 ml 0.7X L-15 medium (no additives) was included.

To lyse the plasma and organelle membranes, the cell pellet was resuspended in 200 μ l TRI-reagent while pipetting the suspension 10 times up and down. The following incubation (for 8 minutes at room temperature) causes the dissociation of any nucleo-protein complexes that might have formed during the procedure. In cases where the actual RNA extraction was performed at a later time point, the obtained cell lysate was stored at -20°C .

RNA extraction was carried out by adding 40 μ l (i.e., 20% vol. of the lysate volume) 1-Brom-3-Chloropropane, followed by intense vortexing for 15 seconds. After incubation for 10 minutes at room temperature, the suspension was centrifuged at $12,000 \times g$ for 15 minutes at 4°C (Eppifuge 5415D, Eppendorf), yielding three phases. The RNA fraction is found in the upper phase, while the interphase and lower phase contain the respective fractions with DNA and proteins. To avoid contamination with traces of DNA, instead of retrieving the entire upper phase only 90 μ l were taken off and used for RNA-precipitation by adding 100 μ l (approx. one vol. of RNA phase suspension) of isopropanol (99% p.a.). After incubation for 10 minutes on ice, the precipitated RNA was pelleted at $12,000 \times g$ for 12 minutes at 4°C (Eppifuge). Sedimented RNA was washed with

Methods

0.5 ml ice-cold ethanol (75% in DEPC-water) while vortexing. A final centrifugation step at $12,000 \times g$ for 12 minutes at 4°C (Eppifuge) was added, the supernatant carefully discarded, and the RNA-pellet was air-dried for 3 minutes at room temperature and dissolved for 10 minutes at 55°C in 20 μl RNase-free water. Concentration of RNA content was measured at 260 nm (Section 4.2.2.7) before the extracted RNA was put to -70°C for storage.

4.2.1.2 cDNA synthesis via reverse transcriptase (RT)-PCR

The extracted RNA was used for subsequent reverse transcription into cDNA. In this process, the reverse transcriptase (RT) allows transcription of single-stranded copy DNA (or cDNA) from an RNA template by executing its RNA-dependent DNA polymerase activity. Furthermore, being a multifunctional enzyme, the reverse transcriptase is capable of acting as well as an RNase. Thereby the RNA from the RNA/DNA hybrids that have formed upon reverse transcription is degraded, yielding pure cDNA¹³⁶. A schematic overview on this process is given in **Figure 10**.

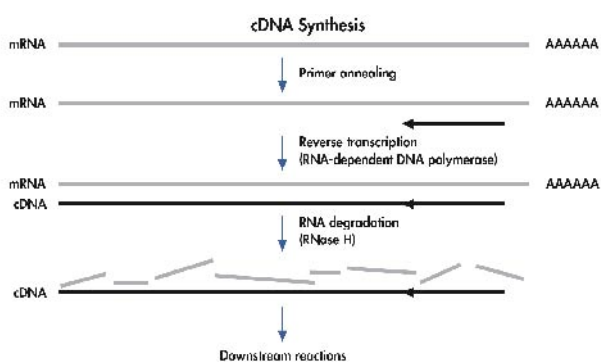


Figure 10. Reverse transcriptase in first-strand cDNA synthesis.

A kit-provided Oligo-d(T) primer anneals at the 3'-poly A⁺ ends of the before isolated mRNA. The reverse transcriptase (RT) allows for the transcription of single-stranded copy-DNA (cDNA) by executing its RNA-dependent DNA polymerase activity. In addition the RT possess RNase activity and thereby degrades any RNA/DNA hybrids that have formed upon reverse transcription, leaving over cDNA only.

cDNA synthesis was carried out according to the manufacturer's protocol using the first-strand cDNA synthesis kit from Roche Applied Sciences (Penzberg, Germany). For this protocol, a so-called Oligo-d(T) primer (kit-included) was used that anneals to the 3'-Poly-A ends (poly A⁺) of the mRNA to be transcribed and is needed for the initiation of the transcription process. RT-PCR was carried out in a 20 μl reaction volume and was set up as described in **Table 1**. The reaction was incubated for 10 minutes at 25°C followed by incubations at 42 and 99°C for 60 and 5 minutes, respectively.

Component (concentration)	Final concentrations	Applied volume (μ l)
Reaction Buffer 10X	1X	2
RNA	~ 1 μ g	variable
MgCl ₂ (25 mM)	5 mM	4
dNTP-Mix (10 mM)	1 mM	2
Oligo-p(dT) ₁₅ -Primer (0.8 μ g/ μ l)	0.08 μ g/ μ l	2
RNase-inhibitor (1000 U)	50 U	1
RT (500 U)	20 U	0.8
Sterile H ₂ O (RNase-free)	-	Δ 20
Total reaction volume		20

Table 1. Reaction setup for reverse transcriptase (RT)-mediated first-strand cDNA synthesis.

4.2.1.3 RACE-PCR on isolated RNA

The specialized PCR technique of Rapid Amplification of cDNA Ends (RACE-PCR) is ideally suited for the purpose of retrieving and amplifying a specific portion that is encoded by the isolated poly A⁺ mRNA.

Here, the SMARTer RACE cDNA Amplification Kit (ClontechLaboratories) was used. This technology combines the generation of full-length cDNAs via reverse transcription with primer-specific amplification of the desired region on the generated cDNA. The reverse transcriptase (RT) used in this kit is a variant of the Moloney Murine Leukemia Virus (MMLV) RT and upon reaching the end of an RNA template, exhibits terminal transferase activity, which in turns leads to the addition of three to five nucleotides to the 3' end of the first-strand cDNA (SMARTer sequence). Those added residues then serve as annealing sites for the SMARTer Oligo, which contains a terminal stretch of modified bases that are complementary to the SMARTer sequence that was added by the RT. The annealed oligo in turn serves as template for the RT, which itself is then able to switch templates from the mRNA to the oligo, thereby generating a complete cDNA copy of the original RNA with the specific SMARTer sequence added at its end (referred to RACE-ready cDNA) (Figure 11).

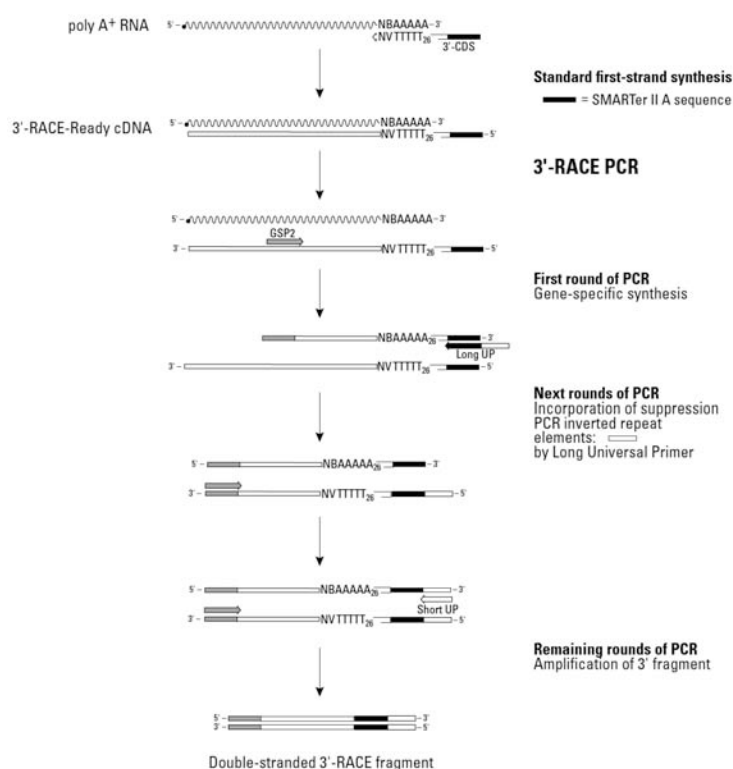


Figure 11. Overview of the 3'-RACE PCR mechanism.

RACE PCR combines in four steps the generation of full-length cDNAs via reverse transcription and subsequent primer-specific amplification of the desired region on the generated cDNA. *Step one:* Upon reaching the end of an RNA template, the RT exhibits terminal transferase activity. Thereby three to five nucleotides are added to the 3' end of the first-strand cDNA (*SMARTer III A sequence*). *Step two:* The added residues subsequently serve as annealing sites for the SMARTer Oligo, which is complementary to the SMARTer sequence that was added by the RT. Upon annealing, this oligo in turn provides the template for the RT, which upon switching templates (from the mRNA to the oligo) generates a complete DNA copy of the original RNA with the specific SMARTer sequence added at its end (referred to as *3'-RACE-Ready cDNA*). *Steps three and four:* Using a gene-specific primer (GSP) along with short and long kit-provided universal primers (UP) actual RACE PCR is carried out. This way a gene-specific double-stranded DNA fragment composing the sequence up to and including the poly A⁺ ends of the initial applied RNA template is obtained. *Figure adapted from SMARTer™ RACE cDNA amplification manual (Clontech Laboratories Inc., CA, U.S.A.).*

To generate RACE-ready cDNA, 1 µg of extracted RNA was mixed with the SMARTer Oligo (Mix 1, Table 2) and briefly centrifuged (Eppifuge) before incubation for two minutes at 70°C with subsequent chilling for 2 minutes on ice took place. Subsequently, Mix 1 was added to Mix 2 (Table 2) and incubated in a hot-lid thermo-cycler for 90 minutes at 42°C. Due to the large amount of initially applied RNA (greater than 200 ng), following cDNA synthesis 100 µl Tricine-EDTA Buffer was added.

Methods

	Component (concentration)	Final concentrations	Applied volume (µl)
Mix 1	RNA	~ 1 µg	variable
	3' coding sequence Primer A (12 µM)	1.2 µM	1
	Sterile H ₂ O (RNase-free)	-	Δ 5
Mix 2	First-strand buffer (5X)	1X	2
	DTT (20 mM)	2 mM	1
	dNTPs (10 mM)	1 mM	1
	SMARTscribe RT (100 U/µl)	10 U/µl	1
Total reaction volume			10

Table 2. Reaction setup for SMARTer RACE cDNA synthesis.

As outlined in Table 3, for RACE-PCR a Polymerase and Primer Mix was prepared. The Advantage 2 Polymerase used here is comprised of a Titanium[®] *Taq* and a proofreading polymerase. The Primer Mix contained the RACE-ready cDNA, a so-called universal primer mix (UPM) and a gene-specific primer (in this case FLXM5_Fw#7 was used).

	Component (concentration)	Final concentrations	Applied volume (µl)
Polymerase Mix	Advantage 2 Buffer (10X)	1X	5
	dNTPs (10 mM)	0.2 mM	1
	Advantage 2 Polymerase Mix (50X)	1X	1
	H ₂ O	-	Δ 41.5
Primer Mix	RACE-ready cDNA	-	2.5
	UPM (10X)	1X	5
	FLXM5_Fw#7 (10 µM)	0.2 µM	1
	Total reaction volume		50

Table 3. Reaction setup for SMARTer 3'-RACE PCR with gene-specific and universal primers.

After both mixes were combined, RACE-PCR was carried out according to the thermo-cycler program that is outlined in Table 4. Note, here no touchdown thermo-cycling program was required.

Methods

Temperature (°C)	Cycle Time (s)	Cycles
94	30	35 ×
68	30	
72	180	

Table 4. Thermal cycling program of SMARTer 3'-RACE PCR.

The product obtained by RACE-PCR was purified (Section 4.2.2.5) and sequenced as described in Section 4.2.2.6.

4.2.2 DNA

4.2.2.1 Polymerase chain reaction (PCR)

By applying specifically designed oligonucleotides (primers), via polymerase chain reaction (PCR) it is possible to *in vitro* amplify a part of a known sequence from a DNA template¹³⁷. Via their complementary sequence the primers flank at 5' and 3' of the region of interest on the single-strands of the template DNA. The PCR cycle starts with heat-denaturation of the double-stranded DNA, is followed by hybridization of the single strands and added primers, and is completed by the eventual synthesis of the complementary strand via DNA polymerase. By repeating those three phases for a certain number of cycles (30 to 50 times), exponential amplification of the synthesized DNA product takes place, yielding large amounts of specific DNA fragments.

4.2.2.2 PCR protocols

4.2.2.2.1 PCR for the cloning of HMM-like Myosin Va and CaMKII- α

PCR was performed as outlined in Table 5 and Table 6 using the Platinum[®] Pfx DNA Polymerase (Invitrogen) along with a specific combination of forward and reverse primers (for a complete list of primers, see Section 3.4) and the purified insert DNA obtained before as template.

Component (concentration)	Final concentrations	Applied volume (µl)
Reaction Buffer 10X	1X	5
Insert-DNA	-	1
dNTP-Mix (10 mM)	0.4 mM	2
Forward Primer (10 µM)	0.5 µM	2.5
Reverse Primer (10 µM)	0.5 µM	2.5
Platinum® <i>Pfx</i> Pol. (250 U)	2.5 U	1
Sterile H ₂ O	-	Δ 50
Total reaction volume		50

Table 5. PCR reaction setup using Platinum *Pfx* polymerase.

Temperature (°C)	Cycle Time (s)	Cycles
94	120	
94	15	
55	45	35
68	180	
68	420	

Table 6 Thermal cycling program for PCR reactions using Platinum *Pfx* polymerase.

4.2.2.2.2 PCR for determining the full-length *Xenopus l.* Myosin Va

All PCR reactions were carried out with Platinum® *Taq* DNA Polymerase High Fidelity (HF). The reaction setup (Table 7) always was the same. Depending on the primer combination and the size of the product to be expected, annealing temperatures as well as extension times were slightly modified (Table 8). In Table 9, the forward and reverse primers that yielded products of approximate correct sizes are listed along with the respective product size and PCR phase of each primer combination. For the specific primer sequences, please refer to Section 3.4.1.

Methods

Component (concentration)	Final concentrations	Applied volume (μ l)
Reaction Buffer 10X	1X	5
cDNA	-	1
MgSO ₄ (50 mM)	4 mM	4
dNTP-Mix (10 mM)	0.3 mM	1.5
Forward Primer (10 μ M)	0.3 μ M	1.5
Reverse Primer (10 μ M)	0.3 μ M	1.5
Platinum [®] Taq HF Pol. (250 U)	1.5 U	0.3
Sterile H ₂ O	-	Δ 50
Total reaction volume		50

Table 7. PCR reaction setup using Platinum Taq High-Fidelity polymerase.

Temperature ($^{\circ}$ C)	Cycle Time (s)	Cycles
94	120	
94	30	
50 to 52	30	30 to 50
72	300 to 420	
72	600	

Table 8. Thermal cycling program for PCR reactions using Platinum Taq High-Fidelity polymerase

PCR Reaction (Phase)	Forward Primer (name)	Reverse Primer (name)	Size of PCR Product (bp)
A	FLXM5_Fw#1	FLXM5_Rv5	3146
B	FLXM5_Fw#5	FLGgM5_Rv4126	1633
C (RACE)*	FLXM5_Fw#7	UPM (RACE-kit)	2500 (approx.)

Table 9. Summary of PCR primers used to obtain the full-length sequence of *Xenopus l.* Myosin Va.

Listed are the forward and reverse primers that were used to obtain the final products of Phases A, B, C as well as of the full-length coding sequence (**Figure 52**). (*) for details on RACE-PCR, refer to Section 4.2.1.3.

4.2.2.2.3 PCR-mediated preparation of the full-length *Xenopus l.* Myosin Va gene for vector cloning

To subsequently clone the gene encoding for the full-length protein of *Xenopus l.* Myosin Va into a suitable transfer vector (pFastBac Dual) the full-length coding sequence DNA was obtained and prepared for further cloning. To either yield 5' (N' in protein sequence) or 3' (C' in protein sequence) FLAG-tagged full-length *Xenopus l.* Myosin Va PCR products, the sequence coding for the FLAG-tag was fused to the 3'- and 5'-ends of the gene. In addition, the forward and reverse primers used in this step likewise contained an NheI and SphI restriction enzyme recognition sequence, respectively. PCR reactions were performed according to the protocol in Section 4.2.2.2 (Table 7 and Table 8). The PCR products were gel-extracted, purified and digested with restriction enzymes NheI and SphI (HF) as described (Sections 4.2.2.4, 4.2.2.5 and 4.2.3.1). For a list of specific primer sequences, please refer to Section 3.4.1.

Product	Primer Names
N' FLAG-tagged FLXMyosin Va	FLXM5_NheIFLAG-Fw
	FLXM5_SphI-Rv
C' FLAG-tagged FLXMyosin Va	FLXM5_Nhe-Fw2
	FLXM5_SphIFLAG-Rv
Untagged FLXMyosin Va	FLXM5_NheI-Fw2
	FLXM5_SphI-Rv

Table 10. PCR primer list.

Forward and reverse primers used for the cloning of untagged and FLAG-tagged full-length *Xenopus l.* Myosin Va into the pFastBac Dual vector.

4.2.2.3 DNA analysis by agarose gel electrophoresis

Unless mentioned otherwise, DNA fragments were separated via (1%) agarose gel electrophoresis. For this, the required amount of agarose was dissolved in TAE buffer (1X). All gels were supplemented with 1% ethidium bromide (10 mg/ml) to easily visualize the acquired DNA products on the gel. Typically, prior loading, the samples were mixed with loading buffer (6X) in a 1:6 ratio. Electrophoresis was performed at 90 V for 10 to 30 minutes. DNA was detected by using a UV light source. To determine the correct size of the product, in addition to the samples a standard 1 kb DNA ladder was always loaded.

4.2.2.4 Gel-extraction of DNA fragments

For the extraction of DNA fragments (e.g., PCR products) from agarose gels post gel electrophoresis, bands of interest were excised with a clean scalpel and subsequently gel-extracted with the Qiaquick[®] Gel Extraction kit (Qiagen) according to the manufacturer's protocol. Depending on the yield in DNA concentration to be expected, elution of the sample took place in 30 to 50 µl Qiagen Elution Buffer. Samples were stored at -20°C.

4.2.2.5 Purification of PCR and restriction-digest products

PCR and restriction enzyme-digested DNA products were purified from any left-over enzymes, nucleotides and salts by using the Qiaquick[®] PCR Purification kit (Qiagen) according to manufacturer's protocol. Typically, purified samples were eluted in 30 µl Qiagen elution buffer. Samples were stored at -20°C.

4.2.2.6 DNA Sequencing

All plasmids and PCR products were purified before sequencing at the Sequencing Service Unit of the LMU (Ludwig-Maximilians-University, Munich, Germany) was carried out. Typically 50 to 200 ng of gel-purified PCR product DNA was mixed with 3.3 pmol sequencing primer in DNA elution buffer (DNA-EB) 1X (Table 11). In cases where purified plasmid DNA was prepared for sequencing, 150 to 300 ng of DNA was required. Sequencing at the service unit was then performed with the "Cycle, Clean & Run" program using BigDye v3.1.

Methods

Component (concentration)	Final concentration	Applied volume (µl)
DNA-EB (1X)	-	Δ 7
Sequ. Primer (3.3 µM)	3 pmol	1
DNA	50 to 200 ng	variable
Total reaction volume		7

Table 11. Reaction setup for “Cycle, Clean & Run” DNA sequencing with BigDye v3.1.

4.2.2.6.1 Sequencing reactions of full-length *Xenopus l.* Myosin Va

All products that were obtained either by RACE- or conventional PCR and that yielded products of approximately the right size (estimated via sequence homology comparison to full-length chicken Myosin Va) were prepared for DNA sequencing (for details on the reaction setup, refer to Table 11).

A list of all the primers that were used to step-by-step sequence the respective PCR products obtained in Phases A through C is provided in Table 12. For a list of the specific primer sequences, please refer to Section 3.4.2.

PCR Product (Phase)	Sequencing Primer (#)	Primer annealing site
A	1	1
	2	672
	3	1349
	4	1927
	5	2488
B	6	3139
	7	3775
C (RACE)	7	3775
	8	4089
	9	4316
Final full-length	10	4528
	1	1
	11	550
	12	1177
	3	1349
	4	1927
	5	2488
	13	3079
	14	3415
	7	3786
15	4316	
9	4528	
16	5269	

Table 12. List of sequencing primers used for the conformation of partial and full-length *Xenopus l.* Myosin Va PCR products.

4.2.2.7 Determination of DNA concentration

The concentration (c) of purified DNA and RNA was measured spectroscopically by determining the optical density (OD) at wavelength (λ) 260. The optical density is a unit-less measure of the transmittance of an optical element for a given length and wavelength. The transmittance is expressed as the fraction of the intensity of the transmitted (I) and incident (I_0) light beam. For liquids the measure of the OD is also referred to as absorbance (A).

Depending on the yield to be expected, 1:100 or 1:200 dilutions of the DNA or RNA sample (in (DEPC)-water) were targeted for concentration determination.

The concentration was calculated according to Equation 2 and Equation 1:

$$OD_{\lambda} = A_{\lambda} = -\log_{10} T = -\log_{10} \left(\frac{I}{I_0} \right)$$

Equation 2

$$c_{\text{DNA/RNA}} = \frac{0.05 \text{ or } 0.04 \mu\text{g}/\mu\text{l}}{\text{Factor}_{\text{Dilution}}} * OD_{260 \text{ nm}}$$

Equation 1

$$\Rightarrow \text{with } OD_{260 \text{ nm}} = 1 \approx 0.05 \mu\text{g}/\mu\text{l DNA}$$

and

$$\Rightarrow \text{with } OD_{260 \text{ nm}} = 1 \approx 0.04 \mu\text{g}/\mu\text{l RNA}$$

4.2.2.8 DNA sequence synthesis of HMM-like Myosin Va loop 2 constructs

The plasmid DNA provided by Purcell, T. J. and colleagues (Stanford University, Stanford, U.S.A.)¹³⁸, containing the Wildtype HMM-like Myosin Va gene, was used as the template plasmid to perform custom DNA synthesis (carried out by SloningBio-Technology, Puchheim, Germany) of the three loop 2 mutations described above.

The so-called Slonomics™ technology relies on a library of standardized DNA building blocks that can be combined to any desired sequence, instead of ligating gene product-specific and individually designed oligo-nucleotides. The loop 2 of Myosin Va is flanked by the two unique restriction sites, SphI and ApaI. This

Methods

rather convenient circumstance was taken advantage of to cut out the loop 2 sequence from the Wildtype version to then synthesize the mutant versions of loop 2.

Eventually, the synthesized mutant versions of loop 2 were cloned back into p2bac/pfastbac transfer vector via the exact same restriction sites. Thereby all the HMM-like Myosin Va loop 2 constructs were cloned into the hybrid transfer vector p2bac/pfastbac¹³⁸ and confirmed by DNA-sequencing (performed by SloningBiotechnology).

4.2.3 Cloning techniques

4.2.3.1 Restriction enzyme-mediated DNA digest

Plasmid DNA or PCR fragments, containing restriction enzyme-specific restriction sites at their ends, were digested via restriction enzyme-mediated digestion according to the enzyme manufacturer's protocol (New England Biolabs, NEB). Typically, digestion was carried out for 2 to 3 hours at the temperature optimum of the respective enzyme. Vector linearization was typically performed with ~ 5 µg of vector DNA in a 30 µl-reaction volume, while for digestion of PCR-products the entire PCR-reaction (50 µl) was applied (Table 13). In cases where simultaneous digestion with two different enzymes was carried out, the buffer suiting both enzymes best was used. Or, in cases where no suitable common buffer could be used, sequential digestion with the two enzymes took place.

Component (concentration)	Final concentration	Applied volume -Vector linearization- (µl)	Applied volume -Test or PCR Digest- (µl)
Rest. Enzyme Buffer (10X)	1X	3	2 or 5.5
DNA	~ 5 µg (vector DNA)	variable	2 or 47
BSA (10 mg/ml) -if required-	~ 0.1 mg/ml	0.3	0.2 or 0.6
Enzyme 1 (10 to 20 U/µl)	0.3 to 0.5 U/µl	1	0.5 or 1
Enzyme 2 (10 to 20 U/µl) -if double-digest is performed-	0.3 to 0.5 U/µl	1	0.5 or 1
H ₂ O	-	Δ 30.3	Δ 20 or 55
Total reaction volume		30.3	20 or 55

Table 13. Reaction setup for restriction enzyme-mediated digest of plasmid DNA or PCR fragments.

Methods

Following DNA digestion, DNA purification of the product was carried out (Section 4.2.2.5).

4.2.3.2 Dephosphorylation of linearized DNA

To prevent religation of linearized (i.e., restriction enzyme-specifically cut) vector DNA, Antarctic Phosphatase (AP; NEB) was used to dephosphorylate the 5' ends of the DNA. For this, typically 1 µg of linearized DNA was incubated with 5 units AP in AP-Buffer (10X) for 1 hour at 37°C (Table 14). It was crucial to heat-inactivate AP by incubating for 5 minutes at 65°C. DNA treated this way can be used for subsequent ligation without any additional purification.

Component (concentration)	Final concentration	Applied volume (µl)
AP Buffer (10X)	1X	3
Linearized DNA	~ 1 to 2.5 µg	26
AP (5 U/µl)	~ 0.17 U/µl	1
Total reaction volume		30

Table 14. Reaction setup for the dephosphorylation of linearized DNA via alkaline phosphatase.

4.2.3.3 Ligation of DNA fragments into linearized vectors

Once linearized by specific restriction enzyme-mediated digestion, those vectors typically now containing so-called sticky (3' and 5' overhangs) ends can be ligated with DNA fragments (inserts) that contain the exact same sticky ends. For the efficient and successful ligation it is crucial that the linearized vector (or insert) is dephosphorylated at the 5' end (Section 4.2.3.2). The ligation reaction is then carried out by T4 DNA Ligase, which catalyzes the formation of a phosphodiester bond between juxtaposed 5' phosphate and 3' hydroxyl termini in duplex DNA (or RNA)¹³⁹.

Typically, ligation was carried out by mixing vector and insert in a 1:3 or 1:5 ratio, with subsequent ligation by 40 units T4 DNA Ligase in Ligase Buffer (10X) overnight at 16°C (Table 15).

Component (concentration)	Final concentration	Applied volume (μ l)
Ligase Buffer (10X)	1X	1
Vector DNA	~ 100 ng	1
Insert DNA	variable	3 to 5
T4 DNA Ligase (400 U/ μ l)	40 U/ μ l	1
H ₂ O	-	Δ 10
Total reaction volume		10

Table 15. Reaction setup for the ligation of linearized vector and insert DNA via T4 DNA ligase.

4.2.3.4 Transformation of chemically competent *E. coli* XL1-Blue cells

To amplify plasmid-DNA that contains the genes encoding the different constructs used in this work, transformation of the plasmid of interest into chemically competent XL1-Blue cells was carried out. Prior transformation, the cells were slowly thawed on ice. Typically, 30-50 μ l of DNA (in general from ligation reactions), were carefully mixed with 200 μ l of XL 1-Blue competent cells and incubated on ice for 20 minutes. To transform the cells, a heat-shock for 45 seconds at 42°C was performed, followed by 2 minutes of incubation on ice. Then, 200 μ l S.O.C. medium was added and the mix was incubated for 1 hour at 37°C on a shaker and afterwards plated on LB-Amp Petri-dishes, which were then kept overnight at 37°C.

For the transformation of synthesis-generated genes from Sloning BioTech, 3 μ g of the lyophilized plasmid DNA was dissolved in 10 μ l TE Buffer (1X), before the transformation into chemically competent XL1-Blue cells.

4.2.3.5 Selection and expansion of transformed *E. coli*

To select for those cells that contained the plasmid coding for the protein of interest and as well the ampicillin-resistance cassette, transformation reactions were plated on LB-Ampicilin plates. Typically, after an overnight incubation at 37°C, for Mini-Plasmid preparation (Mini-Prep) two to ten medium-size colonies were picked to inoculate 2 to 5 ml of LB-Amp liquid medium per tube. Incubation was carried out overnight in a shaker device at 220 rpm and 37°C. The following day, the cells were pelleted and plasmid isolation by using the Qiaprep[®] Miniprep kit (Qiagen) was carried out (for details, see below).

4.2.3.6 Plasmid-DNA extraction from transformed bacteria

As mentioned above, single colonies of the transformation reaction were selected for subsequent DNA isolation and used for the inoculation of a Mini-Prep (4.2.3.5). Cells were pelleted at 2,500 x g for 10 minutes at 4°C (Rotanta 460R swinging bucket centrifuge, Hettich), and plasmid DNA isolation was carried out with the QIAprep[®] Miniprep kit (Qiagen) according to the manufacturer's protocol. Typically, DNA was eluted in 50 µl (pre-warmed) Qiagen Elution Buffer and stored at -20°C.

4.3 Protein Biochemistry

4.3.1 Analytical methods

4.3.1.1 Protein analysis by SDS-polyacryl amide gel electrophoresis (SDS-PAGE)

SDS-PAGE allows the separation of protein bands under denaturing conditions. The highly anionic character of SDS gives all proteins the same negative charge so that separation in an electric field occurs only by differences in size and not by individual native protein charges.

Typically 10 to 12% polyacryl amide gels with 10 or 15 loading pockets were used. Before loading, samples were always boiled in a heat-block at 95°C in SDS 6X sample buffer. Usually 20 to 25 µl of the sample in SDS sample buffer and 5 to 10 µl of protein standard (unstained High Molecular Weight ladder or pre-stained Protein-marker IV) were loaded on the gel. The gels were run for 40 to 60 minutes in electrophoresis buffer (1X) at 20-60 mA with 240 V limit. Protein bands were stained with Coomassie Blue solution. For subsequent imaging or mass spectrometry analysis, Gels were stored in water at 4°C.

4.3.1.2 Protein identification and conformation by mass spectrometry

Expressed and purified proteins of interest but also those protein bands that were of still uncertain identity were confirmed by mass spectrometry analysis. This analytical technique measures the mass-to-charge ratio of charged particles. In principle, the mass spectrometer consists of the following three basic parts: First, an ion source that induces sample ionization; second, an electric or magnetic field

by which based on different ion masses, separation of those ions takes place; and third, a detector system that generates a mass spectrum with the collected mass data ¹⁴⁰. Many different ion sources and analyzers are used for different applications. To identify peptide sequences, at first basic MALDI-TOF (Matrix-assisted laser desorption/ionization-Time of flight) mass spectrometry, and then later on Nanospray-Liquid Chromatography tandem mass spectrometry (Nanospray-LC-MS/MS) was performed by the Zentrallabor für Proteinanalytik (ZfP) of the LMU. Tandem mass spectrometry (MS/MS) involves multiple steps of mass spectrometry analysis, which makes possible multiple rounds of mass spectrometry with different types of analyzers, leading to exact and well-sorted mass data, whereas MALDI-TOF analysis makes only one round of mass spectrometry ¹⁴¹. For LC-MS/MS, an iontrap/orbitrap and quadrupol/time-of-flight (TOF) space-separated analyzer was used. Mass spectrometry was performed from in-gel-digested protein bands.

4.3.1.3 Determination of protein concentration

Unless mentioned otherwise, protein concentration was determined using a Bovine Serum Albumin (BSA)-standard that was included on those SDS-PAGE gels where the purified protein of interest was loaded. The principle of this method is to generate a calibration curve by loading different but defined concentrations of a high-grade pure protein of known molecular weight. Typically five different BSA concentrations (0.1, 0.2, 0.4, 0.6 and 0.8 mg/ml; in H₂O) were loaded next to the protein(s) of interest on SDS-PAGE gels. The calibration curve was generated as follows: the respective TIFF-image of the gel was background-corrected and the intensity of the BSA-specific protein bands of the respective concentration was analyzed with ImageQuant imaging software. Likewise, the intensities of the protein bands of interest were determined and subsequently related to those values obtained from the calibration curve. Using Equation 3, the absolute concentration was converted into the molar concentration of the protein.

$$c_{\text{molar}} (\text{Mol}) = \frac{c_{\text{absolute}} (\text{mg/ml})}{MW (\text{kDa})}$$

⇒ with 1 micromole protein of $MW = x \text{ kDa} \cong x \text{ mg}$

Equation 3

4.3.1.4 Determination of tubulin concentration

To determine the concentration of polymerized microtubules, a 5-fold dilution into 12A25 Buffer 1X supplemented with 20 μM Taxol, and a subsequent 10-fold dilution into Guanidine Hydrochloride (6.6 M) were carried out. Guanidine hydrochloride has chaotropic properties and depolymerizes the microtubule polymers¹⁴². Calibration of the spectrophotometer was carried out at 280 nm with a 10-fold dilution of 12A25 Buffer (1X) supplemented with 20 μM Taxol into guanidine hydrochloride (6.6 M), before 100 μl of the microtubule dilution was measured at 280 nm. The concentration was calculated according to the law of Lambert-Beer (Equation 4).

$$\begin{aligned}\epsilon_{\text{tubulin at } 280\text{ nm}} &= 1.03 \text{ Mol}^{-1} * \text{cm}^{-1} * 10^3 L \\ \Rightarrow \text{with } d &= 1 \text{ cm} \\ c_{\text{molar}} (\mu\text{M}) &= \left(\frac{A_{280\text{ nm}}}{\epsilon_{\text{tubulin at } 280\text{ nm}}} \right) * 10 * \text{dilution factor}\end{aligned}$$

Equation 4

4.3.1.5 Western-blot analysis

Western-blotting is an often-used technique to test for the presence or state of activity (phosphorylated versus non-phosphorylated) of proteins of interest. In brief, proteins that had been separated on a polyacryl amide gel are transferred onto a membrane, which is typically made of nitrocellulose (NC) or polyvinylidene difluoride (PVDF). The blotted proteins are probed with primary antibodies that are specific for the antigens of interest. Then, secondary antibodies, which are conjugated to either a reporter enzyme or a fluorophore and are reactive against the primary antibodies are used for detection. Depending on the detection method, photons emitted from either chemoluminescence or fluorescence are visualized by a photographic sheet of film or a CCD-camera, respectively.

By using a semi-dry transfer apparatus, protein transfer after gel-electrophoresis was achieved by applying a current of 50 to 400 mA for 40 to 120 minutes. Efficiency of protein transfer was tested with Ponceau red. The membranes were blocked with 5% milk solution (in TBST) for 2 to 3 hours at room temperature. Incubation with primary and secondary antibodies (all conjugated to horseradish-

Methods

peroxidase) was performed overnight at 4°C or at room temperature for 1 hour, respectively. Before imaging, blots were always kept in TBS (1X) at 4°C. In-between each step, membranes were washed three times with TBST (1X) for 20 minutes each at room temperature.

Chemiluminescence was generated by applying 1 ml freshly mixed ECL solution, containing cumaric acid and H₂O₂, onto the membrane. Signal detection took place with a sheet of photographic film.

Primary and secondary antibodies were all diluted in 1% milk solution (in TBST). For a complete list of antibodies, please refer to Section 3.7.

4.3.2 Isolation, purification and handling of cytoskeletal Proteins

4.3.2.1 G-actin purification from rabbit muscle tissue

For the isolation of actin, skeletal muscle tissue of rabbits was cut in pieces, briefly washed with cold water to remove any remains of blood and ground with a pre-chilled meat grinder. The protocol refers to purification of G-actin from about 350 g skeletal muscle meat, however it can be scaled-up proportionally. The ground tissue was mixed with 1 L Solution I and stirred for 10 minutes at 4°C. Filtration of the meat suspension through a gauze bandage was carried out and the remainder was dissolved in 2 L Solution II by stirring for 10 minutes at 4°C. After this suspension was filtrated, remainder II was dissolved in 1 L solution III, stirred for 10 minutes at 4°C and filtrated again. Remainder III was mixed with 2 L ice-cold water for 5 minutes and filtrated again. Extraction of the remaining water from the filtrate was accomplished by five times mixing and filtrating with 1 L acetone. To prepare the so-called acetone powder, the filtrate was air-dried on a sterile bench overnight and thereafter aliquots of 10 g were stored at -20°C.

One aliquot of acetone powder was dissolved in 200 ml G Buffer, stirred for 30 minutes at 4°C and afterwards was centrifuged at 35,000 x g for 30 minutes at 4°C (J2-21M/E centrifuge and JA-14 Rotor, Beckman-Coulter). The supernatant of this extraction step was saved and the pellet was resuspended in 200 ml G Buffer and again stirred for 30 minutes at 4°C. The supernatant of this extraction was combined with the supernatant, which has been saved and the total solution was filtrated through a gauze bandage. To polymerize G-actin, 50 mM KCl, 2 mM MgCl₂ and 0.5 mM ATP was slowly applied to one volume of the combined filtrate

Methods

and the mixture was incubated for 30 minutes at room temperature. The polymerized mixture was stirred an additional 30 minutes at 4°C and centrifuged at 100,000 x g for 2 hours at 4°C (L8-70M Ultra-centrifuge and 45Ti Rotor, Beckman-Coulter). The pellet was resuspended in 30 ml G Buffer and homogenized. To depolymerize the actin, the homogenous solution was dialyzed in G Buffer for 46 to 48 hours with three buffer exchanges. Leftover polymerized actin was pelleted by centrifuging the solution at 100,000 x g for 2 hours at 4°C (L8-70M Ultra-centrifuge and 45Ti Rotor, Beckman-Coulter). The supernatant containing the G-actin was applied onto a Sephacryl G-300 HR column (Pharmacia, equilibrated with 5 L G Buffer) and eluted overnight in G Buffer with a flow-rate of 60 ml per hour. The concentration of the different fractions was determined spectroscopically at a wavelength of 290 nm ($OD_{290\text{ nm}}=1$ equals 0.63 mg/ml of G-actin) (for details on determination of protein concentration, refer to Section 4.3.1.3). The purity was confirmed via SDS-PAGE (10%). 1 mg of G-actin together with 2 mg sucrose was lyophilized and stored at -20°C.

4.3.2.2 G-actin polymerization

Purified G-Actin was polymerized by increasing the concentrations of monovalent and divalent cations in the buffer, which bind to sites with low affinity and hence promote polymerization⁴. For the purpose of this work, actin filaments required stabilization, so that experimentation under constant conditions for a sufficient length of time was possible. F-actin polymerization was achieved by including the fungal toxin phalloidin into the polymerization reaction. By binding only to polymeric and oligomeric forms of actin, phalloidin is capable of strongly stabilizing actin filaments¹⁴³.

As shown in Table 16, G-actin was mixed with Assay Buffer (AB, 10X) and phalloidin. The polymerization reaction-mix was incubated for 40 to 60 minutes at room temperature and was then kept on ice at all times. To visualize actin filaments for *in vitro* motility assays, fluorescently labeled tetramethylrhodamine-isothiocyanate (TRITC)- or Atto488-labeled phalloidin instead of the unlabeled phalloidin (used for ATPase assays) was included into the polymerization reaction.

Methods

Component (concentration)	Final concentration	Applied volume (μ l)
G-actin (40 to 80 μ M)	5 μ M	variable
TRITC/Atto488-labeled or unlabeled Phalloidin (100 μ M)	5 μ M	2.5
AB (10X)	1X	5
H ₂ O	-	Δ 50
Total reaction volume		50

Table 16. Reaction setup for actin polymerization from monomeric G-actin.

4.3.2.3 Isolation and purification of porcine tubulin

The tubulin used in this work was isolated from about 700 g of pig brain. For the proper isolation it was crucial to keep the brains on ice at all times. First, connective tissue and superficial capillaries were removed manually at 4°C. 350 g of the cleaned brain tissue together with 1 volume of Buffer A was homogenized by intense mixing until a homogenous consistency was obtained. The homogenate was then cleared by centrifugation at 26,000 \times g for 70 minutes and 4°C (J2-21M/E centrifuge and JA-14 Rotor, Beckman-Coulter). Together with 2 mM Na₂ATP, the supernatants from the first centrifugation step were gently mixed with a quarter of the final volume pre-warmed glycerol. By adding glycerol, the polymerization process even is enhanced. Polymerization took place in a water-bath under constant shaking for 30 minutes at 35°C. The microtubules were then pelleted by centrifugation at 200,000 \times g for 45 minutes and 32°C (L8-70M Ultra-centrifuge and 45Ti Rotor, Beckman-Coulter). Microtubule pellets were then resuspended in 5 ml Buffer C, homogenized in ice-cold homogenizers and incubated on ice for 25 minutes while frequent homogenization in-between (enhances microtubule depolymerization) was carried out. The homogenate was cleared again by centrifugation at 150,000 \times g for 30 minutes at 4°C (L8-70M Ultra-centrifuge and 42Ti Rotor, Beckman-Coulter). The collected supernatant was again polymerized by adding 2 mM Na₂ATP and incubation at 35°C for 30 min. Following sedimentation at 125,000 \times g for 30 minutes at 35°C (L8-70M Ultra-centrifuge and 42.1 Rotor, Beckman-Coulter), the supernatants were discarded and pellets collected. To prevent the binding of microtubule-associated proteins (MAPs) to microtubules, tubulin pellets were resuspended and homogenized in Buffer B (high ionic strength) until a final volume of 50 ml was

Methods

reached. To further depolymerize the microtubules, the homogenate was incubated on ice for an additional 25 minutes. The homogenate was cleared once more by centrifugation at $150,000 \times g$ for 30 minutes at 4°C (L8-70M Ultra-centrifuge and 42.1 Rotor, Beckman-Coulter). The supernatant was mixed with one tenth of volume DMSO, 2 mM ATP and was incubated for 30 minutes at 37°C to induce polymerization. The polymerized microtubules were pelleted at $125,000 \times g$ for 60 minutes at 35°C (L8-70M Ultra-centrifuge and 42.1 Rotor, Beckman-Coulter). By adding 5 ml of Buffer D to the pellet fraction and further homogenization on ice for 30 minutes depolymerization of microtubules was reached. Precipitates were removed by centrifugation at $135,000 \times g$ for 30 minutes at 4°C (L8-70M Ultra-centrifuge and 42.1 Rotor, Beckman-Coulter).

To separate the pure tubulin from remaining MAPs, the material was loaded on a gravity-flow phosphocellulose P11 material-filled column. Equilibration took place in 100 ml Buffer D and tubulin was eluted dropwise in Buffer D. Protein content was checked by calorimetric determination via Bradford reagent. The main fractions of eluted tubulin were combined, mixed with 0.1 mM GTP and aliquots were snap-frozen in liquid nitrogen. For long-term storage aliquots of purified tubulin were kept at -70°C .

4.3.2.3.1 Tubulin polymerization

Taxol (4 mM), an established potent microtubule-stabilizing agent, was included into the polymerization reaction. By binding to the β -subunits, Taxol prevents the individual subunits from dissociating and thereby stabilizes microtubules¹⁴⁴.

4.3.2.3.2 Polymerization of fluorescently labeled tubulin for *in vitro* motility assays

For fluorescent labeling of microtubules, typically Atto488-labeled tubulin was included into the polymerization reaction. The actual labeling of tubulin was carried out exactly as described by Mitchison, T. *et al.* (<http://mitchison.med.harvard.edu/protocols/label.html>).

In a 1:50 stoichiometry, Atto488-labeled tubulin was thoroughly mixed with tubulin and immediately centrifuged at 80,000 rpm for 5 minutes and 4°C (Optima-TL ultra-centrifuge and TLA120 Rotor, Beckman-Coulter) to pellet and remove

Methods

excess dye from the reaction. Polymerization was started upon adding 1 mM GTP to the tubulin-dye mixture and incubation for 20 minutes at 35°C. After this initial polymerization step, 20 µM Taxol was added and the reaction was incubated over night at 35°C.

4.3.2.3.3 Polymerization of unlabeled tubulin for ATPase activity assays

After *in vitro* polymerization, a fraction of tubulin always remains unpolymerized. However, for determining the exact rate of ATP-hydrolysis at a given microtubule concentration, it is crucial to also determine the exact concentration of polymerized tubulin in the assay. Therefore, after initial polymerization one additional centrifugation step at 200,000 × g for 15 minutes at 30°C (Optima-TL ultra-centrifuge and TLA120 Rotor, Beckman-Coulter) through a cushion of sucrose (40% in 12A25 Buffer 1X plus 20 µM Taxol) was included. Thereby the fraction of unpolymerized tubulin was separated from the polymerized microtubules. The pelleted microtubules were washed twice with 100 µl 12A25 Buffer (1X) and dissolved in 100 to 200 µl 12A25 Buffer (1X).

4.3.2.4 Microtubule E-hook removal via Subtilisin digest

E-hooks represent the C-terminal ends (approx. the last 12-18 amino acids) of tubulin and are mainly composed of glutamic acid (E) residues, lending the E-hook its name as well as its negative charge. In previous studies it has been shown that many different members of the kinesin family use those hook-like structures to interact via electrostatic attraction with the microtubule surface^{115,119,145,146,147}. To test for the possible influence of microtubule E-hooks on Myosin Va's ability to interact with microtubules, E-hooks were removed from α - and β -tubulin subunits via limited proteolysis by Subtilisin A, a non-specific protease that belongs to the family of Serine-endopeptidases¹⁴⁸.

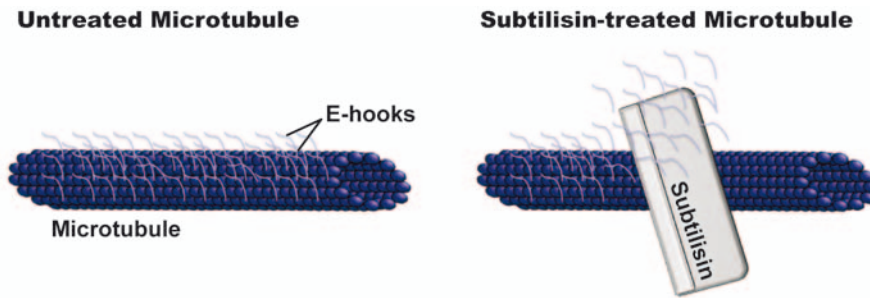


Figure 12. Schematic of E-hook removal from intact microtubules via Subtilisin-treatment.

Microtubules were polymerized *in vitro* from porcine brain tubulin. On intact microtubules (*left*), the highly acidic C'-terminal ends (E-hooks) of the α - and β -tubulin dimer subunits protrude from the microtubule surface and are known to serve as electrostatic tethers for a number of kinesins. If desired, said E-hooks can be removed via limited proteolysis with the Serine-endopeptidase Subtilisin A (*right*).

Here, an established method¹¹⁹ was optimized and adapted to the needs of this work (illustrated in **Figure 12**). In brief, tubulin (3.5 mg/ml) and Atto488 tubulin at a 50:1 ratio was polymerized in BRB80 1X (plus 1 mM GTP) at 36°C for 90 min. Subsequently, microtubules were stabilized with 20 μ M Taxol and incubated for an additional 40 minutes at 36°C. E-hooks were removed by incubation of 0.6 mg/ml with Subtilisin A at 1:0.8 ratio in BRB80-Tx 1X for 45 minutes at 36°C. The reaction was stopped with 2 mM PMSF (dissolved in isopropanol) and incubation at room temperature for 10 minutes. Subtilisin-treated microtubules were pelleted at 27,000 \times g for 25 minutes and 25°C (Optima-TL ultra-centrifuge and TLA120 Rotor, Beckman-Coulter). Pellets were washed with and resuspended in BRB80-Tx 1X (plus 1 mM GTP). To test for the efficiency of E-hook removal, samples were resolved on a 12% SDS-PAGE with subsequent Coomassie-staining or immunoblotting. Together with the HMM-Myosin Va constructs used here, those modified microtubules were then targeted for single-molecule motility assays and were visualized via TIRF microscopy (for schematics, see **Figure 4**, **Figure 5** and **Figure 6**).

4.3.3 Protein expression using the baculovirus expression system

Over the past decade the use of baculoviruses has become an important tool for overexpressing recombinant proteins in eukaryotic cells ^{149,150}. Unlike the bacterial expression systems, this eukaryotic system uses most of the protein modification, processing, folding and transport machinery that is present also in higher eukaryotes. Thus, with this system, most of the over-expressed proteins exhibit proper biological activity and function ¹⁵¹.

For the purpose of this thesis, the expression of the different protein constructs was carried out with the Bac-to-Bac[®] baculovirus expression system (Invitrogen) in the Sf9 insect cell line (Section 4.1.5). One of two major components of the Bac-to-Bac[®]-system is the vector into which the gene or genes of interest is/are cloned. In this thesis, vectors containing one or two promoters, and thus one or two expression cassettes, were used. Dual vectors, i.e., vectors that carry two such expression cassettes, allow for the expression of two different proteins that are encoded by two different genes while cloned into the same plasmid. Both, the polyhedrin (pPH) and the p10 promoter in the wildtype baculovirus AcMNPV promote transcription of two major late viral proteins. Both, the polyhedrin and p10 gene were replaced by a foreign gene in the here used recombinant baculoviruses. Thereby recombinant protein expression under the control of those two promoters was made possible.

The second major component of the Bac-to-Bac[®] system is represented by an *E. coli* strain (DH10Bac[™] Competent *E. coli*) that is used as host for the before generated plasmid, consisting of transfer vector and gene(s) of interest. DH10Bac[™] Competent *E. coli* cells contain a baculovirus shuttle vector, referred to as bacmid. After transformation into these cells, transposition between transposons of the vector and the bacmid occurs. This recombinant bacmid is the basis to then generate the recombinant baculovirus.

An overview of the key steps for baculovirus protein expression is given in **Figure 13**.

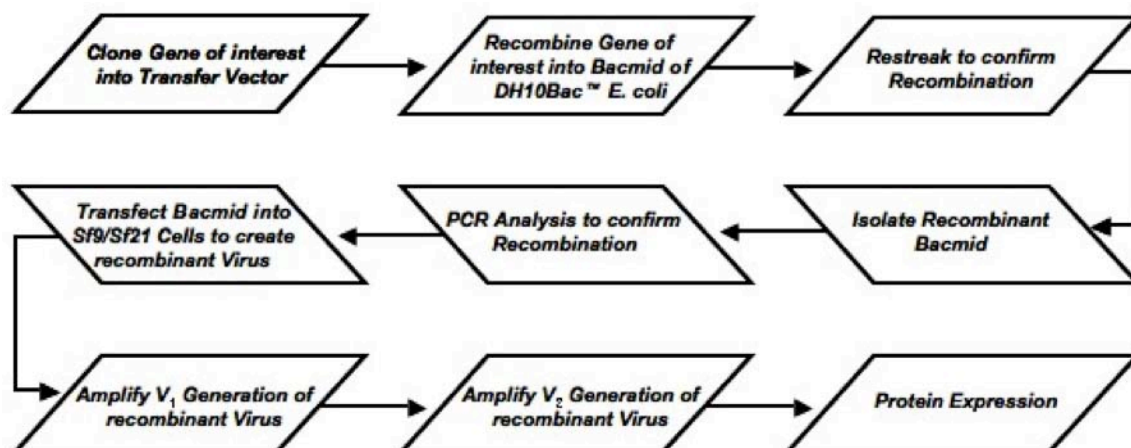


Figure 13. Protein expression via the Baculovirus Bac-to-Bac[®] system – An overview. The flowchart illustrates the required steps for the successful protein expression via the Bac-to-Bac[®] system.

4.3.3.1 Construction of the recombinant transfer vector for protein expression

In this thesis two dual vectors and one mono vector were used to generate recombinant transfer vectors for the expression of the herein used protein constructs (vector maps are provided in Section 7). The two dual vectors, named hereafter p2bac/pfastbac and pFastBac[™] Dual, mainly differ in their multiple cloning sites downstream of the p10 and polyH promoter. The presence of these two strong promoters allows for the simultaneous expression of two different proteins encoded on the same plasmid. The expression cassette is flanked by the left (L) and right (R) arms of Tn7, which are mini Tn7 elements that permit site-specific transposition of the gene of interest into the baculovirus genome¹⁵². It also contains a SV40 polyadenylation signal, which permits efficient transcription termination and polydenylation of mRNA¹⁵³. In addition the vectors contain an ampicillin and gentamicin resistance gene, where the first one allows selection of the plasmid in *E. coli* XL 1-Blue cells, while the latter one permits selection of the recombinant bacmid in *E. coli* DH10Bac[™] cells.

Except for the fact that the mono vector pFastBac[™] 1 possesses the polyH promoter only, all the genes and regions that were described for both the dual vectors are present also in the pFastBac[™] 1 vector (vector maps are provided in Section 7).

4.3.3.2 Generation of the recombinant bacmid

Once the recombinant vector was generated, for transposition into the baculovirus shuttle vector (bacmid) the amplified and purified DNA was transformed into DH10Bac™ *E. coli* cells. This strain of *E. coli* cells contains the bacmid with a mini-*att*Tn7 attachment site, which is inserted in a segment of DNA encoding the LacZ α peptide, and a helper plasmid. Generation of the recombinant bacmid is achieved via site-specific transposition between the mini-Tn7 element of the donor vector and the mini-*att*Tn7 attachment site on the bacmid (Figure 14).

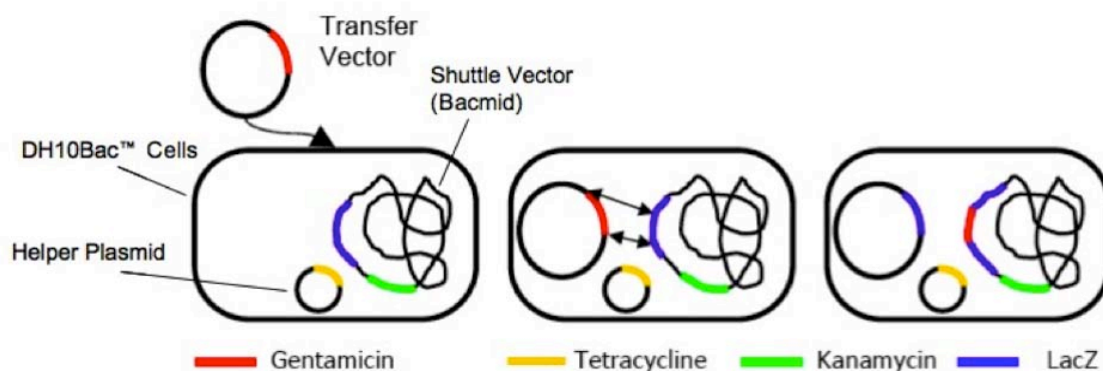


Figure 14. Generation of recombinant bacmid by site-specific transposition.

Left: before transformation of transfer vector into DH10Bac™ cells; *middle:* transposition of the gene of interest and the gene encoding for gentamicin resistance into the bacmid (*black arrows*); *right:* recombinant bacmid with Tn7-element of transfer vector. LacZ gene and genes encoding resistance for indicated antibiotics are color-coded.

For transformation, chemically competent DH10Bac™ *E. coli* cells (aliquots of 50 μ l) were thawed on ice and incubated with 10 ng DNA (in 5 μ l TE buffer) 30 minutes on ice. The heat shock was performed for 45 seconds at 42°C, followed by immediate incubation on ice. Subsequently, 900 μ l of S.O.C. medium was added and the suspension was incubated in a shaker device at 225 rpm, for 4 hours at 37°C. The Tn7 transposition functions are provided by a helper plasmid, which encodes for the transposase and confers resistance to tetracycline. Thus, successful recombination leads to the disruption of the LacZ gene on the bacmid, which in turn allows for blue-white screening in the presence of the chromogenic substrate Bluo-gal and the inducer IPTG.

Therefore, 100 μ l of dilutions 1:10, 1:100 and 1:1000 in S.O.C medium were plated on LB plates supplemented with (100 μ g/ml) Bluo-Gal, (40 μ g/ml) IPTG,

Methods

(50 µg/ml) kanamycin, (7 µg/ml) gentamicin and (10 µg/ml) tetracycline. The plates were incubated for 48 hours at 37°C to grow single colonies. Two to ten single large and white colonies were picked and re-streaked to confirm the white (i.e., recombinant bacmid) phenotype on new LB plates supplemented with same concentrations of kanamycin, gentamicin, tetracycline, Bluo-Gal and IPTG.

4.3.3.3 Isolation of the recombinant bacmid DNA

Single large and white colonies from the re-streak plates were picked and grown to saturation overnight in culturing tubes containing 6 ml LB medium supplemented with kanamycin, gentamicin, tetracycline at the same respective concentrations as the ones applied before. Cells were pelleted at in a Rotanta 460R swinging bucket centrifuge (Hettich) at 2,500 x g for 15 minutes at 4°C (Rotanta 460R swinging bucket centrifuge, Hettich).

Plasmid isolation and purification was performed with buffers P1, P2 and P3 from the Qiagen® Midiprep kit, using the following protocol, while all centrifugation steps were carried out at 16,000 × g for 1 minute at room temperature in an Eppifuge.

Pelleted cells were resuspended in 500 µl of P1 buffer and then lysed by adding 500 µl P2 buffer, followed by incubation for 5 minutes at room temperature. 500 µl of P3 buffer was added and incubated for additional 10 minutes on ice. The solution was cleared by centrifugation for 15 minutes. The supernatant containing the plasmid DNA was briefly mixed with 1.6 ml ice-cold isopropanol and incubated for 30 minutes on ice. The precipitated DNA was pelleted by centrifugation for 15 minutes, followed by a wash step with 1 ml of ethanol (70%) before again pelleted by centrifugation for 5 minutes. The pellets were then air-dried for 15 minutes and subsequently dissolved in 40 to 50 µl of double-distilled water. Before storage at -20°C, the DNA concentration of all purified plasmids was determined (Section 4.2.2.7).

The insertion of the gene of interest was confirmed by PCR using promoter- and gene-specific primers. The correct orientation of the transposon inserted into the bacmid was checked by combining a (gene-) internal forward and an external reverse primer.

4.3.3.4 Transfection of Sf9 insect cells with recombinant bacmid

For transfection it is crucial that the bacmid DNA is clean and free from any salts, as contaminants will kill the cells and salt will interfere with lipid complexing, eventually leading to low levels in transfection efficiency (Invitrogen™, 2004).

For transfection, per probe 2 ml of freshly diluted Sf9 cells at a density of 0.5×10^6 cells/ml were seeded into one well of a 6-well tissue culture plate. The cells were incubated light protected for 15 to 20 minutes at 28°C, allowing the cells to attach to the surface of the tissue culture plate.

In the following, 1 to 10 µl of recombinant bacmid DNA solution was mixed with 5 µl of the cationic lipid Cellfectin® reagent (Invitrogen) into 200 µl Sf-900 II SFM medium (no additives). Cellfectin® is a 1:1.5 (m/m) liposome formulation of the cationic lipid N, N^I, N^{II}, N^{III}-tetramethyl-N, N^I, N^{II}, N^{III}-tetrapalmitylspermine (TM-TPS) and dioleoyl phosphatidylethanolamine (DOPE), which coats the DNA and thereby facilitates transfection (**Figure 15**).

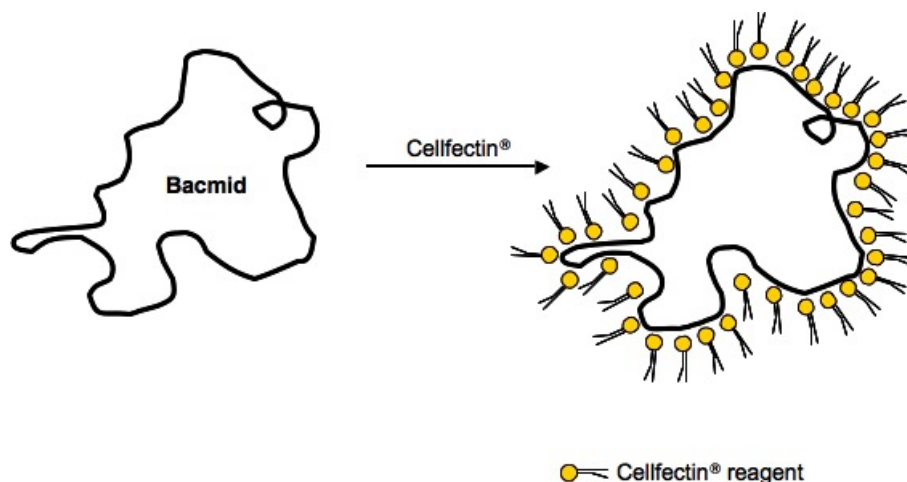


Figure 15. Preparing the bacmid for transfection into insect cells via Cellfectin® reagent.

The cationic lipid (Cellfectin® reagent) coats the bacmid DNA for the subsequent chemical transfection into insect cells.

The mixture was incubated for 15 minutes at 28°C before 1 ml Sf-900 II SFM medium was added. As a next step, the medium from the seeded cells was removed and the cells were washed twice with 2 ml Sf-900 II SFM medium (no additives). Subsequently, the cells were overlaid with the Cellfectin®-DNA suspension, before culture plate was tightly sealed and incubated light protected for 5 hours at 28°C. During this time the lipid-coated DNA enters the cells.

Methods

Then the transfection mix was removed and supplemented with 3 ml of fresh Sf-900 II SFM medium (containing 10% serum and 1% gentamicin, 10 mg/ml), followed by further incubation for two to three days at 28°C.

Virus-infected insect cells are characterized by increased cell size. In addition, after transfection the formerly surface-adhered cells detach from the plate they were seeded on and eventually undergo cell lysis, resulting in the release of virus into the medium (**Figure 16**).

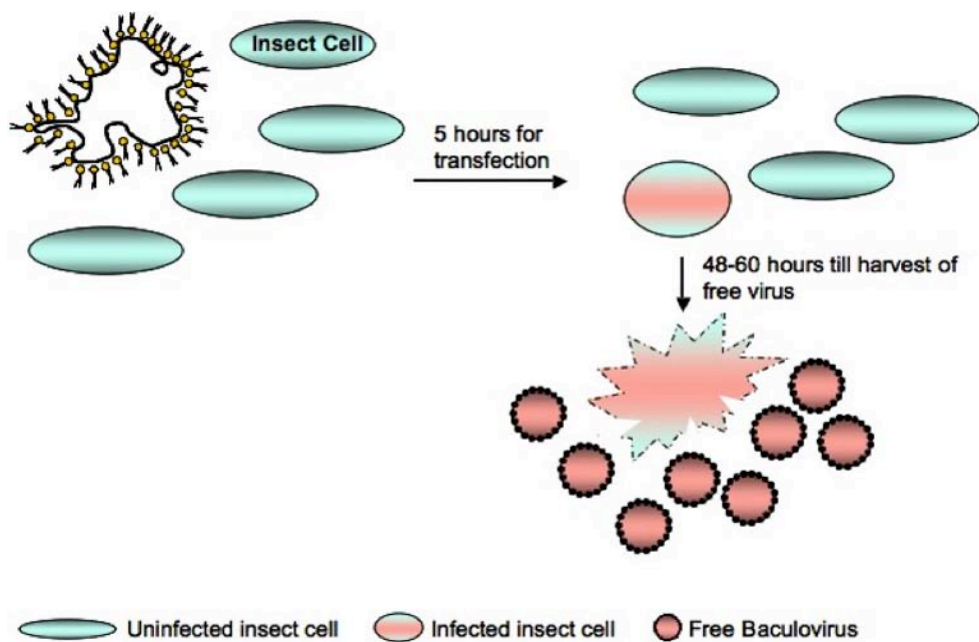


Figure 16. Schematic showing the time course from cell transfection until harvesting of released virus.

Top left: Cellfectin-mediated transfection of insect cells with bacmid DNA; *top right:* following transfection, within approx. 48 to 60 hours cells produce viral proteins, that eventually assemble into intact lytic viral particles; free virus is eventually harvested and used for further virus amplification.

48 to 60 hours after transfection, the initial virus (V_0 generation) was harvested, sterile-filtered using a 0.22 μm syringe filter and stored light-protected at 4°C.

4.3.3.5 Amplification of baculovirus V_0 generation

The V_0 viral stock is a small-scale, low-titer stock and is used to infect a larger volume of yet uninfected cells to generate a high-titer V_1 (or higher) virus generation. For viral amplifications always cells from suspension culture were used. For an efficient amplification, prior infection the viability of the cell stock was supposed to be greater than 95%, while a cell density of $0.5 \cdot 10^6$ cells/ml was

Methods

desired. Typically, 100 ml of uninfected cells were infected with 100 to 300 μ l of V_0 virus. Amplifications were incubated shaking at 110 rpm and 28°C. To determine the progress of the individual amplification cell viability and density was determined daily. As long as the cell density was higher than 0.5×10^6 cells/ml, the cell suspension was diluted to 0.5×10^6 cells/ml, while keeping the volume constant. Virus was harvested when the cell density stayed below 0.5×10^6 cells/ml for additional 48 hours. The harvested V_{1+x} generations can be stored light protected at 4°C up to several months.

4.3.3.6 Protein expression in Sf9 insect cells

For all proteins over-expressed via the baculovirus expression system, expression was carried out in insect Sf9 cells from suspension culture.

300 ml to 800 ml freshly diluted Sf9 cells at a density of 2×10^6 cells/ml (viability greater than 95%) were used for protein expression from suspension culture in 1 to 6 L-glass spinner flasks. Typically, 2 to 5% vol. of recombinant virus encoding for the gene(s) of interest, were used to transfect the cells. Depending on the protein to be expressed, the suspension of transfected cells was incubated for 45 to 80 hours in a shaker device at 110 rpm and 28°C.

4.3.4 FLAG-tag affinity protein purification

All proteins expressed in this thesis contained either a C- or an N-terminal FLAG-tag. The FLAG-tag itself is an octapeptide, which is made up of the amino acid sequence DYKDDDDK (Figure 17).

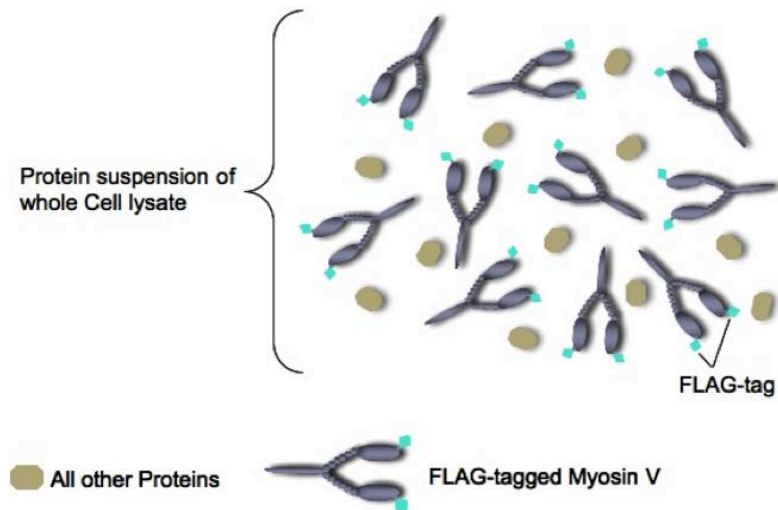


Figure 17. Schematic of FLAG-affinity protein purification – Part 1.

Depicted is the cell lysate fraction containing the overexpressed FLAG-tagged protein of interest (depicted is a double-headed motor protein, e.g. Myosin V).

As for other tags used in molecular biology, the FLAG-tag with its rather unique peptide sequence, is used to affinity-purify only those proteins that contain a FLAG-tag and are over-expressed in Sf9 cells. For this, a commercially available resin that contains agarose-beads to which multiple copies of monoclonal anti-FLAG antibody are attached (Anti-FLAG M2[®] Affinity Gel, SIGMA) was used (Figure 18).

The size of the beads keeps the bound proteins from passing through the membrane of the column. Via competitive elution, where synthetic FLAG-Peptides are applied in excess amount to the solution of antibody-bound protein, the protein of interest is eventually eluted from the column. Statistically the antibody will bind more likely to the highly concentrated FLAG peptides than to the much lower concentrated proteins of interest (Figure 19). This way high yields of relatively clean protein fractions are achieved.

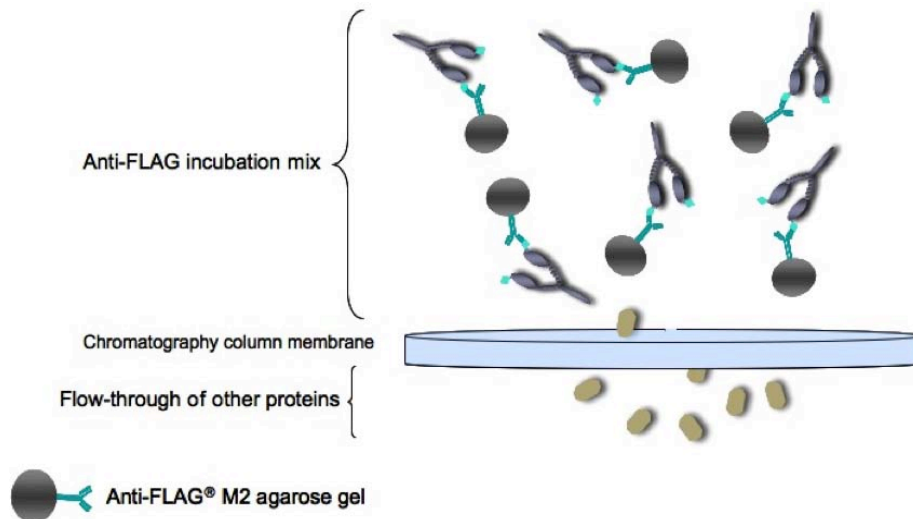


Figure 18. Schematic of FLAG-affinity protein purification – Part 2.

Upon incubation with anti-FLAG[®] M2 agarose resin, FLAG-tagged proteins bind to the resin. Thereby highly efficient separation of the FLAG-tagged protein from other unwanted cytoplasmic protein fractions is achieved.

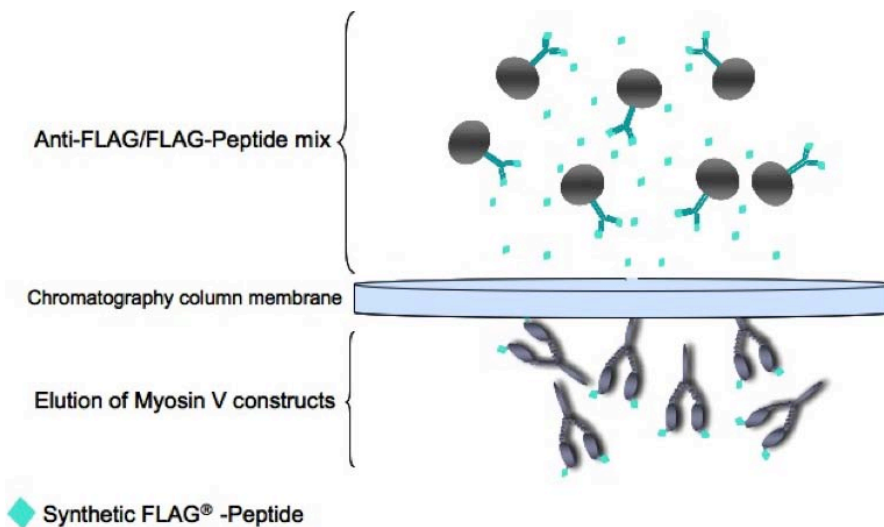


Figure 19. Schematic of FLAG-affinity protein purification – Part 3.

FLAG-tagged protein fraction is eluted from the column by competitive elution applying an excess amount of FLAG-peptides.

4.3.4.1 General FLAG-tag affinity purification protocol

All steps were carried out on ice at all times. Before harvesting of the cells, viability and density was determined for comparison of infection rates. The cells were harvested by centrifugation at 1,500 x g for 15 minutes at 6°C. The pelleted cells were resuspended in approx. 9% vol. (of the initial cell suspension volume) Lysis Buffer (LB) 1X and homogenized in a glass-bounce homogenizer for 5 minutes on ice. The homogenate was cleared by centrifugation at 69,000 x g for 15 minutes at 4°C (L8-70M Ultra-centrifuge and 42.1 Rotor, Beckman-Coulter). The supernatant, containing most of the soluble proteins, was mixed with 3% vol. (of lysis solution volume) anti-FLAG agarose resin (Anti-FLAG M2[®] Affinity Gel). This mixture of anti-FLAG resin and cellular proteins was then incubated rotating for 90 to 120 minutes at 4°C. As a next step, the mixture now containing the antibody-bound FLAG-tagged proteins of interest was applied onto a PolyPrep[®] chromatography column, which was equilibrated with 2 to 3 ml of LB 1X beforehand. The cushion of anti-FLAG resin on the column was washed 8 to 10 times with 2 ml of Wash Buffer (WB) 1X by constant stirring the suspension with a glass-stick. Protein elution from the column took place in 0.5 to 1.5 % vol. (of lysis suspension volume) of Elution Buffer (EB). Before the actual elution was carried out and under constant stirring, EB and the resin mixture were incubated for 30 minutes at 4°C (chromatography column sealed-up). By gently applying air pressure onto the unsealed column, protein elution was carried out. Immediately after elution, via Slide-A-Lyzer[®] dialysis cassettes (0.1 - 0.5 ml or 0.5 - 3 ml capacity, 10 kDa molecular weight cut-off) samples were dialyzed for 60 to 120 minutes at 4°C into 500 ml dialysis buffer (DB, containing 50% glycerol). This step was included to make the purified proteins suitable for long-term storage at -20°C. For SDS-PAGE analysis always 15 to 30 µl of flow-through (FT), wash (W), elution (E, prior dialysis) and dialysis (D) was saved. For those purifications where protein yield was expected to be low, protein concentration was further scaled up with Amicon Ultra-4 centrifugal filter units (10 kD molecular weight cut-off). For this, the filter unites containing the un-dialyzed protein elution, were centrifuged in a swinging bucket centrifuge (swinging-bucket centrifuge, Rotanta 460R, Hettich) at 4,000 x g for 5 to 10 minutes and 4°C.

It is to be mentioned that due to the different downstream applications carried out,

Methods

for subsequent cryo-EM studies the CaMKII- α protein was dialyzed into 10% glycerol (in DB 1X), keeping the protein stable at 4°C for four weeks. If snap-frozen in liquid nitrogen (for biochemical analysis) the protein could be stored at -70°C for up to several months.

For protein-specific buffers used during cell lysis, sample washing and sample elution, please refer to **Table 17**.

	HMM-like Myosin Va	FL-Xenopus Myosin Va	CaMKII-α
Lysis	LB-HMM-M5	LB-XM5	Brickey Buffer
Wash	WB-HMM-M5	WB-XM5	WB-CK
Elution	EB-HMM-M5	EB-XM5	EB-CK
Dialysis	DB-HMM-M5	DB-XM5	DB-CK

Table 17. Listing of the different buffers used during FLAG-tag affinity purification of the different baculovirus-expressed proteins of interest.

4.3.4.2 Optimized protocol for FLAG-tag affinity purification of full-length *Xenopus l.* Myosin Va

For the purification of full-length *Xenopus l.* Myosin Va, in principle the general FLAG-tag affinity purification protocol was followed (for details, refer to Section 4.3.4.1).

Due to strong degradation of the full-length protein, any detergent in the lysis buffer was omitted and instead of Dounce-homogenization, cell lysis was performed via sonication for a total of three minutes (duty cycle: 40%, output control: 4). Cell lysate was cleared at 27,000 \times g (Sorvall RC-5B and SS-34 rotor) for 30 minutes at 4°C. Because of its high molecular weight (larger than 215 kDa), the expression was expected to yield relatively low protein concentrations. Thus, immediately after the first incubation with anti-FLAG resin was completed the mixture was applied onto the column, and the flow-through of this first incubation round underwent a second round of incubation with anti-FLAG resin. Furthermore, two rounds of incubation with EB (1% total vol. of lysis solution volume) were performed while eluting the protein sequentially in-between. Before dialysis into 50% glycerol, protein concentration was typically scaled-up via Amicon Ultra-4 centrifugal filter units (as described in Section 4.3.4.1).

4.3.5 Methods for functional protein analysis

4.3.5.1 *In vitro* motility assays

In vitro motility assays were utilized to test for the functionality of both, recombinant baculovirus-expressed proteins and whole organelles. Furthermore, by performing motility assays it is possible to characterize movement and transport of motor proteins and organelles on actin filaments as well as microtubules, biophysically.

4.3.5.1.1 Flow cell preparation

All *in vitro* (single-molecule, melanosome motility and gliding filament) motility assays were performed using 15- μ l flow cells (area 18 \times 5 mm), covered by a nitrocellulose coverslip. The cells were prepared by greasing a large coverslip (for TIRF microscopy) or microscope slide (for epi-fluorescence) on a flat surface with silicon vacuum grease along the length of the coverslip about 5 mm apart and placing a smaller coverslip on top of the grease. The second coverslip was gently pushed downward so that maximal capillary force for the reagents was achieved. The reagents were pipetted into the opening at one end of the channel created by the grease and the coverslip (**Figure 20**).

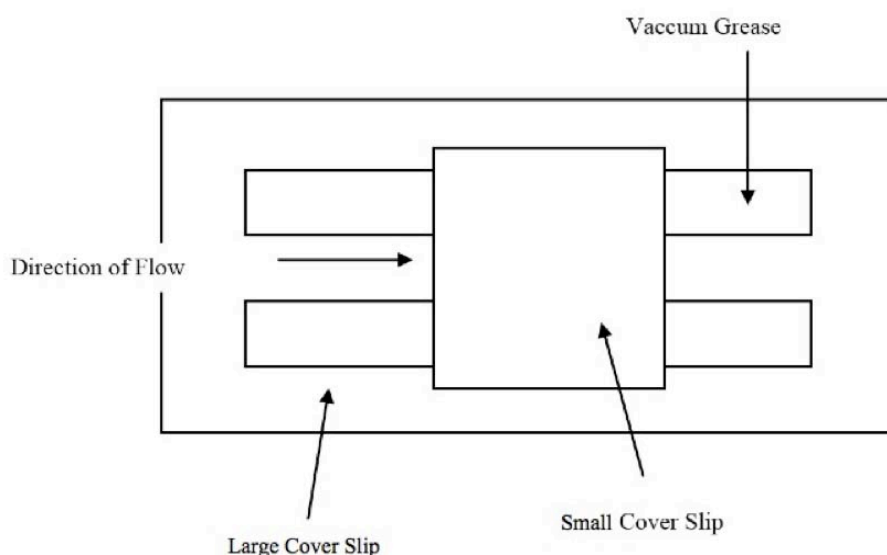


Figure 20. Schematic of the flow cell setup used during *in vitro* motility assays.

For *in vitro* gliding filament or single-molecule motility assays 15 μ l-flow cells (approx. area 18 \times 5 mm) were prepared by applying a small coverslip on top of a larger one, with two stripes of silicon grease in between to create a flow channel.

4.3.5.1.2 Fluorescent labeling of motor proteins

For visualizing individual motor molecules in motility assays on F-actin and microtubules, FLAG-purified myosins to be probed for fluorescence microscopy were conjugated to a monoclonal anti-FLAG Cy3 antibody. For this, the antibody was diluted 20-fold to 0.05 mg/ml in TBS 1X, while being kept on ice. The FLAG-specific labeling was achieved by incubating 40 μ l of 500 nM FLAG-tagged purified protein with 10 μ l of the pre-diluted antibody at room temperature for 5 minutes in AB 1X and subsequent storage on ice. Before use, the mixture was further diluted to the desired motor concentration in AB 1X (containing oxygen-scavenging system).

4.3.5.1.3 Single-molecule motility assays on microtubules and F-actin

For assays with microtubules as the cytoskeletal track, an appropriate dilution of fluorescent microtubules was perfused into the flow cell, followed by a wash with BRB80-Tx (1X), containing 0.7 mg/ml casein to block the flow cell surface. 100 nM of fluorescent-labeled Myosin protein in AB 1X (containing an oxygen-scavenging system) was added to the flow cell. For experiments in which different ionic strength-conditions were applied to the flow cell, the required volume of KCl (1 M) was added, yielding a final assay concentration of 50, 100 or 200 mM KCl (Table 18).

Step	Reagent	Incubation time (minutes)
1	15 μ l dilution of Atto488-labeled microtubules in BRB-Tx (1X)	3
2	50 μ l wash with BRB80-Tx (1X) plus 0.7 mg/ml casein	3
3	100 nM Cy3-labeled Myosin in AB (1X) plus Oxygen Scavenging system	1
or		
4	Step 3 plus: 25, 75, 175 mM KCl (1M)	1

Table 18. Pipetting scheme for *in vitro* single-molecule motility assays with Myosin V on microtubules.

For assays in which actin filaments served as cytoskeletal tracks, flow cells were pre-incubated with 0.1 mg/ml N-ethyl maleimide (NEM)-modified Heavy Meromyosin (HMM)¹⁵⁴ (kind gift of Prof. T. Bausch, Technical University, Munich,

Methods

Germany), rinsed with AB 1X, incubated with an appropriate dilution of TRITC-labeled actin filaments, rinsed with AB 1X and then blocked with BSA (5 mg/ml). 100 nM fluorescently labeled Myosin was applied and incubated for 1 minute, followed by a wash step with AB 1X containing 1 mM ATP (Table 19).

Step	Reagent	Incubation time (minutes)
1	15 μ l NEM-HMM (0.1 mg/ml) in NHB (1X)	3
2	50 μ l wash with AB (1X)	-
3	15 μ l TRITC-labeled F-actin dilution in AB (1X)	3
4	50 μ l wash with AB (1X)	-
5	50 μ l wash with AB (1X) plus 5 mg/ml BSA	5
6	100 nM Cy3-labeled Myosin in AB (1X) plus Oxygen Scavenging system	1
7	50 μ l wash with AB (1X) plus Oxygen Sc. system, 1 mM ATP	1

Table 19. Pipetting scheme for *in vitro* single-molecule motility assays with Myosin V on F-actin.

The oxygen-scavenging system was included to keep photo-bleaching low. In this system, glucose-oxidase catalyzes the oxidation of D-glucose to form D-glucono-1, 5-lactone and hydrogen peroxide. Hydrogen peroxide would severely damage the motor proteins, so that catalase is used to decompose the hydrogen peroxide to water and oxygen (Figure 21).

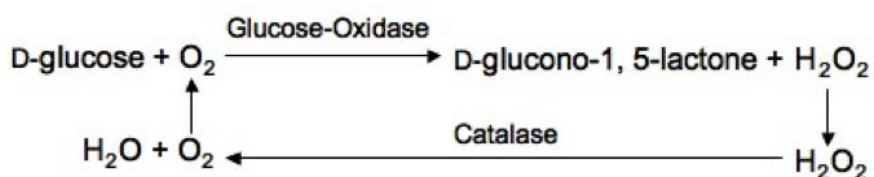


Figure 21. Reaction of the oxygen-scavenging system used in *in vitro* motility assays.

To avoid photo-bleaching of the sample during acquisition, an oxygen-scavenging system containing glucose, glucose-oxidase and catalase was used.

4.3.5.1.4 Gliding filament assays

For gliding filament assays with the full-length *Xenopus l.* Myosin Va, the motor was surface-adhered non-specifically by infusing 50 to 650 nM protein into the flow cell. To prevent unspecific filament binding to the glass-surface, an additional wash step with BSA (5 mg/ml) in AB 1X was included. Then, an appropriate dilution of Atto488-labeled F-actin was perfused into the flow cell, followed by a wash step with BSA (5 mg/ml) in AB 1X. At last motility buffer, containing ATP and oxygen-scavenging system, was applied to the flow cell (Table 20).

Step	Reagent	Incubation time (minutes)
1	15 μ l of 50- 650 nM Myosin in AB (1X)	3
2	50 μ l wash with AB (1X) plus 5 mg/ml BSA	5
3	15 μ l Atto488-labeled F-actin dilution in AB (1X)	3
4	50 μ l wash with AB (1X) plus 5 mg/ml BSA	-
5	50 μ l wash with AB (1X) plus Oxygen Sc. system, 2 mM ATP	3

Table 20. Pipetting scheme for *in vitro* gliding filament assays with F-actin and Myosin V.

4.3.5.2 TIRF and epi-fluorescence microscopy

In vitro motility (Section 4.3.5.1) of HMM-Myosin Va loop 2 mutants, as well as Wildtype full-length *Xenopus l.* Myosin Va was studied by applying fluorescence-microscopy techniques. For assays, where primarily the filament-gliding behavior was studied, both an epifluorescence microscope (Axiovert 200M) equipped with a apochromatic objective lens (100 \times , N.A. 1.4 Oil) and linked to a CCD camera (AxioCaM MRm, Zeiss) as well as the below described TIRF microscope were used (as indicated in the respective figures). For microscopy via epi-fluorescence, a mercury lamp (FluoArc 01.26D, Jena GmbH) along with band-pass filters allowing for fluorophore excitation at 488 and 532 nm was used, while the optical resolution was 10 px/ μ m, and dependent on the duration of image acquisition, integration times varied. In most cases, image acquisition took place for 1 to 3 minutes.

All the single-molecule motility assays where the behavior of HMM-Myosin Va constructs on microtubules and F-actin was examined, were studied with a total

internal reflection fluorescence (TIRF) microscope (IX71), equipped with a Plan objective lens (100 \times , N.A. 1.65 Oil) and linked to a front-illuminated CCD camera (C-9100, Olympus). Fluorophores were excited with a solid-state laser at wavelengths of 532 or 488 nm. The optical resolution was 160 nm per 2 \times 2 - binned pixel, with integration time 200 ms. Typically, 350 images were recorded for a total of 70 s.

4.3.5.3 ATPase activity assays

ATPase activity was determined in a coupled enzymatic assay^{35,155} (Figure 22). In this assay, ATP hydrolysis is linked to the oxidation of NADH, which is measured spectroscopically at 340 nm by its decrease in concentration. The coupling takes place via phosphoenol pyruvic acid (PEP), pyruvic acid kinase (PK) and lactate dehydrogenase (LDH), which is referred to as ATP regenerating system.

To study the filament-stimulated ATPase activity of the assayed motor proteins,

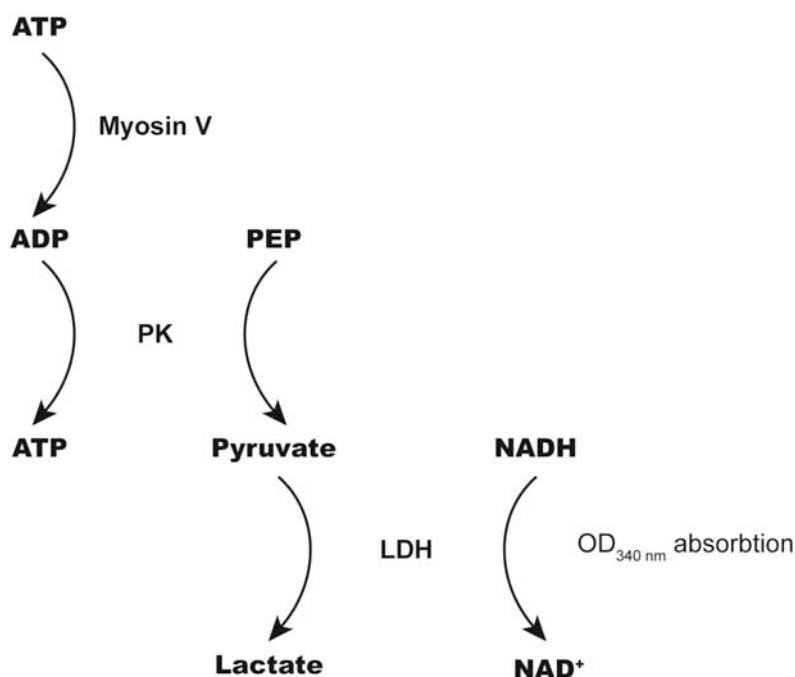


Figure 22. Schematic of the coupled enzymatic steady-state ATPase assay.

Myosin Va hydrolyzes ATP to ADP and inorganic phosphate, while simultaneously the regenerating system recycles the generated ADP back into ATP. Therefore, the system maintains a steady state ATPase of Myosin Va. Via the enzymatic action of pyruvate kinase (PK), for each ATP molecule generated, one NADH molecule is oxidized by lactate-dehydrogenase (LDH) to NAD⁺. The resulting decrease in absorption can be measured at 340 nm.

Methods

measurements at different F-actin or microtubule concentrations were carried out. With the output value of absorption (A) in OD per second, the molar absorptivity (ϵ) of NADH at 340 nm and the diameter of the well, the NADH concentration in the activated ATPase assay can be determined by applying the law of Lambert-Beer (see Equation 5).

$$A_{\lambda} = \epsilon_{\lambda} * d * c$$
$$\epsilon_{\text{NADH at 340 nm}} = 6.22 \text{ Mol}^{-1} * \text{cm}^{-1}$$
$$d = 0.3125 \text{ cm}$$

Equation 5 (Haid *et al.*, 1975)¹

The amount of NADH that is oxidized per second corresponds to the amount of hydrolyzed ATP per second, which in turn reflects the maximal rate of ATP hydrolysis (V_{max}). K_m expresses the motor concentration that yields the half-maximal reaction rate. k_{cat} or the catalytic constant expresses the number of hydrolyzed ATP molecules per motor head (or motor dimer) per second, and was calculated according to Equation 6.

$$k_{\text{cat}} = \frac{C_{\text{ATP}} * S^{-1}}{C_{\text{myosin}}}$$

Equation 6

The ATP regenerating system was prepared by mixing gently all reagents (Table 21) on ice. 2.3 μl ATP regenerating system per well was applied to the reaction.

Components for ATP Regenerating System (concentration)	Final concentration (139.3 μl)	Final Concentration per 96-Well (50 μl)
NADH (solid) in HEPES Buffer (1X)	32.3 mM	1.5 mM
PEP (solid) in KMg50 Buffer (1X)	189.5 mM	3 mM
PK (700 U/ml)	34.2 U/ml	1.6 U/ml
LDH (1000 U/ml)	48.8 U/ml	2.2 U/ml
H ₂ O	(Δ 139.3 μl)	-

Table 21. Final concentrations of ATPase regenerating system components.

Methods

It was crucial that ATP was added to the reaction immediately before the plate-reading was started. All components were pipetted into the wells by following a strict order, which is outlined in **Table 22**.

Order for the application of assay-components (volume)	Applied volume/concentration
Step 1 (10 μ l)	100 nM HMM-Myosin Va 2.3 μ l ATP regenerating system Δ 10 μ l KMg50 Buffer (1X)
Step 2 (37 μ l)	F-actin or microtubules at desired concentrations Δ 37 μ l KMg50 Buffer (1X)
Step 3 (3.3 μ l)	3.3 μ l MgATP at desired concentration
Total reaction volume	50 μ l

Table 22. Reaction setup for actin- or microtubule-stimulated ATPase activity assays with Myosin V.

Volumes and concentrations refer to one well.

ATPase activity assays were carried out in 96-well plates using a spectrophotometer at an excitation wavelength of 340 nm and 23°C. The data were analyzed with Kaleidagraph software (Synergy, Pittsburgh, U.S.A.) and fitted to the Michaelis-Menten function¹⁵⁶ as is described in more detail in Section 4.4.5.

4.3.5.4 Microtubule-affinity co-sedimentation assays

Microtubules were polymerized from porcine tubulin overnight and their concentration was determined as described in Section 4.3.1.4. Typically, 0.5 to 1 ml purified tubulin was diluted 3-fold in BRB80 1X so that after polymerization a microtubule concentration of 200 μ M was yielded. 375 μ g of the microtubule stock solution was treated with Subtilisin A (for experimental details see Section 4.3.2.4). After E-hook digestion was completed, the mixture was cleared by centrifugation at 27,000 \times g for 25 minutes and 25°C (Optima-TL ultra-centrifuge and TLA120 Rotor, Beckman-Coulter). The pellet was resuspended in 135 μ l BRB80-Tx 1X (containing 1 mM GTP), yielding a final microtubule concentration of 50 μ M. Likewise the untreated microtubule stock solution was diluted to 50 μ M in BRB80-Tx 1X.

Methods

Co-sedimentation assays were carried out at constant microtubule (1 μM) and motor protein (850 nM) concentrations, while the ionic strength of the assay milieu differed (25 to 200 mM KCl final concentration) (for details see Table 23). To ensure that all reactions took place under zero ATP, the non-hydrolyzable ATP analogue AMP-PNP as well as the phosphatase Apyrase (hydrolyzes all residual ATP to AMP and P_i) were included.

The reactions were incubated for 20 minutes at 30°C before centrifugation through a sucrose cushion (40% in BRB80 1X) at 280,000 $\times g$ for 10 minutes at 25°C (Optima-TL ultra-centrifuge and TLA120 Rotor, Beckman-Coulter) was carried out. For further SDS-PAGE analysis, a sample aliquot of the supernatant from each of the reactions was saved. Before aspirating the sucrose cushion, it was washed once with AB 1X. The pellet, now containing the microtubule-bound Myosin Va fraction, was washed twice with AB 1X and for the subsequent SDS-PAGE analysis was resuspended in 20 μl AB1X.

Component (concentration)	Final concentration	Applied volume (μl)
Microtubules, treated/untreated (50 μM)	5 μM	variable
Myosin Va (850 nM)	5 μM	2.5
Apyrase (1000 U ml^{-1})	5 U ml^{-1}	1
AMP-PNP (0.1 M)	1 mM	2
	25 mM or	-
	50 mM or	5
KCl (1 M), if applicable	100 mM or	15
	125 mM or	20
	200 mM	35
AB (10X)	1X (includes 25 mM KCl)	20
H ₂ O	-	Δ 200
Total reaction volume		200

Table 23. Reaction setup for ionic strength-dependent microtubule-affinity co-sedimentation assays with Myosin V.

Methods

4.3.5.5 CaMKII- α autophosphorylation assays

The autophosphorylation reaction was set-up by mixing calmodulin and the so-called Ca²⁺ reaction mixes (2.5X), each of which contained a different concentration of free Ca²⁺. The mixture was incubated with 0.1 mM ATP and temperature-equilibrated on a shaking heat-block for 2 minutes at 25°C before purified C' or N' FLAG-tagged CaMKII- α (0.15 mg/ml) was added. Reactions were stopped after 0 (immediate stop), 2 or 3 minutes by adding Stop Solution, containing 9% SDS and 3% β -mercaptoethanol.

The analysis was carried out by resolving the individual reactions via 10% SDS-PAGE (Section 4.3.1.1) with subsequent targeting of the resolved samples for immunoblotting against total CaMKII- α protein and phospho-Thr286 of CaMKII- α (for details on immunoblotting, refer to Section 4.3.1.5).

For detailed information on the applied volumes and final concentrations for the various assay ingredients, please refer to **Table 24** and **Table 25**.

	Ca²⁺ Reaction Mix 2.5X	BSA (2 mg/l)	Calmodulin (1 mg/ml)	KCl (3M) in 50 mM TrisCl	H₂O	ATP (2 mM)	CaMKII Mix (0.15 mg/ml)		
	(μ l)	(μ l)	(μ l)	(μ l)	(μ l)	(μ l)	(μ l)		
Sample	Final Ca ²⁺ conc. (mM)								
	0	1.73	300						
Zero	80	-	-	40	4	10	36	10	20
Low	-	80	-	40	4	10	36	10	20
High	-	-	80	40	4	10	36	10	20

Table 24. Reaction setup for autophosphorylation assays with CaMKII- α at different calcium concentrations.

The ability of CaMKII- α to undergo autophosphorylation was assessed at zero, low (1.73 μ M) and high (300 μ M) concentrations of free Ca²⁺. Concentrations of all other components were kept constant. Prior the addition of CaMKII- α , reactions were equilibrated at 25°C for 2 minutes (including 0.1 mM ATP).

Methods

Sample	Total Ca ²⁺ (μ M)	Free Ca ²⁺ (μ M)	Mg ⁺ (mM)	EGTA (mM)	ATP (mM)	KCl (mM)	Calmodulin (mg/ml)	CaMKII (mg/ml)	CaMKII (μ M)	
Zero	0	0	1	0.4	0.1	150	0.02	1.18	0.015	0.27
Low	379	1.73	1	0.4	0.1	150	0.02	1.18	0.015	0.27
High	700	300	1	0.4	0.1	150	0.02	1.18	0.015	0.27

Table 25. Final concentrations of CaMKII- α autophosphorylation assay components.

4.3.5.6 Assays to monitor CaMKII- α -mediated Myosin V release from melanosomes

At first, melanosomes from eight to ten confluent flasks of cultured *Xenopus l.* melanophores were isolated according to the procedure outlined in Section 4.1.4. However, for this assay serum-deprived cells were rinsed once with PBS 0.7X and then again with AB 1X before being scraped into 2 ml of AB 1X (containing protease inhibitor). Subsequent lysis by Balch-homogenization and all the centrifugation steps were performed as described above. Before proceeding to the release-assay, isolated melanosomes were kept suspended in 800 μ l AB 1X (containing protease inhibitor) on ice. Just before the assay, the granules were pelleted at 2,500 \times g for 5 minutes and 4°C (Hettich, Rotina 420R) and resuspended in 100 μ l PBS 0.7X (containing protease inhibitor).

The fact that Myosin V release via CaMKII- α is possible only if the kinase is in its active form required a set-up where the CaMKII- α autophosphorylation assay (outlined in 4.3.5.5) is combined with the isolated melanosomes. The different Ca²⁺ reaction mixes (2.5X), calmodulin and 0.1 mM ATP were equilibrated on a shaking heat-block for 2 minutes at 25°C before activation of the kinase was induced in high Ca²⁺ (300 μ M free Ca²⁺) for 30 seconds at 25°C. Lastly, melanosomes were added to the mixture for zero (immediately stopped with AB 10X), 2, 4 or 5 minutes shaking at 25°C (Table 26). Reactions were stopped by mixing AB 10X with the sample in a 1:10 ratio. To separate melanosomes from supernatant, samples were centrifuged at 5,000 \times g for 10 minutes and 4°C (Biofuge 15R, Heraeus). Both, supernatant and pelleted melanosomes were mixed with SDS 6X sample buffer, and resolved by SDS-PAGE. Subsequently, samples were analyzed by immunoblotting against the antigen of interest.

Methods

The final concentrations of the assay components were identical to those of the auto-phosphorylation assays (Table 25).

	Ca²⁺ Reaction Mix 2.5X	BSA (4 mg/l)	Calmodulin (1 mg/ml)	KCl (3M) in 50 mM TrisCl	H₂O	ATP (4 mM)	CaMKII Mix (0.28 mg/ml)	Mel.	
	(μ l)	(μ l)	(μ l)	(μ l)	(μ l)	(μ l)	(μ l)	(μ l)	
Sample	Final Ca ²⁺ conc. (mM)								
	0	300							
Zero	40	-	5	2	5	20	2.5	5	20
High	-	40	5	2	5	20	2.5	5	20

Table 26. Reaction setup for the CaMKII- α -mediated Myosin V-release from melanosomes.

The ability of CaMKII- α to trigger the release of Myosin V from melanosomes (from *Xenopus* melanophores) was assayed at zero and high (300 μ M) concentrations of free Ca²⁺, while having 0.01 mM ATP present. All reactions were carried out at 25°C. The final concentrations of the applied assay components are identical to those used in the CaMKII- α -autophosphorylation assays (Table 25).

4.4 Data Analysis

Unless mentioned otherwise in the detailed description of the respective method, data was analyzed as described below.

4.4.1 Fluorescence microscopy data analysis: Single-molecule motility measurements

Diffusion events were defined as follows: Those events in which the Myosin V molecule moves on microtubules in both directions (for > 300 nm) were classified as diffusive events.

For the characterization of Myosin V diffusion on microtubules, the following parameters were determined: i) *maximum speed* of diffusion for a given encounter was defined as the maximum displacement along the microtubule during one frame interval (i.e., 5 frames per s); ii) *scan distance* for a given encounter was calculated as the distance between the two extreme positions of the microtubule, on which the respective Myosin V molecule has diffused along; iii) *association time* (t_A) was defined as the total time an individual Myosin V

Methods

molecule spent on the microtubule during recording. The individual values for t_A of the respective Myosin V constructs were obtained from an exponential fit as described¹¹⁶.

The mean square displacement (MSD) for all diffusion events was calculated as described in¹⁵⁷, plotted as a function of time and fitted to linear function.

Single displacements of individual diffusion events for a given Myosin V construct were plotted as a displacement histogram. A single Gaussian was fitted to the data according to Equation 7.

$$y = a \cdot \exp \left[-\left((x - x_0) / b \right)^2 \right]$$

Equation 7

Based on the Gaussian fit curve for the respective displacement histogram, the variance $\sigma = b^2$ was calculated. From these data, the diffusion coefficient (D) was determined according to the *1st law of diffusion*-derived equation, $D = \sigma / 2t$, where t is the time interval between successive images.

Quantification of microtubule association and diffusion was carried out with the data obtained from the single-molecule experiments on microtubules. For each microtubule, the numbers of diffusing and stationary particles during a 70-second period were counted. The numbers of diffusing and stationary particles on microtubule lengths of 1000 to 3000 μm were added and divided by the corresponding microtubule lengths and time of measurement. By this procedure, the number of associated and diffusing Myosin V particles per microtubule unit length and time at the respective salt concentration (25, 50, 100 and 200 mM KCl) was obtained. Quantification on S-microtubules is based on data obtained from experiments in 25 mM KCl.

On actin, only events of individual Myosin V molecules ($n \geq 25$) walking along the filaments with an interaction time ≥ 2 s were classified as processive. The length of a processive run was determined manually with CellR software (Olympus Biosystems, Germany). Runlength and velocity distributions were obtained from the single exponential and Gaussian fit as described by Helenius *et al.*¹¹⁶ and Equation 7, respectively.

4.4.2 Fluorescence microscopy data analysis: Gliding-filament motility measurements

Only those filament-gliding events ($n \geq 30$) where the transport of an individual filament lasted for longer than 5 s and remained uninterrupted during that time period were taken into consideration. As for the single-molecule motility analysis of Myosin V on F-actin described above, the gliding velocity of individual actin filaments was determined using CellR software and IMAGEJ (NIH, Bethesda, U.S.A.). The mean-values for gliding velocity were obtained from the single Gaussian fit according to Equation 7.

4.4.3 Fluorophore measurement and statistical analysis

Distances and single displacements were measured by brightest centroid tracking, using MTrackJ for IMAGEJ. Single-displacement boxplots as well as all other data plotting and fitting, but also the statistical analysis was performed with IgorPro software (WaveMetrics, Inc., Portland, U.S.A.).

Kymographs of representative video sequences from the performed single-molecule TIRFM assays on actin and microtubules were generated with the MultipleKymograph macro for IMAGEJ.

4.4.4 Quantitation of data obtained from microtubule-affinity co-sedimentation

Band intensities of the respective supernatant and pellet fractions were determined with the digital gel-analysis software ImageQuant (Version TL 7.0, GE Healthcare). By determining the average pixel value adjacent to the measured band of interest, background subtraction was carried out. The obtained background-corrected values of the reactions were subtracted by the median of the calculated ratio of the values determined for the control reactions (i.e., microtubules and Myosin V only). This way, all band intensities were not only background-corrected but also correction of potential assay-derived probe leakage into the supernatant and/or pellet fraction was included. As a last step, the obtained value of the respective sample (e.g., supernatant of reaction x) was related to the determined value of the respective control reaction (e.g., supernatant Myosin V only). This way the percentage of microtubule-bound

Methods

Myosin V relative to the situation where no microtubules are present at all could be calculated. Finally, the obtained values of all reactions from one assay were compared to the value of the 25 mM salt condition (set to 100%).

4.4.5 Analysis of data obtained from ATPase assays on actin and microtubules

Microtubule- and actin-activated ATPase activity of Myosin V was determined in a coupled enzymatic assay (4.3.5.3) with a final MgATP concentration of 1 mM and concentrations of Myosin V and F-actin or microtubules described above. Measurements were carried out in 96-well plates (Greiner, Frickenhausen, Germany) using a spectrophotometer (Biotek-Greiner, Frickenhausen, Germany) at an excitation wavelength of 340 nm and 23°C. The data were analyzed with Kaleidagraph 3.6 (Synergy Software, Reading, U.S.A.) software and fitted to the Michaelis-Menten function¹⁵⁶ to determine the maximum ATPase rate (k_{cat}) and the actin concentration at which Myosin V is activated half-maximally (K_m).

4.4.6 Sequence alignment

Sequence alignment of the herein determined full-length Myosin Va sequence from *Xenopus l.* and full-length sequences from other species was performed using Megalign (DNASStar, Madison, WI, U.S.A.) and the blosum62 amino acid table. The full-length Myosin Va sequence from *Xenopus l.* was aligned from N'-to C'-terminus to Myosin Va from chicken (*Gallus gallus*, accession number: NP_990631), mouse (*Mus musculus*, accession number: CAX15576.1) and human (*Homo sapiens*, accession number: NP_000250.3) using a progressive pairwise methods. Sequence data were obtained from the NCBI database.

5 Results

5.1 One-dimensional diffusion of Myosin Va on microtubules

5.1.1 Strategy

5.1.1.1 Generating HMM-like Myosin Va loop 2 mutants

All Myosin Va constructs assayed in this work were cloned from the previously described pFastBac-dhM5-CaM plasmid¹⁵⁸. The myosin encoded by this plasmid corresponds to the Wildtype form of chicken Myosin Va, which is truncated at the position D1098, and is thus lacking the Carboxy (C')-terminal globular tail domain (GTD). In the literature, this truncated version of Myosin Va is also referred to as the heavy meromyosin (HMM)-like fragment of Myosin V. To ensure dimerization, a leucine zipper motif was fused in-frame to the native coiled-coil. In this thesis the term mutant refers exclusively to changes of the amino acid composition within the actin binding-loop (loop 2) of Wildtype Myosin Va. The complete amino acid sequence of Wildtype HMM-like Myosin Va can be found in Section 7.

5.1.1.2 Designing and cloning of HMM-like Myosin Va loop 2 mutants

The plasmid encoding for the double-headed Wildtype HMM-like Myosin Va used in this thesis was a kind gift of Purcell, T. J. and colleagues (Stanford University, Stanford, U.S.A.)¹³⁸. It served as a template to design the loop 2 mutants. To facilitate purification, double-headed Myosin Va contains an amino (N')-terminal FLAG-tag. As for other HMM-like Myosins that have been studied previously, the constructs described in this work contain all six IQ motifs of the lever arm region (**Figure 23**).

The actin-binding loop commonly referred to as loop 2 is a well-defined region of ~ 44 amino acids near the so-called 50/20 kDa junction of the head domain. It has been implicated in binding the motor domain to actin^{35,111} and recently has been suggested to also mediate the interaction of Myosin V with microtubules¹⁰⁷. It is surface-exposed and exhibits a net positive charge of +5.

To dissect the contribution of the Myosin V loop 2 to the interaction with microtubules, we have generated two HMM-like Myosin V mutants with surplus net negative charge (referred to as *Minus4* and *Minus13*). For Myosin Va *Minus4*, all lysines and arginines within loop 2 were changed to alanines (K607A, R619A,

Results

R624A, K628A, K631A, R633A, K639A, K642A, K643A). For Myosin Va *Minus13*, all lysines and arginines were substituted with glutamic or aspartic acid (K607E, R619D, R624E, K628E, K631D, R633E, K639E, K642E, K643E) (Figure 23).

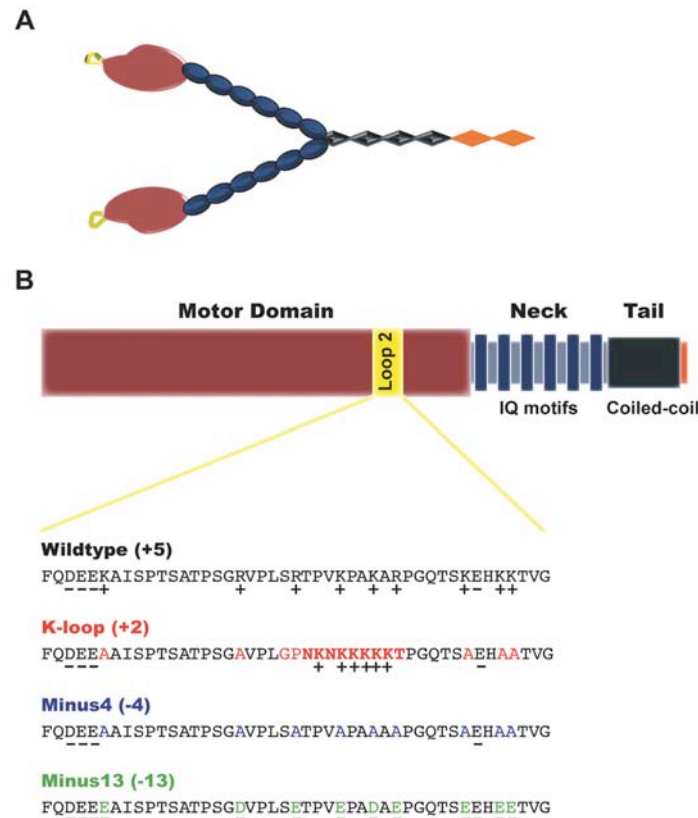


Figure 23. Schematic representations of the Myosin Va loop 2 constructs.

(A) Schematic domain model of the homodimeric truncated (HMM-like) Myosin V. The regions are color-coded for each structural motif. The same set of colors is used also in B. (B) Schematic diagram depicting the domain structure of Myosin V with its surface-exposed loop 2 shown in yellow. The C-terminal GCN4 motif ensures dimerization. Lower part of B: comparison of the loop 2 sequences from Myosin Va *Wildtype*, *K-loop*, *Minus4* and *Minus13*. Mutants *Minus4* (blue) and *Minus13* (green) were designed by altering positively charged amino acids (lysines and arginines) to alanine and glutamic/aspartic acid, respectively. For *K-loop* a positively charged stretch within the loop 2 sequence (positions 625-633) was substituted with the *K-loop* sequence of kinesin KIF1A, flanked by GP as helix breaker. (+) and (-) indicate positively and negatively charged amino acids, respectively. The net charge of each construct is indicated in brackets next to the respective construct.

To directly assess the role of the negatively charged E-hook of tubulin¹¹⁹ as a potential microtubule-binding site for Myosin Va, an additional mutant containing the surface loop sequence NKNKKKKKT¹¹⁹ of kinesin KIF1A was designed. For this, the entire stretch of loop 2 amino acids S623 to R633 was replaced with the sequence encoding for the microtubule-interaction loop (K-loop) of kinesin KIF1A. Except for the helix breaker residues G623 and P624, all the amino acid residues

Results

flanking the K-loop sequence correspond to those of the *Minus4* mutant. In the following this mutant containing two positive net charges on its loop 2 is referred to as *K-loop* mutant. The complete protein sequence of *Wildtype* HMM-Myosin Va can be found in Section 7.

The loop 2 sequences of the respective mutants were obtained by custom DNA synthesis (carried out by SloningBio-Technology, Puchheim, Germany). Details of the DNA sequence synthesis and cloning procedure are described in Section 4.2.2.8.

The baculovirus-compatible transfer vector plasmid was generated in such a way that the myosin gene itself was cloned downstream of the p10 promoter (P_{P10}) of the dual p2bac/pfastbac transfer vector (Purcell *et al.*, 2005)¹³⁸, using the restriction sites NotI and Sall. In addition, via restriction enzyme-mediated cloning with NheI and KpnI the light chain calmodulin was cloned downstream of the poly H promoter (P_{PH}) (see vector maps in Section 7).

Sections 4.3.3.6 and 4.3.4 outline the steps from the generation of baculovirus to protein purification.

5.1.1.3 Actin- and microtubule-activated ATPase activity of HMM-like Myosin Va constructs

Microtubule- and actin-activated ATPase activity of HMM-Myosin Va was determined with a final MgATP concentration of 1 mM. For this, the NADH-coupled ATPase assay was carried out as described in Section 4.3.5.3.

The ATP hydrolysis by Myosin Va was determined with 100 nM motor protein (in KMg50 Buffer) using 0 to 20 μ M F-actin or 0 to 35 μ M microtubules (in 12A25 Buffer). The concentration of polymerized actin was not determined because statistically nearly all monomers will polymerize in the presence of phalloidin¹⁵⁹. In contrast, for assays where microtubules were used, the microtubule concentration was determined post-polymerization as described in 4.3.1.4.

5.1.1.4 Microtubule-affinity co-sedimentation assays with HMM-like Myosin Va constructs

To test for the capability to interact with the filament, the four HMM-like Myosin Va constructs were assayed by the so-called microtubule-affinity co-sedimentation assay. A detailed protocol for this assay can be found in Section 4.3.5.4. In this assay, microtubules and the respective motor protein are mixed and subsequently ultra-centrifuged through a high-percentage sucrose cushion. Thereby, motor proteins that did not bind to the filaments remain in the supernatant on top of the cushion, while all filament-bound protein is present in the microtubule pellet. In addition to testing the affinity on untreated microtubules, the four Myosin Va constructs were tested as well in combination with subtilisin-treated microtubules lacking E-hooks (see also Section 4.3.2.4). Furthermore, all assays were carried out at different ionic strength conditions.

Results

5.1.2 Results

5.1.2.1 Purification of HMM-like Myosin Va loop 2 constructs

The four different HMM-like Myosin Va loop 2 constructs were expressed and purified as described in Section 4.3.4.2. **Figure 24** shows eluted and dialyzed fractions of the various constructs. Typically, when over-expressing the respective constructs in 300 to 350 ml of Sf9 cell suspensions, protein concentrations ranged between 5 and 10 μM in a total volume of 400 to 500 μl . The Myosin Va heavy chain corresponds to the 134 kDa-band, which is visible on the PAGE-photograph in **Figure 24**. The band that appears at roughly 100 kDa was identified by mass-spectrometry as a degradation product of Myosin Va. The protein fractions were dialyzed into 50% glycerol and storage buffer AB 1X containing 25 mM KCl and were stored at -20°C to avoid any freeze-thaw cycles. They could be readily used for all subsequent experiments that were carried out in this study.

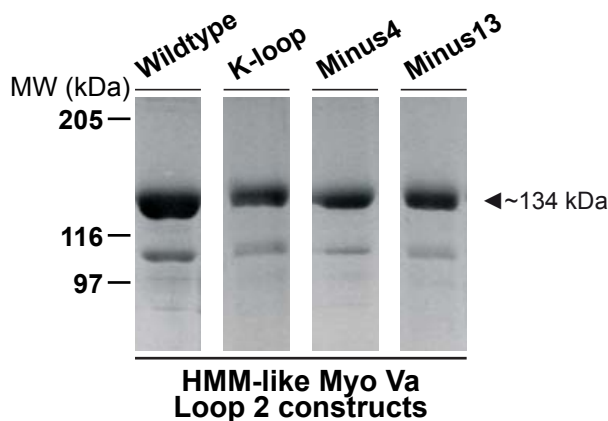


Figure 24. FLAG-affinity protein purification of Myosin Va loop 2 constructs.

Protein was expressed in Sf9-insect cells via the baculovirus expression system, and was FLAG-affinity purified from suspension culture. Cropped images of Coomassie blue-stained polyacrylamide (10%) gels show the respective fractions of the purified and eluted protein of each Myosin Va loop 2 construct (indicated on top). Approximate product size is indicated on the right.

5.1.2.2 Loop 2 is not the prime determinant of the interaction between Myosin V and microtubules

To uncover the role of electrostatic interactions via loop 2 of Myosin Va with microtubules, I assessed the effects of increasing KCl-concentrations on the *Wildtype* and loop 2 mutants by quantifying the number of microtubule-interacting Myosin Va molecules. I discriminated between microtubule-colocalization events (defined as *association* events) and events where association was followed by subsequent diffusion (defined as *diffusion* events). The number of events per microtubule unit length and time period was determined at KCl concentrations of

Results

25, 50, 100 and 200 mM. An increase in ionic strength decreased microtubule association of *all* four constructs (grey bars in Figure 25 and Table 27), though to different extents.

Table 27. Summary of microtubule association and diffusion of various constructs at increasing salt-concentrations.

	Ionic strength condition ($C_{(KCl)}$ in mM)	MT associations (particles · (mm min) ⁻¹)	Myo Va diffusions (particles · (mm min) ⁻¹)	Fraction of Myo Va diffusion events (% of total MT associations)
<i>Wildtype</i>	25	55.4 ± 5.0	17.6 ± 3.7	31.7
<i>K-loop</i>		102.9 ± 10	28.4 ± 5.3	27.6
<i>Minus4</i>		51.3 ± 8.6	7.0 ± 2.4	13.6
<i>Minus13</i>		12.8 ± 2.5	2.1 ± 1.3	16.7
<i>Wildtype</i>	50	45.9 ± 6.1	4.7 ± 1.7	10.3
<i>K-loop</i>		86.5 ± 7.0	21.3 ± 4.4	8.9
<i>Minus4</i>		33.4 ± 5.0	4.3 ± 1.8	12.9
<i>Minus13</i>		13.0 ± 3.3	1.8 ± 1.1	13.9
<i>Wildtype</i>	100	10.9 ± 2.5	0.4 ± 0.4	3.5
<i>K-loop</i>		22.4 ± 4.3	4.6 ± 2.3	20.4
<i>Minus4</i>		25.2 ± 5.2	0.0 ± 0.0	0.0
<i>Minus13</i>		5.6 ± 2.0	0.8 ± 0.8	14.6
<i>Wildtype</i>	200	6.4 ± 2.6	0.6 ± 0.6	9.7
<i>K-loop</i>		10.9 ± 3.8	0.0 ± 0.0	0.0
<i>Minus4</i>		11.2 ± 3.7	0.0 ± 0.0	0.0
<i>Minus13</i>		0.0 ± 0.0	0.0 ± 0.0	n.a.

Values for microtubule association were calculated as mean ± S.E.M. from the total count of microtubule-associated (stationary and diffusing) molecules per unit length and time at the indicated salt-concentrations (*left column*). Among those, the diffusing fraction of motors was determined and calculated as mean ± S.E.M. of the total number of diffusing motors per unit length and time. The portion of diffusing molecules is expressed in % of the total number of microtubule-associated molecules (*right column*). For details of the conditions for counting refer to Section 4.4.1. *n.a.*, not applicable.

The *Minus13* mutant, in particular, showed the most dramatic reduction of microtubule association, even at moderate ionic strength (Figure 25). This behavior can be attributed to a pronounced repulsion between the highly negatively charged motor loop and the negatively charged surface of the microtubule¹⁶⁰.

Results

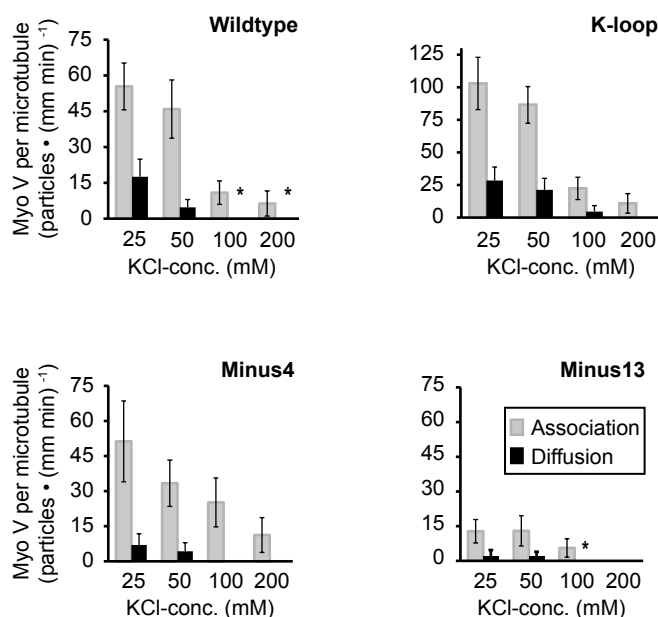


Figure 25. Interaction of Myosin Va with microtubules under increasing ionic strength conditions.

TIRFM movie sequences of single-molecule experiments with 100 nM Cy3-labeled Myosin Va *Wildtype*, *K-loop*, *Minus4* and *Minus13* on Atto488-labeled microtubules under increasing salt concentrations (i.e., 25, 50, 100 and 200 mM KCl), were analyzed for microtubule-association and subsequent diffusion. For this, the total number of microtubule-associated Myosin Va particles (*shaded*) and the number of diffusing particles (*solid*) per unit length of the microtubules are plotted as a function of KCl concentration. (*) indicates that in those cases only one event in total was counted. Error bars represent mean \pm confidence interval ($\alpha=0.95$).

Conversely the *K-loop*, a motif that specifically interacts with the E-hook of microtubules, boosts association with microtubules (Figure 25). Interestingly, even though more than twice as many *K-loop* mutant molecules interact with microtubules compared to the *Wildtype* construct, the strong ionic strength-dependent association behaviors of the two constructs hardly differed from each other. Therefore, it is conceivable that for the *K-loop* mutant possessing an additional and specific microtubule-binding motif, an additional binding mode is triggered on microtubules.

In an alternative approach, the potential of Myosin Va to bind to microtubules in an ionic strength-dependent manner was assayed in microtubule affinity co-sedimentation assays. For this microtubules and the respective Myosin Va loop 2 construct were mixed and ultra-centrifuged through a sucrose cushion (Section 5.1.1.4). Here, microtubules alongside with bound Myosin V protein are found in the pellet fraction, whereas unbound myosin is present in the supernatant. The intensity-quantified data of the SDS-PAGE-resolved pellet and supernatant

Results

fractions imply that both constructs containing a net positively charged loop 2 bind to microtubules in a strongly salt-dependent manner. In contrast, for the *Minus4* and *Minus13* mutant, microtubule binding remains relatively subtle under increasing ionic strength conditions (Figure 26). These findings are in concordance with the behavior observed at the single-molecule level, where for *Wildtype* and *K-loop* Myosin Va, a significant drop in microtubule-association was seen already at 50 mM salt. In contrast, for the *Minus4* and *Minus13* mutant a significant decrease in microtubule association was not observed below 200 mM added salt (Figure 25 and Figure 26). Even though in this assay it was not possible to distinguish association from diffusion events, the results clearly support the findings obtained by the microscopic assay (Figure 25).

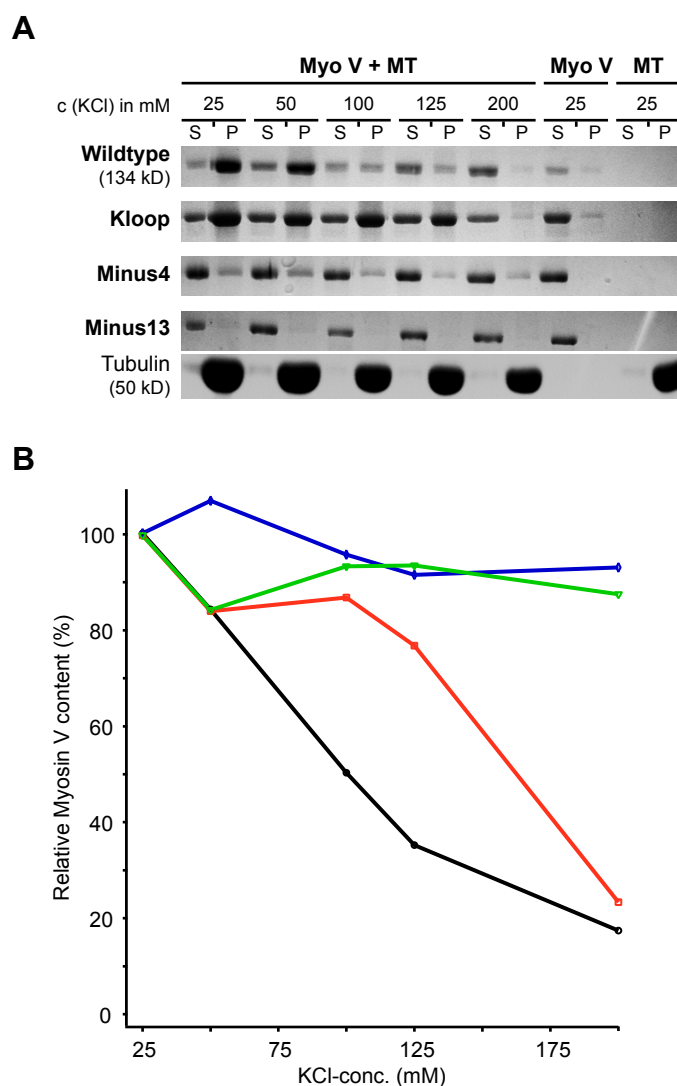


Figure 26. Microtubule-affinity co-sedimentation with Myosin Va loop 2 constructs under increasing ionic strength conditions.

Microtubules (1 μ M) together with purified (850 nM) Myosin Va *Wildtype*, *K-loop*, *Minus4* and *Minus13* under increasing salt concentrations (i.e., 25, 50, 100 and 200 mM KCl) were targeted for co-sedimentation at 280,000 \times g through a sucrose cushion (40%). The microtubule-bound (i.e., the pellet) and unbound (i.e., supernatant) protein fractions were resolved on a polyacryl amide (12%) gel (A) and quantified as described in 4.4.4. To compare the association behavior under increasing ionic strength conditions, the obtained values for each condition and construct were related to the values determined at 25 mM salt condition, which for the illustration was set to 100%. (B) Graph shows normalized relative content of microtubule-bound Myosin Va under increasing ionic strength.

Results

Although these findings indicate that the surface-exposed loop 2 may indeed participate in Myosin Va's affinity for microtubules, the observed attraction cannot be primarily attributed to simple charge-charge interactions between the negatively charged microtubule and the normally positively charged loop 2, for two obvious reasons: first, the positively *and* the negatively charged loop 2 constructs display a similar salt-dependent decrease in microtubule association (grey bars in **Figure 25**); second, despite carrying opposite net charges on loop 2, *Wildtype* and *Minus4* show comparable levels of association at 25 mM salt (**Table 27**).

Taken together, these results make testable predictions for Myosin V's capability to diffuse on the microtubule. If, as previously proposed ¹⁰⁷, the interaction between Myosin V and microtubules were exclusively dependent on electrostatic forces, only *Wildtype* Myosin Va with its positive loop 2 net charge (and most likely also the *K-loop* construct) would be expected to show diffusion on microtubules. However, if this interaction depends either on additional attraction forces or/and domain regions other than loop 2, the two negatively charged constructs, *Minus4* and *Minus13*, should diffuse along the negatively charged microtubule lattice as well.

Indeed, irrespective of their net charge, all four Myosin Va constructs showed diffusion along microtubules (**Figure 25**, black bars). Due to the clear salt-dependent interactions shown here, charge-charge interactions are likely to dominate the binding of Myosin Va to microtubules. Notably, not only at low-salt conditions but also at 100 mM KCl (*Wildtype*, *K-loop* and *Minus13*) and 200 mM KCl (*Wildtype*) diffusion was observed (black bars in **Figure 25**, **Table 27**, Video 1). Hence it can be concluded that electrostatic attraction mediated by loop 2 cannot be considered the sole molecular determinant for microtubule association. Therefore, it cannot be ruled out that other attraction forces (e.g., non-ionic interactions) co-determine Myosin Va's affinity toward microtubules.

Results

5.1.2.3 All Myosin Va loop 2 charge mutants show unperturbed diffusion on microtubules

Next, the behavior of the diffusion events for Myosin V *Wildtype* and the loop 2 mutants on microtubules was characterized (Figure 27, Figure 28, Figure 29, Figure 30 and Figure 32, Videos 2 and 3). In Figure 27 A, a representative image section from the single-molecule assays acquired by TIRF microscopy for each of the Myosin V loop 2 constructs is provided. In addition, Figure 27 B shows an image sequence of *Wildtype* Myosin Va diffusing on microtubules.

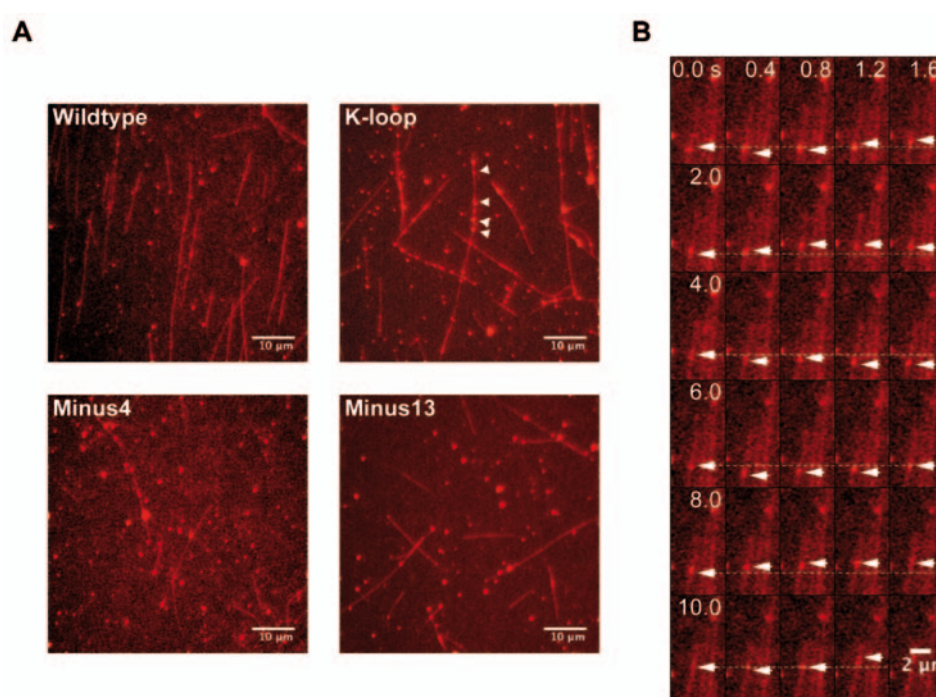


Figure 27. Single-molecule TIRF microscopy of Myosin Va loop 2 constructs on microtubules.

(A) 100 nM Cy3-labeled Myosin Va *Wildtype*, *K-loop*, *Minus4* and *Minus13* (bright particles) were infused into a flow cell containing surface-attached Atto 488-labeled microtubules (dim filaments in background). *White arrowheads* indicate representative single Myosin Va molecules that co-localized with microtubules and subsequently started to show diffusive motion on microtubules. Assay was performed in 25 mM KCl. *Scale bar* represents 10 μm. (B) Representative TIRF microscopy image sequence of a single Cy3-labeled Myosin Va *Wildtype* molecule (indicated by *white arrowheads*) on a microtubule. The position of the myosin at the beginning of each time row is indicated (*white dotted line*). Wave-like dispositions over time reflect characteristic unbiased one-dimensional diffusion behavior of Myosin Va on microtubules. Excitation wavelength in A and B was 532 nm and representative image sections were false-colored. In B the same image section (5 × 10 μm) was taken over time. *Scale bar* represents 2 μm.

The kymographs in Figure 28 A show the traces for the diffusive motion that each of the loop 2 constructs generated during its interaction with microtubules. The

Results

subsequent biophysical and statistical analysis of the diffusive motion of Myosin Va on microtubules is based on such kymograph-derived traces. Diffusion of *Wildtype* yielded a diffusion constant ($D= 0.113 \mu\text{m}^2/\text{s}$) which is in good agreement with previous work¹¹⁰ (Figure 28 B ,Table 28 and Video 2). Strikingly, the analysis demonstrates that the diffusion coefficients of the loop 2 mutants were similar to those of *Wildtype* (Figure 28 B and Table 28). The diffusion-derived single displacements of all three constructs distributed as zero-centered Gaussians, as expected for one-dimensional Brownian motion (Figure 28 B)¹⁶¹.

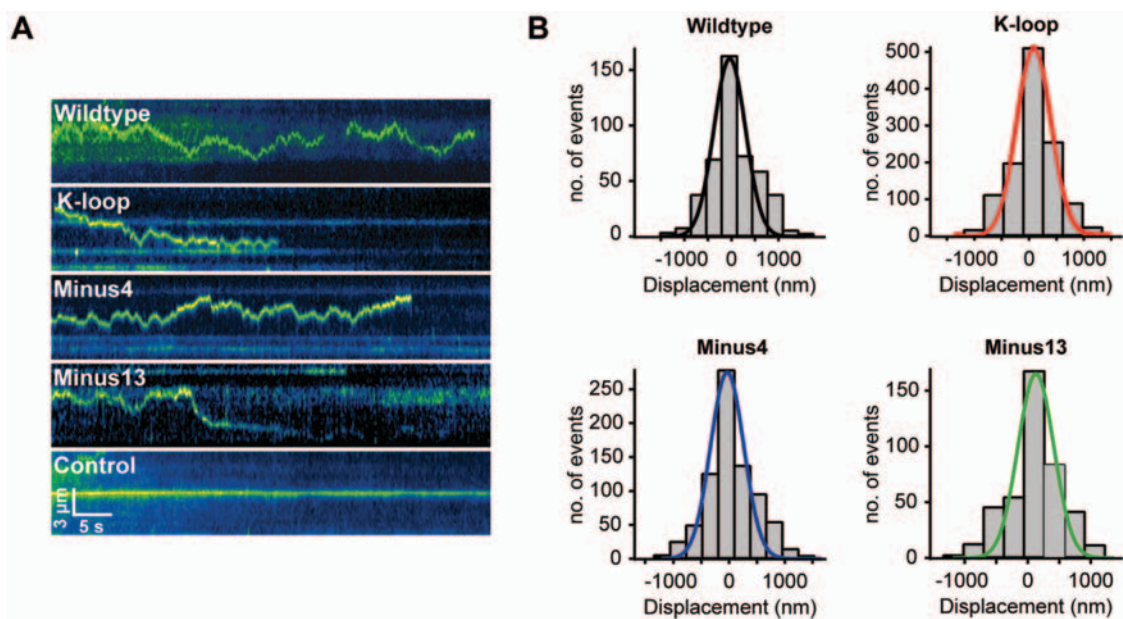


Figure 28. One-dimensional diffusion of Myosin Va loop 2 constructs on microtubules.

(A) Kymographs of sequential frames depicting diffusive movement of single Cy3-labeled Myosin Va *Wildtype*, *K-loop*, *Minus4* and *Minus13* molecules (top to bottom, pseudo-colored green) on Atto488-labeled microtubules in 25 mM KCl. Microtubules are not shown for this purpose. Control represents a stationary, non-diffusing motor molecule on the microtubule. (B) TIRF microscopy movie sequences of single Myosin Va molecules on microtubules in 25 mM KCl were analyzed and then plotted as a displacement histogram. A single Gaussian (solid color-coded lines) was fitted to the data using Equation 7 (Section 4.4.1). From the obtained fit, the variance was used to calculate the diffusion coefficient D according to the equation, $\text{variance} = 2Dt$, where t is the time interval between images, resulting in $D_{\text{WT}} = 0.113 \mu\text{m}^2 \text{s}^{-1}$ ($n = 464$), $D_{\text{K-loop}} = 0.097 \mu\text{m}^2 \text{s}^{-1}$ ($n = 1225$), $D_{\text{Minus4}} = 0.089 \mu\text{m}^2 \text{s}^{-1}$ ($n = 801$) and $D_{\text{Minus13}} = 0.081 \mu\text{m}^2 \text{s}^{-1}$ ($n = 425$). Black, blue and green color-coded fit-lines depict the Gaussian fit for the individual displacement distribution of Myosin Va *Wildtype*, *K-loop*, *Minus4* and *Minus13*, respectively.

Results

Table 28. Key parameters of diffusion of Myosin V (*Wildtype*) and three Myosin V loop 2 mutants.

	Diffusion coefficient (D) ($\mu\text{m}^2 \text{s}^{-1}$)	Maximum speed (V_{max}) ($\mu\text{m} \text{s}^{-1}$)	Scan distance (x_{scan}) (μm)	Association time (t_A) (s)	n Diffusions	n Displacements
<i>Wildtype</i>	0.113 ± 0.004	1.04 ± 0.06	2.21 ± 0.27	14.1 ± 0.5	31	464
<i>K-loop</i>	0.097 ± 0.002 **	0.86 ± 0.04 **	2.05 ± 0.13 *	20.5 ± 1.0 ***	77	1225
<i>Minus4</i>	0.089 ± 0.003 ***	0.99 ± 0.06 *	2.95 ± 0.28 *	23.8 ± 3.2 ***	35	801
<i>Minus13</i>	0.081 ± 0.003 ***	0.84 ± 0.06 **	2.07 ± 0.23 *	16.2 ± 0.8 **	32	425
<i>on S-microtubules</i>						
<i>Wildtype</i>	0.226 ± 0.006 ***	1.21 ± 0.09 *	3.02 ± 0.34 *	12.4 ± 2.7 *	20	327

Diffusion coefficients (D) were measured from the variance of the Gaussian fit function of the displacement histogram (**Figure 28 B**). Values for maximum speed (V_{max}) reflect the maximum displacement along a microtubule during one frame interval and diffusion event. Scan distances (x_{scan}) were calculated as the distance between the two extreme positions the motor has scanned on the microtubule during one diffusion event. Association times (t_A) represent the total time a Myosin V molecule spent on the microtubule during one diffusion event. Mean values for t_A were measured from the exponential fit of the plotted histogram of single t_A -values (**Figure 30**). Diffusion events are defined as events during which the Myosin V molecule has bound to the filament and subsequently started diffusing. Diffusion was quantified by single displacement measurements. Parameters of Myosin V diffusion on subtilisin-treated microtubules (*S-microtubules*) for *Wildtype* are shown in the bottom part. All parameters were obtained from experiments in 25 mM KCl. Values represent mean \pm S.E.M. Statistical significance at * $P > 0.05$, ** $P < 0.05$ and *** $P < 0.005$ vs. *Wildtype* was determined using Student's t-Test.

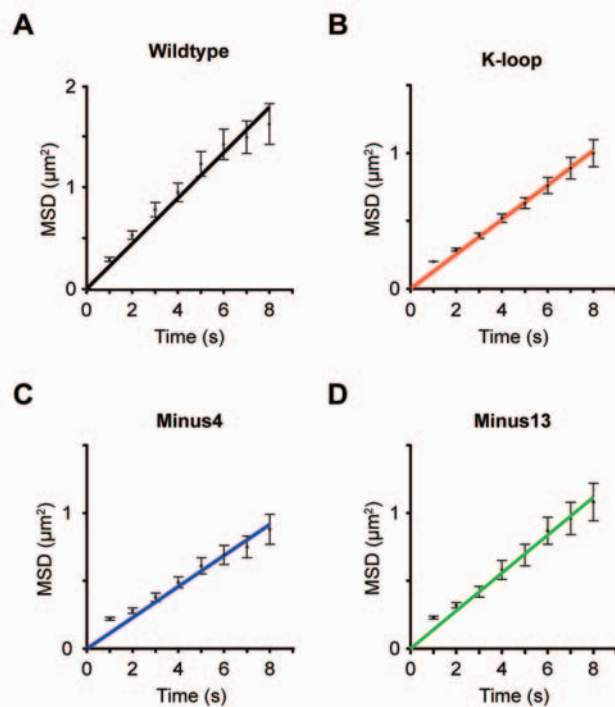


Figure 29. Mean-squared displacement analysis of diffusive motion of the four Myosin Va loop 2 constructs on microtubules.

(A-D) The mean-squared displacement (MSD) data of Myosin Va *Wildtype*, *K-loop*, *Minus4* and *Minus13* are plotted versus time, with the individual slopes providing an estimate of the respective D -values. The following D -values were calculated: $D_{Wildtype} = 0.11 \mu\text{m}^2 \text{s}^{-1}$ ($\pm 0.004 \mu\text{m}^2 \text{s}^{-1}$ S.D.), $D_{K-loop} = 0.07 \mu\text{m}^2 \text{s}^{-1}$ ($\pm 0.001 \mu\text{m}^2 \text{s}^{-1}$ S.D.), $D_{Minus4} = 0.06 \mu\text{m}^2 \text{s}^{-1}$ ($\pm 0.002 \mu\text{m}^2 \text{s}^{-1}$ S.D.) and $D_{Minus13} = 0.07 \mu\text{m}^2 \text{s}^{-1}$ ($\pm 0.002 \mu\text{m}^2 \text{s}^{-1}$ S.D.). Data were obtained from single-molecule TIRFM experiments with 100 nM Cy3-labeled Myosin Va on Atto488-labeled microtubules in 25 mM KCl. Error bars represent the S.E.M. of the squared displacement values.

Results

Additional support came from the linear increase in mean square displacement (*MSD*) over time (Figure 29)^{162,163,164}. As expected, by calculating *D* from the slopes in the *MSD*-plots, the validity of the Gaussian-based *D*-value calculations could be confirmed.

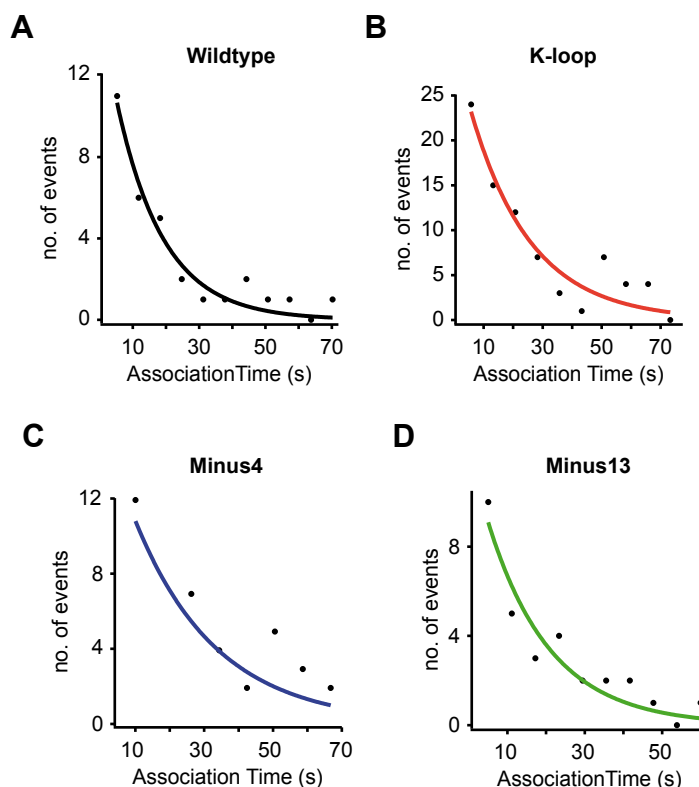


Figure 30. Interaction lifetime of diffusing Myosin Va on microtubules.

(A-D) The distribution of the association times (t_A) for Myosin Va *Wildtype*, *K-loop*, *Minus4* and *Minus13* were plotted as histograms. Data were obtained from single-molecule TIRFM experiments with 100 nM Cy3-labeled Myosin V on Atto488-labeled microtubules in 25 mM KCl. Exponential curves fitted to the respective histograms (solid lines) yield mean t_A -values of 14.1 s (n= 31), 20.5 s (n=77), 23.8 s (n= 35) and 16.2 s (n= 32) for Myosin Va *Wildtype* (A), *K-loop* (B), *Minus4* (C) and *Minus13* (D), respectively.

During diffusion, the time of association with the microtubule (t_A) for all four constructs distributed exponentially (Figure 30). Individual mean values of t_A (Table 28) ranged from 14.1 s to 23.8 s, with t_A of *Wildtype* being the shortest. Finally, the average distance scanned during diffusional events did not vary significantly amongst *Wildtype* and *Minus13* and was only slightly larger for *Minus4* (Table 28). Furthermore, in microtubule-stimulated ATPase assays it could be excluded that microtubules stimulate Myosin Va's ATPase activity (Figure 32).

Results

Control experiments confirmed that diffusion was not caused by the antibody that coupled the motor to the fluorophore, nor did the antibody display any specific association with microtubules. In line with the Myosin V-microtubule *association* analysis, the *diffusion* analysis strongly supports the notion that the interaction between the motor and the microtubule is not restricted to loop 2-conveyed electrostatic forces. Most notably, *Minus13*, a construct carrying 13 negative net charges on loop 2, shows a similar diffusion behavior as the positively charged *Wildtype* (Figure 28 B).

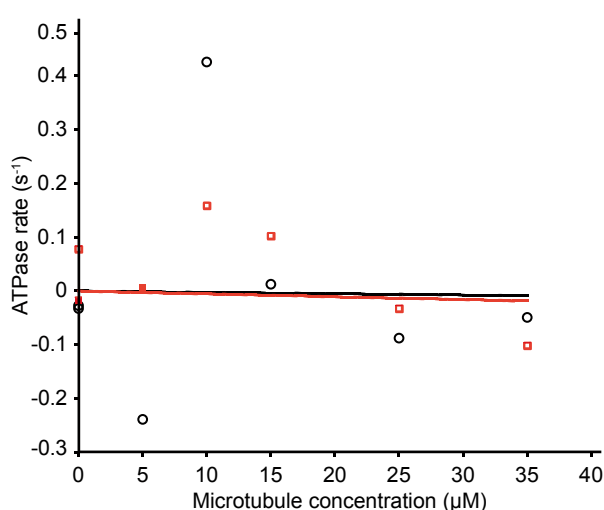


Figure 32. ATPase activity of Myosin Va on microtubules.

Microtubule-activated ATPase for Myosin Va *Wildtype* (black, open circles) and *K-loop* (orange, open squares) was measured with the NADH-coupled enzymatic assay and plotted as a function of microtubule concentration (Myosin Va concentration, 100 nM). The data were fitted to the Michaelis-Menten equation. As expected, Myosin V's ATPase activity could not be stimulated by microtubules.

In addition to the TIRF microscopy experiments, also electron microscopy of Myosin Va on microtubules was carried out. A representative negative stain image of the *Wildtype* Myosin Va construct is provided in Figure 31, illustrating Myosin Va's ability to bind to microtubules.

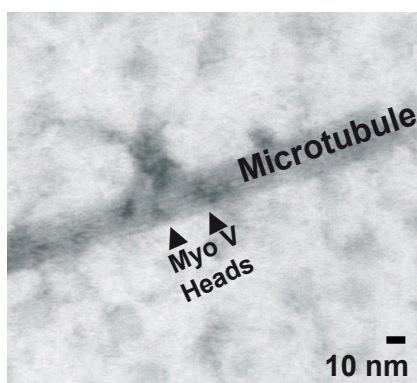


Figure 31. Electron micrographs of Myosin Va on microtubules.

HMM-like Myosin Va *Wildtype* (160 nM) was mixed with microtubules (approx. 1 μM) and thereafter briefly centrifuged (low-speed) to remove unbound motor. As desired, different dilutions of the pellet fraction were used for the preparation of negative-stains. Representative negative stain image shows an HMM-like Myosin Va molecule bound to the surface of a microtubule (as indicated). Scale bar represents 10 nm.

Results

Next, the proposed role of the negatively charged E-hooks (Ali *et al.*, 2007) in tethering Myosin V to the microtubule surface was assessed.

5.1.2.4 Myosin Va diffusion takes place without the help of E-hooks

To test if the negatively charged E-hooks play a substantial role in microtubule association and diffusion of the Myosin V constructs, we made use of limited proteolysis by subtilisin to generate S-microtubules that lack the E-hook^{119,162}. E-hook removal was confirmed by SDS-PAGE and Western-blot analysis (Figure 33)
113,119,145

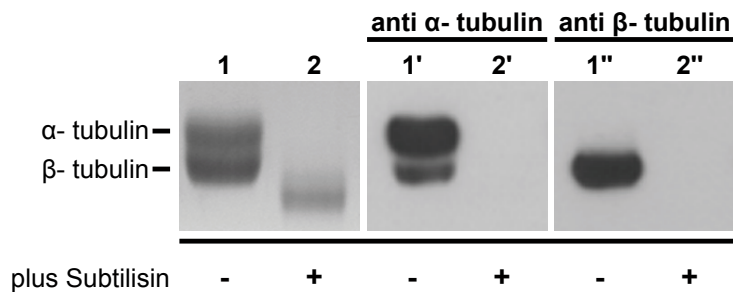


Figure 33. Removal of the Carboxy-terminal E-hook from microtubules.

(Left panel) Coomassie-blue stained SDS polyacrylamide gel (12%) shows untreated microtubules (lane 1), and microtubules after subtilisin-treatment (lane 2). (Middle and right panel) Western-blot analysis of both lanes with anti-α or anti-β tubulin antibodies. Subtilisin-treatment resulted in the complete loss of epitope reactivity, hence complete E-hook removal can be assumed.

In favor of the non-ionic attraction model, the absence of E-hooks does not interfere with the ability of *Wildtype* to associate with microtubules (Figure 34 and Table 29). Moreover, for all four loop 2 constructs the number of associated motors per microtubule unit length leveled off (grey bars in Figure 34, Table 29).

Results

Table 29. Summary of association and diffusion of various constructs on S-microtubules.

	MT associations (particles · (mm min) ⁻¹)	Myo V diffusions (particles · (mm min) ⁻¹)	Fraction of Myo V diffusion events (% of total MT associations)
<i>Wildtype</i>	58.2 ± 6.7 *	7.3 ± 2.4 **	12.5
<i>K-loop</i>	49.3 ± 6.5 *	3.1 ± 1.5 **	6.3
<i>Minus4</i>	65.0 ± 6.9 *	0.0 ± 0.0 ***	0.0
<i>Minus13</i>	50.8 ± 6.5 ***	0.0 ± 0.0 *	0.0

Values for microtubule association and diffusion were calculated as described in **Table 27**. Data were obtained from single-molecule studies on subtilisin-treated microtubules (*S-microtubules*) in 25 mM KCl. Significance levels in association and diffusion on *S-microtubules* vs. untreated microtubules (*P > 0.05, **P < 0.05 and ***P < 0.005) (**Table 27**) were determined using Student's t-Test. For details of the counting conditions applied refer to Section 4.4.1.

For the most negatively charged *Minus13* construct, E-hook removal resulted in a significant increase in microtubule association by 75 % (**Table 27** vs. Table 29). For the *K-loop* construct with its E-hook-specific motif, on the other hand, the association with S-microtubules decreased significantly by 50 % (p < 0.005) (**Table 27** vs. Table 29).

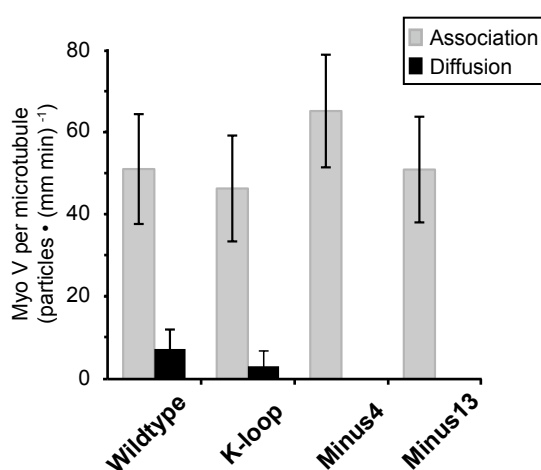


Figure 34. Interaction of Myosin Va with S-microtubules.

TIRFM movie sequences of single-molecule experiments with 100 nM Cy3-labeled Myosin V *Wildtype*, *K-loop*, *Minus4* and *Minus13* on Atto488-labeled S-microtubules, in 25 mM KCl were analyzed for microtubule-association and subsequent diffusion. The total number of S-microtubule-associated and diffusing Myosin V particles per unit length of the microtubules is plotted as category plot for the respective Myosin V constructs. Error bars represent mean ± confidence interval (α = 0.95).

Therefore, as already predicted and assumed from the findings in section 5.1.2.2, the observed boost in association with untreated microtubules ceases as soon as the K-loop-specific binding-motif on microtubules, the E-hook, is removed.

Myosin Va's attraction for microtubules lacking the E-hook was also assayed by means of microtubule-affinity co-sedimentation assays under increasing salt conditions (**Figure 35**, for experimental details, see Section 5.1.1.4).

Results

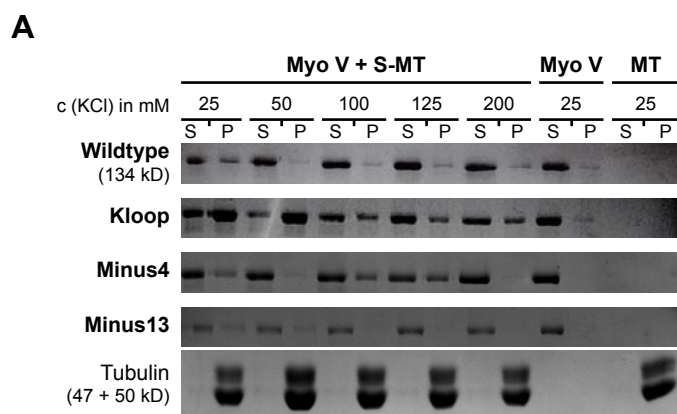
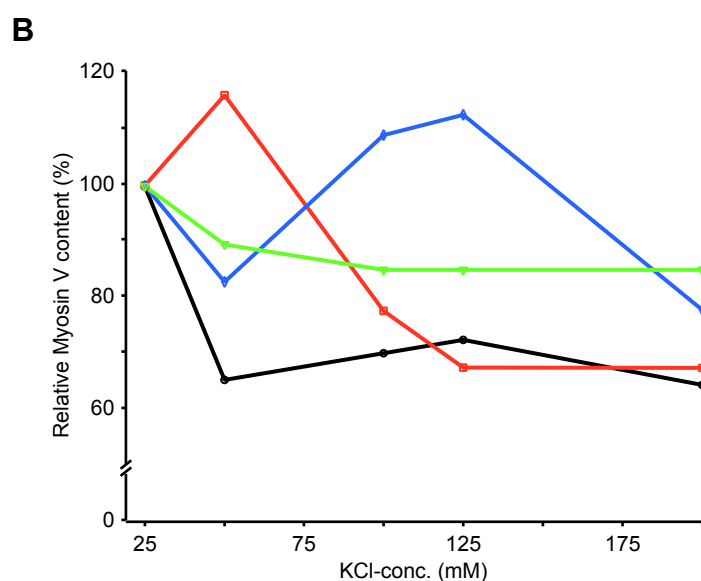


Figure 35. Affinity co-sedimentation assays with various Myosin Va loop 2 constructs and S-microtubules under increasing ionic strength conditions.

1 μ M S-microtubules and 850 nM purified Myosin Va *Wildtype*, *K-loop*, *Minus4* and *Minus13* under increasing salt concentrations (i.e., 25, 50, 100 and 200 mM KCl) were targeted for co-sedimentation and analyzed as described for **Figure 26**. To compare the association behavior under increasing ionic strength conditions, the obtained values for each condition and construct were related to the values determined at 25 mM salt condition, which for the illustration was set to 100%. (**B**) Graph shows normalized relative content of microtubule-bound Myosin Va under increasing ionic strength. S-microtubules were generated as described (Section 4.3.2.4).



In contrast to the behavior on untreated microtubules, neither positively nor negatively charged loop 2 mutants show a salt-dependent association with S-microtubules (**Figure 26**). Here the lowest level of relative Myosin Va content was about 65% (*Wildtype*, at 50 mM salt), whereas on untreated microtubules at 200 mM salt, microtubule-association of the *Wildtype* construct was reduced to 20%. Interestingly, for *Minus4* and *Minus13* the association at increasing ionic strength hardly differed from that on untreated microtubules (**Figure 26**). The fluctuations in values for relative Myosin V content are reflected in the standard deviations of the data of **Figure 34** and **Table 29** and are most likely due to experimental difficulties arising from dealing with S-microtubules.

Most importantly, the removal of E-hooks did not interfere with the ability of *Wildtype* or *K-loop* Myosin V to diffuse along S-microtubules. The diffusion behavior of *Wildtype* on S-microtubules meets all the criteria of a one-dimensional

Results

diffusion process (Figure 36) ^{107,161,162,163,164}.

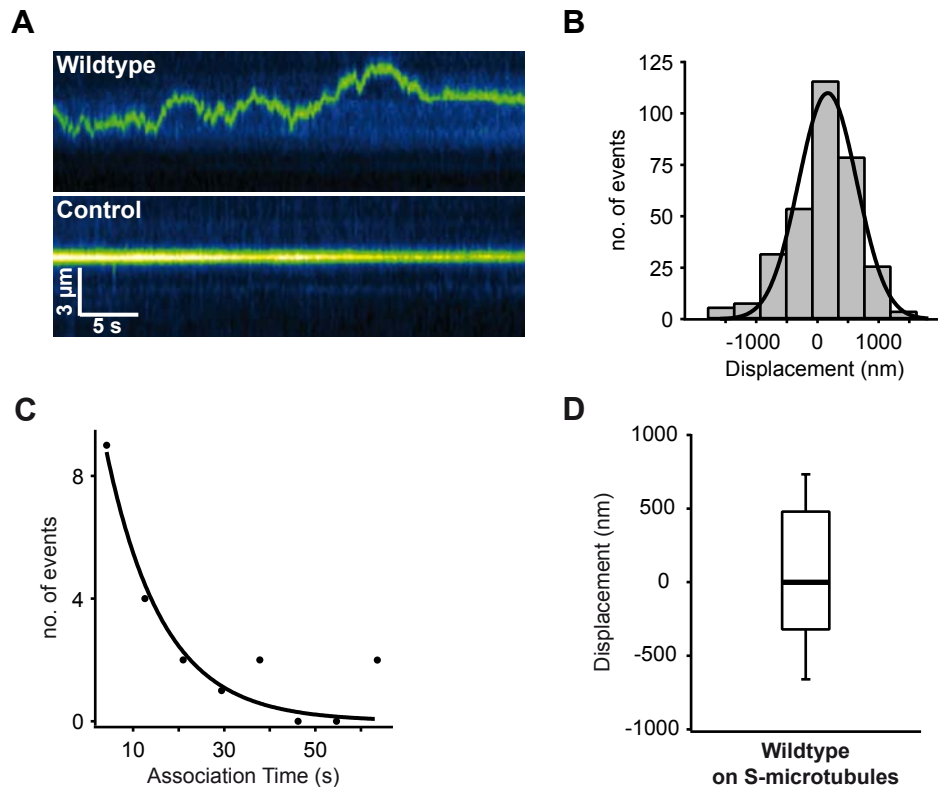


Figure 36. One-dimensional diffusive motion of Myosin Va on microtubules lacking the E-hook.

(A) Kymograph of sequential frames depicting the diffusive motion of a single Cy3-labeled Myosin Va *Wildtype* molecule (pseudo-colored green) on Atto488-labeled microtubules (for this purpose not visualized). Control represents a stationary, non-diffusing motor molecule on the microtubule. (B) The displacement between successive image frames of diffusive movements for Myosin Va *Wildtype* on S-microtubules was determined. TIRF microscopy movie sequences of 100 nM Cy3-labeled Myosin Va *Wildtype* on Atto488-labeled microtubules were analyzed and plotted as a displacement histogram. The diffusion coefficient D was calculated according to the equation, $\text{variance} = 2Dt$, where t represents the time interval between images. The variance was obtained from the Gaussian fit (solid line), resulting in $D = 0.226 \mu\text{m}^2 \text{s}^{-1}$ ($n = 327$). (C) The distribution of the values for t_A is plotted as histogram with an exponential curve fit (solid line), yielding a mean t_A -value of 12.4 s ($n = 20$). (D) Here, the displacement distribution of Myosin Va *Wildtype* on S-microtubules is plotted as Box-Whisker Plot, where the top and bottom of the boxes indicate the 75 and 25 percentile, the whiskers indicate the 90 and 10 percentile, while the solid line within the box represents the median. As it was observed for Myosin Va *Wildtype* on untreated microtubules (Figure 28 B), also on S-microtubules Myosin Va *Wildtype* exhibits no net displacement during diffusion and hence the median centers at zero.

The maximum speed of Myosin V diffusion on S-microtubules ($1.21 \pm 0.09 \mu\text{m} \text{s}^{-1}$) is higher than that on untreated microtubules and shows a trend towards prolonged scan distances ($3.02 \pm 0.34 \mu\text{m}$). However, the average association time of 12.4 s remained essentially unchanged (Table 28 and Figure 36). Notably, the diffusion coefficient $D = 0.226 \mu\text{m}^2/\text{s}$ was twice as high as that of *Wildtype* on untreated microtubules (Table 28 and Figure 36).

5.1.2.5 Non-electrostatic attraction forces contribute to the interaction of Myosin Va with microtubules

The striking observation that irrespective of the net charge of loop 2 all four constructs bind to S-microtubules, while only *Wildtype* and *K-loop* (Figure 34, Figure 36, Table 29 and Video 4) diffuse, raises the question whether additional attraction forces besides electrostatics contribute to the interaction between Myosin V and microtubules. I propose that due to the E-hook removal, the formerly homogeneously negatively charged microtubule is now marked by negative and also positive surface charges^{160,165}. Hence, formerly prevalent electrostatic *repulsion* forces (negative loop 2 vs. negative E-hooks) are now eliminated and electrostatic *attraction* forces (negative loop 2 vs. positive patches on the microtubule surface) are free to exert their effects. The absence of the 4 nm E-hook spacers would enhance additional, non-ionic attraction forces that have strong effects over short distances, thereby preventing the individual molecule from advancing from an associative to a diffusive state (as is the case for *Minus4* and *Minus13*) (Figure 34). Under such circumstances, only constructs bearing a residual ionic repulsive capacity (positive loop 2 vs. positive patches on the microtubule surface), such as *Wildtype* or *K-loop*, display diffusion (Figure 34). Taken together, the data presented here suggest that additional, non-electrostatic attraction forces contribute to Myosin V's interaction with microtubules.

5.1.2.6 A negative charge on loop 2 impairs the Myosin Va interaction with actin filaments whereas Myosin Va carrying a Kinesin-loop is functional on F-actin

To assess the intrinsic functionality of the four Myosin Va loop 2 constructs, single molecule motility as well as ATPase activity measurements on F-actin were carried out. In Figure 38 A, a representative image from the single-molecule assays acquired by TIRF microscopy for each of the respective Myosin V loop 2 constructs on F-actin is provided. In addition, in Figure 38 B an image sequence of *Wildtype* Myosin Va showing directed walking along one or even two actin filaments (see also, Video 8).

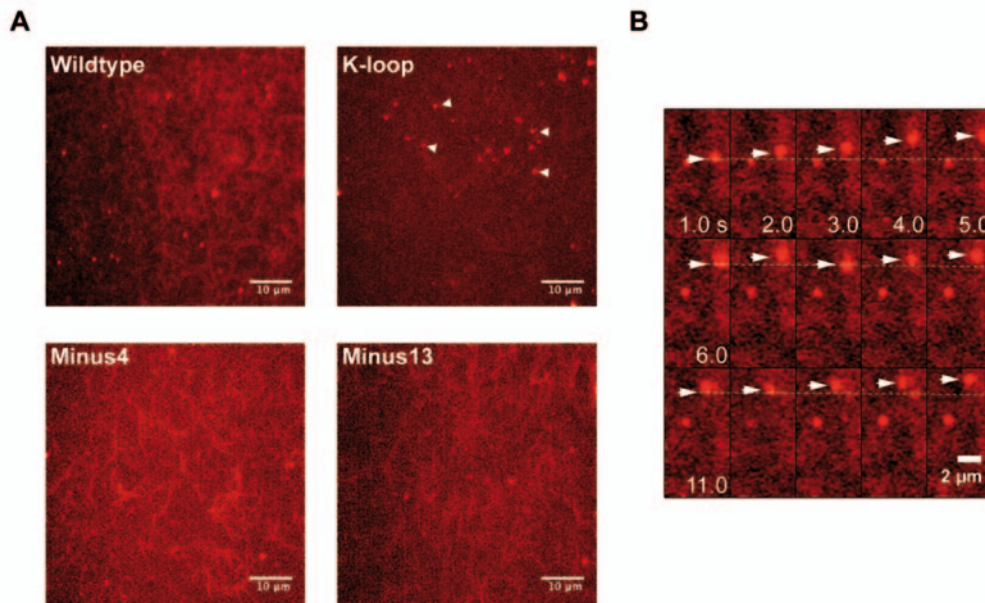


Figure 38. Single-molecule TIRF microscopy of Myosin Va loop 2 constructs on F-actin.

(A) 100 nM Cy3-labeled Myosin Va *Wildtype*, *K-loop*, *Minus4* and *Minus13* (bright particles) was infused into a flow cell containing surface-attached Atto488-labeled F-actin (fuzzy filaments in background). *White arrowheads* indicate representative single Myosin Va molecules that co-localized with actin filaments and subsequently exhibited directed movements on F-actin. Assays were performed in 25 mM KCl and 1 mM ATP. *Scale bar* represents 10 μm . (B) Representative TIRF microscopy image sequence of a single Cy3-labeled Myosin Va *Wildtype* molecule (indicated by *white arrowheads*) on F-actin. The position of the motor molecule at the beginning of each time row is indicated (*white dotted line*). The continuous edging up of displacements over time reflects the characteristic processive walking behavior of Myosin Va on actin filaments. Excitation wavelength in A and B was 532 nm and representative image sections were false-colored. In B the same image section (5 \times 10 μm) was taken over time. *Scale bar* represents 2 μm .

As for the interaction with microtubules, in **Figure 37** a representative negative stain image of the *Wildtype* Myosin Va construct, is shown. Both heads bound to the actin filament and also the motor's stalk region is clearly visible.

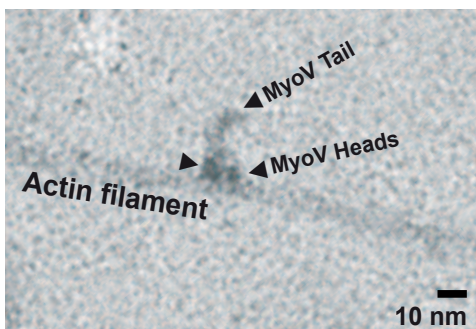


Figure 37. Electron micrographs of Myosin Va on F-actin.

HMM-like Myosin Va *Wildtype* (160 nM) was mixed with F-actin and 1 mM AMP-PNP. The unbound motor fraction was removed by brief (low-speed) centrifugation. As desired, different dilutions of the pellet fraction were used for the preparation of negative-stains. Representative negative stain image shows an HMM-like Myosin Va molecule that is bound to an actin filament (as indicated). *Scale bar* represents 10 nm.

Results

Table 30. Summary of behavior of Myosin Va loop 2 constructs on F-actin.

	Velocity (nm s ⁻¹)	Runlength (μm)	n	K _m (μM)	k _{cat} (mol of ATP s ⁻¹ · (mol of myosin) ⁻¹)
<i>Wildtype</i>	230 ± 4	1.41 ± 0.04	62	2.6	4.3
<i>K-loop</i>	140 ± 4 ***	1.51 ± 0.04 *	65	7.4	4.5
<i>Minus4</i>	n.m.	n.m.	n.m.	n.m.	n.m.
<i>Minus13</i>	n.m.	n.m.	n.m.	n.m.	n.m.

Velocities and runlengths of the single-molecule measurements on F-actin were obtained at 1 mM ATP. Values for velocity and runlength are mean ± S.E.M. from Gaussian and exponential fits to the data (**Figure 41**), respectively. *n* is the number of processive runs. *K_m* represents the actin concentration at which the ATPase rate is half the maximal rate, determined from the Michaelis-Menten curve fit (**Figure 39**). *k_{cat}* shows the maximum rate of ATP turnover as determined from fitting the data to the Michaelis-Menten equation (**Figure 39**). *n.m.*, not measurable.

In line with previous studies where a decrease of the positive net charge on loop 2 led to a diminished affinity for actin^{35,111,166}, in Myosin V constructs carrying a negative net charge on loop 2, actin-stimulated ATPase activity was nearly (*Minus4*) or completely (*Minus13*) abolished (**Figure 39** and Table 30).

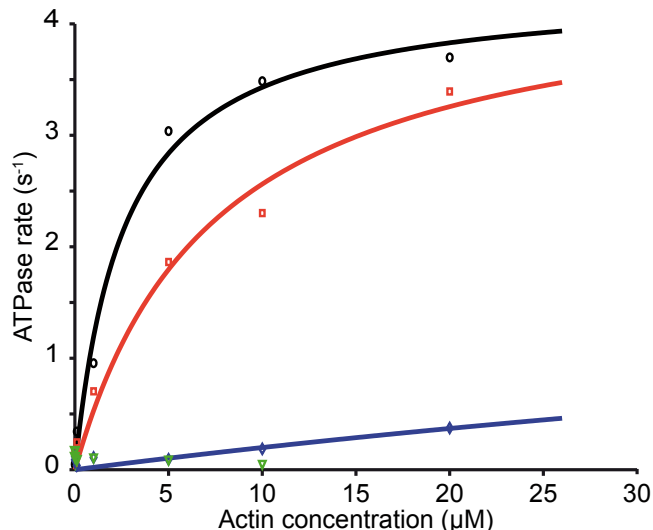


Figure 39. ATPase activity measurements of the four Myosin Va loop 2 constructs on F-actin.

Actin-activated ATPase for Myosin Va *Wildtype* (black, open circles), *K-loop* (orange, open squares), *Minus4* (blue, open diamonds) and *Minus13* (green, open triangles) were measured with the NADH-coupled enzymatic assay and plotted as a function of actin concentration (Myosin V concentration, 100 nM). The data were fitted to the Michaelis-Menten equation to determine the maximum ATPase rate (*k_{cat}*) and the actin concentration at which Myosin Va is activated half-maximally (*K_m*). Due to the negatively charged loop 2 motifs of *Minus4* and *Minus 13* hardly any and no stimulation by actin was observed, respectively. Data-set shown is representative and was reproducible.

Results

Accordingly, in *in vitro* motility studies only occasional brief attachments of single *Minus4* and *Minus13* molecules were recorded, but no single molecule runs (Figure 38 A, Video 5). Thus only a positively charged loop 2 promotes a productive interaction with actin.

The kymographs in Figure 40 show the traces of directed movement of *Wildtype* and *K-loop* Myosin Va (see also, Videos 6, 7 and 8) constructs during their interaction with actin filaments. Biophysical and statistical analyses of these movements of Myosin Va were performed using such kymograph-derived traces.

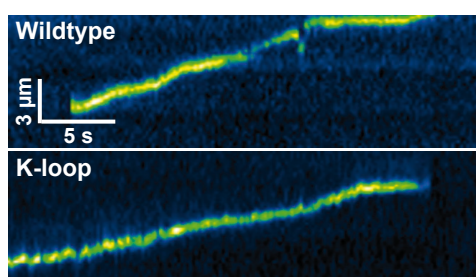


Figure 40. Processive walking of Myosin V *Wildtype* and *K-loop* on F-actin.

Kymographs of representative walking events of single Cy3-labeled Myosin Va *Wildtype* and *K-loop*, on Atto488-labeled F-actin in buffer containing 25 mM KCl and 1mM ATP. On F-actin, no movement for *Minus4* and *Minus13* was observed and thus no kymographs are depicted.

Strikingly, with its +2 net charge, the *K-loop* mutant was not only capable of binding to actin, it also displayed numerous walking events (Figure 40, Figure 41, Videos 6 and 7). However, its average velocity was decreased compared to *Wildtype* (140 vs. 230 nm s⁻¹) (Figure 41 and Table 30), while the runlength distribution coefficient remained essentially unchanged (Figure 41 and Table 30).

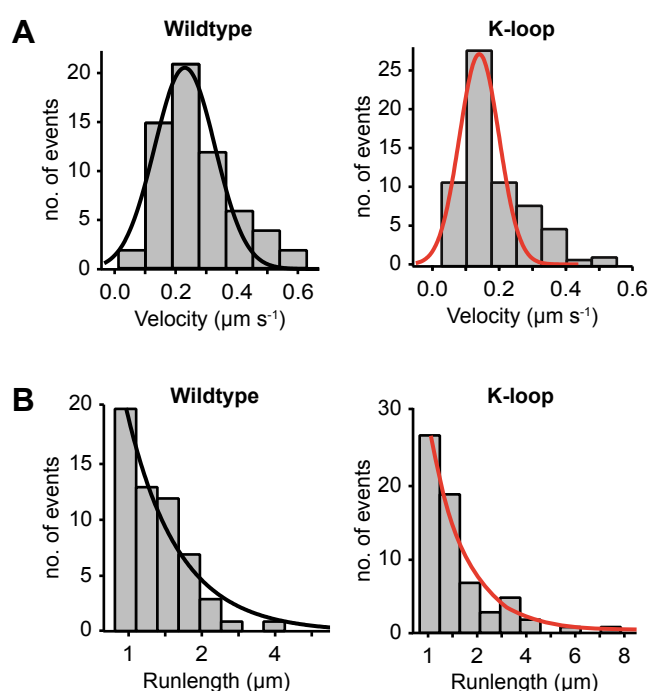


Figure 41. Biophysical analysis of processive walking behavior of Myosin V *Wildtype* and *K-loop* on F-actin.

Velocity (A) and runlength (B) distributions of Myosin Va *Wildtype* (left panels) and *K-loop* (right panels) were plotted as histograms. Data were obtained from single-molecule TIRFM experiments, where 100 nM Cy3-labeled Myosin Va was incubated with Atto488-labeled F-actin in 25 mM KCl and 1 mM ATP. In (A) the data were fitted to a single Gaussian (according to Equation 7), yielding a mean velocity of 0.23 μm² s⁻¹ (n= 62) and 0.14 μm² s⁻¹ (n= 65) for *Wildtype* and *K-loop*, respectively. For the runlength distribution in (B) an exponential curve was fitted to the histograms (solid lines), resulting in mean values of 1.41 μm (n= 62) and 1.51 μm (n= 65) for *Wildtype* and *K-loop*, respectively.

Results

The *in vitro* single-molecule velocity and runlength measurements (Table 30), as well as the ATPase activity values of HMM-like *Wildtype* Myosin Va were in good agreement with those reported previously (Figure 39 and Table 30)^{38,44,45,111,167}.

When comparing the ATPase activity measurements of the *Wildtype* and *K-loop* construct, the K_m -value of *K-loop* was decreased three-fold. This finding points to a decreased binding affinity of *K-loop* for actin, while yielding almost the same k_{cat} -value as the *Wildtype* construct (Figure 39 and Table 30).

In summary, only a positively charged loop 2 strongly promotes productive interaction with actin, even if it comes from the loop of a kinesin motor.

5.2 Studying the effects of Calcium-/Calmodulin-dependent Kinase II- α on melanosome-associated Myosin V

Karcher and colleagues (2001)¹²¹ showed that incubation of melanosomes with mitotic cell extract from *Xenopus l.* oocytes leads to the release of melanosome-associated Myosin V. In addition, the authors provided evidence that the observed release was due to Calcium-/Calmodulin-dependent Kinase II- α (CaMKII- α)-mediated phosphorylation of a specific Serine residue within the tail domain of Myosin V. With this in mind, I decided to take a closer look at the role of CaMKII- α in melanosome transport.

Therefore, my primary goal was to set up an assay where melanosomes that contain Myosin Va are targeted for CaMKII- α -mediated release *in vitro*. Such a method would for the first time allow for the specific manipulation of melanosome transport *in vitro*. Thus it would be finally possible to determine *in vitro* using a native cellular cargo, if and how Myosin V might assist the Kinesin-2-driven cargo transport on microtubules (for a detailed protocol, refer to Section 4.3.5.6).

5.2.1 Results

5.2.1.1 Cloning and purification of baculovirus-expressed CaMKII- α

Most studies that in the past dealt with the characterization of CaMKII, used protein that had been purified from rat brain, simply because in the forebrain CaMKII composes up to 1% of the total protein¹⁶⁸. However because of two fundamentally important reasons, in this work I aimed on setting up a protocol for the purification of baculovirally expressed recombinant CaMKII- α : i) enhancing the yield of total kinase protein, while lowering the required labor time; and ii) not being reliant on supply of rat brain as a natural source. This section provides a brief summary of the cloning, and purification procedure of baculovirus-expressed CaMKII- α .

The coding sequence of CaMKII- α (kindly provided by Prof. Y. Hayashi, RIKEN institute, Saitama, Japan), was originally blunt-end cloned into the pBluescript SK (-) vector via EcoRI. Therefore, the coding sequence, which at this point still also contained a portion of non-coding region (approx. 200 bases), was retrieved via restriction enzyme-mediated digestion with EcoRI (Figure 42 A).

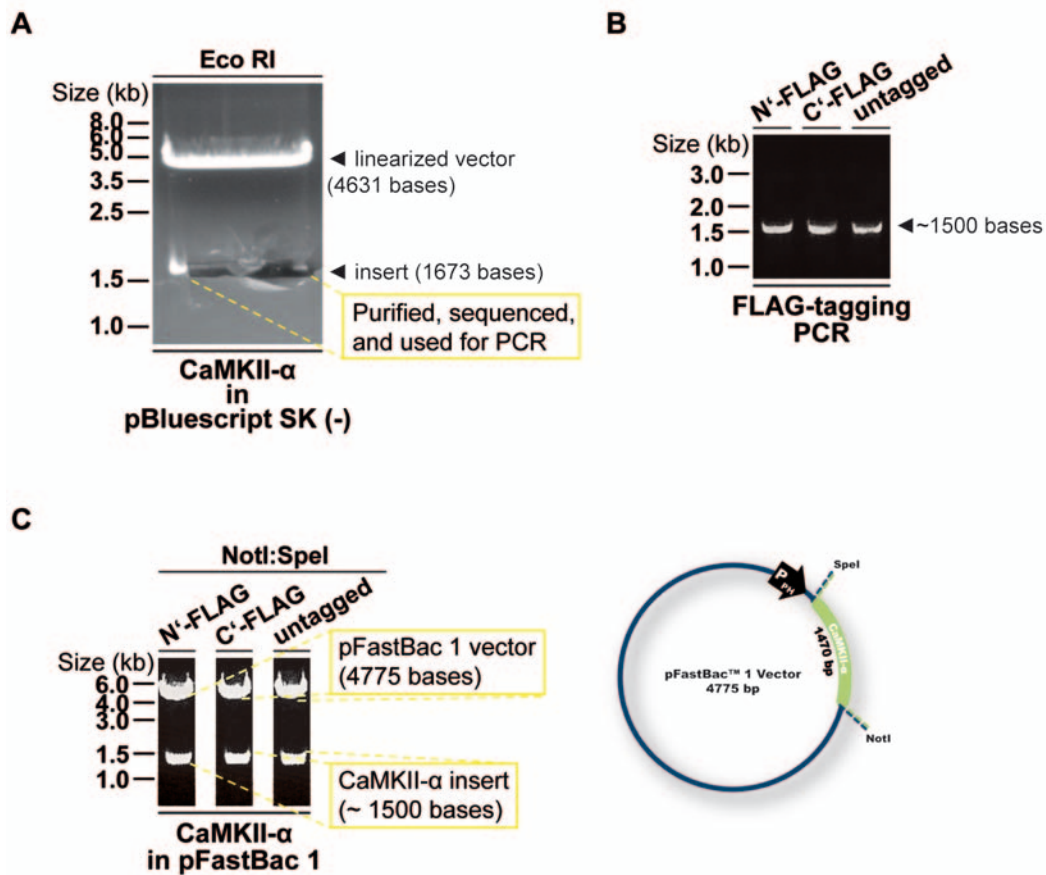


Figure 42. Cloning of FLAG-tagged CaMKII- α for baculovirus expression.

(A) The CDS (and approx. 200 bases non-coding region) encoding for CaMKII- α was retrieved from the pBluescript SK (-) vector by restriction enzyme-mediated digest with EcoRI. The purified fragment of size 1673 bp subsequently was sequenced and used as template during further cloning. (B) The sequence encoding for the FLAG-tag motif was fused 5' and 3' of the CaMKII- α gene, by using forward and reverse primers containing respectively SpeI- and NotI-restriction sites along with the FLAG-encoding sequence. The amplified product (approx. size 1500 bp) was used for the subsequent cloning into the pFastBac 1 vector. (C) Successful cloning of the FLAG-tagged as well as untagged CaMKII- α gene into pFastBac 1 was confirmed via restriction enzyme-mediated test digestion with SpeI and NotI (*left part*). A schematic of the insert and vector along with the respective product sizes is provided on the *right*.

To amplify the coding region from the template sequence and to add the sequence encoding for the FLAG-tag (either to the 3' or 5' ends), PCR was carried out (for a complete list of primers as well as details on the specific PCR performed, see Sections 3.4 and 4.2.2.2.1). An N', C'FLAG-tagged as well as an untagged version containing SpeI- (3') and NotI-restriction sites (5'), were generated (Figure 42 B). The two FLAG-tagged constructs are 1470 bp long, the untagged version only 1437 bp. All three constructs were pre-digested with SpeI and NotI, and purified as described (4.2.3.1 and 4.2.2.5). Via their restriction sites

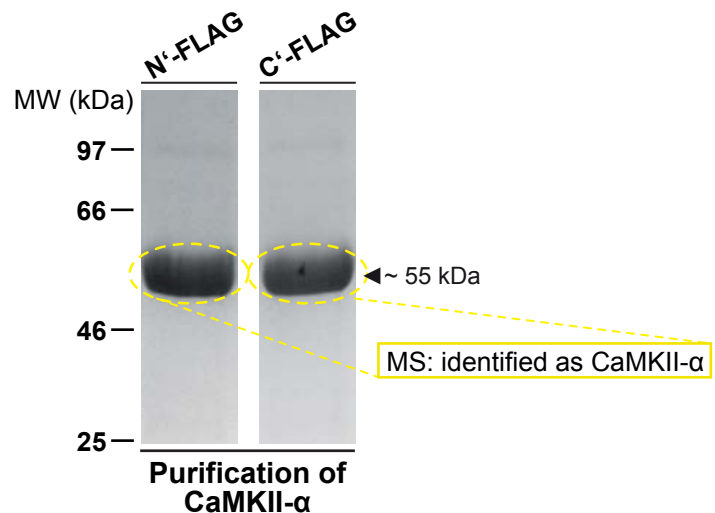
Results

NotI and SpeI, each of the three insert sequences was cloned under the control of the polyhedrin promoter of the baculovirus-specific transfer vector pFastBac 1 (Figure 42 C, see Section 7 for vector maps).

FLAG-affinity purification of the CaMKII- α protein was carried out from 300 to 350 ml of Sf9 cell suspension culture (for details of the purification protocol, refer to Section 4.3.4). Typically concentrations of approx. 20 μ M CaMKII- α (corresponds to approx. 1.1 mg/ml protein) in a final volume of 300 to 400 μ l were yielded (Figure 43).

Figure 43. FLAG-affinity protein purification of N' and C'FLAG-tagged CaMKII- α .

Protein was expressed in Sf9-insect cells via the baculovirus expression system, and was FLAG-affinity purified from suspension culture. Cropped images of Coomassie blue-stained SDS polyacryl amide (10%) gels show the eluted fraction of purified N' and C'FLAG-tagged CaMKII- α . Both products were confirmed by mass-spectrometry analysis. Approximate product size is indicated on the right.



5.2.1.2 Autophosphorylation of CaMKII- α

For CaMKII- α to become an active enzyme, it requires auto-phosphorylation of Thr286 (T286)^{169,170}. Therefore, it was important to pinpoint under which conditions CaMKII- α autophosphorylation was strong or weak when compared to the inactive state. For this study, via Western-blot analysis against phosphorylated Thr286 (pT286) of CaMKII- α the kinase's ability to undergo autophosphorylation was tested (a detailed protocol can be found in Section 4.3.5.5).

To this end, the kinase was incubated with 300 μ M free Ca²⁺ and ATP (0.1 mM) for different time periods, and auto-phosphorylation was assayed via Western-blot analysis using an antibody against the phosphorylated T286 (pT286) of CaMKII- α (Figure 44).

Results

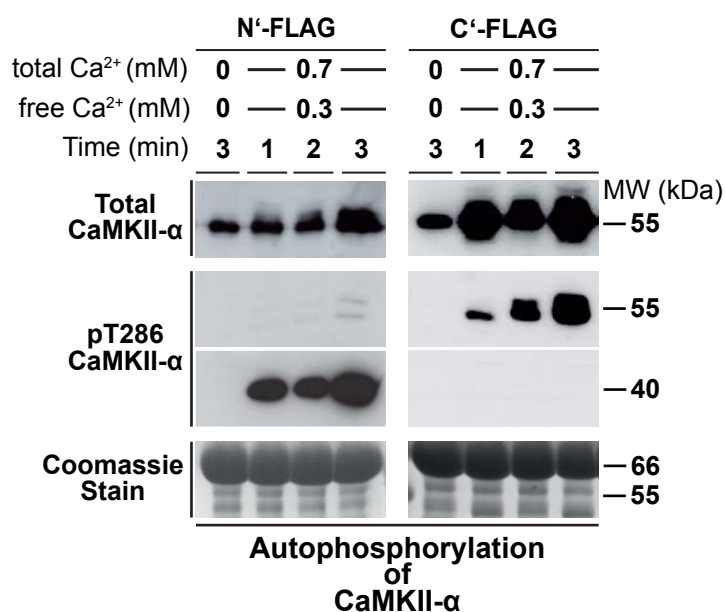


Figure 44. Autophosphorylation of N' and C'FLAG-tagged CaMKII- α .

Both, N'FLAG- (*left panel*) and C'FLAG-tagged (*right panel*) CaMKII- α , were tested for their ability to undergo autophosphorylation at T286. For this 270 nM purified kinase protein was stimulated for one to three minutes with 0.1 mM ATP and 0.3 mM free Ca²⁺ (conditions labeled at the *top*). *Top and middle part*: Semi-quantitative Western-blot analysis against total kinase protein and phosphorylated T286 (pT286). *Bottom part*: Coomassie blue-stained SDS polyacryl amide gels (10%) sections showing the kinase bands at 55 kDa. The 66 kDa-product comprises BSA, which was included in the assay. *Control (left-most lane)*: Here, no Ca²⁺ was included, thus stimulation of the kinase cannot occur. Product sizes (in kDa) are indicated on the right.

As expected, at 300 μ M free Ca²⁺ and 0.01 mM ATP CaMKII- α showed high levels of pT286. However, while for the C'FLAG-tagged version the size of the auto-phosphorylated product corresponded to the molecular weight of monomeric CaMKII- α (approx. 55 kDa), for the N'FLAG-tagged construct strong pT286 auto-phosphorylation was detected in a product of approximately 40 kDa. It should be noted that at the longest reaction time (i.e., three minutes) also at 55 kDa a faint duplex band was detected. In addition, with increasing reaction time (i.e., one to three minutes) the degree of auto-phosphorylation was increased (**Figure 44**). Perhaps due to a calcium-SDS gel artifact, the detection levels of total CaMKII- α protein were higher when Ca²⁺ was included in the reaction. Judging from the Coomassie-stain (**Figure 44**), it is unlikely that unequal sample loading accounted for the higher intensities in the blots. Under zero-Ca²⁺ conditions, no activation was observed. Thus the C'FLAG-tagged CaMKII- α construct is fully functional under the conditions used here.

5.2.1.3 Initial structural analysis of CaMKII- α by cryo-electron tomography

Besides providing the biochemical evidence for the kinase's functionality, in collaboration with the laboratory of Prof. W. Baumeister and Dr. V. Lucic (Max-Planck-Institute for Biochemistry, Martinsried, Germany), cryo-electron tomography (cryo-EM) studies have been initiated and are still ongoing. For these experiments, exclusively the C'FLAG-tagged CaMKII- α was used. In **Figure 45 A** and **B**, representative negative stain electron micrographs of the dialyzed kinase are shown. At a 10-fold dilution of the protein solution several thousands of (non-aggregated) holoenzyme-assembled particle images could be acquired. An excellent sample quality was crucial for the cryo-EM work and the following three-dimensional (3D) reconstruction (**Figure 45 C** and **D**). In **Figure 45 A**, an overview image of the sample is shown, whereas **Figure 45 B** shows one optimally plane-oriented holoenzyme kinase particle (black square box). Already on the level of conventional electron microscopy (EM), the reported hexagonally shaped holoenzyme structure becomes visible. Furthermore, a pore-like structure in the middle of the holoenzyme was observed (**Figure 45 A**), confirming earlier reports of EM structures of the CaMKII- α holoenzyme¹⁷¹. Preliminary 3D reconstructions, obtained from approx. 80,000 single particles, impressively show the unstimulated (non-autophosphorylated) as well as the stimulated (autophosphorylated) state of C'FLAG-tagged CaMKII- α (**Figure 45 C** and **D**, resolution of approx. 30 Å). The quality of the kinase preparation even allowed for reconstructions where the kinase can be looked at from different perspectives (top- and side-view). From these reconstruction images, it seems as if upon stimulation, the holoenzyme swivels out the N-terminal portion of each of the six duplex-arranged kinase molecules (**Figure 45 C** and **D**).

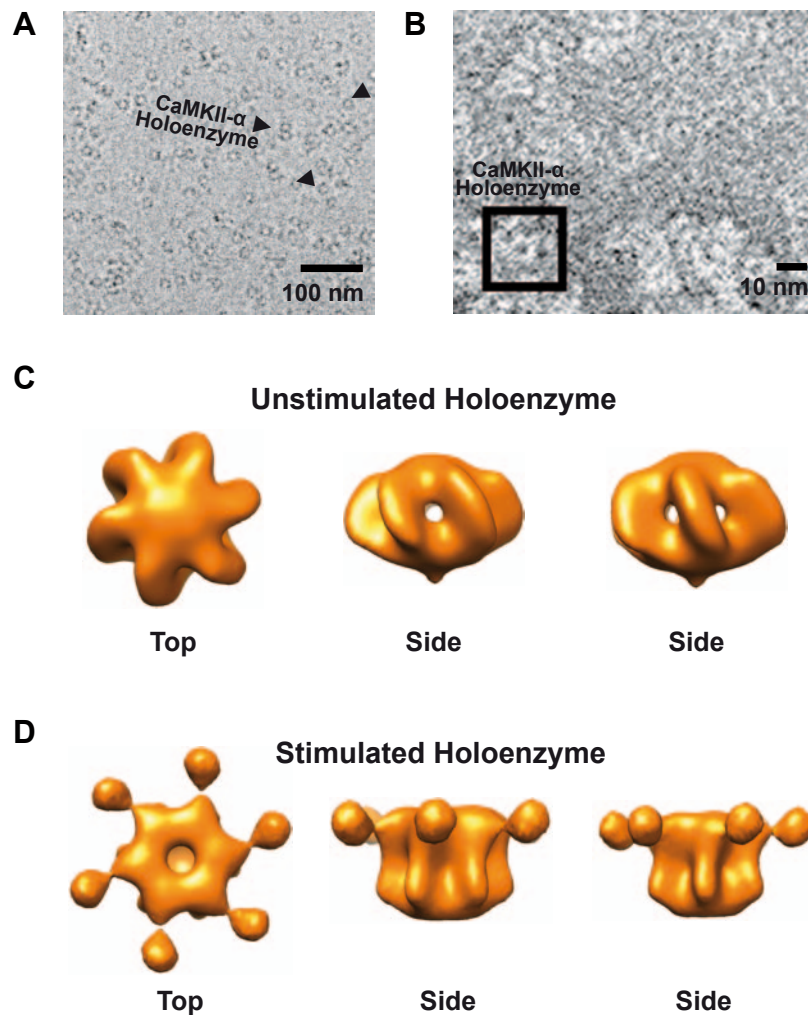


Figure 45. Structural analysis of CaMKII- α by cryo-electron tomography.

(A and B): Representative negative stain electron micrographs of purified C'FLAG-tagged CaMKII- α ; *scale bars* provided in the lower right. The overview-image section in (A) shows that with the applied dilution (0.5 to 2 μ M) of the kinase sample an even distribution of fully assembled holoenzyme-particles without any signs of protein aggregation was achieved. Under the applied conditions, purified C'FLAG-tagged kinase assembles into the characteristic petal-like hexagonal holoenzyme structure (B). (C and D) Three-dimensional (3D) reconstructions of unstimulated (no Ca²⁺, C) and stimulated (plus Ca²⁺, D) CaMKII- α . For this, approx. 80,000 particles from cryo-tomograms of both the conditions were aligned in three dimensions followed by 3D-averaging. Depicted are reconstructions showing the holoenzymatic structure from three different orientations (*top* and *side* views) with an approx. resolution of 30 Å. Images provided by Z. Kochovski, Baumeister-laboratory, MPI for Biochemistry, Germany.

Taken together, I could provide evidence that the purified C'FLAG-tagged CaMKII- α exhibits full autophosphorylation activity (Figure 44, Section 5.2.1.2). Furthermore, cryo-EM (performed by Z. Kochovski, Baumeister-Lab, MPI for Biochemistry, Martinsried, Germany), demonstrated that the kinase assembles into a functional, but more importantly dynamic holoenzyme (Figure 45).

Results

5.2.1.4 Assaying the interaction of CaMKII- α and melanosomes

With the fully functional protein I set out to establish a release assay to better understand the effect on melanosome-bound Myosin V (for experimental details, refer to Section 4.3.5.6). For this assay, a high-Calcium concentration (300 μM free Ca^{2+}) was applied to ensure that the kinase is active and able to phosphorylate Myosin Va as the potential substrate. Once stopped, the samples were briefly centrifuged to separate the melanosome fraction from potentially released Myosin Va molecules. Subsequently both the supernatant and the pellet fraction were subjected to Western-blot analysis.

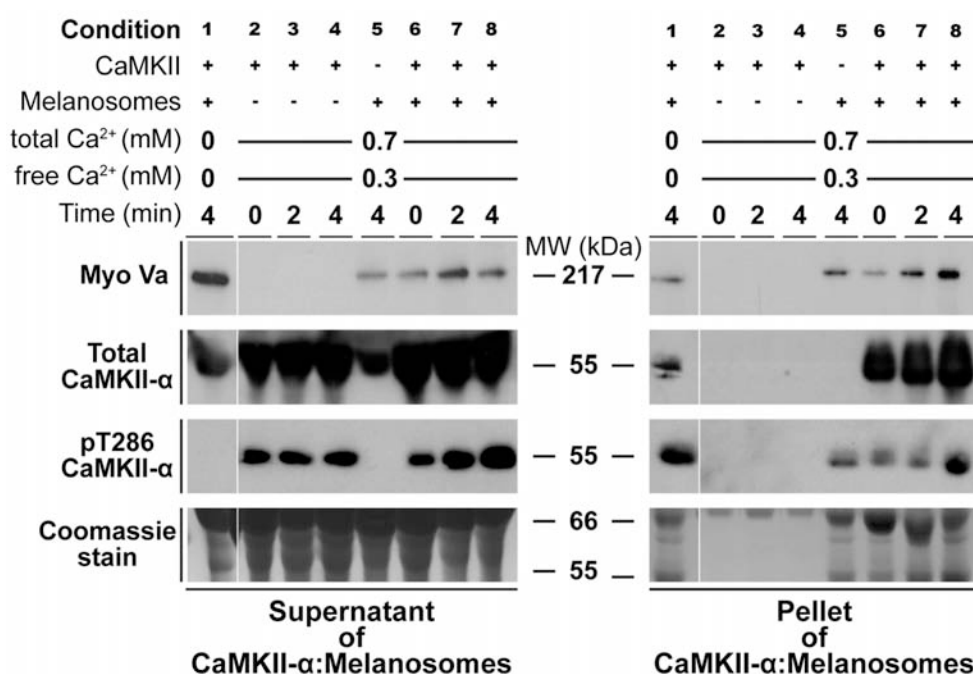


Figure 46. CaMKII- α -mediated Myosin V release from melanosomes.

Melanosomes, isolated from *Xenopus l.* melanophores, were targeted for the herein introduced release-assay (outlined in Section 4.3.5.6) to investigate the potential of (endogenous as well as exogenous) CaMKII- α to trigger Myosin Va-release from the melanosome. *Left and right panels:* after completion of the respective reaction, by brief sample centrifugation the supernatant and pellet fraction was obtained. This way, Myosin Va-release from and also any potential kinase-recruitment onto the melanosome could be assessed by immunoblotting against Myosin Va, total kinase protein and autophosphorylated kinase at T286 (indicated to the *left* of each row). *Bottom row:* Coomassie blue-stained SDS polyacrylamide gel (10%) image sections; the respective conditions applied are labeled on *top* of the image sections; product sizes (in kDa) are indicated in-between both panels. The relative intensities of the herein presented semi-quantitative Western-blot analysis is provided in **Figure 47**.

As expected, high autophosphorylation (i.e., active state turned on) was observed in the supernatant fractions, under conditions where free Ca^{2+} was present and

Results

where purified kinase was added. The different reaction times of kinase activation did not yield significant differences in the level of autophosphorylation (anti-pT286 CaMKII- α of **Figure 46**). As shown in lane 1 of the SN-fraction, purified kinase does not undergo autophosphorylation under Ca²⁺-free conditions (anti-pT286 CaMKII- α of **Figure 46**). Furthermore, according to the band intensity quantification, it made no significant difference whether melanosomes were present in the reaction or not (**Figure 47**).

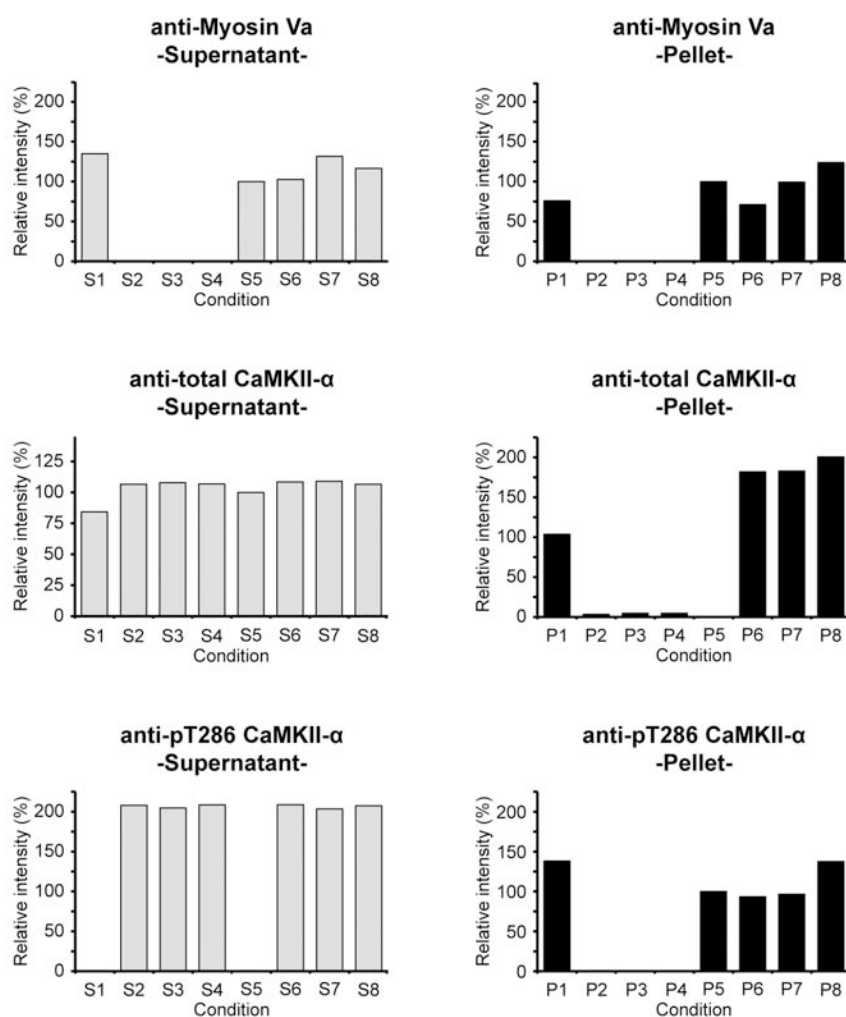


Figure 47. Semi-quantitative analysis of CaMKII- α -mediated Myosin V release.

Left and right panels: Intensities were determined for each protein product at the given condition (#1 through 8, for details refer to **Figure 46** from both the supernatant (*left panel*) and pellet fractions (*right panel*). Barcharts display the relative intensities, normalized to the intensity values of condition #5 (i.e., melanosomes only). For the purpose of correct visualization, intensities of condition #5 were set to 100% when significantly higher than the background value, while they were set to 0% when below the background value. *x-axis:* reaction conditions of the pellet (P) and supernatant (S) fractions are labeled #1 through 8; *y-axis:* relative intensity are given in %; the respective protein product analyzed and quantified is indicated on *top* of each diagram.

Results

It should be mentioned that the added kinase does not pellet as such (anti-total CaMKII- α and pT286 CaMKII- α of **Figure 46**). However, under conditions where melanosomes are present, total and even active CaMKII- α protein is found in the pellet fraction (**Figure 46** and **Figure 47**). Another rather surprising finding was that under Ca²⁺-free conditions highly active CaMKII- α was detected in the pellet even though in the bulk of the supernatant no activated kinase could be detected (anti-total CaMKII- α and pT286 CaMKII- α of **Figure 46** and **Figure 47**). The level of activity was identical to the autophosphorylation level determined for the pelleted kinase fraction under high-Ca²⁺ conditions at the longest activation period (anti-pT286 CaMKII- α of **Figure 46** and **Figure 47**). Furthermore, high autophosphorylation in the presence of melanosomes but not in their absence was observed when no exogenous pre-activated kinase was included to the assay (compare SN and P lanes 5 of anti-pT286 CaMKII- α of **Figure 46**). It made no difference whether non-pre-activated or pre-activated (2 minutes) purified kinase was added (**Figure 46** and **Figure 47**). Under conditions where no exogenous kinase was added, CaMKII- α is largely confined to the supernatant fraction (anti-total CaMKII- α of **Figure 46** and **Figure 47**). Taken together, the kinase is found in the pellet only when melanosomes are present. Moreover, active *endogenous* kinase is very likely capable of binding to melanosomes.

The fact that active endogenous CaMKII- α might associate with melanosomes strengthens the hypothesis of CaMKII- α -mediated regulation of melanosome-associated components. As shown in **Figure 46** and **Figure 47** along with the band intensity quantifications, significant amounts of full-length Myosin Va were detected in the supernatant. This strongly suggests that Myosin V-specific release from the melanosome surface takes place even under conditions where no exogenous kinase was added. Strikingly, the relative amount of released Myosin Va and melanosome-associated active kinase show strong correlation (compare lanes of SN and P for anti-Myosin Va and anti-pT286 CaMKII- α , respectively).

These data provide evidence that endogenous active melanosome-bound CaMKII- α has a role in releasing Myosin Va from the melanosome. However, under the conditions used, a complete release of Myosin Va from the melanosome was not achieved by either the endogeneously expressed or exogenously added and melanosome-bound kinase.

5.3 Purification of isolated melanosomes via MACS technology

The novel technique described here deals with the further purification of melanosomes that had been isolated the conventional way and therefore still contain contaminating cytoplasmic proteins.

Motivated by the problem that for very sensitive analytical methods, like mass-spectrometry, the conventional method for the isolation of melanosomes is hardly suitable, I combined the established gentle two-step centrifugation method with a magnetic bead-based enrichment technology (MACS). So far MACS has been used primarily in immunobiological research, where cells rather than organelles are sorted and enriched.

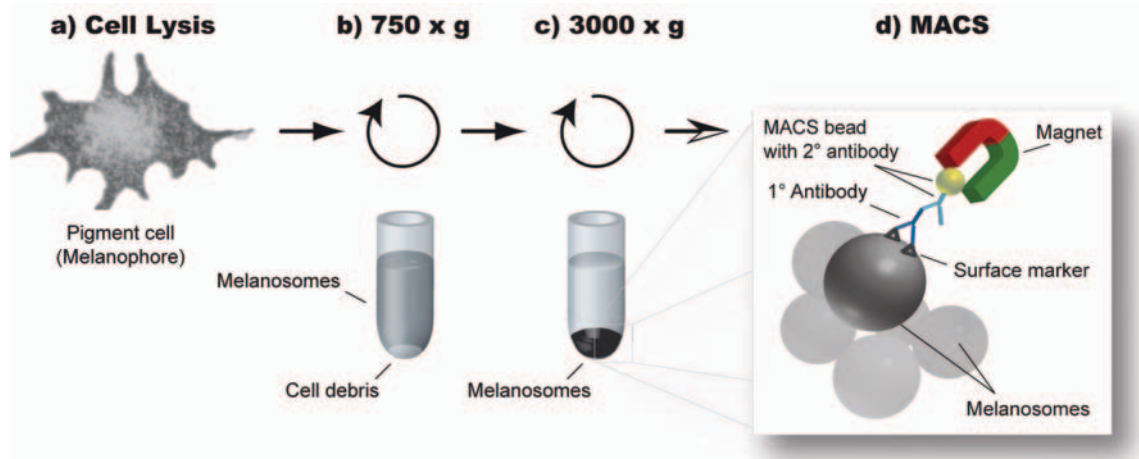


Figure 48. Schematic of MACS bead-assisted melanosome purification.

(a) Melanophores from *Xenopus l.* were harvested and lysed via Balch-homogenization. (b) To separate cell debris (e.g., membranes) from cytoplasmic proteins, the lysate was centrifuged at $750 \times g$. (c) The melanosome fraction was separated from low molecular weight proteins and other small cytoplasmic molecules by centrifugation at $3,000 \times g$. The pellet fraction from c is here referred to as “crudely” isolated melanosome fraction. (d) For further purification by MACS, the pelleted melanosome fraction from c was incubated with surface marker-specific primary (1°) antibodies. Here, Tyrosine-related protein 1 (Trp1) was chosen as marker, as it represents a transmembrane and thus is an integral part of the protein melanosome membrane. Antibody-labeled melanosomes were subjected to incubation with paramagnetic MACS[®] microbeads, which are conjugated to secondary (2°) antibodies that are reactive against the earlier applied 1° antibodies. By using a strong magnet, almost like using a fishing-rod, the magnetically labeled organelles are attracted toward the magnet and can eventually be eluted. Sizes of cells, organelles and other components here depicted are schematics and are not drawn to scale.

In brief, magnetic beads bind specifically via bead-conjugated secondary antibodies to the target (i.e., melanosomes), which in turn is marked with surface-marker-specific primary antibodies. This way, no additional centrifugation step is

Results

required, and only those organelles that contain the marker against which the beads are reactive are purified. For details on the protocol for MACS bead-assisted purification of isolated melanosomes, refer to Section 4.1.4 and the schematic in **Figure 48**.

5.3.1 Results

5.3.1.1 Comparative analysis of the different purification methods

The main goal of this work was to establish a protocol that yields highly pure but intact melanosomes. In brief, melanosome isolation from melanophores was carried out according to the established isolation protocol^{65,93}, yielding a crudely isolated melanosome ($\text{Mel}_{\text{crude}}$) fraction. This was followed by density gradient ultra-centrifugation purification (DC). Using SDS-PAGE and mass-spectrometry, melanosome fractions purified by the standard crude method or by DC were compared (**Figure 49**).

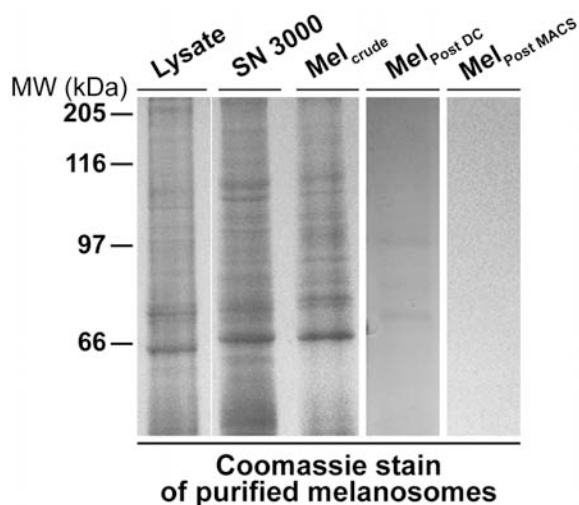


Figure 49. Comparison of the different melanosome purification procedures.

Image sections of Coomassie blue-stained SDS polyacrylamide gels (12%), showing lanes of the cell lysate, cytosolic (SN 3000) and melanosome ($\text{Mel}_{\text{crude}}$) fractions after centrifugation of the lysate at $3,000 \times g$ (*first three lanes*); in *lanes 4 through 6* the purified melanosome fractions after density gradient ultra-centrifugation ($\text{Mel}_{\text{Post DC}}$) or magnetic-bead assisted sorting ($\text{Mel}_{\text{Post MACS}}$) are provided. Virtually all proteins detected by Coomassie-staining are depleted upon purification via DC and MACS. Sizes of proteins (in kDa) are indicated on the left.

The appearance of the Coomassie-stained bands from the cell lysate, cytosolic (SN 3000) and crude melanosome ($\text{Mel}_{\text{crude}}$) fractions hardly differed from each other (**Figure 49**). In contrast, in both the tested purification methods (DC and MACS) in principle all the protein bands that were obtained at the $\text{Mel}_{\text{crude}}$ isolation stage became absent in the process of further purification (**Figure 49**). In collaboration with the Zentrum für Proteinanalytik (ZfP, LMU Munich, Germany) the DC-purified and crude melanosome fractions were subjected to tandem mass-spectrometry (the list of protein hits obtained, is provided in Section 7).

Results

For the Mel_{crude} fraction, mass-spectrometry provides a long list of proteins, of which only very few could be matched to proteins or protein families that are known to be associated with the (still poorly) characterized melanosome proteome. This is consistent with the many Coomassie-stained protein bands detected by SDS-PAGE (Figure 49, the list of protein hits is provided in Section 7).

For the Mel_{Post DC} probe, mass spectrometry gave improved spectra along with several significant peptide matches (the complete list of protein hits is provided in Section 7). In addition, a reasonable portion of the Mel_{Post DC} results matched previous reports of mass-spectrometric analyses of melanosomes from mouse melanocytes (see complete list of protein hits is provided in Section 7). More importantly, the reliability of the analysis was underlined by the fact that tyrosinase-related protein 1 (Trp1), a melanosome-specific surface marker protein, was identified with the highest protein score among the proteins identified. However, despite the improved quality in the mass-spectra, none of the known melanosome-associated motor proteins could be detected.

For melanosomes isolated via MACS, at this point only preliminary mass-spectrometry results could be obtained (data not shown). However, the fact that for the first time also motor proteins (myosins, kinesins and dynein) as well as melanosome-specific adaptor-molecules (dynactin) could be identified is encouraging. This and the fact that the MACS-purification was carried out via the melanosome surface marker Trp1, makes this novel purification technique superior to the other two procedures used here.

5.3.1.2 Qualitative analysis of the purity of MACS-purified melanosomes

To determine the degree of contamination of melanosomes purified by MACS, Western-blot analysis against ubiquitous cellular proteins was performed. β -tubulin was chosen because it is an abundant cytoskeletal protein. The glycolytic enzyme GAPDH is a housekeeping enzyme that is present in almost all cell types¹⁷², and is representative of the cytosolic protein fraction. And Myosin Va was chosen because it is a melanosome-specific marker that is expected to remain on the melanosome during the purification procedure.

Results

In **Figure 50**, a Western-blot of a representative preparation of MACS-purified melanosomes is shown, from which three important conclusions could be drawn: i) GAPDH is present in the lysate and SN3000 fraction, but is nearly absent (only a faint band remained) in the melanosome fraction after the second centrifugation step; ii) even though clearly reduced, the melanosome probe from this second centrifugation step still contained β -tubulin. Importantly however, after the MACS bead-purification, the contaminating β -tubulin fraction vanished; and iii) even though each step in the purification procedure was accompanied by a slight reduction in the content of Myosin Va, a significant portion of this melanosome surface marker stayed associated with the organelles. Therefore, the two contaminating cytoplasmic proteins, GAPDH and β -tubulin, could be successfully depleted from the melanosome fraction by the MACS protocol (**Figure 50**).

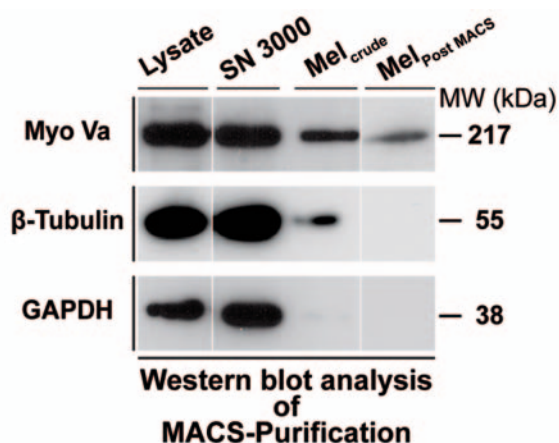


Figure 50. Qualitative analysis of MACS-purified melanosomes.

Via Western-blot analysis, the amounts of Myosin Va, β -tubulin and GAPDH, representing proteins from the melanosome-bound transport machinery, cytoskeleton and cytosol, respectively, in the cell lysate and cytosolic fraction, as well as crudely purified melanosome fraction were compared with equal amounts from the MACS-purified melanosome fraction (from left to right). Protein product sizes (in kDa) are indicated on the right.

5.3.1.3 Analysis of the MACS-purification protocol by FACS

To quantitatively determine the specificity of this novel melanosome purification technique, Fluorescent Activated Cell Sorting (FACS) analysis with the crudely isolated but not yet MACS-purified melanosomes was carried out. By applying the same primary and secondary antibodies at dilutions identical to those used for MACS-purification, via FACS the antibody-specific binding of the melanosomes can be monitored and quantified.

In **Figure 51** representative plots for melanosomes stained with anti-Trp1 and Kinesin-2 antibody are presented. As controls, unstained melanosomes as well as melanosomes stained with secondary antibody only were included. Approximately 11,000 melanosomes per antigen and condition were analyzed in one run.

Results

Comparing the respective peaks of the green curve (melanosomes plus primary and secondary antibody) to the red and blue curves of the control measurements, in both sets (anti-Trp1 and anti-Kinesin-2) an obvious shift toward higher mean intensity for the green curves is observed (Figure 51).

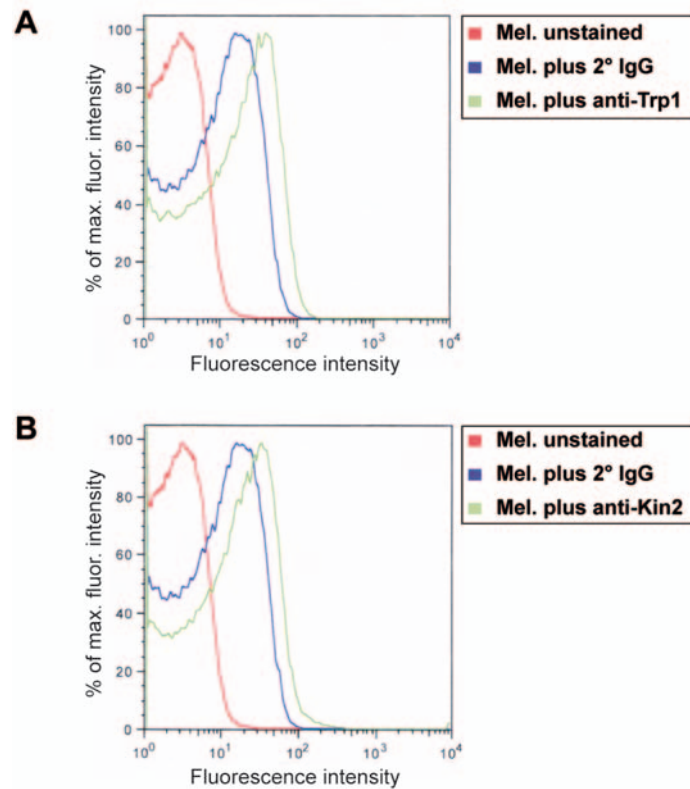


Figure 51. Surface marker-specific FACS analysis on isolated melanosomes.

Depicted are two representative histogram overlays for the surface marker-specific staining of crudely isolated melanosomes (*green lines*) of Tyrosinase-related protein 1 (Trp1, *upper panel*) and Kinesin-2 (*lower panel*). As *Controls* unstained melanosomes (*red lines*) as well as melanosomes stained with the respective secondary antibody only (*blue lines*) were subjected for FACS analysis. Histogram overlays are plotted as fluorescent intensity of phycoerythrin (*x-axis*) versus % of maximum fluorescence (*y-axis*). The latter is calculated by setting the highest count of one fluorescent intensity unit to 100%. Thereby, it is possible to compare the two controls to the specific staining.

This finding clearly demonstrates the specific binding of the Trp1 antibody to the crudely isolated melanosomes, and thereby encourages further use of the current protocol of the MACS-purification technique.

5.4 Determining the full-length sequence of *Xenopus l.* Myosin Va

One of the goals of this work was to obtain the complete full-length sequence of *Xenopus l.* Myosin Va and to subsequently clone the complete gene into a baculovirus-specific transfer vector for the expression in insect cells. Lots of biologically relevant applications could be tackled if it was possible to produce this important organelle transporter as recombinantly over-expressed protein. In addition, once successfully cloned the Wildtype full-length version can easily be mutated and then studied both, *in vivo* and *in vitro*.

5.4.1 Strategy

To obtain the full-length sequence of *Xenopus l.* Myosin Va the following five steps were performed: First, mRNA was isolated from cultured *Xenopus l.* melanophores followed by reverse transcription into cDNA (Sections 4.2.1.1 and 4.2.1.2); second, with the cDNA at hand PCR with gene-specific forward and reverse primers as well as RACE-PCR was performed (Sections 4.2.2.2.2 and 4.2.1.3). Via this gradual retrieval of new sequence fragments, the stepwise proceeding toward the end of the coding sequence was achieved; and third, before restriction-mediated cloning of the obtained gene into a baculovirus transfer vector, the sequence was confirmed by DNA sequencing (Section 4.2.2.6).

5.4.1.1 Step-by-step PCR on cDNA from *Xenopus l.* melanophores

Based on the known approximate molecular weight of 215 kDa, the coding sequence for the full-length Myosin Va from *Xenopus l.* would be expected to be almost 6000 base pairs (bp) long. However, the sequence that has been published as coding sequence for *Xenopus l.* Myosin Va (accession number: NM_001087248), with 1760 bp hardly covers one third of the expected full-length sequence.

To provide the entire sequence, reverse transcribed cDNA from *Xenopus* melanophores served as template for as series of PCR reactions, which for reasons of clarity are sub-divided into the three distinct but overlapping phases A, B and C (**Figure 52**).

Results

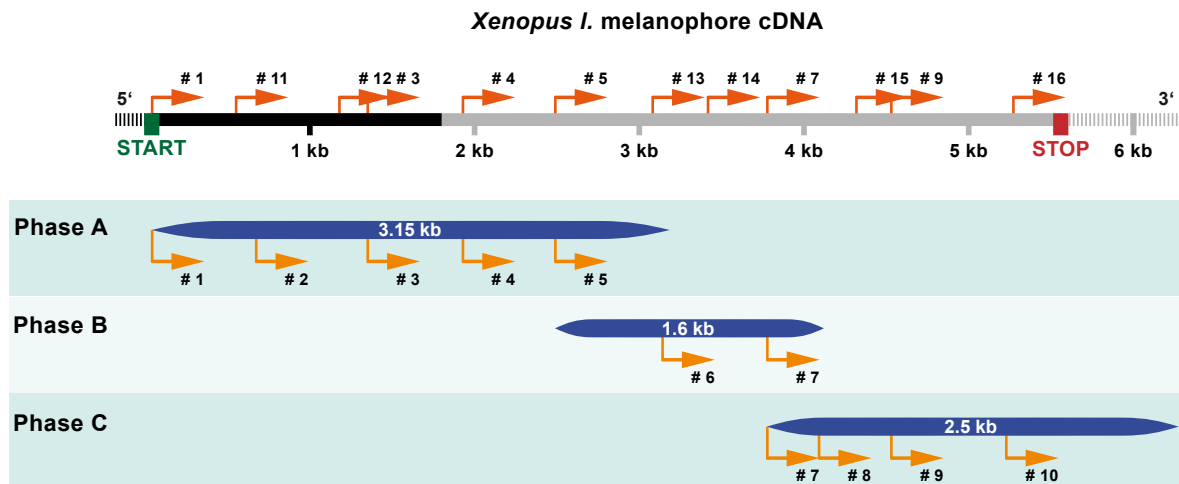


Figure 52. Obtaining the full-length Myosin Va sequence from *Xenopus I. melanophore* cDNA – Overview.

In the three overlapping *Phases A, B* and *C* the full-length *Xenopus I.* Myosin Va sequence from melanophore cDNA was obtained. *Phase A:* By using forward and reverse primers that were specific for the published but incomplete Myosin Va gene (*solid black* portion of the cDNA), a product of 3.15 kb was retrieved. *Phase B:* PCR on the not known sequence (*grey portion* of the cDNA) was performed by using a combination of forward and reverse primers annealing at the 3'-end of the Phase A product and the related full-length Myosin Va gene from chicken, respectively (1.6 kb-product yielded). *Phase C:* The remaining 1.8 kb of the coding sequence (*solid grey*) were obtained by RACE PCR, using a Phase B gene product-specific forward primer along with a reverse primer that was specific for the poly A⁺ tail of the cDNA. Products yielded by PCR are depicted as *blue* portions for the respective phases (indicated on the left). A schematic of the cDNA containing the coding sequence of the full-length Myosin Va gene is provided at the very top. Arrows along with primer numbers indicate the carried out sequencing reactions in Phases A through C (*yellow*) and prior to the subsequent cloning of the full-length product (*orange*).

5.4.1.1.1 Overview on Phases A, B and C

Phase A primarily served the purpose of validating and correcting the published but yet incomplete sequence, hence primers used during Phase A were designed on the basis of this incomplete Myosin Va coding sequence.

The fact that 3' of the sequence that had been obtained during Phase A, no further sequence information was available, made a *Xenopus I.* Myosin Va gene-specific primer design impossible. Therefore, as an alternative approach for Phase B reverse primers were designed on the basis of the published and complete full-length Myosin Va gene from chicken.

PCR reactions of Phase A and B were carried out with overlapping primer combinations, so that the newly retrieved sequence fragments could be easily aligned and compared to each other. This way, new preliminary template sequences could be obtained. For primer design it was important to not consider

the very end of the sequences for primer annealing because errors are more likely to occur towards the ends of the sequencing reaction, which would ultimately result in erroneous design of new primers. Therefore, primers were designed such that annealing could occur close (i.e., 20 to 50 nucleotides inward) but not at the very 3'-end of the respective sequence template.

The third and final phase aimed at the retrieval of the remaining approx. 2 kb of the full-length Myosin Va coding sequence. For this, the more specialized PCR technique of Rapid Amplification of cDNA Ends (RACE-PCR) was used, as it is ideally suited for amplifying a certain portion of a given gene sequence encoded by the isolated poly A⁺ mRNA.

For details on the PCR reactions of phases A, B and C and a summary list of the primers used, please refer to Section 4.2.2.2 and 4.2.1.3. A list of all primers that were used to step-by-step sequence the respective PCR products is provided in Section 3.4.2.11.

5.4.1.2 Cloning of full-length *Xenopus l.* Myosin Va for baculovirus expression in Sf9 cells

To express the full-length protein in insect cells, the coding sequence coding for the full-length protein was cloned into the pFastBac Dual transfer vector under the control of the p10 promoter. By using forward and reverse primers that contained both, the sequences for the restriction enzyme-specific recognition sites (NheI and SphI) as well as the FLAG-coding sequence motif, the full-length Myosin Va coding sequence was N' or C'FLAG-tagged and prepared for restriction enzyme-mediated cloning via NheI and SphI. This way expression of the full-length protein in insect cells with the subsequent purification via FLAG-affinity chromatography became possible. For more detailed information about the preparation of the full-length Myosin Va gene for vector cloning, please refer to Section 4.2.2.2.3.

Both versions, N' and C'FLAG-tagged full-length *Xenopus l.* Myosin Va, were expressed in insect cells via the baculovirus expression system and subsequently FLAG-tag affinity-purified (for more details, refer to Sections 4.3.3.6 and 4.3.4.2).

Results

5.4.2 Results

5.4.2.1 Sequence retrieval of full-length *Xenopus l.* Myosin Va

The goal of the Phase A work was to check the already published but incomplete sequence for errors and/or point mutations. A product constituting the first 3146 bases of the gene (Figure 53 A) revealed five point mutations and six base insertions within the published sequence, including a 5 bp insertion at position 1754 (GTAAG). The base shift generated by the absence of this quintet generates a STOP-codon, ending the published coding sequence at position 1760. In addition, at position 2708 a Thymidine was inserted.

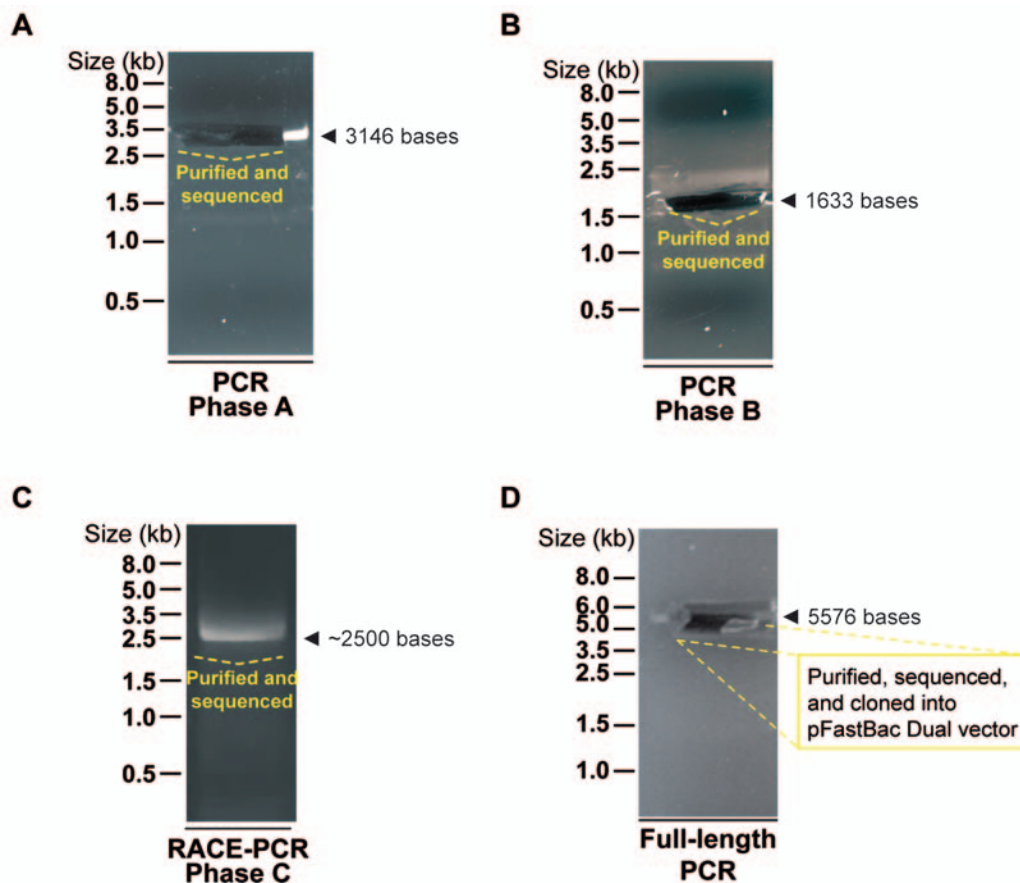


Figure 53. Obtaining the full-length Myosin Va sequence from *Xenopus l. melanophore* cDNA

(A) Phase A: By PCR on cDNA from *Xenopus l. melanophores* with *Xenopus l.* sequence-specific primers, a product of 3146 bp was obtained. Forward primers of Phase B derived from the assembled sequence obtained in Phase A. (B) Phase B: PCR on cDNA with a Phase A-sequence-derived forward primer and a chicken Myosin Va-specific reverse primer, yielded a product of 1633 bp. The forward primer used in Phase C derived from the assembled sequence obtained in Phases A and B. (C) Phase C: RACE PCR on RACE-ready cDNA, using a Phase B-derived forward primer and an universal primer (kit-provided) as reverse primer. The product obtained (approx. 2500 bp) contained the missing last 1784 bp along with approx. 700 bp of untranslated region. (D) By using the in-silico assembled full-length coding sequence, forward and reverse primers containing restriction site-specific sequences for NheI and SphI, were used to amplify the full-length product (5576 bp) from *Xenopus l. melanophore* cDNA. For primers used along with sequences, refer to Sections 3.4.1 and 4.2.2.2.2.

Results

By combining a forward primer annealing close to the 3'-end of the newly obtained sequence and a reverse primer specific for a portion of the published full-length chicken Myosin V, in Phase B additional 1633 bases were retrieved (Figure 53 B). The remaining portion of the coding sequence (approx. 2 kb) was retrieved via RACE PCR (Phase C).

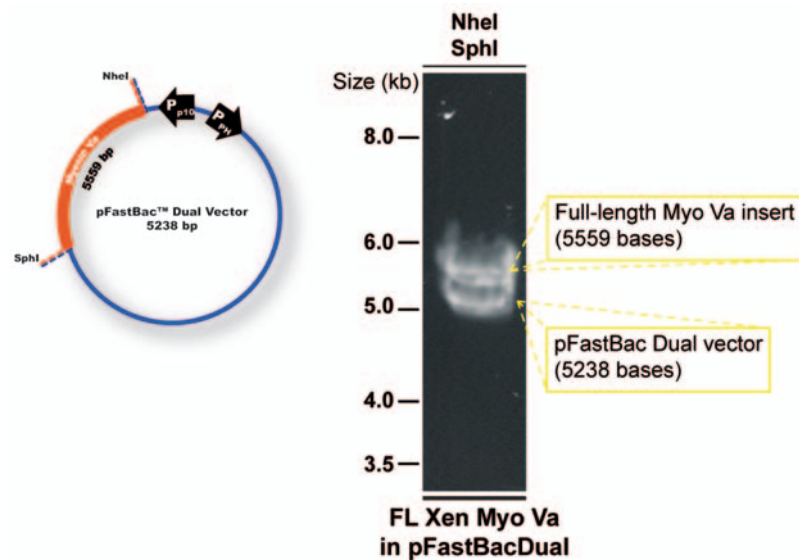


Figure 54. Cloning of the full-length *Xenopus l.* Myosin Va gene for baculovirus expression.

Test digest of the pFastBac Dual vector containing the full-length Myosin Va sequence from *Xenopus l.* with restriction enzymes NheI and SphI. *Right:* A schematic of the insert and vector along with the respective product sizes is provided.

The obtained product of approx. 2.5 kb, contained the remaining 1.8 kilobases of the coding region, along with about 700 bases of untranslated region (Figure 53 C). Via conventional gene-specific PCR, the final full-length product (total length, 5559 bp) including the restriction sites specific for NheI (5') and SphI (3') could be obtained and prepared for the cloning into the pFastBac Dual transfer vector (Figure 53 D and Figure 54, for details refer to Section 5.4.1.2).

Results

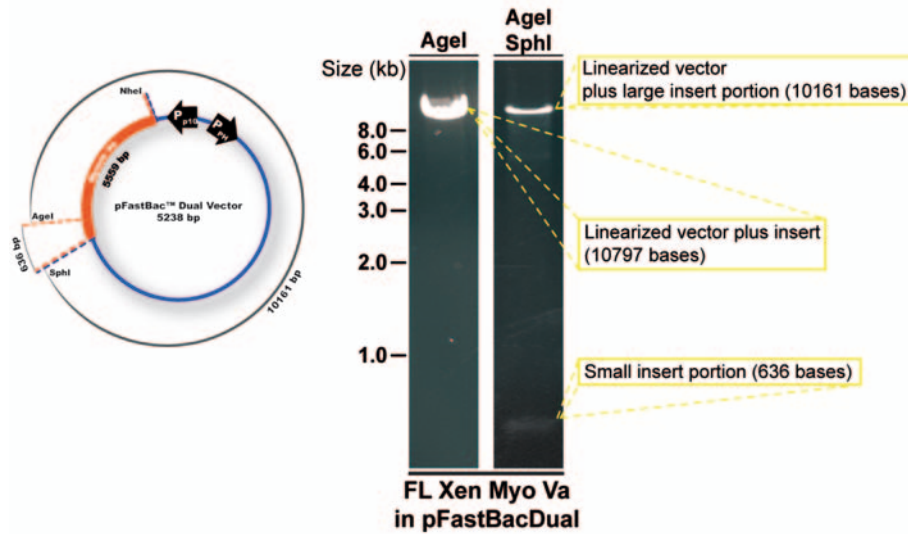


Figure 55. Confirming the correct insertion of full-length *Xenopus I.* Myosin Va into the pFastBac Dual vector.

Test digest of the pFastBac Dual vector containing the full-length sequence of Myosin Va from *Xenopus I.* with restriction enzymes Agel and SphI or Agel only to confirm the correct insertion into the vector. Agel was used as it represents a unique restriction site within the insert. A schematic of the insert and vector along with the respective product sizes is provided on the right.

In Figure 55 the plasmid was digested with restriction enzymes Agel/SphI, to show more clearly that the insert is of the right size and was inserted correctly. Representing a gene-internal restriction site (near the 3'-end/C'-terminus of the insert), Agel was used to confirm the correct insertion direction into the vector. Additional PCR was carried out to generate N' (5'-end) and C' (3'-end) FLAG-tagged full-length constructs. As for the untagged version, both FLAG-tagged constructs were provided with NheI and SphI restriction sites at the 5'- and 3'-end, respectively (Figure 56; a list of primers sequences is provided in Section 3.4.1).

Results

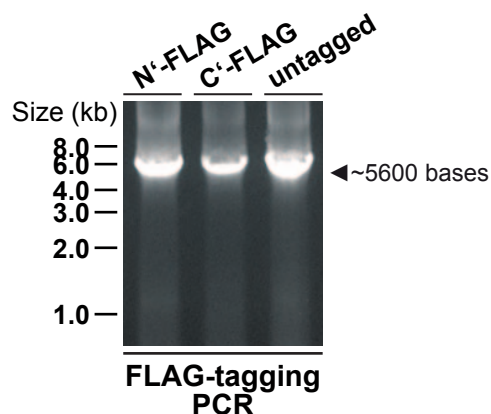


Figure 56. Cloning of FLAG-tagged full-length *Xenopus l.* Myosin Va for baculovirus expression.

The sequence encoding for the FLAG motif was fused to the 5'- and 3'-ends of the full-length Myosin Va gene, by using forward and reverse primers containing respectively NheI- and SphI-restriction sites along with the FLAG-encoding sequence. The amplified product (approx. size 5600 bp) was used for the subsequent cloning into the pFastBac Dual vector.

5.4.2.2 Domain analysis and comparative alignment

To identify both the conserved and rather divergent regions, the deduced amino acid sequence of the full-length *Xenopus l.* Myosin Va was compared to published Myosin Va sequences from chicken (*Gallus gallus*), mouse (*Mus musculus*) and human (*Homo sapiens*) (for the complete sequence *alignment*, refer to Section 7). The protein sequence comparison focused on the head, neck, stalk and tail domains and is summarized in the following. Figure 1 in Section 1.3.1 shows the individual domains of Myosin V.

As was reported previously for Myosin Va from other species^{173,174,175}, the head domain (aa1-775) represents a highly conserved region (see also complete sequence alignment in Section 7). For instance the ATP-binding (aa167-177) as well as loop 1 regions (aa193-203) are identical among the four Myosin Va species (Figure 57).

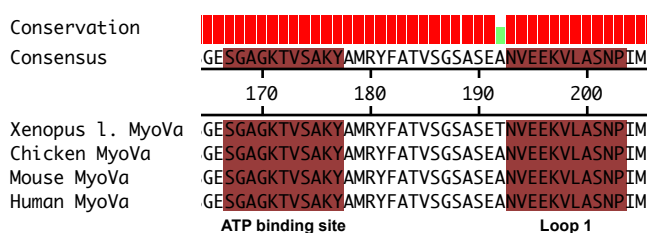


Figure 57. Comparative sequence alignment of full-length *Xenopus l.* Myosin Va with other class V myosins – ATP binding site and loop 1.

The sequence of the full-length Myosin Va from *Xenopus l.* was aligned with class V myosins from chicken, mouse and human. The depicted section shows the ATP binding site and loop 1 within the highly conserved head domain. The regions and motifs of interest are labeled and color-coded. For more details on the alignment, refer to the complete alignment in Section 7.

Results

The actin-binding region (aa505-532) is similar (four differences out of 28 amino acids) to the actin-binding regions from the other three Myosin Va species (Figure 58).

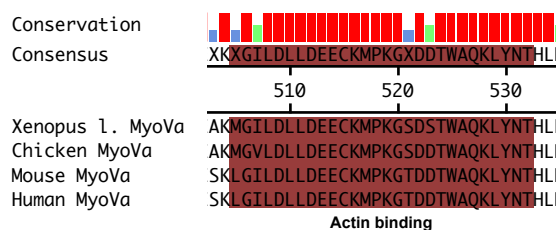


Figure 58. Comparative sequence alignment of full-length *Xenopus l.* Myosin Va with other class V myosins – Actin-binding region.

The sequence of the full-length Myosin Va from *Xenopus l.* was aligned with class V myosins from chicken, mouse and human. The depicted section shows the actin-binding region within the highly conserved head domain. The regions and motifs of interest are labeled and color-coded. For more details on the alignment, refer to the complete alignment in Section 7.

By contrast, in the loop 2-sequence (aa594-639) representing a region of the head domain crucial for the actin-binding-mediated phosphate release, almost half of the residues (21 out of 46 amino acids) are divergent (Figure 59). Interestingly, more than half of those divergences come from the *Xenopus l.* Myosin Va alone. The remaining (C-terminal) approx. 140 aa of the head domain (including the loop 3 region) are highly conserved among the four species. However, from the eight divergences in this region, six are found in *Xenopus l.* Myosin Va alone.

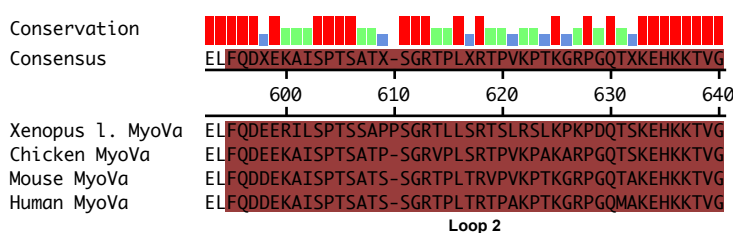


Figure 59. Comparative sequence alignment of full-length *Xenopus l.* Myosin Va with other class V myosins – Loop 2 region.

The sequence of the full-length Myosin Va from *Xenopus l.* was aligned with class V myosins from chicken, mouse and human. The depicted section shows the loop 2 region within the otherwise highly conserved head domain. Loop 2 in the *Xenopus* Myosin Va shows high divergence in comparison to Myosin V from the other species. The regions and motifs of interest are labeled and color-coded. For more details on the alignment, refer to the complete alignment in Section 7.

Results

The neck domain (aa776-908) shows obvious differences compared to the other three Myosin Va species. While the consensus sequence IQxxxRGxxxRxxY of the IQ repeats is conserved, in particular the repeats IQ₃, IQ₄ and IQ₅ diverged more than the other three IQ-motifs (Figure 60).

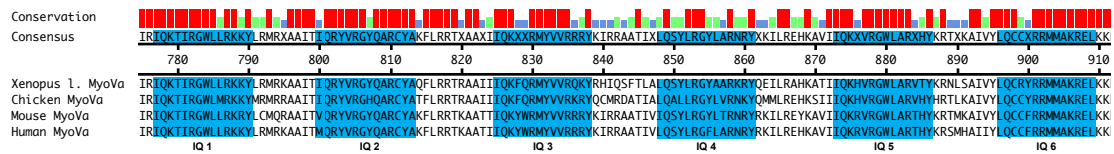


Figure 60. Comparative sequence alignment of full-length *Xenopus l.* Myosin Va with other class V myosins – IQ motifs.

The sequence of the full-length Myosin Va from *Xenopus l.* was aligned with class V myosins from chicken, mouse and human. The depicted section shows the six IQ motifs of the lever arm domain. While the IQ repeat consensus sequence is kept, some minor divergences for the *Xenopus* Myosin Va exist. The regions and motifs of interest are labeled and color-coded. For more details on the alignment, refer to the complete alignment in Section 7.

The proximal tail or rod domain (aa 915 through approx. aa 1320) is marked by two extensive coiled-coil regions (CC#1 and CC#2), which are separated by a calpain-sensitive PEST site. The four sequences diverge in 79 of the 202 amino acids that comprise CC#1. Nearly half of these, i.e., 35 residues, are found in *Xenopus l.* Myosin Va (see also complete sequence alignment in Section 7). While the PEST site shows high similarity among the species (Figure 61), with 22 out of 81 residues diverging, CC#2 again shows high sequence-variability. Again, most of these divergences were found only in the *Xenopus l.* sequence.

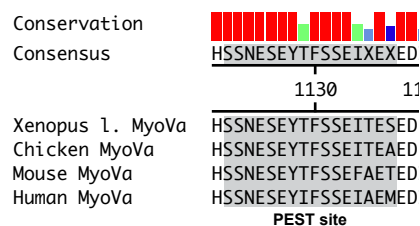


Figure 61. Comparative sequence alignment of full-length *Xenopus l.* Myosin Va with other class V myosins – PEST site.

The sequence of the full-length Myosin Va from *Xenopus l.* was aligned with class V myosins from chicken, mouse and human. The depicted section shows the calpain-sensitive PEST site of the rod (proximal tail) region. While this region in general shows high sequence variability (see complete alignment in Section 7), the PEST motif is highly conserved. The regions and motifs of interest are labeled and color-coded.

Just before the beginning of CC#3, a stretch of 27 amino acids (consensus sequence, aa1324-1351) is present in mouse and human Myosin Va but missing in *Xenopus l.* as well as chicken Myosin Va (Figure 62).

Results

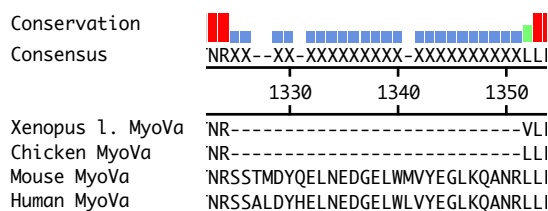


Figure 62. Comparative sequence alignment of full-length *Xenopus I.* Myosin Va with other class V myosins – Sequence deletion in the distal rod region.

The sequence of the full-length Myosin Va from *Xenopus I.* was aligned with class V myosins from chicken, mouse and human. The depicted section shows a stretch just before the third coiled-coil of the distal rod region, where for *Xenopus* and chicken Myosin V a sequence deletion (27 residues) was detected. The regions and motifs of interest are labeled and color-coded. For more details on the alignment, refer to the complete alignment in Section 7.

In contrast, the distal rod region (aa1321-1430), marked by a third coiled-coil (CC#3), shows high sequence similarity and conservation among the four species. However, the second half of CC#3 has an insertion of 25 amino acid residues in *Xenopus I.* Myosin Va, (Figure 63).

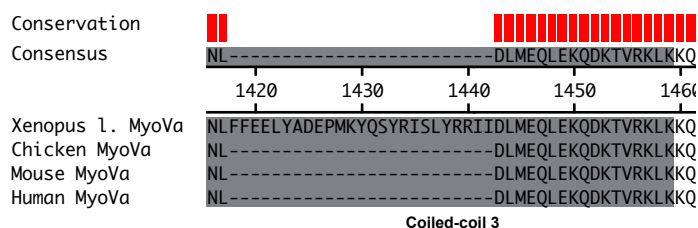


Figure 63. Comparative sequence alignment of full-length *Xenopus I.* Myosin Va with other class V myosins – Unique sequence insertion in the distal rod region.

The sequence of the full-length Myosin Va from *Xenopus I.* was aligned with class V myosins from chicken, mouse and human. The depicted section shows the second half of the third coiled-coil region. Normally this portion of the tail domain shows high sequence similarity, but for *Xenopus* Myosin Va a unique insertion of 25 amino acids was detected. The regions and motifs of interest are labeled and color-coded. For more details on the alignment, refer to the complete alignment in Section 7.

To summarize, while a large portion of the head and distal tail domains are highly conserved, parts of the neck and most of the proximal stalk/tail are highly divergent in *Xenopus I.* Myosin Va.

Results

5.4.2.3 FLAG-affinity purification of full-length *Xenopus l.* Myosin Va

The initial purification of both the N' and C'FLAG-tagged construct was carried out from as few as 200 ml of Sf9-cell suspension (Figure 64).

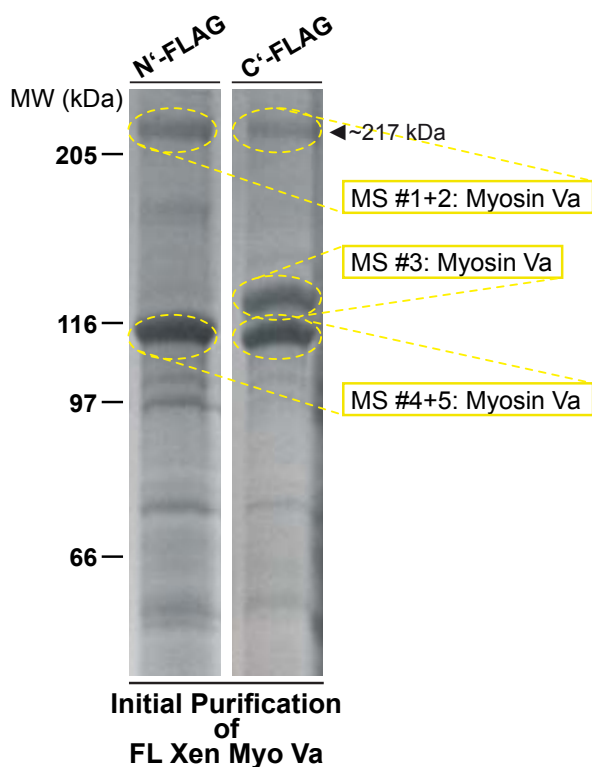


Figure 64. Initial FLAG-tag affinity purification of N' and C'FLAG-tagged full-length *Xenopus l.* Myosin Va.

Proteins were expressed in Sf9-insect cells via the baculovirus expression system, and FLAG-affinity purified from suspension culture (200 ml). Cropped images of Coomassie blue-stained SDS polyacrylamide (12%) gels show the eluted fraction of purified N' and C'FLAG-tagged full-length *Xenopus l.* Myosin Va. Bands of the full-length (bands #1 and #2), but also of three lower-running protein products (bands #3, #4 and #5) were confirmed by mass-spectrometry as Myosin Va. Approximate size of the full-length protein is indicated on the right.

Via mass-spectrometry, both full-length protein products were confirmed as Myosin Va (Table 31). The prominent degradation bands at approx. 110 and 125 kDa (only for the C'FLAG version) that along with the full-length protein product were co-eluted (Figure 64), via mass-spectrometry were clearly identified as Myosin Va derivatives (Table 31).

Table 31. Mass-spectrometry analysis of FLAG-tag affinity-purified full-length *Xenopus l.* Myosin Va.

Sample #	Match to (Protein/Species)	Score	Sequence coverage (%)
1	MyoVA/Gallus g.	3247	30
2	MyoVA/Gallus g.	5428	19
3	MyoVA/Gallus g.	1307	22
4	MyoVA/Gallus g.	5336	30

Results

For optimized full-length Myosin Va purification (Figure 65), protein expression and purification had to be fine-tuned. It was most important to scale up the virus titer as well as to increase the number of cells to be infected. Also, two cycles of FLAG-resin incubation were required, and twice the amount of FLAG-peptides was included during the elution process.

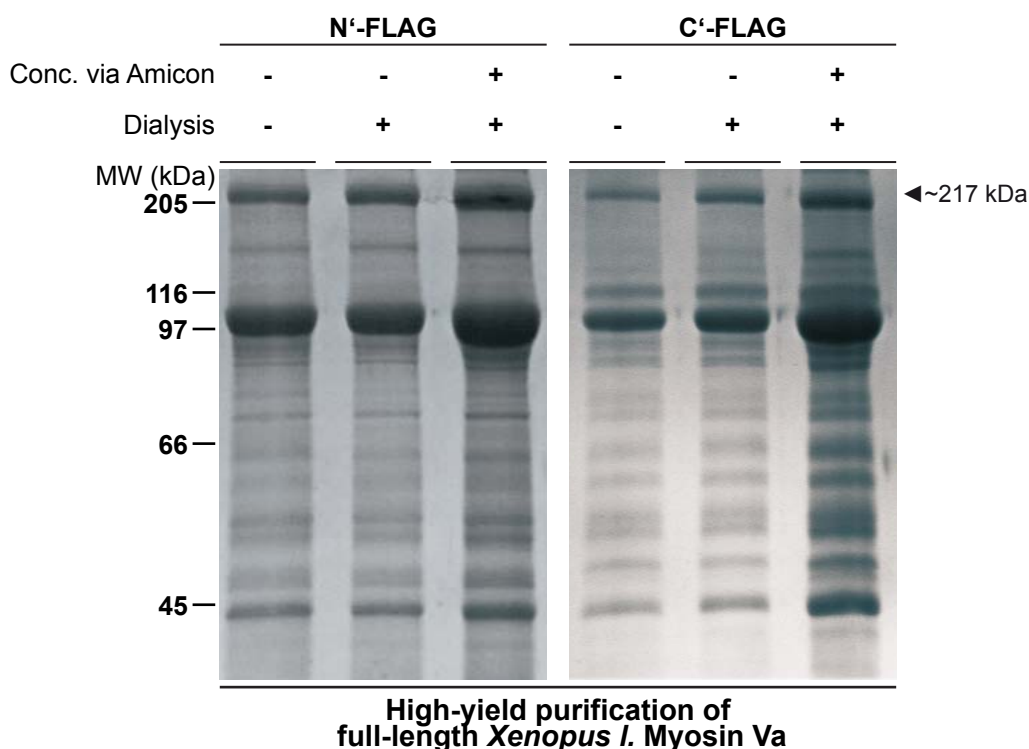


Figure 65. Optimized and large-scale FLAG-tag affinity purification of N' and C'FLAG-tagged full-length *Xenopus I.* Myosin Va.

Left and right panel: N' and C'FLAG-tagged proteins were expressed in Sf9-insect cells via the baculovirus expression system, and FLAG-affinity purified from suspension culture (800 ml). After elution of the purified protein (*left lanes*), one fraction was further dialyzed in buffer containing 50% glycerol (*middle lanes*), followed by an additional concentration via Amicon-Ultra device (*right lanes*). Cropped images of Coomassie blue-stained SDS polyacrylamide (12%) gels show the respective fractions of the purified N' and C'FLAG-tagged full-length *Xenopus I.* Myosin Va. Approximate size of the full-length protein is indicated on the right.

5.4.2.4 *In vitro* gliding motility of full-length *Xenopus I.* Myosin Va on F-actin

Both, the N' and C'FLAG-tagged version of the full-length protein were assayed for their capabilities to bind to, and move, actin filaments. Intuitively, one might expect the C'FLAG-tagged version to be better suited for gliding assays because a tag at the head domain might interfere with motor function. Under zero-ATP conditions both full-length protein constructs perfectly bind to actin filaments

Results

(Figure 66 A and Figure 67 A). However, upon the addition of 2 mM ATP, the observed gliding motion of the C'FLAG-tagged version was clearly impaired (Figure 66 B and Video 9) when comparing it to the N'FLAG-tagged full-length construct (presented in the next paragraph). In other words, only the mechanical force generation and/or catalytic activity of the C'FLAG-tagged molecule are disturbed, while its ability to bind to F-actin seems not to be affected.

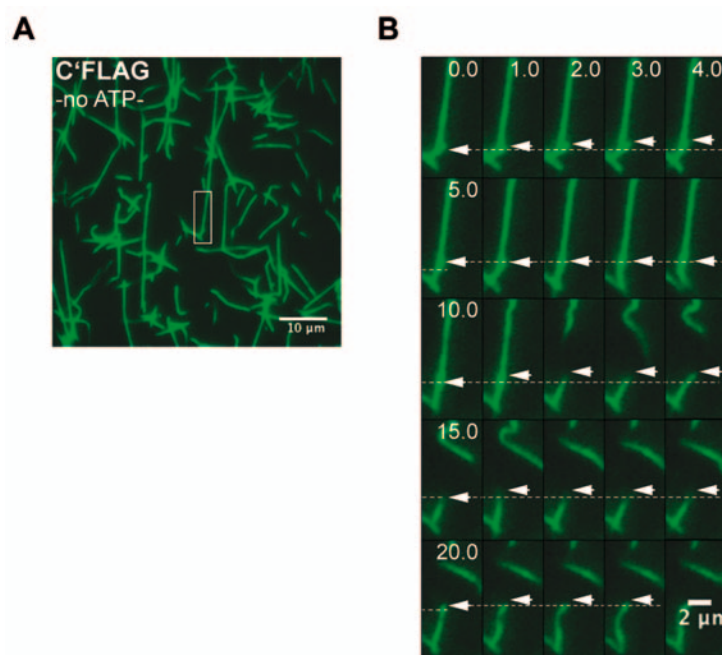


Figure 66. Filament gliding assay with the C'FLAG-tagged version of full-length *Xenopus I.* Myosin Va

(A and B) Atto488-labeled F-actin (green filaments) was infused into a flow cell containing surface-attached C'FLAG-tagged full-length *Xenopus I.* Myosin Va. (A) Directly after infusion, filaments were tightly bound to the surface by myosin. Assay was performed in 25 mM KCl, without ATP, thus no movement could be observed. White frame box indicates the region from where a close-up is provided in B. Scale bar represents 10 µm. (B) Representative TIRF microscopy image sequence of an Atto488-labeled actin filament (indicated by white arrowheads), which is bound to the coverslip by surface-adhered full-length *Xenopus I.* Myosin Va (at 25 mM KCl and 2 mM ATP). The position of the filament at the beginning of each time row is indicated (white dotted line). Also, the position of the filament at the end of one row is marked in the first frame of the row below (dotted white line on the left). Despite the presence of ATP, hardly any filament gliding was observed. Excitation wavelength in A and B was 488 nm. In B same image section (5 × 10 µm) was taken over time with scale bar representing 2 µm.

In contrast, with ATP (2 mM) present, the N'FLAG-tagged full-length Myosin Va practically moves all of the bound actin filaments (Figure 67 B and C, Videos 10 and 11). The fact that without ATP no gliding motility was observed (Video 12) indicates that the post-purification dialysis of the protein solution effectively removes any ATP that had been present during the purification procedure.

Results

Furthermore, the results imply that the initial binding to F-actin happens also in the absence of ATP. The rapid tearing-apart of the transported filaments (compare Figure 67 A and B), most likely is due to the high density of surface-attached motor molecules and the resulting intense pulling force on the filaments.

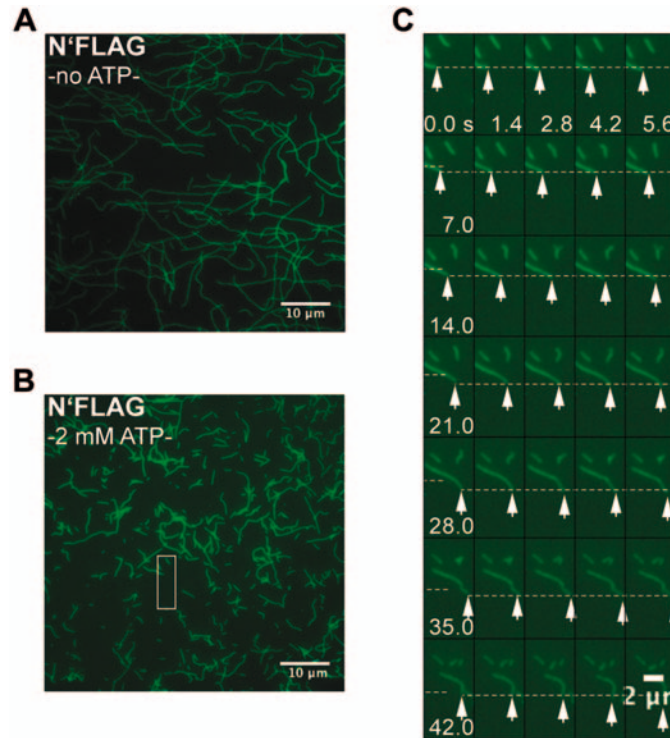


Figure 67. Filament gliding assay with the N'FLAG-tagged version of full-length *Xenopus l.* Myosin Va

(A) Atto488-labeled F-actin (green filaments) was infused into a flow cell containing unspecifically surface-attached N'FLAG-tagged full-length *Xenopus l.* Myosin Va. As for the C'FLAG-tagged version, directly after infusion filaments were tightly bound to the surface. Assay was performed in 25 mM KCl and zero ATP, thus no movement could be observed. (B) To the experiment from A, 2 mM ATP was added and directly thereafter filament gliding of the before tightly bound actin filaments was observed. White frame box indicates the region, from where in C a close-up is provided; Scale bars in A and B represent 10 µm. (C) Representative TIRF microscopy image sequence of an Atto488-labeled actin filament (indicated by white arrowheads), which is bound to the coverslip by surface-adhered full-length *Xenopus l.* Myosin Va. The position of the filament at the beginning of each time row is indicated (white dotted line). Also, the position of the filament at the end of one row is marked in the first frame of the next row (dotted white line on the left). An obvious downward movement over time was measured (compare positions at the beginning and end). Excitation wavelength in A through C was 488 nm. In C same image section (5 × 10 µm) was taken over time with scale bar representing 2 µm.

The gliding events lasted on average for 31.4 s with an average gliding distance of 3.8 µm (Table 32). A gliding velocity histogram yielded a single-Gaussian fit (Figure 68) with a deduced mean value for the gliding velocity of 131.2 nm s⁻¹. This corresponds to velocities that have been reported for the

Results

Myosin V-driven melanosome transport on F-actin *in vivo*¹⁷⁶ and *in vitro* (D. Zimmermann & A. Oberhofer, unpublished data).

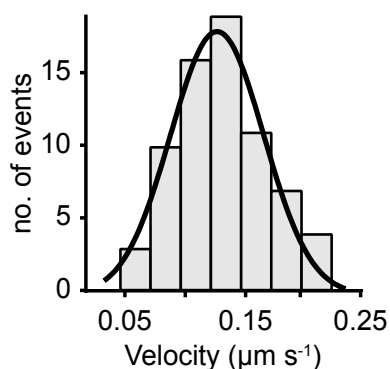


Figure 68. Analysis of filament gliding behavior of N'FLAG-tagged full-length *Xenopus I.* Myosin Va.

Filament gliding velocity distribution was plotted as histogram. Data were obtained from filament gliding experiments, where 500 nM full-length *Xenopus I.* Myosin Va (N'FLAG-tagged version) was adhered to the surface of a coverslip and incubated with Atto488-labeled F-actin in 25 mM KCl and 2 mM ATP. The data were fitted to a single Gaussian (according to Equation 7), yielding a mean velocity of $0.13 \mu\text{m s}^{-1}$ ($n=70$).

Table 32. Summary of the filament gliding behavior of N'FLAG-tagged full-length *Xenopus I.* Myosin Va.

	Velocity ($\mu\text{m s}^{-1}$)	Distance (μm)	Duration (s)	n
FL Myo Va	131.2 ± 6.5	3.8 ± 0.2	31.4 ± 1.7	70

Mean filament gliding velocities, distances and durations for the full-length *Xenopus I.* Myosin Va (N'FLAG-tagged version, 500 nM) were obtained from gliding filament assays at 2 mM ATP and 25 mM KCl. Mean gliding velocity was determined from the Gaussian fit to the histogram data provided in **Figure 68**. All values represent the mean \pm S.E.M with n as the number sampled for this summary.

To test for single-point attachments indicative of processive movement (**Figure 69** and Video 13), the motor concentration was reduced to 200 nM while keeping the F-actin concentration constant. Expectedly, this led to a decrease in filament binding events. However, those filaments that were bound to the surface of the flow cell mostly were bound through the action of only one or a few motors (indicated by white arrowheads in **Figure 69**). Even though this decreased the likelihood of smooth filament gliding, the typical filament threading where one processive motor molecule takes multiple consecutive power-strokes, could be observed.

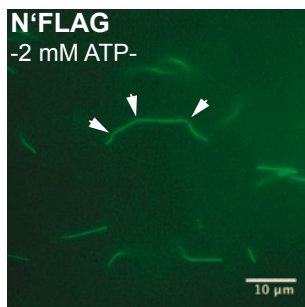


Figure 69. Filament gliding assay with the N'FLAG-tagged full-length *Xenopus I.* Myosin Va showing single-point attachments.

Atto488-labeled F-actin (green filaments) was infused into a flow cell containing 200 nM unspecifically surface-attached N'FLAG-tagged full-length *Xenopus I.* Myosin Va. Immediately after infusion, filaments were bound to the surface and started to show movements. Due to the low number of filament-bound motor molecules, the filament gliding was hardly as smooth as observed in Figure 67. However, the filament threading by single motor molecules implies processive movement of the assayed motor protein. White arrowheads indicate said single-point attachments by (in this case) three Myosin V molecules. Assay was performed in 25 mM KCl and 2 mM ATP; excitation wavelength was 488 nm; scale bar represents 10 μm.

With this finding, evidence was provided that single full-length Myosin Va molecules exhibit ATP-dependent, but most importantly, processive movement.

5.4.2.5 *In vitro* single-molecule motility of full-length *Xenopus I.*

Myosin Va on F-actin

The motile behavior of full-length *Xenopus I.* Myosin Va was studied in single-molecule motility assays. To this end, motors were labeled at their head domain with a FLAG-tag reactive Cy3-labeled antibody (for experimental details, see Section 4.3.5.1.2). In the presence of 2 mM ATP, single fluorescently labeled motor molecules landing on surface-adhered F-actin were observed (Figure 70 A, Video 14). However, only infrequently an actin-bound Myosin Va molecule was also observed to move (Figure 70 B, Video 15). This finding shows that in principle the tracking of single full-length *Xenopus I.* Myosin Va motor molecules is possible.

Results

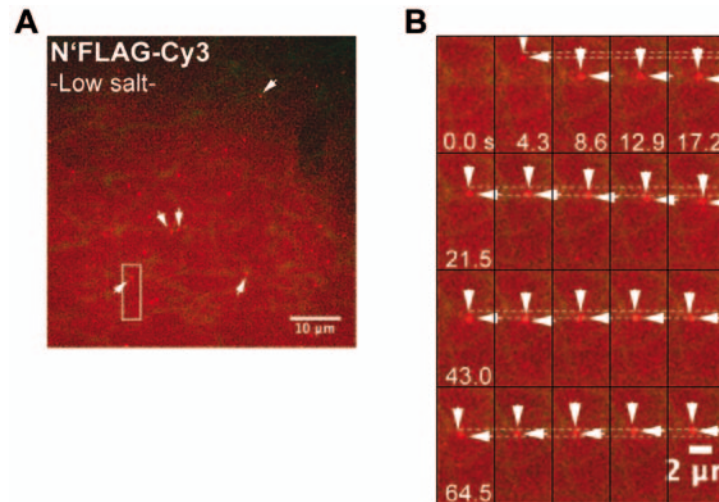


Figure 70. Single-molecule motility of N'FLAG-tagged full-length *Xenopus I.* Myosin Va on F-actin.

(A and B) 100 nM Cy3-labeled N'FLAG-tagged full-length *Xenopus I.* Myosin Va (bright particles) were infused into a flow cell containing surface-attached Atto 488-labeled F-actin (fuzzy green filaments in background). (A) *White arrowheads* indicate representative single Myosin Va molecules that co-localized with actin filaments. Assay was performed in 25 mM KCl and 2 mM ATP. Myosin was excited at 532 nm and F-actin at 488 nm; *scale bar* represents 10 µm; white frame box indicates the region from where a close-up is provided in B; (B) Image sequence of a single Cy3-labeled full-length *Xenopus I.* Myosin Va molecule (indicated by *white arrowheads*) on F-actin. The vertical as well as horizontal position of the motor molecule at the beginning of each time row is indicated (*white dotted lines*). The continuous edging up of displacements over time reflects the characteristic processive but slow walking behavior of the full-length motor molecule on F-actin. The same image section (5 × 10 µm) was taken over time. *Scale bar* represents 2 µm.

As is known from previous studies on full-length Myosin Va from other species^{54,177,178,179}, under low-salt and low Ca^{2+} conditions the globular tail domain almost always folds back onto the two heads, causing auto-inhibition. Thus, though the mechano-catalytic function is inhibited, the capability to bind to F-actin is not affected⁵⁵.

One possibility to overcome this problem is to test the single-molecule behavior of the full-length protein under high-salt conditions (150 mM). Compared to the low-salt condition, the overall specific binding of Myosin Va to F-actin was decreased, however, still only infrequently directed movements along F-actin were observed (Figure 71 A and B, Video 16).

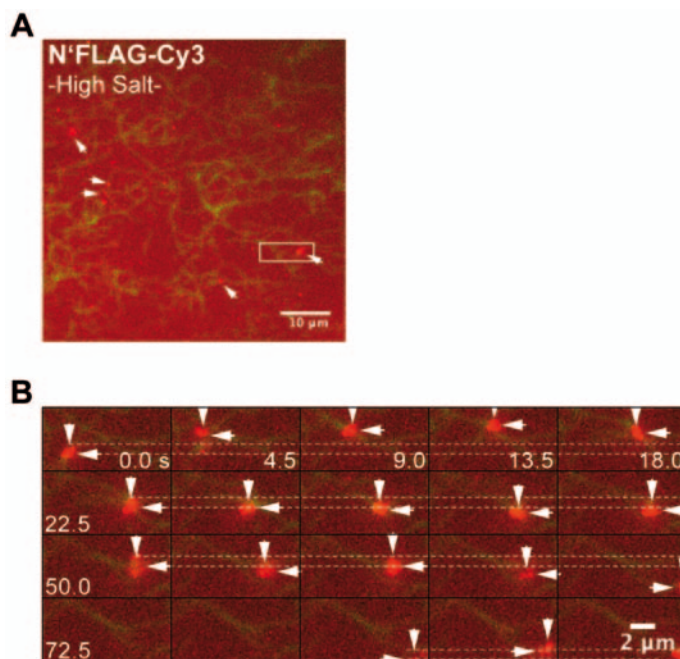


Figure 71. Single-molecule motility of N'FLAG-tagged full-length *Xenopus I.* Myosin Va on F-actin – High salt.

(A and B) Setup of this experiment was the same as described for Figure 70, except that 150 mM salt instead of 25 mM salt was included. (A) *White arrowheads* indicate representative single Myosin Va molecules that co-localized with actin filaments. Myosin was excited at 532 nm and F-actin at 488 nm; *scale bar* represents 10 μm ; white frame box indicates the region from where a close-up is provided in B; (B) Image sequence of a single Cy3-labeled full-length *Xenopus I.* Myosin Va molecule (indicated by *white arrowheads*) on F-actin. The vertical as well as horizontal position of the motor molecule at the beginning of each time row is indicated (*white dotted lines*). In this sequence the molecule of interest shows strong rightward movement at the beginning but then also starts to move vertically. The same image section (5 \times 10 μm) was taken over time. *Scale bar* represents 2 μm .

Unfolding the auto-inhibited molecule by the binding of an artificial cargo to the C-terminal domain was a second approach to revoke auto-inhibition. Analogous to the fluorescent labeling with anti-FLAG-Cy3 antibody, the C'FLAG-tagged full-length version was conjugated to an anti-FLAG-Biotin antibody and thereby biotinylated. This way, quantum dots (Qdots) coupled to streptavidin can bind to the tail domain, imitating motor-bound cargo. The fact that control experiments (i.e., same Qdot concentration but no motor protein) showed only very few unspecific surface-attached Qdots, indicates that the Qdot-coupling works well (Figure 72).

Results

However, no directed motion could be observed. Whether this is because unfolding via the Qdot-tail conjugation simply does not work or because the C'FLAG-tagged version's walking ability in general is impaired, remains to be shown.

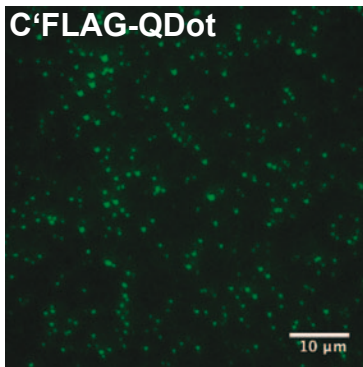


Figure 72. Single-molecule TIRFM measurement of Quantum dot-labeled full-length Myosin Va on F-actin.

A final concentration of 10 nM full-length *Xenopus l.* Myosin Va (C'FLAG-tagged version) conjugated to Qdots (bright particles; 2.5 motor molecules per Qdot) were infused into a flow cell containing surface-attached Atto488-labeled F-actin (not visible in this setup). In the here presented and representative image section (60 × 60 μm, false-colored) only static non-motile particles were observed. Assay was performed in 25 mM KCl and 2 mM ATP at 532 nm excitation wavelength. *Scale bar* represents 10 μm.

Future experiments will show whether under optimized high ionic-strength conditions and with sufficient amounts of applied motor protein, movement of single Myosin Va molecules can be visualized or whether certain modifications have to be made to turn the full-length protein constitutively active.

6 Discussion

6.1 Movement of Myosin Va loop 2 mutants on F-actin and microtubules

In all myosins the loop 2-motif represents a crucial surface structure that lies between the upper and lower 50 kDa sub-domain of the head domain. While the conventional class II myosins contain a relatively short loop 2 (18 to 24 amino acids), in Myosin Va it is 45 amino acids in length and highly positively charged (net charge +5)^{35,112,180}. Loop 2 lies at the actin-binding site of Myosin V²⁴ and is most widely believed to be responsible for the initial weak binding to actin via electrostatic interactions between the positively charged amino acids of loop 2 and negatively charged residues in the subdomain-1 of actin¹⁸¹. Upon binding to actin, the initial stereospecific actin-binding interface is created eventually culminating in rapid phosphate release^{24,111,182,183,184}. In recent years, the functional role of the Myosin V loop 2 has been studied with mutants, where single lysine residues at the C- or N-terminal Myosin V-specific amino acids have been substituted with neutral or negative residues^{35,111}. By substituting all nine positively charged amino acids with either neutral or negative residues, in this study two novel mutants with a negative net charge on loop 2 were created. In addition, by inserting a microtubule E-hook-binding loop motif from a class 3 kinesin into the central part of loop 2, a third mutant was generated here. The behavior of the three Myosin Va loop 2 mutants along with the *Wildtype* Myosin V was studied on F-actin as well as on microtubules.

6.1.1 Myosin Va loop 2 mutant behavior on F-actin

It has been suggested that loop 2 is pivotal for the coupling of ATP hydrolysis to the actual mechanical work. Therefore the behavior of the four Myosin Va loop 2 constructs on F-actin was assayed for actin-stimulated ATPase activity and in single-molecule motility assays yielding unexpected results.

For the *Wildtype* construct, the ATPase activity values were in good agreement with those reported previously (Figure 39 and Table 30)^{35,44}. This confirmed the integrity and functionality of the motor proteins. In contrast, in mutants containing a negative loop 2 net charge (*Minus4* and *Minus13*), ATPase activity was

Discussion

abolished completely (**Figure 39**). This is consistent with findings of previous studies where a so-called AAA-mutant with a decreased positive loop 2 net charge showed a decrease in ATPase activity^{35,111,166}. In contrast to the *Minus4* and *Minus13* mutants, the AAA-mutant ATPase activity was not abolished completely, most likely because its loop 2 still contained an overall positive net charge (+2) and thus the K_m was decreased by only a factor of 5³⁵. At the molecular level this is explained by the fact that for Myosin Va to trigger phosphate and ADP-release it is a prerequisite to weakly bind to actin, for which electrostatic attraction of loop 2 towards F-actin is crucial^{24,111,183,184}. If however electrostatic attraction is changed into electrostatic repulsion (i.e., negative charge on loop 2 and on sub-domain1 of F-actin), then actin-stimulation of the ATPase cycle cannot occur. Along this line, if the initial weak binding does not function properly, then essential intramolecular rearrangements within the upper and lower sub-domains of the head domain cannot occur, culminating in impaired mechanical force generation^{24,111,183,184,185}. Therefore, no persistent walking events were observed in the single molecule assays of *Minus4* and *Minus13* mutants (**Figure 38 A** and Video 5).

Strikingly however, the loop 2 mutant carrying the microtubule E-hook-binding motif from kinesin KIF1A (kinesin-3), exhibited proper ATPase activity as well as single-molecule motility on F-actin (**Figure 38 A**, **Figure 39**, **Figure 40**, Table 30, Videos 6 and 7). While both, Myosin Va *Wildtype* and *K-loop*, showed highly similar values for k_{cat} (i.e., actual hydrolysis rate of ATP mol⁻¹ s⁻¹), in comparison to *Wildtype*, the K_m of the *K-loop* mutant was increased almost three-fold (Table 30). This finding indicates that *K-loop* can hydrolyze ATP at the same rate as *Wildtype*, but to achieve the same performance it however must be stimulated with three times higher actin concentrations. In other words, ATP hydrolysis was not impaired or harmed but the affinity by which the weakly-bound actin state is achieved was significantly lower. A similar observation was made by Yengo, CM and colleagues (2004)³⁵, who reported that compared to *Wildtype* Myosin Va the K_m of the AAA-mutant (2 instead of 5 positive net charges) was decreased five-fold.

Across all the myosins classes, actual ATP-hydrolysis takes place in the absence of actin. Hence, for this the lower affinity of *K-loop* for F-actin would be irrelevant. However, a myosin molecule can only re-bind a new ATP molecule for the next

Discussion

round of ATP-hydrolysis, if the hydrolysis products inorganic phosphate (P_i) and ADP were released. This in turn is only possible, if the initial binding to actin is properly achieved, which according to the ATPase data for *K-loop* is three times less likely or can be assumed to take place at three times slower pace.

Therefore, if it took the *K-loop* mutant longer to re-bind to actin and initiate product release, then how does it catch-up to re-bind fresh ATP within the same cycle time as the *Wildtype* construct? The single-molecule motility analyses revealed that the mean velocity of *K-loop* was half as fast as *Wildtype* Myosin Va (Table 30). Slower speed means that less distance within the same time frame was covered. Thus per given time interval fewer steps (i.e., power-strokes) were taken along the filament. According to recent models, the power-stroke of the lever-arm does not happen before P_i release but rather directly before or during release of ADP^{24,33,185,186,187,188}. As mentioned, P_i release happens only after the binding to F-actin was successfully initiated by loop 2. It has been shown that for the electrostatic weak binding, only the net charge and not the size of loop 2 matters¹¹¹. Thus for *K-loop* with its lower positive net charge on loop 2, fewer power-strokes are triggered, resulting in slower walking.

In processive myosins like Myosin V, the rate-limiting step is ADP release from the binding pocket of the head domain. Compared to the rapid phosphate release, the release of ADP is very slow ($12\text{-}16\text{ s}^{-1}$)³². Thereby processive motors such as Myosin Va ensure to stay attached long enough attached with one (the leading) head, while the second, detached (trailing) head hydrolyzes the bound ATP ($> 250\text{ s}^{-1}$)³², and via diffusive search finds the next actin-binding site^{45,46}. This leads to the fact that in the presence of ATP, Myosin V spends more than 70% of its kinetic cycle strongly bound to actin³². Interestingly, even though the *K-loop* mutant showed slower walking speed (i.e., decreased mean velocity), the same average runlength as for *Wildtype* was obtained (Figure 41 and Table 30). With runlength being a measure of processivity, this suggests that the rate-limiting ADP release step remained unaltered. Given that processivity must not change and that ADP release succeeds phosphate release and that the weak- to strong-binding transition occurs after the initial loop 2-contact has been made¹⁸⁹, then it seems plausible that phosphate release entails the automatic delay in ADP release. Thus slower cycle rates (i.e., k_{cat}) would be expected. For the *K-loop* mutant, however, this discrepancy between the predicted outcome and the actual

Discussion

findings might be explained as follows: Once weakly bound to actin (i.e., during P_i release and subsequent power stroke), the cluster of positively charged lysines in the central part of loop 2 enforces the faster transition to the strong binding state, which in turn would cause ADP to be released faster. This way, the slower phosphate release would be caught up by the accelerated ADP release. This would imply that unlike for the initial weak binding to actin, for Myosin Va to successfully complete multiple ATPase cycles, the distribution of charged residues and not only the total net charge, could play a role. This is in line with a previous study, where it was shown that the specific distribution of charged amino acid residues on their binding partners was more important than the net charge in the vicinity of the binding site ¹⁹⁰. My work here shows that a Myosin V that contains a microtubule-binding motif from kinesin within its conserved loop 2 region is still functional, despite exhibiting lower velocities ¹⁹¹.

Furthermore, it is not unlikely that besides loop 2 also additional structural motifs ensure and maintain the correct initial binding to the actin filament. To obtain a better view of all the potential factors that play important roles at the myosin-actin interface, over the past decade a number of structural simulation and modeling studies have been undertaken. However, the nature of the actin-myosin interface is still a matter of speculation and details are lacking ^{189,192}, which is mainly because to date there is no structure of an actin filament available ¹⁹³. Therefore, studying of the actual binding interface is hard and thus relies on models that are based on results from cross-linking studies and the docking of high-resolution structures of myosin into more or less well-resolved cryo-EM density maps ^{194,195,196,197,198}. In those models it was suggested that besides the electrostatic binding by loop 2 also hydrophobic attraction from loop 2 and other loops (e.g., cardiomyopathy-loop) takes place at the interface ¹¹². Mutations within those regions caused partial or complete ATPase activity abrogation ¹⁸⁴. Furthermore, besides the binding to the major actin monomer (i.e., AC3), more recent simulations showed that most likely by using surface loops 3 and 4, the myosin also binds to the first (i.e., AC1) of the five involved actin monomers ^{112,194}.

Therefore, in the future it will be worth investigating, if for the *K-loop* mutant the hypothesis that the distribution of positive charges rather than the total net charge, holds true and whether additional motifs of the Myosin V head contribute to this intriguing and novel finding.

6.1.2 Role of the loop 2 net charge for its interaction behavior with microtubules

The observation that not only positively but also *negatively* charged loop 2 constructs displayed a salt-dependent decrease in microtubule association (Figure 25) allows the following two conclusions. First, electrostatic interaction is indeed the prevailing force mediating the association of Myosin Va with microtubules. Second, loop 2 is not the site responsible for such attraction because the oppositely charged loop 2 constructs *Wildtype* and *Minus4* (+5 vs. -4) display equivalent salt-sensitive binding behavior. Along with the observation that the *Wildtype* and *Minus4* mutants associate at equivalent levels with microtubules further supports the notion that loop 2 neither mediates nor maintains the interaction between Myosin Va and microtubules (Figure 25). Thus another charged patch (or even multiple patches) on the Myosin Va surface, mediating the observed salt-dependent interaction with the microtubule, need to be considered. If, as hypothesized here, the electrostatic interaction between Myosin Va and microtubules is not mediated by the previously proposed myosin loop 2-microtubule E-hook interaction, then the *K-loop* construct with its E-hook-specific binding motif would be expected to yield higher association rates than the *Wildtype* construct. Notably, as was shown in Figure 25 the *K-loop* mutant indeed showed the most efficient association with microtubules. This implies that the previously proposed interaction between loop 2 of Myosin Va and the microtubule E-hooks can take place, but only if the E-hook-specific binding motif K-loop is present on the loop 2 of Myosin Va. This is in line with a previous study, where the K-loop motif induced diffusional motility when introduced into the head domain of the normally non-diffusive but processive class 1 kinesin Kif5¹⁴⁶. Similarly, the diffusive behavior of MCAK (class 13 kinesin) that had lost the ability to diffuse was restored when introducing the K-loop motif into the motor/microtubule-binding domain of this prototypical diffusional kinesin¹⁹⁹.

Conversely, as soon as enough negative charges were introduced into loop 2 of Myosin Va (e.g., *Minus13*), microtubule “affinity” for Myosin Va was significantly reduced (Figure 25). Those two findings suggest that for the *Minus13* mutant strong repulsion forces arise from the evenly distributed negative charges, while for the

K-loop construct the additional E-hook binding motif and not net charge itself accounts for the observed additional microtubule binding events.

Taken together, the results suggest that the dominating force that tethers Myosin Va to the microtubule is due to charge-charge interactions. However, those interactions are by no means mediated by loop 2. In addition to electrostatic forces, non-electrostatic forces may exert a significant influence at the Myosin Va-microtubule interface.

Most strikingly, and contrary to the predictions inferred from the electrostatic model, the charge of loop 2 neither determines nor limits the diffusion behavior of Myosin Va. The similarity of the diffusion constants ($0.113 \mu\text{m}^2 \text{s}^{-1}$ of *Wildtype* to $0.089 \mu\text{m}^2 \text{s}^{-1}$ of *Minus13*) (Figure 28 and Table 28) argues against a loop 2-biased charge-dependence in diffusion. The diffusion constants not only are comparable to each other, but also are in fine agreement with diffusion constants obtained for other microtubule-binding proteins and even proteins diffusing along DNA 107,116,164,200.

6.1.3 Role of the microtubule E-hooks for the interaction of Myosin Va with microtubules

The fact that on the side of the interactor (i.e., Myosin Va) loop 2 as the potential electrostatic tether structure is neither required for the binding to nor for the diffusion along microtubules, prompted us to dissect the potential contributions of the substrate (i.e., microtubule) to Myosin Va association and diffusion. If indeed attraction forces other than electrostatic tethering contribute to the interaction between Myosin Va and microtubules, then microtubule E-hooks representing the proposed electrostatic tethering structures should be dispensable.

Indeed, on S-microtubules lacking E-hooks, association levels for *Wildtype* and *Minus4* remained unchanged compared to untreated microtubules (Figure 34 vs. Figure 25), demonstrating that E-hook-mediated tethering is not involved in microtubule association of Myosin Va. In fact, these effects were readily revoked after the repulsive microtubule element (i.e., E-hooks) was removed (compare Figure 34 with Figure 25). This leads to the proposal that E-hooks impact the association behavior of *K-loop* (with its E-hook-specific motif) and *Minus13* (with

Discussion

its extensive negative charge) only if the interacting molecule (here Myosin Va) carries the specific E-hook binding motif or provides an abnormally high repulsion. As mentioned earlier, the K-loop represents only an additional and KIF1-specific E-hook binding loop¹⁴⁶. Being intrinsically monomeric, KIF1A cannot move along the microtubule in a hand-over-hand fashion and thus relies on the ability to exhibit diffusional displacements. Therefore, for KIF1A a K-loop comes handy because it ensures weak binding and thus provides the basis for one-dimensional diffusion along the microtubule¹¹⁹. However, other kinesins such as MCAK almost exclusively exhibit diffusional motility on microtubules but at the same time lack the K-loop structure^{116,146}. In that respect, it has been shown for a number of kinesins that for weak binding (required for one-dimensional diffusion along the lattice) to the microtubule surface, the electrostatic interaction with E-hooks is not essential. For instance, via its surface loop L7 class 3 kinesins bind to the β -tubulin subunit of the protofilament directly^{201,202,203}. Also, such highly conserved structures like the α -helical segments 4, 5 and 6 together with loop L8 (all part of the motor head-domain) were shown to mediate the weak binding to the microtubule surface via electrostatic interaction¹⁴⁶. In addition, from structural studies on the MCAK kinesin it is known that not always a specific binding motif, such as the K-loop or the myosin loop 2 is required to initiate weak binding, but rather unspecific binding via unstructured and flexible regions would be sufficient^{116,199,204}. Taken together, even kinesins show diverse ways and structural motifs (mostly within the motor's head domain) to weakly interact with microtubules. With this in mind, it is just logical that Myosin Va, which so far has not been conceived as a classical microtubule-associated protein, uses different ways and structures than those used for the initial binding to actin filaments.

While the capacity to interact with S-microtubules did not differ significantly, diffusion was observed only with the *Wildtype* and *K-loop* construct (Figure 34 and Table 29). In other words, on microtubules lacking E-hooks, the fraction of associated motors remains high, though fewer of the attached Myosin Va molecules advance to the diffusive state and thus remain stationary. As soon as the nearly homogeneous mantle of negatively charged E-hooks is removed, non-ionic forces (e.g., van-der-Waals interactions) that show strong effects over short distances^{205,206} become a substantial attraction force. This is well reflected again

by the fact that on S-microtubules salt-sensitivity for all four Myosin Va constructs is decreased (compare **Figure 26** and **Figure 35**).

This suggests that non-ionic attraction forces account for the observed decrease in diffusion for all four Myosin Va constructs, while the overall affinity remains comparable to that of *Wildtype* Myosin Va on untreated microtubules. In addition, when E-hooks are present, they may act as negatively charged 4 nm spacers^{160,161} that via repulsion facilitate transitions from the stationary to the diffusion phase. Hence on microtubules that lack E-hooks, constructs containing a pronounced negatively charged loop 2 region (*Minus4* and *Minus13*) are now free to productively interact with the unshielded positive patches on the "naked" microtubule surface^{160,165} (**Figure 34**). In contrast, the *Wildtype* and *K-loop* constructs with their net positive loop 2 charge, retain some residual ionic repulsive capacity (positive loop 2 vs. positive patches on the microtubule surface) and thereby on S-microtubules still manage to advance into the diffusive state (**Figure 34**, **Figure 36**, Video 4).

This suggests that only these two constructs are capable of balancing the interplay between ionic and non-ionic effects, making them almost "immune" to harsh changes on the microtubule. A closer look at the diffusion behavior of *Wildtype* Myosin Va reveals that compared to untreated microtubules, its diffusion along S-microtubules in fact is smoother (larger single displacements), yielding an increased diffusion constant (**Figure 36** and Table 28).

6.1.4 Conclusion and Outlook

To gain detailed mechanistic insights into the unbiased diffusion of Myosin Va, in this study association of Myosin Va with microtubules (i.e., binding without additional quantification of subsequent diffusion events) was distinguished from diffusion *per se*. Also, by assaying monomeric and dimeric Myosin Va mutants (*Wildtype* loop 2) that contained the head-domain only, microtubule interaction and one-dimensional diffusion by Myosin Va can be assumed to be limited to the head domain (preliminary data not included in this work). Even though only preliminary, these results now provide a robust basis to perform further studies, aiming on revealing the definite site(s) within the head domain responsible for the interaction between Myosin Va and microtubules.

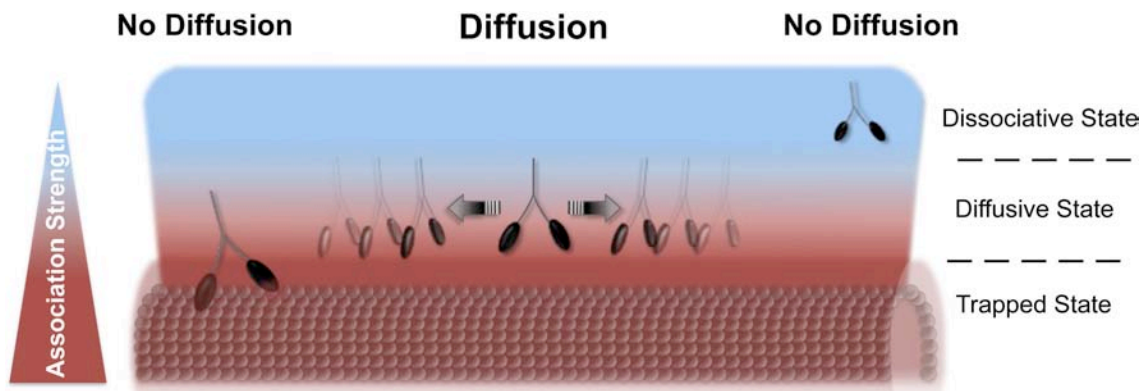


Figure 73. The balance between attraction forces determines the diffusive state of Myosin V on microtubules.

(Left part) Strong attraction forces prevent microtubule-bound Myosin V molecules from advancing to the diffusive state. This *Trapped State* is achieved, if in addition to electrostatic also non-ionic attraction forces become increasingly dominant (*Minus4* and *Minus13* on S-microtubules). (Middle part) Diffusion takes place if for Myosin V the attraction toward the microtubule is of moderate strength. This *Diffusive State* in general is achieved when attraction and repulsion outweigh each other. Two different possibilities might account for that behavior. First, electrostatic and non-electrostatic interaction forces at the Myosin V binding-interface are well-balanced (*Wildtype* on untreated and S-microtubules); second, strong loop 2-derived ionic attraction is dominated by ionic repulsion elements (E-hooks) on the microtubule binding-interface (*Minus4* on untreated microtubules). (Right part) Weak attraction toward microtubules prevents Myosin V from binding effectively to the filament, and hence diffusion becomes unlikely. This *Dissociative State* is given, if electrostatic repulsion via hydrophilic surface structures (E-hooks) becomes predominant (*Minus13* on untreated microtubules). Red and blue colors indicate strong and weak attraction forces toward the microtubule surface, respectively.

In analogy to recent findings by Minoura *et al.*¹⁶¹, the here presented findings suggest the following two-phase model for diffusion of Myosin Va on microtubules. *Phase One* is the initial association with the filament. This step represents a prerequisite for diffusion and is accomplished as long as electrostatic surface effects exerted from both, the interactor and the substrate, cause attraction rather than repulsion. *Phase Two* is the advancement to the diffusive state. This phase heavily depends on a balanced interplay between attractive and repulsive forces of Myosin Va and microtubules. Here, it is crucial that the strength of attraction is limited to such an extent that the motor is free to move laterally. Simply put, strong attraction forces may bind a high number of motor molecules to the surface but they also prevent those motors from moving (*Minus4* and *Minus13* on S-microtubules); conversely, weak attraction favors the diffusion along filaments, but at the same time gives the molecule a hard time to initially bind (*Minus13* on untreated microtubules). Since the dosage makes the difference, in this specific case the dosage of electrostatic vs. non-ionic attraction

on the surface determines the strength of binding and the likelihood of moving (Figure 73).

Compared to motor-driven directed movement, unbiased one-dimensional diffusion is faster over short distances and does not consume energy, thus representing a supportive mechanism for intracellular transport processes^{25,108,147,164,207}. In addition to Myosin Va, in most recent years a number of kinesins and other microtubule-binding proteins (e.g., MCAK, Dam1 complex, Ncd80 complex, tau and XMAP215) have been shown to exhibit unbiased (non-directional) one-dimensional diffusion^{116,200,208,209,210}. Despite all those candidates so far identified, to date most of the hypotheses brought forward base on knowledge that has been acquired from the well-studied phenomenon of one-dimensional unbiased diffusion of DNA-binding proteins along DNA strands^{211,212,213,214}. Interestingly, the diffusion constants for proteins exhibiting diffusional motility along microtubules ($0.1 - 0.4 \mu\text{m}^2 \text{s}^{-1}$) are in the same range as those of diffusion along DNA^{107,116,164,200}. However, the mechanism of protein diffusion on microtubules is still unclear. However, based on the previous and now here presented findings, it becomes evident that an even more complex and multilayered picture of the interaction modes between Myosin Va (and perhaps further microtubule- and non-microtubule binding proteins) and microtubules emerges.

Furthermore, as long as atomic structures of the microtubule are missing, it will be difficult to predict the exact binding events on the microtubule lattice. Another important aspect that so far has not been paid attention to is that posttranslational modifications of the track might affect the diffusion of interacting proteins. From a previous study of DNA-DNA methyl-transferase interaction, it is known that the enzyme's diffusional motility was enhanced drastically when it encountered hemimethylated DNA. Since in a cell tubulin is known to be heavily modified both post-translationally as well as post-polymerisationally^{215,216,217}, this aspect will need to be investigated in more detail.

In this respect unbiased diffusion of Myosin Va contrasts with biased diffusion of certain kinesins such as MCAK along microtubules, which is E-hook-dependent^{116,218}. A different kinesin motor, kip3 from yeast, which belongs to the kinesin-8 class, also diffuses on microtubules, but does so without the help of E-hooks²¹⁹.

Discussion

Thus different types of motors can diffuse on microtubules, but the underlying mode of interaction differs.

However, the E-hook-independent mode of interaction displayed by Myosin Va offers an attractive explanation for the recent *in vitro* observation that Myosin Va might increase kinesin's run length on microtubules¹¹⁰. The here presented results point to a possible synergism between E-hook-independent tethering by Myosin Va to microtubules that might enhance the E-hook-dependent processive movement of kinesin. However, Myosin V-mediated runlength-enhancement of Kinesin-2 has been assayed in a rather artificial *in vitro*-system, where purified Kinesin-2 and truncated Myosin Va were attached to Qdots to mimic cargo¹¹⁰.

To better study the proposed role of Myosin Va, in future studies it would be appealing to use a more biologically relevant system. For this, it would be ideal to use a cellular cargo, which contains the necessary motor make-up, in an *in vitro* assay similar to what Ali *et al.* were using. Melanosomes would be ideally suited for this because if isolated carefully, melanosomes retain all three motor protein classes (cytoplasmic dynein, Myosin Va and Kinesin-2) and transport on microtubules^{65,74} as well as actin filaments can be reconstituted *in vitro* (D. Zimmermann & A. Oberhofer, manuscript in preparation). To test whether Myosin V's ability to interact with microtubules indeed assists the kinesin-driven transport on microtubules, the transport of normal and Myosin V-deficient melanosomes would have to be assayed and compared. If indeed Myosin V enhances runlength, then the Myosin V-containing melanosomes would be expected to yield longer transport ranges on microtubules than melanosomes lacking Myosin V. It will by no means be trivial to obtain melanosomes that lack Myosin V on their surface. However, Karcher *et al.* showed that the Calcium-/Calmodulin-dependent kinase II (CaMKII) in mitotic *Xenopus* egg-cell-extract is capable of releasing Myosin V from melanosomes¹²¹.

Therefore, it would be highly valuable to investigate whether purified CaMKII can indeed specifically remove Myosin Va from melanosomes, while leaving the other melanosome-associated motor proteins (especially kinesin) untouched. Such a study would also provide further insights about the interplay between the CaMKII and melanosomes.

6.2 Studying the effects of Calcium-/Calmodulin-dependent Kinase II- α on melanosome-associated Myosin Va

6.2.1 Expression and purification of functional recombinant CaMKII- α

CaMKII- α is one of the most abundant proteins in the brain and thus has been thoroughly studied over the past two to three decades, in the majority of cases the full-length native-form CaMKII- α has been purified from rat brain ^{220,221}. Even though, isolating the kinase from rat brain is a tedious procedure that requires high amounts of brain material (about 20 rat brains), with at the end relatively low yields in protein concentration (Z. Kochovski, personal communication). In cases, where only a kinase fragment (e.g., the active N-terminal portion) is needed, it has become a standard procedure to express such constructs in *E.coli* ²²². However, due to high cytotoxicity of the constitutively active kinase fragment, protein yields are very low when using this procedure ²²³. By contrast, high yields of the fragment can be expected when over-expressed in insect cells via the baculovirus system ²²². The initial attempt to express recombinant full-length CaMKII- α via the baculovirus system was made by Brickey and colleagues two decades ago ²²⁴. However, most likely due to the laborious additional purification via calmodulin-sepharose (which is rather expensive, if purchased commercially) and FPLC, which is required when purifying untagged recombinantly over-expressed proteins, only very rarely the full-length protein has been retrieved this way ^{122,225}.

One goal of this work was to set up a protocol that allows for FLAG-tag affinity purification of the baculoviral-expressed full-length protein. Therefore a FLAG-tag was fused to either the later N- or C-terminus of the full-length CaMKII- α -encoding cDNA from rat brain (**Figure 42** and **Figure 43**, Section 5.2.1.1). This way, the time-consuming and expensive additional purification steps, which at the same time also entail further protein loss, could be omitted from the procedure. The expression and purification protocol used here yielded high (> 20 μ M) protein concentrations for both the C' and N'FLAG-tagged kinase version (**Figure 43**).

6.2.2 Functional analyses of FLAG-tag affinity-purified CaMKII- α

6.2.2.1 Biochemical analysis

In contrast to the constitutively active chymotryptic N-terminal kinase fragment, the full-length kinase has been shown to be capable of phosphorylating substrates only if it first underwent autophosphorylation at Threonine 286 (T286)^{169,170}. Therefore, to test whether the FLAG-tag affinity purified CaMKII- α shows the ability to activate itself, autophosphorylation assays with both, the purified N' and C'FLAG-tagged kinase versions, were performed (for experimental details, see Section 4.3.5.5).

While for the C'FLAG-tagged CaMKII- α the expected autophosphorylation at T286 took place, for the N'FLAG-tagged version strong autophosphorylation of a 40 kDa-fragment was detected (**Figure 44**). The fact that the 40 kDa-fragment exhibited autophosphorylation implies that the T286 autophosphorylation site of the regulatory domain R1 was not affected^{226,227,228}. Also, the often used constitutively active chymotryptic N-terminal fragment is not capable of triggering autophosphorylation^{170,229,230,231,232}. This indicates that 40 kDa-fragment must be different. Furthermore, it is important to keep in mind that *in vivo* and in solution the monomeric kinase assembles into a dodecameric holoenzyme^{122,123,124,171}, only when the C-terminal hub domain is present^{123,124}. Therefore, the functional kinase fragment contains the C-terminal hub domain (approx. 150 amino acids) for certain. On the other hand, autophosphorylation has been shown only to take place, if upon Ca²⁺/CaM binding onto the regulatory subunit R3 the inhibitory bond between T286 of R1 and the N-terminal kinase domain is released^{124,233}. Therefore, the N-terminal FLAG-tag of the non-shortened kinase protein is very likely to be involved in the formation of this inhibitory bond and thus might keep the kinase locked in the non-autophosphorylatable state.

It is worth noting, that the shortened but autophosphorylatable product was detected only in Western-blot, indicating that low concentrations of the 40 kDa-kinase fragment yield pT286-levels nearly as high as those detected of the C'FLAG-tagged CaMKII- α construct.

Due to the unusual and yet not fully understood autophosphorylation behavior of the N'FLAG-tagged kinase version, in all subsequent experiments the C'FLAG-tagged version of CaMKII- α was used.

6.2.2.2 Structural analysis by cryo-electron tomography

CaMKII- α with its highly conserved dodecameric holoenzyme structure^{122,123,124} has the most complex and unique structure among all protein kinases identified so far. Therefore, the FLAG-tagged CaMKII- α was studied also by cryo-electron tomography (carried out by Z. Kochovski, from the Baumeister-Lab, MPI for Biochemistry, Martinsried, Germany). For cryo-EM, only samples of high purity can be processed. The uniform distribution of holoenzyme-like particles in negative-stain images (**Figure 45 A and B**) offered two important insights for the continuation of this project: i) neither any protein precipitation nor aggregation takes place using the FLAG-tag affinity purification protocol; and ii) by assaying multiple independent protein preparations of C'FLAG-tagged CaMKII- α , the assembly into the proposed hexagonal holoenzymatic structure was observed repeatedly (**Figure 45 B**).

One of the advantages of cryo-EM is that images of assembled structures in their native state can be obtained^{234,235}. Also, “snapshots” of differently oriented particles can be acquired, which then allows for high-resolution 3D-reconstructions. With the recent progress in cryo-EM, it has become possible to determine 3D structures to near atomic resolution, allowing the reconstruction of full atom models of multi-subunit proteins^{234,236,237}. The quality of recombinantly expressed CaMKII- α was confirmed by our preliminary 3D reconstructions (**Figure 45 C and D**). Up to this point, the reconstructions are based on approx. 80,000 particles, providing an approximate resolution of 30 Å.

The reconstructions presented in this work provide clear evidence that the stimulated and unstimulated holoenzymes have structurally distinct conformations. This is an important observation, as over the past years there has been intense debate on what the real holoenzyme structure of CaMKII- α looks like and whether dynamic conformational changes between the unstimulated and stimulated state exist at all. Based on computational simulation models from crystal structures of kinase subunit fragments, a number of different structures describing the autoinhibited as well as non-inhibited state have been put forward^{122,171,238,239,240}. Based on the most recent structural information that mainly has been obtained from small-angle X-ray scattering (SAXS) studies^{122,123,240,241}, Chao and colleagues have now presented a crystal structure of the full-length

Discussion

autoinhibited CaMKII- α (4.0/3.6 Å)¹²⁴. This structure shows a very compact arrangement of the kinase domains around the hub domain (core). The kinase domains of the twelve individual holoenzyme subunits are arranged as two hexameric rings, which are stacked in a petal-like structure above and below the core. This general concept in principle accords with the initial EM-studies, which had proposed a similar structure a decade ago¹⁷¹. However, still contrasting is the fact, that in EM the kinase domains of the individual subunits of the autoinhibited holoenzyme were shown to extend outward, while in the most recent crystal structure by Chao *et al.* all twelve kinase domains are tightly packed and thus are not accessible for Ca²⁺/CaM^{124,171}. In addition Chao and colleagues added that according to computational kinetic simulation analyses it is very likely that parallel to the compact holoenzyme structure, also a semi-extended though still autoinhibited state exists. This semi-extended conformation is proposed to facilitate the otherwise impossible binding of Ca²⁺/CaM to the regulatory domains, thereby allowing for the initial autophosphorylation at T286, which concomitantly leads to a complete pop-out of the kinase domain (extended non-autoinhibited state)¹²⁴.

With the current means in crystallography it will be highly unlikely to confirm the true existence of the recently proposed (auto-inhibited) semi-extended model structure. And to solve the fully extended (auto-activated) structure of the holoenzyme will be almost impossible when using crystallography. The preliminary cryo-EM results nicely show that under non-stimulating conditions (i.e., no Ca²⁺/CaM), the kinase adopts a rather compact structure without showing any domains extending outward (**Figure 45 C**). This contrasts with the previously proposed auto-inhibited EM structure by Kolodziej, S. *et al.* (2000)¹⁷¹, but is in agreement with the recently presented crystal structure of the autoinhibited full-length CaMKII- α ¹²⁴. The 3D-reconstructed cryo-EM structure of the stimulated CaMKII- α presented here clearly shows six presumably N'-terminal kinase domains extending outward (**Figure 45 D**). This underlines that upon stimulation obvious conformational rearrangements within the holoenzyme take place.

At the current resolution of 30 Å, the structures here presented are still subject to interpretation and speculation. Critically speaking, the here observed extended structure in **Figure 45 D** could as well represent the semi-extended and still autoinhibited state that has been documented by Chao *et al.*¹²⁴. This assumption

is however unlikely, as in **Figure 44** it was shown that at stimulating conditions, CaMKII- α clearly becomes autophosphorylated and thus exists as a stimulated molecule. The fact that in this study only the subunits from the upper ring show the characteristic outward extending, is simply due to the tilt-angle used during the herein applied 3D-reconstruction modeling. By taking a closer look at the side-view of the 3D-reconstruction of stimulated CaMKII- α , in the lower part indicated structures in-between the extended subunits of the upper ring become apparent. Therefore, at this point the structure of the stimulated CaMKII- α most certainly represents the extended and fully active state of the holoenzyme.

To date, crystallography studies have only predicted but they could never directly show holoenzymatic dynamics of the full-length CaMKII- α . Even though still preliminary, the cryo-EM structures of the stimulated and unstimulated CaMKII- α presented here for the first time provide direct evidence that in solution the CaMKII- α holoenzyme undergoes drastic conformational changes. To further improve the resolution and thereby obtain further proof, 3D-reconstructions from over 160,000 single cryo-EM particles will be carried out.

6.2.3 Studying the interaction between CaMKII- α and melanosomes

First and foremost, this project was motivated by the fact that Rogers *et al.* (1999)¹⁰³ reported on the specific release of Myosin Va from melanosomes when incubated with mitotic *Xenopus* egg-cell extract. Shortly thereafter, Karcher and colleagues (2001)¹²¹ could provide evidence that the observed release was mediated by CaMKII- α -specific phosphorylation of Serine 1650 within the distal tail domain of Myosin Va. Based on those findings, my goal was to establish an *in vitro* assay by which the following questions could be easily addressable: First, does endogenous CaMKII- α from *Xenopus l.* melanophores interact with melanosomes? Second, if indeed such an interaction between melanosomes and endogenous CaMKII- α exists, then to which extend does Myosin V release take place? And third, via the *in vitro* release-assay system introduced here, would a complete Myosin Va-release from the melanosome be enforced when using the recombinant purified CaMKII- α ?

Indeed, autophosphorylated CaMKII- α was detected, even though no exogenous recombinant CaMKII- α was included (condition 5, **Figure 46**). This implies that

Discussion

endogenous CaMKII- α from *Xenopus l.* melanophores interacts with melanosomes, while being active (i.e., autophosphorylated). Importantly, for the respective supernatant of this condition no autophosphorylation was detected at all, suggesting that (i) only activated autophosphorylated CaMKII- α interacts with the melanosome fraction; or (ii) endogenous CaMKII- α is turned active only when bound to melanosomes. As was shown in the autophosphorylation tests (**Figure 44**), the recombinant and purified CaMKII- α does not undergo any autophosphorylation at condition 1. Also, the supernatant of this condition did not show any autophosphorylation, while at those conditions where Ca^{2+} /CaM was added together with recombinant purified CaMKII- α only (conditions 2 through 4) high activity for the supernatant fraction was observed. This underlines that even though in condition 1 exogenous kinase was present, the detected autophosphorylation must be attributed to the endogenous melanosome-bound CaMKII- α .

Also, the endogenous kinase was turned active most likely before or during the isolation procedure because it was detected as activated kinase at condition 1, where neither Ca^{2+} nor calmodulin had been added (**Figure 46**).

It should be mentioned that only very low levels of total endogenous kinase protein in the pellet were detected (condition 5), while clearly under those conditions active kinase was present in the pellet fraction. This is most likely attributed to the fact that compared to the exogenously added purified kinase the amount of total kinase protein bound to the melanosome was below the antibody's sensitivity.

Importantly, the Myosin Va release (supernatant fractions of conditions 1 and 5 through 8) seems to correlate with the amount of melanosome-bound active (i.e., autophosphorylated) kinase (compare Myosin V supernatant with pT286 pellet fractions). The fact that under zero Ca^{2+} /CaM conditions exogenously added kinase was believed to be inactive, while endogenous melanosome-associated CaMKII- α showed clear signs of activation, leads to the assumption that Myosin Va release is due to the active endogenous and not the exogenously added purified kinase.

Previous studies showed that once activated, the CaMKII- α exhibits its kinase activity in a completely Ca^{2+} -independent manner^{242,243,244}. This fits the notion

Discussion

that the release takes place even though no $\text{Ca}^{2+}/\text{CaM}$ was added, implying that for the kinase to phosphorylate its substrate (e.g., Myosin V) it is sufficient to being autophosphorylated rather than requiring additional supplies of $\text{Ca}^{2+}/\text{CaM}$. Importantly, even though the amount of total kinase protein on the melanosome was significantly higher under conditions where exogenous CaMKII- α was added (conditions 6 through 8), Myosin Va release was hardly increased. This implies that the exogenously added purified kinase most likely did not contribute to Myosin Va release. This in turn might be explained by the fact that the melanosome-bound purified CaMKII- α seems to reside in the inactivate state. This is underlined by the finding that the association of exogenous purified kinase takes place only if $\text{Ca}^{2+}/\text{CaM}$ was present (compare pellet fraction of conditions 1 and 6 through 8), while showing unperturbed autophosphorylation when in solution. Therefore, it seems as if the exogenously added kinase is clearly capable of binding to the melanosome, it however does not undergo autophosphorylation in this state even though sufficient amounts of $\text{Ca}^{2+}/\text{CaM}$ are present.

In conclusion, only the endogenous CaMKII- α is turned active when bound to the melanosome, while in solution it seems to reside in the auto-inhibited state. Myosin Va-specific release doubtlessly takes place, although it was not as complete as suggested by the previous study of Karcher *et al.* (2001)¹²¹.

It is important to mention that the release in Karcher's work was triggered primarily upon the addition of mitotic frog egg-cell extract. By contrast, here the Myosin Va-specific release was mediated solely by the endogenous activated melanophore-borne CaMKII- α . In this context, it is worth mentioning that due to the actions of CaMKII- α , during mitosis, motor-activity is preferentially down-regulated²⁴⁵. Furthermore egg-cells can be assumed to show higher rates in proliferation than dermal pigment cells, thus more mitosis events would be expected to occur. Therefore it is very likely that frog egg-cells contain higher amounts of CaMKII- α than melanophores. It has been shown that in HeLa cells moderate levels of active CaMKII- α are required for proper cell cycle progression²⁴⁶. Therefore, due to moderate expression levels of CaMKII- α , significant but incomplete motor release from the melanosome would indeed be a logical consequence. Additionally, in contrast to an egg-cell the primary task of

melanophores is pigment distribution, which would be largely abrogated if important parts (e.g., Myosin V) of the transport machinery were deleted.

6.2.4 Conclusion and Outlook

In further studies one of the major goals will be to find optimal conditions under which the enforced release of Myosin Va from the melanosome via specific activation of melanosome-hooked CaMKII- α becomes possible. Furthermore, to find out why for the endogenous CaMKII- α only the activated state was found on melanosomes will be a major question in future studies. Lastly, it will be important to determine why the purified kinase stimulated without having melanosomes around while being recruited to the melanosome exclusively as inactive kinase.

Costa *et al.* provided evidence that on vesicles from nerve terminals, CaMKII- α binds to the medial tail of Myosin Va, activating Myosin V in a Ca²⁺-dependent manner, most likely with Myosin V acting as a Ca²⁺-transferring unit²⁴⁷. Those findings support the notion that only the active form of endogenous CaMKII- α was detected on the melanosome, which was accompanied by the release of Myosin Va.

The fact that exogenous CaMKII- α was capable of binding to melanosomes but remained attached in an inactive state, could indicate that the exogenous kinase does not bind properly to Myosin Va and thus is not activated properly. In that sense, Myosin Va would act as a melanosome-specific co-factor that regulates the activation of the kinase and thus its own release from its cargo.

In that respect, one option to further explore the melanosome-specific activation of CaMKII- α , would be to perform pull-down assays with purified full-length *Xenopus l.* Myosin Va and melanophore cell extract. This might reveal if any endogenous non-melanosome-associated CaMKII- α is capable of binding to *Xenopus l.* Myosin Va.

If CaMKII- α binds Myosin Va directly, then both the kinase and the full-length *Xenopus l.* Myosin Va can be studied under varying conditions by cryo-EM. In addition, one could assess the complex interaction between Myosin Va and the CaMKII- α on intact isolated melanosomes.

Both approaches would ask similar questions. Are accessory proteins involved in the interaction between Myosin Va and CaMKII- α ? If yes, can those accessory

proteins be confirmed also biochemically? Finally, with further co-factors identified and visualized, would it be possible to reconstitute protein CaMKII- α :Myosin Va complex *in vitro*?

In addition, it would be highly interesting to reveal whether in melanophores CaMKII- α functions differently in anterograde or retrograde melanosome transport. If indeed the release of Myosin V from the melanosome surface takes place *in vivo*, what factors would be involved in the regulation of this phenomenon.

6.3 Purification of isolated melanosomes via MACS technology

For the past three decades, the majority of studies on melanosome transport focused on characterizing the components by fluorescence microscopy and biochemistry, or by making use of reconstituted motility experiments. However, with the rapid progress in proteomic tools, the analysis of whole proteomes of certain organelles via mass-spectrometry adds an additional facet. Over the past years a number of pivotal factors involved in melanosome transport could be elucidated^{63,68,73,75,104,131,132,248,249} (for reviews, see also^{70,72,94,250,251,252,253,254}). As a next step, it would be important to unravel the regulation of those factors on the melanosome, for which a proteomic “bottom-up” approach might bear a great potential.

To date only two studies from the same laboratory used the bottom-up approach to analyze the melanosome and its associated proteome via (conventional) mass-spectrometry^{125,126}. Those studies were performed on human melanoma (MNT-1) cells, but as yet a similar approach has not been applied to the otherwise very well studied pigment cells from *Xenopus l.*

Due to its high sensitivity²⁵⁵, mass-spectrometry allows to identify many proteins while requiring only very small amounts of protein. However, the sensitivity of proteomics goes along with the demand for pure protein samples. In the two studies mentioned, sample purity was achieved by applying sucrose density gradient centrifugation (DC)^{125,126}, which primarily has found usage for the purification of other organelles (e.g., mitochondria)^{127,128,129,130}. An often-encountered problem with DC-based organelle purification is, however, that the organelle’s functionality is harmed or that only incomplete proteome fractions are

retained and purified ²⁵⁶, thus making the subsequent analysis prone to misinterpretation.

In this part of the work I focused on establishing a novel method by which functionally intact but at the same time also pure organelle fractions are obtained. To reach this ultimate goal, two rather unrelated techniques were combined here. The first is the conventional and established melanosome isolation protocol ^{65,249}, which in the past has been successfully utilized for numerous *in vitro* melanosome motility studies ^{65,74}. Due to two low-speed centrifugation steps, this method results in gently handled (important for functionality) but quite crudely isolated melanosome fractions with many cellular contaminants. Therefore, as an additional purification step the likewise gentle and highly specific MACS[®] (magnetic activated cell sorting)-technology was applied. MACS is based on the magnetic sorting of surface-marked particles and most commonly is used to sort a certain cell type or population depending on its specific surface-marker composition ²⁵⁷. By combining both these techniques, neither harsh centrifugation steps nor contaminating additives (e.g., sucrose, percoll etc.) are being used.

6.3.1 Efficiency of MACS-based melanosome isolation

To assess the efficiency of this novel melanosome purification technique, the post-MACS fraction was compared to melanosome probes that had been purified either by DC or crude isolation (no additional purification). As illustrated in **Figure 49** all three techniques resulted in the removal of virtually all protein bands detected via Coomassie-stained SDS-PAGE.

The analysis by tandem mass-spectrometry revealed that for fractions that had not been further purified (i.e., Mel_{crude}, **Figure 49**), a relatively long list of proteins with significant hit -scores was identified. However, the great majority of those proteins belonged to the family of elongation factors, ribosomal proteins, and cytoskeletal proteins (actin, tubulin and members of the intermediate filament proteins). Mitochondrial proteins as well as mitochondrial precursors were among those proteins identified with the highest score (for a complete list of protein hits, refer to Section 7). The presence of mitochondria-derived proteins is most likely due to the fact that mitochondria are highly similar to melanosomes in terms of size and density and thus hard to separate from melanosomes by the two-step centrifugation procedure. Taken together, this particular purification procedure

Discussion

fails to eliminate the cytosolic factors, which seem to overwhelm the melanosome-derived peptide signals (personal communication with mass-spectrometry core facility).

When melanosomes were further purified by DC, a larger fraction matched those proteins that were proposed to belong to the melanosome proteome^{125,126} (color-coded in the listing of mass-spectrometry results, Section 7). This result implies that, even though the majority of cytoplasmic contaminants remain present in the probe, the proportion of contaminants was reduced, enabling the detection of the less abundant melanosome-associated components (color-coded in respective list of protein hits, Section 7). However, a fair number of proteins that do not belong to the melanosome-associated group of proteins (e.g., elongation factors, ribosomal and mitochondrial proteins), are also listed in the studies by Basrur *et al.* and Chi *et al.*^{125,126}.

Compared to the crude isolation procedure, in DC a 50 times higher centrifugation force is applied to the probe, leading to the detachment or disruption of parts of the melanosome-associated transport machinery most likely due to the high shear-forces applied on the organelle²⁵⁶. In fact, DC-purified melanosomes never displayed any movement in *in vitro* reconstitution motility assays. To conclude, even though DC yields improved results in terms of eliminating cytosolic contaminants, the method is not well suited to identify motility-related factors on melanosomes.

Although in the past DC has been used for the purification of blood or immune cells, specific membrane fractions, or organelles such as mitochondria^{128,129,130,258,259}, two major disadvantages come along with this method: i) it is a time-consuming method for which access to an ultra-centrifuge is required; and ii) contaminations of the sample by sucrose are not unlikely and may interfere with subsequent mass-spectrometric analysis. Even though by additional purification steps such contaminations could be removed further losses of the limited sample material might ensue.

By contrast, MACS purification is less time-consuming and omits any harsh centrifugation steps. The MACS method takes advantage of the fact that the antibody-antigen bond is among the strongest non-covalent bonds in biology^{260,261}. With Trp1 a melanosome-specific surface marker was chosen to further enhance binding specificity. Removal of unspecifically bound material was

Discussion

ensured by multiple washes in large volumes of buffer, so that aggregation became less likely.

Western-blot analysis of each step during the isolation/purification procedure showed that the three target proteins herein assayed (β -tubulin, GAPDH and Myosin V) turned up in high and comparable amounts in both, the lysate (membranes, cytoplasmic and nuclear proteins, melanosomes) as well as in the SN 3000 (cytoplasmic proteins only) fraction (**Figure 50**). This finding was not surprising because for GAPDH and β -tubulin, as abundant cytoplasmic proteins¹⁷², the cell extract as well as the cytoplasmic fraction are expected to contain both of these marker proteins. Myosin Va, constituting the prototypical actin-based cargo transporter protein, is detected in high amounts in both, the lysate and the SN 3000 fraction. In the crude fraction (i.e., no additional purification by MACS), clearly less Myosin Va is present, implying that in the second centrifugation step ($3,000 \times g$) most of the cytoplasmic (non-melanosome-associated) Myosin Va was successfully depleted (**Figure 50**). However, with β -tubulin, as the second marker protein and representing the cytoskeletal protein fraction in the cell, in **Figure 50** evidence is provided that without further purification still contaminations by this protein (and most likely other abundant proteins) takes place. The more striking is the fact that for those samples that underwent additional purification by MACS, the usually omnipresent β -tubulin fraction was removed, while the Myosin Va fraction remained associated with the probe. The fact that only about 20% (quantification not included) of the detected Myosin Va in the crude fraction got lost during the purification by MACS while the abundant β -tubulin could be removed (**Figure 50**), demonstrates the specificity and efficiency of the here introduced technique. It furthermore shows that in addition to the commonly used GAPDH, other likewise abundant protein markers should be included to show the purity of an organelle preparation by immunoblotting. These include Golgin97, KDEL, Rab4, lamins A and C or β -actin, representing markers of the Golgi apparatus, endoplasmic reticulum, endosomes, nucleus and cytoskeleton, respectively.

The efficiency in immuno-labeling melanosomes by using the melanosome-specific surface marker Trp1 was determined by FACS (fluorescent activation cell sorting) analysis, a commonly used tool in the field of immunology. To my

knowledge, FACS has never before been performed on melanosomes before, so that in addition to testing the melanosome-specific transmembrane protein Trp1, Kinesin-2 as a known surface-bound (but not membrane-integrated) protein was selected as a test-candidate (Figure 51 A and B). Regardless of the surface marker tested (Trp1 or Kinesin-2), the FACS analysis showed clear detection-specificity for melanosomes containing either one of those markers (Figure 51). First and foremost, this underlines the functionality and integrity of the here presented MACS bead-assisted melanosome purification via the surface marker protein Trp1. And secondly, with the performed FACS analysis clear evidence is provided that even Kinesin-2 would be a highly sensitive marker and thus could be used for melanosome purification via MACS.

6.3.2 Summary and Outlook

The herein presented MACS-bead-assisted melanosome purification not only fulfills all the required needs for a functional but still pure isolation, it also represents a technique that is very flexible and can be adapted to any specific needs. For instance, besides targeting exclusively those antigens/surface markers that are known to be stably associated with the melanosome, marker proteins known to be associated with melanosomes only under certain conditions or at specific cellular stages, could be used. This additional aspect of condition-specific melanosome sorting would significantly add to the initially intended goal of simply purifying the otherwise crudely isolated melanosomes. It also holds the promise of answering yet unaddressed questions, whether during melanosome aggregation and dispersion certain proteins are transiently recruited or released to and from the melanosome surface. Furthermore, cell state-specific markers could easily be used to select for only those organelles that actually derive from the one or the other state.

Though final *in vitro* motility experiments will be required for proving full functionality of MACS-purified melanosomes, the here presented biochemical analysis demonstrates, that this methodology marks a significant progress in obtaining purer melanosome fractions while remaining functional, as suggested by the retained presence of motor proteins.

By using FACS in combination with the MACS-based melanosome purification, it becomes possible to analyze and compare individual purifications from

consecutive stages. The fact that per FACS-analysis typically 10,000 to 12,000 particles (in this context, organelles) are analyzed, allows for robust quantitative statistical analyses. By searching for additional and new surface markers, perhaps an even better antigen-antibody combination can be identified, by which even higher amounts of MACS-purified melanosomes will be yielded.

The major advantages of the here presented MACS-based melanosome purification are: i) no additional centrifugation steps are required; ii) the technique is less time-consuming and easier to perform than the conventional purification by DC; and iii) it omits further application of shear-forces on the applied probe. Most importantly, the quality of the purified melanosome probe can be monitored by FACS analysis.

6.4 Determining the full-length sequence of *Xenopus l.* Myosin Va

6.4.1 Comparative sequence-analysis

The deduced amino acid sequence of the here determined coding sequence of the full-length *Xenopus l.* Myosin Va altogether shows strong homology to the three Myosin Va sequences (chicken, mouse and human). However, certain parts such as the loop 2 region (head domain), neck domain and portions of the proximal tail displayed more divergence than others (for the complete alignment, refer to Section 7). The homology of the functionally and structurally important regions infers that the secondary structure of the protein is most likely conserved, while the amino acid usage in the *Xenopus l.* version is different, as has been described previously for other proteins¹⁷³.

Interestingly, with four instead of five net positive charges, loop 2 of *Xenopus l.* Myosin Va, carries one positive net charge less than the three other myosins assayed (Figure 59). In addition, the sequence length of the *Xenopus l.* Myosin Va loop 2 with 46 amino acids is one residue longer than the loop 2 of chicken, mouse and human Myosin Va. In previous studies, it has been shown that the number of positive net charges on loop 2 positively correlates with the exhibited actin-binding affinity during the initial filament encounter^{24,111,183,184}. In addition, loop 2 is known to interlink the initial actin binding to subsequent phosphate release. This in turn initiates the strong-binding state upon which the rate-limiting

Discussion

ADP-release step occurs^{24,33,111,183,184}. In this respect, the lower positive net-charge on loop 2 of *Xenopus l.* Myosin V, might affect its behavior on F-actin. Previous studies on Myosin V mutants showed that a less positively charged loop 2 results in decreased ATPase activity^{35,44}. Decreased ATPase activity typically also leads to decreased speed in motility, as it takes the myosin longer to complete the mechano-kinetical cycle. So far only addressed by a number of preliminary motility studies, the here described full-length Myosin Va protein indeed showed slightly lower velocities on F-actin compared to the three homologous Myosin V species^{35,38,43,45,48,167,179,262}.

The neck domain (or lever arm) is an extended helix that fulfills regulatory as well as structurally important functions. It contains six of the so-called IQ motifs that preferentially bind calmodulin or calmodulin-like light chains^{34,166,263}. Even though the IQ motif as such is conserved, compared to the head domain it (in particular IQ motifs #3, #4 and #5) displays more divergence (77.4 % identity) (**Figure 60**). At this point still speculative but nevertheless also likely is the notion that Myosin Va from different species might employ different regulatory conditions such as for instance Ca^{2+} concentrations^{264,265,266}. Therefore, by keeping the consensus motif (IQxxxRGxxxRxxY) similar, the neck domain primarily ensures the Ca^{2+} -dependent binding of those light chains. However, the binding affinity depends on the cellular environment of the respective Myosin V and therefore might be subject to fine-tuning for cell-specific functions by the described sequence diversity.

The divergence that was observed for the proximal tail domain (#915-1320 of complete alignment in Section 7) encompasses both, the first and second coiled-coil region. Both coiled-coil domains, as part of the stalk-like structure, are required for the efficient dimerization of the molecule^{34,263,264}. Interestingly, this portion shares only 60% identity, while most of it is accounted by the stretch that follows the last IQ repeat (up to position #1064). A similar observation was made in a study dealing with the analysis of the *Squid* Myosin Va¹⁷³, implying that this portion of the primary protein sequence allows for more sequence variability. This variability most likely is due to the fact that coiled-coil motifs represent α -helical segments that via heptad-repeats mediate exclusively dimerization^{265,267,268}. Therefore, unlike the ATP- or actin-binding site, a coiled-coil motif does not constitute a site that is to be recognized by a specific tertiary structure of another

Discussion

protein or chemical and thus allows for higher variability in between the crucial heptad-repeats.

By contrast, the so-called PEST site (**Figure 61**), which in class V myosins separates the first two coiled-coil regions from each other^{34,267}, shows high conservation among the four species. Mainly this is because it serves as recognition sequence for the endoprotease Calpain, which is known to cleave Myosin Va at this site *in vitro*^{34,267}. Furthermore, the PEST-site has been suggested to function as a means of specific regulation by proteolytic-based depleting of the Myosin V on neuronal vesicles^{269,270}. Thus the PEST-site would be expected of being subject to strong sequence conservation.

In contrast to the rather divergent proximal tail domain (for the complete alignment, refer to Section 7), the first 60 amino acid residues of the distal tail portion show high sequence identity (90%) for all four Myosin V sequences. Along with chicken, the *Xenopus l.* Myosin Va lacks a stretch of 25 amino acids just before the beginning of coiled-coil #3, while both the mammalian sequences contain this exact portion (**Figure 62**). Interestingly, towards the end of the otherwise very conserved coiled-coil #3, at position # 1385, the *Xenopus l.* sequence is characterized by a unique insertion of 25 amino acids (**Figure 62**). With 99 amino acids in length, the coiled-coil #3 portion from *Xenopus l.* is significantly longer than the third coiled-coil of mouse, human and chicken Myosin Va. In addition, due to this insertion, the *Xenopus l.* construct is predicted to form a coiled-coil only upto residue #1361 while continuing as rather unstructured helical region to the end of the described sequence (for the complete alignment, refer to Section 7). In line with this, more recently it has been proposed that the elongation of a given coiled-coil sequence can as well lead to destabilization, rather than hydrophobic density-mediated stabilization of the structure²⁶⁵.

The distal tail portion, at large is constituted of the globular tail domain (GTD or cargo binding domain) and is a distinct feature of the class V myosins. Being used primarily for the binding to cargo molecules such as vesicles, mRNA, ER to name a few, the functions of the GTD overlap across all the Myosin Va from different species and/or different cell types. This and the fact that GTD-mediated cargo-binding of any sort preferentially occurs via the tripartite adaptor complex Myosin Va-Melanophilin-Rab27a (reviewed in^{34,263}), accounts most likely for the

observed strong conservation of the distal tail portion across the four Myosin Va sequences.

6.4.2 Expression and purification of full-length *Xenopus l.* Myosin Va

In addition to determining the complete full-length sequence of the *Xenopus l.* Myosin Va, as is shown in Section 5.4.2.3 of this work, the full-length protein (size of dimer: 434 kDa) was successfully expressed and FLAG-affinity purified. At this point, typically concentrations of approx. 0.3 mg/ml in considerably large final volumes (i.e., greater 500 μ l) of dialyzed (i.e., zero ATP) full-length protein are obtained (Figure 65). To set the basis for increased protein yields, baculovirus-titers as well as the amount of cells to be infected have been scaled up. The initial problem of having had lost large amounts of protein after the FLAG-affinity column, was solved by performing an additional incubation round with fresh anti-FLAG agarose. Thereby at least twice as high protein concentrations were obtained. Also, by using higher concentrations of FLAG-peptides during the elution, along with three to five successive elution cycles, protein yield was significantly increased. Most importantly, by simply prolonging the time period after the infection with baculovirus and prior cell harvesting to at least 75 hours, a significant increase in protein yield was achieved. This way over-expression of the full-length protein could be improved, while keeping protein degradation at similar levels as before.

Besides yield, purity of the overexpressed protein is usually an issue. Here, relative to the increased yield in full-length protein, protein degradation was slightly reduced by omitting any detergent during the process of breaking up the cells. In turn, to still obtain high cell-lysis yields, sonication instead of glass dounce-homogenization was used to break up the cells.

As shown in Figure 64, the prominent bands running at lower sizes than the full-length protein band, via mass-spectrometry were confirmed to be truncation products of the purified full-length protein (Table 31) and thus most likely represent degradation products. Except for the band at approx. 125 kDa (C'FLAG-tagged version only), all the appearing bands were observed for both, the N' and C'FLAG-tagged version of the full-length Myosin Va. This implies that the large majority of the "by-products" resolved via SDS-PAGE, are missing most likely

parts somewhere between the N- and C-terminal domain, rather than missing the N- or C-terminus itself.

In general, for Myosin Va being a large (217 kDa per heavy chain), complex (dimer-forming molecule with light chains bound to the neck domain) protein that in addition contains proteolysis-sensitive recognition motifs (e.g., PEST site), the half life is expected to be rather short mainly due to intracellular degradation^{267,271,272}. Even though not of immediate interest, to investigate the nature of the observed degradation, several approaches could be undertaken. For instance, one could perform western-blot analyses against certain regions of the protein to thereby localize the approximate regions of preferred degradation. Subsequently, further analyses involving mass-spectrometry or N-terminal Edman-sequencing²⁷³ in combination with 2D-SDS-gel electrophoresis could be carried out.

In addition to further up-scaling the protein yield, the next and most important step will involve the further purification by either size-exclusion or ion-exchange chromatography FPLC (Fast Performance Liquid Chromatography). By the fact that with approx. 140 kDa the largest prominent degradation product runs almost 80 kDa lower than the full-length protein (217 kDa), size-exclusion chromatography will most likely serve the purpose. FPLC in combination with MALS (multi-angle light scattering) will be required to confirm the efficiency in homo-dimerization of the heavy chains of the full-length Myosin Va.

6.4.3 *In vitro* motility of full-length *Xenopus l.* Myosin Va

In this work initial motility assays were carried out to determine the functional behavior of the full-length *Xenopus l.* Myosin Va on F-actin *in vitro*.

In gliding-filament assays, immediate binding-down of actin filaments by both the N' and C'FLAG-tagged full-length Myosin Va, was observed (Figure 66 A and Figure 67 A, Videos 9 and 12). In agreement with previous work, the initial weak binding to F-actin is an ATP-independent process^{112,181,182}. For both the versions no noteworthy difference in their capability to bind to F-actin was observed, indicating that neither the N- nor the C-terminal FLAG-tag seem to impact on the actin-binding capacity of the respective construct. Studies using recombinant HMM-like Myosin Va protein constructs (i.e., lacking most of the tail portion; for details, see also Section 5.1.1.1) have revealed that both C' and N'FLAG-tagged HMM-like Myosin V constructs are likewise proficient in binding to F-actin^{110,189}.

Discussion

In contrast, upon addition of 2 mM ATP, a major difference in the gliding behavior of the two FLAG-versions was displayed. While for the N'FLAG-tagged version nearly all before rigor-bound filaments showed long-range gliding motility (Figure 67 B and C, Videos 10 and 11), for the C'FLAG-tagged construct only very few of the bound filaments showed directed and smooth gliding movements (Figure 66 B, Video 9). This observation was made repeatedly with independent batches of protein purifications, and including probes from simultaneously purified N' and C'FLAG-tagged constructs using the same protocol and buffer components. Thus, the high fraction of non-motile C'FLAG-tagged Myosin Va molecules is highly unlikely due to erroneous protein purification. The FLAG-tag at the C'FLAG-tagged Myosin Va seems to affect the regions responsible for the actual ATPase or/and power-stroke activity but not actin binding (Figure 66).

Further support for this notion comes from the finding that the N'FLAG-tagged Myosin Va at high concentrations is capable of fully disintegrating the long actin filaments (compare Figure 67 A and B, Videos 10 and 12) upon the addition of ATP, while for the C'FLAG-tagged construct such observation could not be made (Figure 66 A, Video 9). The here described filament-rupturing showed clear ATP-dependence, which disproves the possibility of accidentally co-purified gelsolin or severin being responsible for this observation, as both proteins sever F-actin in an ATP-independent manner^{274,275}.

With 70 individual gliding events obtained from the N'FLAG-tagged Myosin Va the first biophysical characterization of this motor species was performed (Figure 68 and Table 32). Smooth and continuous filament gliding was determined to take place for on average 31.4 seconds, while covering an average distance of nearly 4 μm . The average single gliding-filament velocity as determined from the obtained Gaussian-fit function was 131.2 nm s^{-1} (Figure 68 and Table 32). This value is highly similar to what Wu *et al.* reported for the *in vivo* Myosin Va-driven melanosome transport (140 nm s^{-1})^{106,174}.

As shown in Figure 69 (and Video 13), by reducing the amount of surface-adhered motor protein, single-point attachments of actin filaments via the involvement of single Myosin Va molecules were achieved. Now on single-molecular level, this finding underlines even more the notion that an individual *Xenopus l.* Myosin Va motor is capable of transporting actin filaments in a processive manner.

Discussion

In the initial single-molecule motility assays, with N'FLAG-tagged *Xenopus I.* Myosin Va attached to the glass surface, only infrequent but unambiguous walking events lasting three seconds or longer could be acquired. This behavior is most likely attributed to the fact that under the here assayed conditions (i.e., no Ca^{2+}) the full-length *Xenopus I.* Myosin Va resides in an inactive though actin-bound state.

This assumption is based on results from studies, where at low Ca^{2+} concentrations for the full-length Myosin Va from mouse virtually no activity has been observed^{54,178,276}. Further studies involving analytical ultracentrifugation provided first evidence that at low Ca^{2+} concentrations the full-length Myosin Va adopts a rather compact structure²¹, whereas at high Ca^{2+} concentrations this structure becomes less compact^{53,266}. Via advanced techniques in the 3D-reconstruction of EM negative-stain and tomographical images, Liu *et al.* confirmed that the inhibited (i.e., without calcium) full-length Myosin Va from mouse adopts a compact triangular-like shape⁵⁵. In this state, the two lever arms along with the motor domains fold onto lobes of the cargo-binding domain (CBD). Thereby the molecule's ATPase activity becomes basically abrogated, while actin-binding remains unaffected⁵⁵.

In line with this, for the here assayed full-length *Xenopus I.* Myosin Va, actin binding was by no means affected and therefore over time increasing numbers of single Myosin Va molecules could be observed binding to the immobilized F-actin (**Figure 70 A and B**, Videos 14 and 15). Furthermore, when bound to an actin filament the lever arm of the inhibited full-length Myosin Va was reported to adopt the post-power-stroke conformation, inferring that inhibited Myosin Va resides in a strongly-bound state on the actin filament⁵⁵. This fits the herein obtained observation that once bound to actin, the actin-bound full-length *Xenopus I.* Myosin Va molecules remained stationary and hardly ever detached (Videos 14 and 15). The same observation was made in the very recent study by Armstrong, *et al.*¹⁷⁹.

In this very same study, the authors showed that *in vitro* a small fraction of full-length (mouse) Myosin Va turns infrequently active before it becomes again switched off via the previously shown head-tail interaction²⁷⁷. The authors argue that in cases where the full-length Myosin Va is assayed under low ionic strength (50 mM or lower) conditions without tail-bound cargo, the equilibrium between the

Discussion

closed (i.e., inactive) and open (i.e., active) conformation is shifted towards the closed state ¹⁷⁹. It was further proposed that this equilibrium can be shifted towards the unfolded, non-inhibited state when elevating the salt concentration in the assay to 150-200 mM.

However, such putative unfolding was not observed with the full-length *Xenopus l.* Myosin Va at 150 mM final salt concentration (Figure 71 A and B, Video 16). Based on studies dealing with the regulation of chicken and mouse Myosin V ^{54,278}, it is fairly likely that the *Xenopus l.* Myosin Va for instance exhibits a yet unknown light chain-binding behavior and thus for its re-activation would require more than just an increase in ionic strength.

Interestingly, it has been shown that cargo-binding domain (CBD)-lacking HMM-like Myosin V exhibits high ATPase activity independent of the Ca²⁺ concentration that is present ^{51,279}. It was therefore speculated that the CBD might play an essential role for the regulation of Myosin V. While previous ATPase activity studies demonstrated that high Ca²⁺ concentrations or high ionic strength leads to the re-activation of inhibited full-length Myosin V ⁵², for full-length Myosin Va it has not yet been shown that cargo-binding to the CBD indeed unfolds and thereby activates the auto-inhibited Myosin Va. However, due to the fact that kinesin motors show a highly similar inactivation pattern and are known to be re-activated upon cargo-binding ²⁸⁰, it is conceivable that receptor-specific cargo binding would compete with and disrupt the intramolecular interaction between the CBD and motor domain ⁵⁵.

To assay whether unfolding of the full-length Myosin Va would be achieved via attaching an artificial cargo (e.g., QDot), in this work the C'FLAG-tagged full-length Myosin Va version was targeted for tail-specific QDot-labeling (Figure 72). This idea based on previous studies, where for the purpose of optical trap assays full-length (chicken) Myosin Va was attached to polystyrene beads and was thereby forced to unfold ³⁸. While the applied conditions resulted in the efficient labeling of full-length *Xenopus l.* Myosin Va with QDots, unfortunately no movement but instead only stationary actin-bound Qdots could be observed. This observation could be explained by at least two reasons: One, the potential improper protein integrity of the C'FLAG-tagged construct (as earlier no filament-gliding motility was observed, discussed above); or two, the here performed

QDot-Myosin conjugation was simply not proficient in unfolding the auto-inhibited motor protein.

Therefore, further experiments will be required to pinpoint the walking behavior of individual full-length *Xenopus l.* Myosin Va molecules on F-actin.

6.4.4 Summary and Outlook

In this work, the complete coding sequence of the full-length Myosin Va from *Xenopus l.* was determined. On protein level, the primary sequence shows high similarity to Myosin Va from other species. Besides a less positively charged loop 2 sequence, the *Xenopus l.* Myosin Va sequence has an extended third coiled-coil region, that is unique among the four species herein compared. Similar to what has been reported for Myosin Va sequences from other species, the highest divergence was observed within the proximal tail region, while the head and distal tail domain (contains the cargo-binding domain) constitute the most conserved domains as expected.

In addition to the described successful sequence retrieval, in this work the expression and subsequent purification of this large and complex protein was achieved. However, due to the large size (217 kDa), its complexity and potential degradation sites (e.g., PEST site) of the full-length Myosin Va, instant degradation of the over-expressed protein still poses a problem. The optimized protein expression, will now allow further purification of the full-length protein by native size-exclusion chromatography. Along with the enriched full-length protein the dimerization-state can now be determined via MALS.

Herein performed *in vitro* gliding-filament motility assays revealed the unperturbed movement of the N'FLAG-tagged full-length Myosin Va version, while exhibiting velocities similar to those reported for Myosin Va-driven melanosome transport inside cells¹⁰⁶. Initial experiments provided evidence that single full-length Myosin Va molecules can be visualized either by Cy3-conjugated anti-FLAG antibody or by Quantum dot labeling. However, up to this point only very few single-molecule walking events could be recorded, most likely due to auto-inhibition of the full-length protein, as has been previously reported for the full-length Myosin Va from mouse and chicken^{21,50,51,52,53,266,276}. Further experiments will be required to find experimental conditions under which the auto-inhibited full-length Myosin Va can be re-activated into a constitutively active motor protein. For this, not only the

Discussion

efficiency in fluorescent single-molecule labeling but also adaptation of the optimal ionic strength and Ca^{2+} concentrations will be necessary. The putative head-tail interaction that is proposed to mediate auto-inhibition can be disrupted by generating C-terminally truncated Myosin Va constructs, lacking the C-terminal globular tail domain^{51,279}. Another way to prevent auto-inhibition, would be to introduce a stretch of amino acids (e.g., glutamic acids) that make the molecule inapt of folding back and thus would turn it intrinsically active^{179,281}, while retaining the globular tail domain. *In vivo*, cargo-binding to the CBD of Myosin Va occurs via recruiting the tripartite adaptor protein complex melanophilin:Rab27a:Myosin Va^{57,58,59,92}. However, presently melanophilin is the only confirmed cargo-receptor for Myosin Va and has been shown to be capable of markedly increasing ATPase activity of the auto-inhibited full-length mouse Myosin Va²⁷⁹. For this reason, currently I have been over-expressing recombinant FLAG-tagged melanophilin, to then assess whether auto-inhibited full-length *Xenopus l.* Myosin Va can be re-activated *in vitro*.

Once re-activation is successful, the *in vitro* behavior of the here introduced and described motor protein will be compared and correlated to the well studied intracellular Myosin Va-driven transport behavior on F-actin inside *Xenopus l.* melanophores.

While for the auto-inhibited form of the full-length chicken Myosin Va electron-microscopy deduced high-resolution structures have been useful in providing useful insights, for the open unfolded full-length version, via x-ray crystallography only parts (head, neck and globular tail domain) of the full-length Myosin Va were successfully resolved^{192,282,283,284,285}. With this gap of structural knowledge, any descent structure-prediction via the currently available software remains impossible, leaving the field with an incomplete view of this (not only in pigment cells) important molecular transporter. Now that the full-length Myosin Va from *Xenopus l.* can be expressed and purified as recombinant protein, in the future it should be focused on also obtaining the extended non-inhibited structure of the full-length Myosin Va by either (cryo) electron microscopy.

How exactly does the previously reported tail-phosphorylation of the full-length Myosin Va regulate Myosin V-driven transport in *Xenopus l.* melanophores? As this question has still remained poorly answered, rather than using a short tail construct from mouse^{88,103,106,286}, with the now available *Xenopus*-specific tail

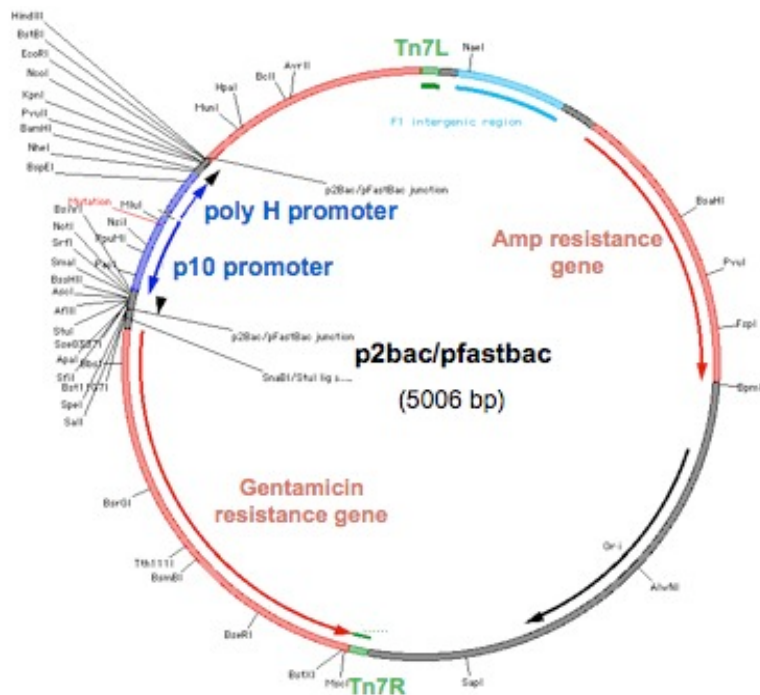
Discussion

domain the specific phosphorylation sites of e.g., PKA and CaMKII- α can now be investigated biochemically *in vitro*^{121,287}. Furthermore, with the purified full-length protein it will be possible to study the interaction of those but also other kinases or phosphatases as well as other proposed Myosin V-interacting and adaptor proteins (e.g., melanophilin) *in vitro*.

At last with the here provided full-length sequence of the *Xenopus l.* Myosin Va, a tail construct similar to the short-tail construct from mouse, can be generated and used for dominant-negative over-expression in *Xenopus l.* melanophores. This way for the first time it would be possible to study Myosin Va's role during intracellular cargo transport in a species-specific background. Based on the here determined sequence of the full-length *Xenopus l.* Myosin Va, it now has become possible to generate specific Myosin Va mutants, by which sequence-specific and/or structural clues regarding the Myosin Va-driven cargo transport inside melanophores can then be elucidated *in vivo*.

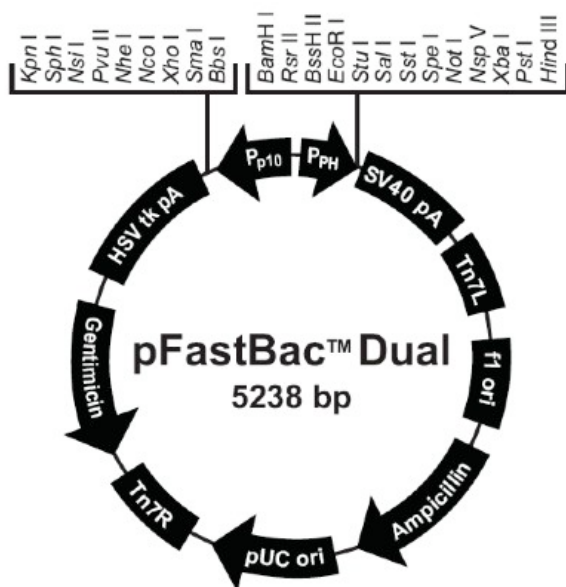
7 Supporting Information

7.1 Maps of baculovirus transfer vectors



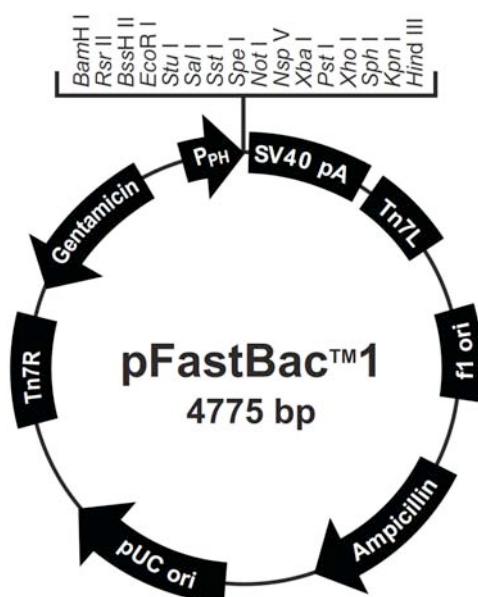
Vector map and features of p2bac/pfastbac baculovirus transfer vector.

The two promoters (poly H and p10, *dark blue*) of this vector allow for simultaneous overexpression of two different proteins encoded on the same plasmid. The expression cassette is flanked by the left (L) and right (R) arms of Tn7, which are mini Tn7 elements that permit site-specific transposition of the gene of interest into the baculovirus genome (*green*). The antibiotic resistance genes encoding for ampicillin and gentamicin are also depicted (*light red*). This vector was used for the overexpression of HMM-like Myosin V loop 2 constructs in insect cells. While the gene encoding for myosin was cloned under the control of p10, the calmodulin gene was cloned under the control of poly H. *Courtesy of J. Spudich (Stanford University, Stanford, U.S.A.).*



Vector map and features of pFastBac™ Dual baculovirus transfer vector.

As for the p2bac/pfastbac vector, with the polyhedrin (here PH) and p10 promoters the pFastBac Dual vector (Invitrogen) contains the same two promoters, allowing for simultaneous overexpression of two different proteins encoded by the same vector. Except for the multiple cloning sites of each of the two promoters, antibiotic resistance genes as well as left and right Tn7 transposons are the same as for the p2bac/pfastbac vector. This vector was used for the overexpression of the N' and C'FLAG-tagged full-length *Xenopus l.* Myosin Va (loned under the control of p10). *Vector map adapted from Invitrogen™ life technologies (Grand Island, U.S.A.).*



Vector map and features of pFastBac™ 1 baculovirus transfer vector.

This vector was used to overexpress N' and C'FLAG-tagged CaMKII- α as well as calmodulin. While pFastBac 1 encodes for the same antibiotic resistances (ampicillin and gentamicin) as the p2bac/pfastbac or pFastBac Dual vectors, it contains only one promoter (PH) and expression cassette. *Vector map adapted from Invitrogen™ life technologies (Grand Island, U.S.A.).*

7.2 Mass-spectrometry on crudely isolated melanosomes and melanosomes purified by density gradient ultra-centrifugation

Tables 1 and 2: Samples of crudely isolated melanosomes (*Table 1*) as well as of melanosomes that had been further purified by density gradient ultra-centrifugation (DC, *Table 2*) were resolved on a 12% SDS polyacryl amide gel (Section 5.3.1.1). Following the standard trypsin in-gel digestion, the protein samples were subjected to Nanospray-LC tandem mass-spectrometry (for more details, refer to Section 4.3.1.2). All identified proteins that gave significant spectra-deduced protein hits (i.e., above unspecific spectra background) are listed according to their respective protein search scores (from high to low, sixth column from left). Protein scores derived from ions scores as a non-probabilistic basis for ranking protein hits. Ions scores refer to $-10 \cdot \log(p)$, where p is the probability that the observed match is a random event. The Mascot protein search was conducted using protein sequence libraries from *Xenopus l.* In those cases, where peptide matches were obtained but the given protein has not yet been annotated, a subsequent species-independent BLAST search was performed (forth column from left). In addition, all proteins here identified are annotated to the respective protein group to which they belong (fifth column from left). The bioinformatical analysis was carried out by the Zentrum für Proteinanalytik (ZfP, LMU, Munich, Germany). The herein identified proteins were compared to two studies that applied proteomics on melanosomes from human melanoma cells. *Green and yellow shading:* indicates consistency with proteins identified by Basrur *et al.*¹²⁵ (green) and/or Chi *et al.*¹²⁶ (yellow).

7.2.1 **Table 1: Crudely isolated melanosomes**

gi identification number	Protein name	Protein group	Search Score	Nominal Mass	Queries matched	Calc. pI
1	ATP synthase subunit alpha, mitochondrial	Mito Pr	3261	59060	131	3.56
2	Voltage-dependent anion-selective channel protein 2	Mito Pr	2027	30109	76	3.82
3	Vimentin-1/2	IF Pr	1983	52869	128	6.36
4	Actin, cytoplasmic 2	Actin	1912	42108	112	4.69
5	Elongation factor 1-alpha, somatic form	Ribo Pr	1657	50524	104	3.02
6	Actin, alpha cardiac muscle 1	Actin	1220	42331	80	2.09
7	Vimentin 4	IF Pr	1220	53521	92	2.72
8	Heat shock protein 70	Chaperone	1037	72705	62	1.12
9	40S ribosomal protein S3-A	Ribo Pr	901	27156	55	4.05
10	Citrate synthase, mitochondrial	Mito Pr	863	51999	76	1.22
11	Tubulin beta-4 chain	Tubulin	846	50240	60	1.43
12	Succinate dehydrogenase subunit A	Mito Pr	667	73835	45	0.69
13	Succinate dehydrogenase subunit B	Mito Pr	596	73791	39	0.48
14	Putative ATP-dependent RNA helicase an3	RNA-BP	569	77597	33	0.45
15	14-3-3 protein zeta	14-3-3 Pr	452	27940	24	1.2
16	60S ribosomal protein L4-A	Ribo Pr	435	45192	44	1.02
17	40S ribosomal protein S8	Ribo Pr	434	24354	34	1.46
18	Elongation factor 1-gamma-A	Ribo Pr	407	50101	48	1.15
19	60S ribosomal protein L8	Ribo Pr	398	28128	34	1.19
20	Transitional endoplasmic reticulum ATPase (VCP)	ER Pr	389	89760	33	0.38
21	Elongation factor 1-alpha, somatic form	Ribo Pr	377	50524	27	0.46
22	Cytoplasmic poly(A)-binding protein 1-A	RNA-BP	359	70651	30	0.51
23	40S ribosomal protein S4	Ribo Pr	330	29874	45	2.95
24	60S ribosomal protein L10a	Ribo Pr	305	24931	36	1.73
25	Heat shock protein 70	Chaperone	291	71270	18	0.2

gi identification number	Protein name	Protein group	Search Score	Nominal Mass	Queries matched	Calc. pI
26	Presequence protease, mitochondrial	Mito Pr	279	117746	41	0.35
27	Elongation factor 1-alpha, somatic form	Ribo Pr	242	50524	16	0.46
28	Probable mitochondrial import receptor subunit TOM40 homolog	Mito Pr	219	36278	27	0.55
29	Malate dehydrogenase, cytoplasmic	Mito Pr	208	36687	24	0.68
30	14-3-3 protein beta/alpha-A	14-3-3 Pr	199	27856	25	1.47
31	Sodium/potassium-transporting ATPase alpha-1 chain	TM Pr	191	114323	17	0.12
32	T-complex protein 1 subunit gamma (chaperonin CCT3)	Chaperone	183	61225	15	0.11
33	Nucleolin	Nuclear Pr	181	70210	18	0.32
34	60S ribosomal protein L5-A	Ribo Pr	177	34312	17	0.45
35	40S ribosomal protein S6	Ribo Pr	176	28830	16	0.73
36	Elongation factor 1-alpha	Ribo Pr	164	50433	12	0.14
37	Elongation factor 1-alpha	Ribo Pr	136	50433	9	0.21
38	Elongation factor 1-alpha, somatic form	Ribo Pr	124	50524	9	0.13
39	Heterogeneous nuclear ribonucleoprotein A2 homolog 1	Nuclear Pr	115	36651	17	0.41
40	Heterogeneous nuclear ribonucleoprotein A2 homolog 2	Nuclear Pr	106	38020	19	0.52
41	Glyceraldehyde-3-phosphate dehydrogenase	Housekeeping	101	36017	9	0.19
42	Heat shock protein 70	Chaperone	91	72705	14	0.14
43	Tyrosyl-tRNA synthetase, cytoplasmic	Cytoplasmic Pr	86	59236	3	0.06
44	Heterogeneous nuclear ribonucleoprotein A3 homolog 1	Nuclear Pr	80	38728	16	0.51
45	Elongation factor 1-alpha	Ribo Pr	80	50433	11	0.21
46	Elongation factor 1-alpha, somatic form	Ribo Pr	80	50524	18	0.29

gi identification number	Protein name	Protein group	Search Score	Nominal Mass	Queries matched	Calc. pI
47	Nucleolin	Nuclear Pr	77	70210	6	0.1
48	Transforming growth factor beta regulator 4	GF	68	72377	9	0.05
49	Elongation factor 1-alpha, somatic form	Ribo Pr	53	50524	6	0.07
50	Sodium/potassium-transporting ATPase alpha-1 chain	TM Pr	45	114323	4	0.06
51	Keratin, type 1 cytoskeletal 47 kDa	IF	43	29888	5	0.24
52	Elongation factor 1-alpha	Ribo Pr	29	50433	4	0.07
53	Elongation factor 1-alpha, somatic form	Ribo Pr	29	50524	5	0.07
54	Elongation factor 1-alpha, somatic form	Ribo Pr	24	50524	6	0.07
55	WD repeat protein 24	Cytoplasmic Pr	20	90173	3	0.04
56	Elongation factor 1-gamma-A	Ribo Pr	15	50101	2	0.07

7.2.2 *Table 2: DC-purified melanosomes*

	gi identification number	Protein name	BLAST search	Protein group	Search Score	Nominal Mass	Sequence coverage	Calc. pI
1	gi 148223219	Tyrosinase-related protein 1		Mel		61776	32	5.33
2	gi 148233183	Eukaryotic translation elongation factor 1 alpha, somatic form		Ribo Pr	1012	50524	51	9.1
3	gi 120577575	Eukaryotic translation elongation factor 1 alpha 1		Ribo Pr	810	51238	35	9.2
4	gi 148232467	Eukaryotic translation elongation factor 1 alpha 2		Ribo Pr	728	50773	30	9.1
5	gi 138531	Vimentin-1/2		IF Pr	555	52869	47	5.16
6	gi 148231554	Cold inducible RNA-binding protein		RNA-BP	543	17949	41	9.21
7	gi 148235865	Cold-inducible RNA binding protein 2		RNA-BP	411	17844	57	9.12
8	gi 138532	Vimentin-4		IF Pr	328	53521	26	5.08
9	gi 148223359	ATP synthase, H+ transporting mitochondrial F1 complex, beta subunit		Mito Pr	308	56395	20	5.25
10	gi 464252	Nucleolin		Nuclear Pr	242	70210	19	4.86
11	gi 1703123	Actin, cytoplasmic type 5		Actin	223	42165	19	5.3
12	gi 148226518	Nucleolin		Nuclear Pr	209	75533	16	4.79
13	gi 147900289	Beta-actin		Actin	208	69494	8	8.58
14	gi 52345478	RAB1A		Rab Family	163	22875	22	5.93
15	gi 147905648	LOC100036902 in <i>Xenopus laevis</i>	Actin, cytoplasmic type 2	Actin	151	42303	15	5.31
16	gi 148235659	Chaperonin		Chaperone	150	61767	12	5.65
17	gi 227525	ATP dependent RNA helicase		RNA-BP	147	77601	8	5.96

gi identification number	Protein name	BLAST search	Protein group	Search Score	Nominal Mass	Sequence coverage	Calc. pI
18	gi 147901291 Ribosomal protein S8 (rpS8B)		Ribo Pr	134	22170	26	10.09
19	gi 56118925 RAB7A		Rab Family	134	23808	15	6.62
20	gi 4506713 Ubiquitin and ribosomal protein S27a precursor		Ribo Pr	116	18296	22	9.68
21	gi 37719618 Tyrosinase		Mel	114	29547	11	5.2
22	gi 34536534 Tyrosinase		Mel	114	18273	19	4.7
23	gi 148228352 Chaperonin		Chaperone	107	50727	4	7.57
24	gi 148226947 Glucose regulated protein, 58kDa		ER Pr	104	56486	5	5.72
25	gi 50417653 Hypothetical protein LOC397850 in Xenopus laevis	Heat shock protein 70	Chaperone	104	72739	8	4.96
26	gi 147906703 Heat shock protein 70		Chaperone	104	72489	9	5.03
27	gi 114535 ATP synthase subunit alpha, mitochondrial		Mito Pr	99	59060	11	8.86
28	gi 148237590 Mitochondrial malate dehydrogenase 2a		Mito Pr	99	35915	19	8.93
29	gi 66910737 LOC733250 in Xenopus laevis	Transmembrane Glycoprotein nmb	TM-Pr	94	66015	2	7.61
30	gi 122034 Histone H2B 1.2		Histone	83	13897	34	10.31
31	gi 125858696 LOC100037232 in Xenopus laevis	Eukaryotic translation initiation factor 4B	Tr IF	77	39473	11	5.74
32	gi 147900738 Annexin A1		PLipid-BP	77	38499	11	7.56
33	gi 147904224 Desmin		IF	69	52926	9	5.25

gi identification number	Protein name	BLAST search	Protein group	Search Score	Nominal Mass	Sequence coverage	Calc. pI
34	gi 4503499 X-linked eukaryotic translation initiation factor 1A in Homo Sapiens		TF	68	16564	11	5.07
35	gi 147898544 MGC80893 in Xenopus laevis	TAF15 RNA polymerase II	RNA-BP	66	51350	12	8.94
36	gi 140245 Nuclease-sensitive element-binding protein 1		DNA-BP	66	34613	4	9.17
37	gi 147902910 Histone cluster 1, H2ad		Histone	62	13984	28	10.88
38	gi 125112 Keratin, type II cytoskeletal 8		IF	61	55645	4	5.3
39	gi 114145561 Keratin complex 2, basic, gene 8 in Mus musculus		IF	61	54531	5	5.7
40	gi 148222597 Heat shock protein 70		Chaperone	58	71372	8	5.43
41	gi 6678469 Tubulin, alpha 1C in Mus musculus		Tubulin	57	50562	3	4.96
42	gi 50603788 Heat shock protein 70		Chaperone	57	71563	6	5.41
43	gi 148231322 Putative 60S ribosomal protein L21		Ribo-Pr	49	18737	15	10.82
44	gi 27370929 Annexin A1, isoform CRA_b		PLipid-BP	43	28587	14	6.06
45	gi 148229707 Succinate dehydrogenase complex, subunit A		Mito Pr	42	73791	2	6.5
46	gi 54311369 Saf-A protein		Nuclear Pr	42	86340	6	5.03
47	gi 169641972 PMEL17 protein/SILV protein		Mel	41	78157	3	4.46
48	gi 148222693 Annexin A1		PLipid-BP	40	37512	8	6.92
49	gi 148229965 Heat shock protein 70		Chaperone	40	69803	5	5.68
50	gi 62533196 LOC733201 in Xenopus laevis	Rab/GAP TBC domain-cont. Protein	unknown	39	66954	0	6.27

gi identification number	Protein name	BLAST search	Protein group	Search Score	Nominal Mass	Sequence coverage	Calc. pI
51	gi 147907415 Roppurin-1-like		Rho-BP	39	24678	4	4.66
52	gi 148223936 Solute carrier family 25, mitochondrial member 3 carrier		Mito Pr	38	40337	5	9.23
53	gi 148237836 Lysosomal-associated membrane protein 2 (LAMP2)		Mel	37	45371	3	4.97
54	gi 147906628 ATPase, H+ transporting, lysosomal (vacuolar proton pump)		Lyso+LRP	36	56754	11	5.56
55	gi 148229393 Cathepsin D		Lyso+LRP	35	43700	6	5.98
	gi 1710623 Heterogeneous nuclear ribonucleoprotein A2 homolog 1		Nuclear Pr	35	36651	11	8.28
56	gi 147900863 Dolichyl-diphosphooligosaccharide-protein glycosyltransferase 48 kDa subunit		ER Pr	35	48739	1	5.35
57	gi 148229101 RAB10		Rab Family	35	22783	12	8.59
58	gi 148229927 Annexin A1		PLipid-BP	34	37841	7	6.2
59	gi 147901235 Syntaxin 7 [Xenopus laevis]		Endo Pr	34	29361	3	5.14
60	gi 82210031 Actin-binding protein anillin		Actin-BP	33	124009	0	8.42
61	gi 148227544 Translation initiation factor eIF-5A		Tr IF	33	16978	15	5.49
62	gi 115528305 A kinase (PRKA) anchor protein 8		AKAP	32	54678	1	8.74
63	gi 148229220 Signal peptidase complex (18kD)		ER Pr	32	20590	5	9.12

gi identification number	Protein name	BLAST search	Protein group	Search Score	Nominal Mass	Sequence coverage	Calc. pI
64	Tyrosine-related protein 2		Mel	31	58847	4	5.93
65	Mannosidase, alpha, class 2C, member 1		GA Pr	31	119931	1	6.12
66	Insulin-like growth factor I receptor		TM Pr	31	69460	0	5.08
67	Internexin neuronal intermediate filament protein		IF Pr	29	55014	5	5.4
68	Neurofilament protein		IF Pr	29	102774	3	4.27
69	Dihydroipoamide S-succinyltransferase		Mito Pr	29	49255	1	8.85
70	Nuclear/mitotic apparatus protein		Nuclear Pr	29	73297	2	5.45
71	Ras-GTPase-activating protein SH3-domain-binding protein		Nuclear Pr	29	52741	11	4.99
72	High mobility group HMG-17		Chromatin	29	9485	14	10
73	Histone H2A		Histone	28	14907	5	10.05
74	ATP synthase, H+ transporting, mitochondrial F1 complex, delta subunit		Mito Pr	28	16892	17	4.74
75	FXR1		Ribo Pr	27	73283	4	6.24
76	DEAD (Asp-Glu-Ala-Asp) box polypeptide 1		Rec Pr	27	83321	1	7.05
77	CSE1 chromosome segregation 1-like		Chromatin	27	110776	2	5.38
78	Myosin alkali light chain 6, smooth muscle form		Myosin	26	16917	15	4.45

Supporting Information

gi identification number	Protein name	BLAST search	Protein group	Search Score	Nominal Mass	Sequence coverage	Calc. pI
79	RAB32		Rab Family	26	25159	8	5.36
80	Flap endonuclease 1		Nuclear Pr	25	43054	2	8.03
81	ATPase, H+ transporting, lysosomal 70kDa, V1 subunit A		Lyso+LRP	23	68823	7	5.53
82	Heterogeneous nuclear ribonucleoprotein K		Nuclear Pr	22	44141	16	6.64
83	Pre-mRNA binding K protein		Nuclear Pr	22	43890	13	8.23
84	Syndecan binding protein (syntenin)		Nuclear Pr+PM	22	32129	26	7.05
85	Minichromosome maintenance complex component 7		Nuclear Pr	22	82625	1	6.03
86	Chain B, Complex Between Nucleosome Core Particle (H3,H4,H2a,H2b)		Histone	22	9962	11	11.19
87	Similar to arginine/serine-rich 5 splicing factor		RNA-BP	20	29545	4	10.76
88	Tyrosine 3-monooxygenase/tryptophan 5-monooxygenase activation protein		14-3-3 Pr	20	27885	5	4.71
89	Tyrosine 3-monooxygenase/tryptophan 5-monooxygenase activation protein		14-3-3 Pr	20	28046	6	4.69
90	ATPase, sodium-potassium pump alpha1 subunit		TM Pr	19	114138	4	5.33

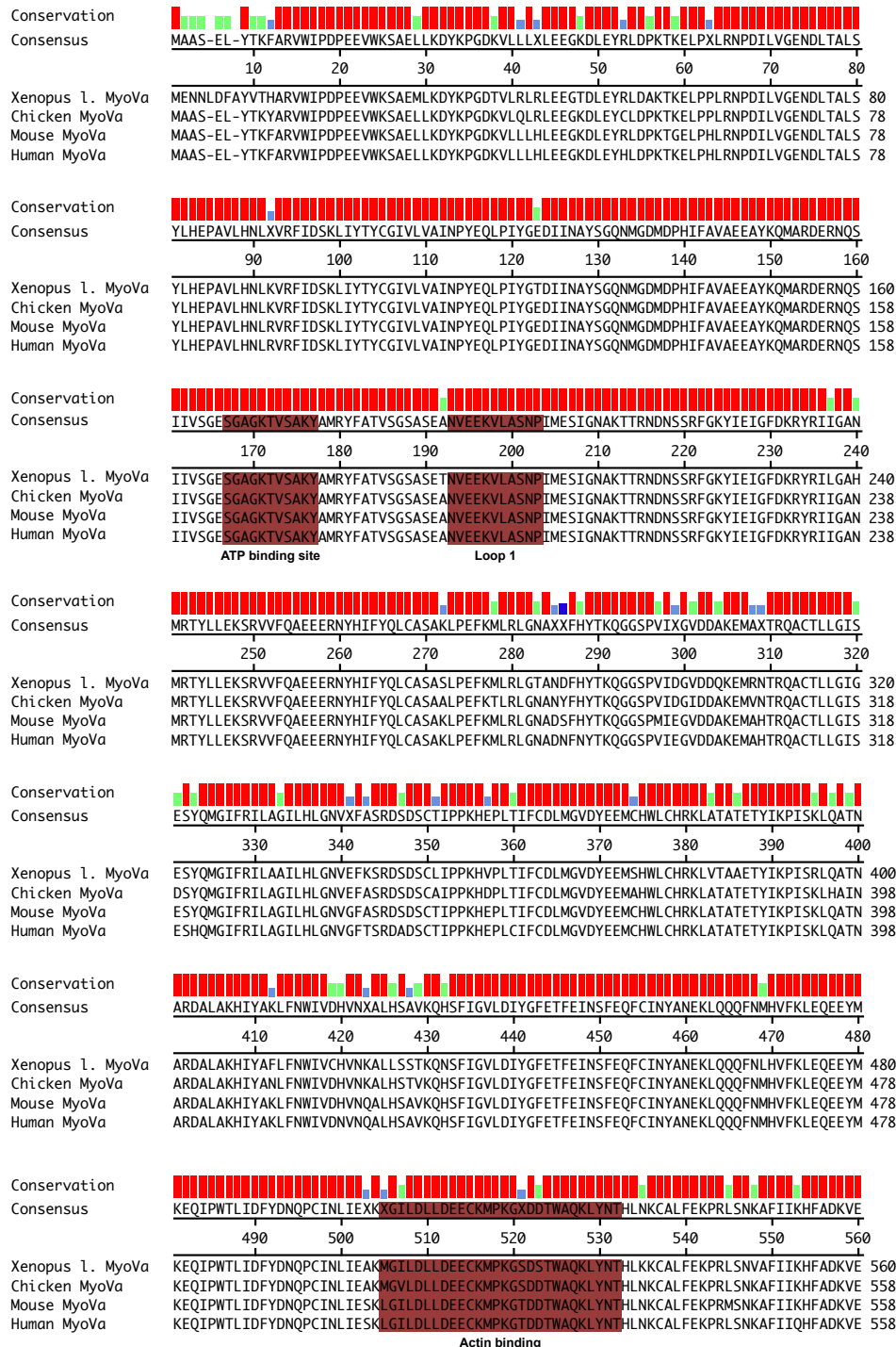
	gi identification number	Protein name	BLAST search	Protein group	Search Score	Nominal Mass	Sequence coverage	Calc. pI
91	gi 27503841	Nuclease sensitive element binding protein 1		DNA-BP	19	34370	4	9.46
92	gi 49257996	Phospholipase A2 activating protein (Plaa)		PLipid-BP	18	91283	1	5.4
93	gi 147901554	Na ⁺ /K ⁺ -ATPase alpha 3 subunit		TM Pr	18	114308	4	5.3

Designated protein categories	
14-3-3 Pr	Members of the 14-3-3 protein family
Actin	Actin isoforms
Actin-BP	Actin-binding proteins
AKAP	A-kinase anchoring proteins
Chaperone	Chaperone-related proteins
Chromatin	Chromatin-binding proteins
Cytoplasmic Pr	Abundant proteins that predominantly localize to the cytoplasm
DNA-BP	DNA-binding proteins
Endo Pr	Endosomal proteins
ER Pr	Proteins that primarily localize to the endoplasmic reticulum
GA Pr	Golgi-apparatus related proteins
GF	Members of the growth-factor family
Histone	Histone (or histone-associated) proteins
Housekeeping	Members of the housekeeping protein family
IF Pr	Intermediate filament proteins
Lyso+LRP	Lysosomes and lysosome-related proteins
Mel	Melanosome (-associated) proteins
Mito Pr	Mitochondrial (or mitochondria-associated) proteins
Myosin	Proteins of the myosin superfamily
Nuclear Pr	Proteins that primarily localize to the nucleus
PLipid-BP	Phospholipid-binding proteins
Rab family	Proteins of the Rab family
Rho-BP	Rho-binding proteins
Ribo Pr	Ribosomal (or ribosome-associated) proteins
RNA-BP	RNA-binding proteins
TM-Pr	Transmembrane Receptor proteins
Tr IF	Translation initiation factor proteins
Tubulin	Tubulin isoforms

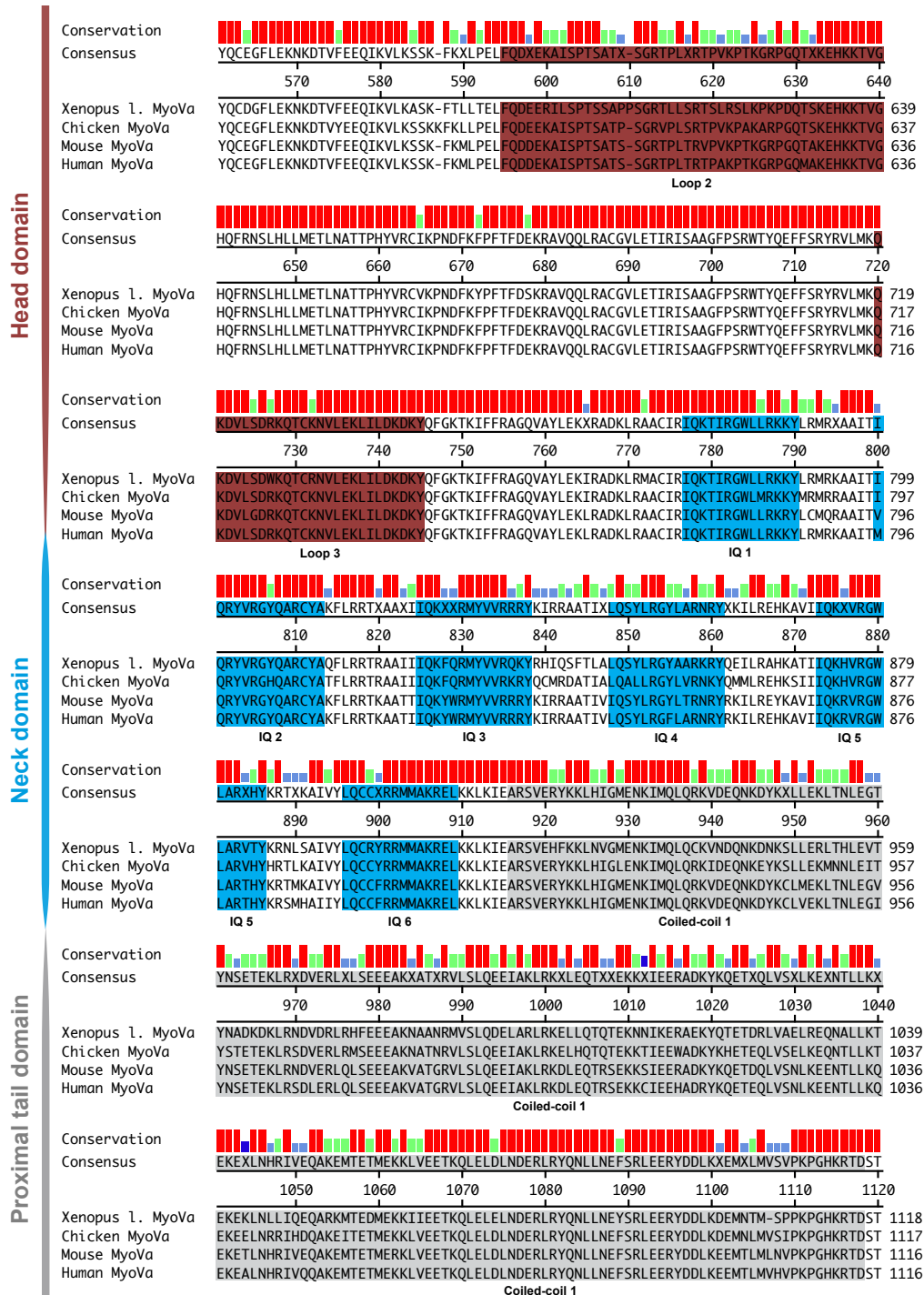
7.3 Comparative sequence alignment of full-length Myosin Va from *Xenopus l.* with other vertebrate class V myosins

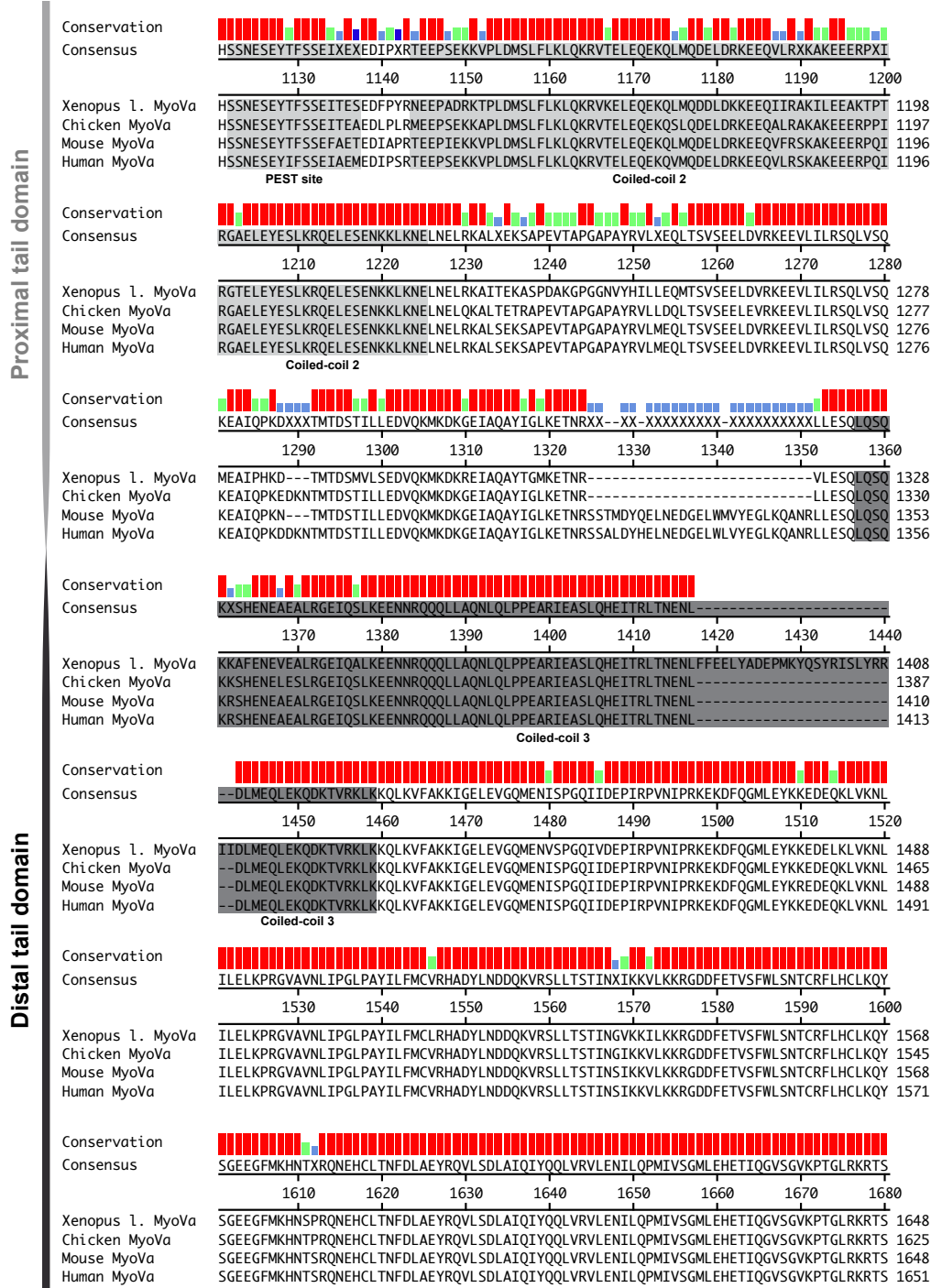
The here determined full-length Myosin Va from *Xenopus laevis* was aligned with the class V myosins from chicken (*Gallus gallus*, accession number: NP_990631), mouse (*Mus musculus*, accession number: CAX15576.1) and human (*Homo sapiens*, accession number: NP_000250.3). The conserved motifs and/or regions of interest in the head, neck and tail domain are labeled and color coded. The sequence alignment was performed using Megalign 2.1.0.97 (DNASStar) and the blosum62 amino acid table. The classification of the structural relevant motifs was adapted from Espreafico *et al.* (1992) and Larson *et al.* (1996)^{288,289} as follows. *Head domain* (aa1-775, maroon color): ATP binding site (aa167-177), Loop 1 (aa193-203), Actin-binding region (aa505-532), Loop 2 (aa594-639) and Loop 3 (aa719-744). *Neck domain* (aa776-908, blue color): Six IQ motifs (aa776, 799, 824, 847, 872, 895). *Proximal tail domain*, also referred to as rod region (aa915-approx. 1320, light grey color): Coiled-coil 1 (aa915-1116), PEST site (aa1119-1135) and Coiled-coil 2 (aa1142-1223). *Distal tail domain* (aa1321-1852, dark grey color): Coiled-coil 3 (aa1325-1427) and Dilute (DIL) domain, composing the globular domain that mediates cargo binding (aa1683-1789). The here named amino acid (aa) positions refer to those of the full-length Myosin Va sequence from *Xenopus l.* Conservation for a given aa among the species here tested, is indicated by red (identical), green (one divergence), light blue (two divergences) and dark blue (all four species diverge at the given aa) bars.

Head domain

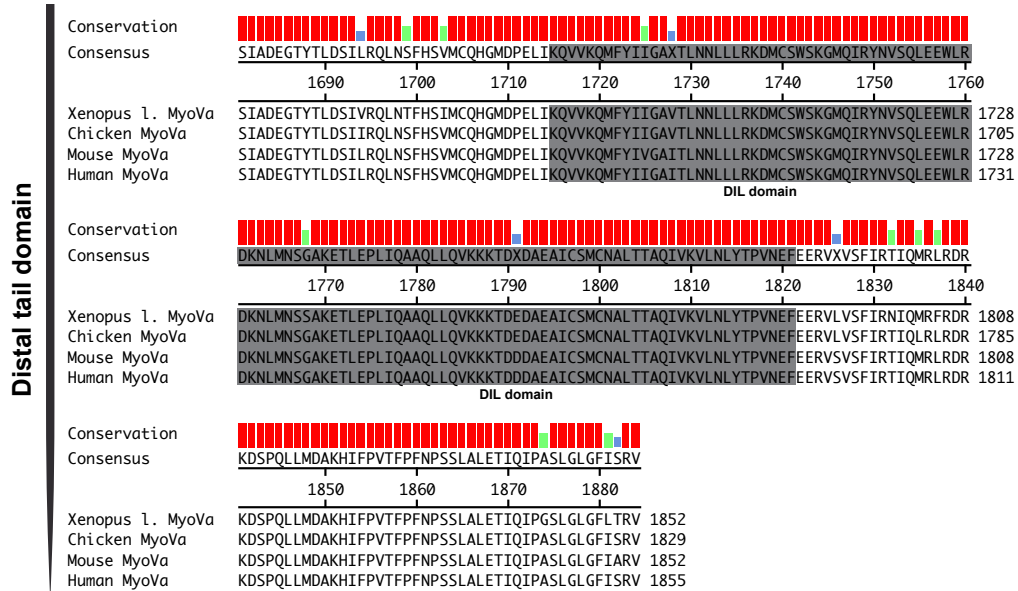


Supporting Information





Supporting Information



7.4 Protein sequences

7.4.1 HMM-like Myosin Va Wildtype (*Gallus gallus*)

M **DYKDDDDK** GAASELYTKYARVWIPDPEEVWKS AELLKDYKPGDKVL
QLRLEEGKDLEYCLDPKTKELPPLRNPDILVGENDLTALSYLHEPAVLHN
LKVRFIDSKLIYTYCGIVLVAINPYEQLPIYGEDIINAYSGQNMGDMDP
HIFAVAEAEAYKQMARDERNQSIIVSGESGAGKTVSAKYAMRYFATVSG
SASEANVEEKVLASNPIMESIGNAKTTRNDNSSRFGKYIEIGFDKRYRII
GANMRTYLLEKSRVVFQAEERNYHIFYQLCASAALPEFKTLRLGNANY
FHYTKQGGSPVIDGIDDAKEMVNTRQACTLLGISDSYQMGIFRILAGIL
HLGNVEFASRSDSDSCAIPPKHDPLTIFCDLMGV DYEEMAHWLCHRKL
ATATETYIKPISKLHAINARDALAKHIYANLFNWIVDHSV NKA LHSTVKQH
SFIGVLDIYGFETFEINSFEQFCIN YANEKLQQQFNMHVFKLEQEEYMK
EQIPWTLIDFYDNQPCINLIEAKMGVLDLLDEECKMPKGSDDTWAQKL
YNTHLNKCALFEKPRLSNKA FIIKHFADKVEYQCEGFLEKNKDTVYEEQI
KVLKSSKKFKLLPEL **FQDEEK AISPTSATPSGRVPLSRTPVKPAKARPGQ**
TSKEHKKT V G HQFRNSLHLLMETLNATTPHYVRCIKPNDFKFPFTFDEKR
AVQQLRACGVLETIRISAAGFPSRWTYQE FFSRYRVL MKQKDVLSDRK
QTCKNVLEKLILDKDKYQFGKTKIFFRAGQVAYLEKIRADKLRAACIR |
QKTIRGWL MR KKYMRMRRAAIT **QRYVRGHQAR** CYATFLRRTRAAII |
QKFQRM YVVR KRYQCMRDATIA **LQALLRGYLVR** NKYQMMLREHKSII |
QKHVRGWLAR VH YHRTLKAIVY **LQCCYRRMMAK** RELKCLKIEARSVER
YKKLH **I GLENKIMQLQRKVDEQNKD YKCLMEKLTNLEGVYNSETEKLRN**
DVERLQLS EEEAKVATGRVLSLQEEIAKLRKDLEQTRSEKKSIEERADKY
KQETDQLVSNLKEENTLLKQEKETLNHRIVEQAKEMTETMERKLV EETK
QLELDLNDERLRYQ NLLNE FSRLEERYDDLKEEMTLMLNV **MKQLEDKVE**
ELLSKNYHLENEVARLKKLVGE

Color code: **FLAG** **Loop 2** **IQ-motifs** **Rod** **GCN4**

7.4.2 Calmodulin light chain (*Drosophila melanogaster*)

MADQLTEEQIAEFKEAFSLFDKDG DGTITTKELGTVMRSLGQNPTEAEL
QDMINEVDADGNGTIDFPEFLTMMARKMKD TDSEEEIREAFRVFDKDG
NGYISAAELRHVMTNLGEKLTDEEVDEMIREADIDGDGQVNYEEFVQ
MMTAK

7.4.3 Essential Light Chain (*Dictyostelium discoideum*)

MSASADQIQECFSIFDKDNDGKVSVEDIGACLRSLGKSPTMADIEALK
TEIGAKEFDINTLKSIIYKKPNIKTPQEQQKEMLD AFKALDKEGHGTIQG
AELRQLLTTLGDYLSAEVDEL FKEISVDSTTGAVSYASLVNTIVSGYPEF
RHKFQSGFRVKREHYHQF

7.4.4 Calcium-/calmodulin-dependent kinase II- α (N'-FLAG-tagged)

M **DYKDDDDK** GAPATITCTRFTEEYQLFEELGKGAFSVVRRVCVKVLAG
QEYAAKIINTKKLSARDHQKLEREARICRLKHPNIVRLHDSISEEGHHY
LIFDLVTGGELFEDIVAREYYSEADASHCIQQILEAVLHCHQMGGVVHR
DLKPENLLLASKLKGAAVKLADFGLAIEVEGEQQAWFGFAGTPGYLSP
EVLRKDPYGKPVLDWACGVILYILLVGYPPFWDEDQHRLYQQIKAGA
YDFPSPDWDTVTPEAKDLINKMLTINPSKRITAAEALKHPWISHRSTVAS
CMHRQETVDCLKKFNARRKLGAILTTMLATRNFSGGKSGGNKKNDG
VKESSESTNTTIEDEDTKVRKQEIIKVTEQLIEAISNGDFESYTKMCDPGM
TAFEPEALGNLVEGLDFHRFYFENLWSRNSKPVHTTILNPHIHLMGDES
ACIAYIRITQYLDAGGIPRTAQSEETRVWHRRDGKWQIVHFHRS GAPS
VLPH

Color code: FLAG

7.4.5 Calcium-/calmodulin-dependent kinase II- α (C'-FLAG-tagged)

MATITCTRFTEEYQLFEELGKGAFSVVRRVCVKVLAGQEYAAKIINTKKLS
ARDHQKLEREARICRLKHPNIVRLHDSISEEGHHYLIFDLVTGGELFEDI
VAREYYSEADASHCIQQILEAVLHCHQMGGVVHRDLKPENLLLASKLKG
AAVKLADFGLAIEVEGEQQAWFGFAGTPGYLSP EVLRKDPYGKPVLD
WACGVILYILLVGYPPFWDEDQHRLYQQIKAGAYDFPSPDWDTVTPE
AKDLINKMLTINPSKRITAAEALKHPWISHRSTVASC MHRQETVDCLKKF
NARRKLGAILTTMLATRNFSGGKSGGNKKNDG VKESSESTNTTIEDED
TKVRKQEIIKVTEQLIEAISNGDFESYTKMCDPGMTAFEPEALGNLVEG
LDFHRFYFENLWSRNSKPVHTTILNPHIHLMGDESACIAYIRITQYLDAG
GIPRTAQSEETRVWHRRDGKWQIVHFHRS GAPS VLP H GAP **DYKDDDD**
K

Color code: FLAG

7.5 Videos/DVD

The provided DVD contains video material from single-molecule motility as well as filament gliding experiments of HMM-like Myosin V loop 2 mutants and the full-length Myosin Va from *Xenopus l.* For details, please refer to the respective video legend (below and as a pdf-file on DVD).

In addition, a copy of the publication that deals with the first part of this thesis (Zimmermann *et al.*, PLoSOne, 2011)¹⁹¹ is attached on the provided DVD.

7.5.1 Video Legends

Video 1

One-dimensional diffusion of *Wildtype* Myosin V on microtubules under high ionic strength.

Cy3-labeled HMM-like Myosin V *Wildtype* (bright particles) was infused into a flow cell containing surface-attached Atto 488-labeled microtubules (dim filaments). Assay was performed in 100 mM KCl. Excitation wavelength was 532 nm and representative image sequences were false-colored. This movie (89 frames) was recorded at 5 frames s⁻¹ and is displayed at three-fold speed. *Scale bar* represents 2 μ m.

Video 2

One-dimensional diffusion of *Wildtype* Myosin V on microtubules.

Cy3-labeled HMM-like Myosin V *Wildtype* (bright particles) was infused into a flow cell containing surface-attached Atto 488-labeled microtubules (dim filaments). Assay was performed in 25 mM KCl. Excitation wavelength was 532 nm and representative image sequences were false-colored. This movie (236 frames) was recorded at 5 frames s⁻¹ and is displayed at three-fold speed. *Scale bar* represents 2 μ m.

Video 3

One-dimensional diffusion of *Minus13* Myosin V on microtubules.

Cy3-labeled HMM-like Myosin V *Minus13* (bright particles) was infused into a flow cell containing surface-attached Atto 488-labeled microtubules (dim filaments). Assay was performed in 25 mM KCl. Excitation wavelength was 532 nm and representative image sequences were false-colored. This movie (272 frames) was recorded at 5 frames s⁻¹ and is displayed at three-fold speed. *Scale bar* represents 2 μ m.

Video 4

One-dimensional diffusion of *Wildtype* Myosin V on microtubules lacking E-hooks.

Cy3-labeled HMM-like Myosin V *Wildtype* (bright particles) was infused into a flow cell containing surface-attached Atto 488-labeled subtilisin-treated microtubules (dim filaments). Assay was performed in 25 mM KCl. Excitation wavelength was 532 nm and representative image sequences were false-colored. This movie (328 frames) was recorded at 5 frames s⁻¹ and is displayed at three-fold speed. *Scale bar* represents 2 μ m.

Video 5

Negatively charged *Minus4* Myosin V shows strongly impaired binding to F-actin.

Cy3-labeled HMM-like Myosin Va *Minus4* (bright particles) was infused into a flow cell containing surface-attached Atto-488-labeled F-actin (fuzzy filaments). Assay was performed in 25 mM KCl and 1 mM ATP. Excitation wavelength was 532 nm and representative image sequences were false-colored. This movie (200 frames) was recorded at 5 frames s⁻¹ and is displayed at six-fold speed. *Scale bar* represents 10 μm.

Video 6

Processive movement of the K-loop containing Myosin Va loop 2 mutant on F-actin.

Cy3-labeled HMM-like Myosin Va *K-loop* (bright particles) was infused into a flow cell containing surface-attached Atto-488-labeled F-actin (fuzzy filaments). Assay was performed in 25 mM KCl and 1 mM ATP. Excitation wavelength was 532 nm and representative image sequences were false-colored. This movie (270 frames) was recorded at 5 frames s⁻¹ and is displayed at six-fold speed. *Scale bar* represents 10 μm.

Video 7

Processive walking behavior of *K-loop* Myosin Va on F-actin – A closeup.

Here, a closeup (20 × 20 μm) of the image sequence from Video 6 is presented. This movie (250 frames) was recorded at 5 frames s⁻¹ and is displayed at six-fold speed. *Scale bar* represents 5 μm.

Video 8

Processive movement of *Wildtype* Myosin Va on F-actin.

Cy3-labeled HMM-like Myosin Va *Wildtype* (bright particles) was infused into a flow cell containing surface-attached Atto-488-labeled F-actin (fuzzy filaments). Assay was performed in 25 mM KCl and 1 mM ATP. Excitation wavelength was 532 nm and representative image sequences were false-colored. This movie (197 frames) was recorded at 5 frames s⁻¹ and is displayed at six-fold speed. *Scale bar* represents 10 μm.

Video 9

Actin filament gliding behavior of C'FLAG-tagged full-length Myosin Va from *Xenopus l.*

Atto488-labeled F-actin (green filaments) was infused into a flow cell containing surface-adhered C'FLAG-tagged full-length *Xenopus l.* Myosin Va. Assay was performed in 25 mM KCl and 2 mM ATP. Excitation wavelength was 488 nm and representative image sequences were false-colored. This movie (330 frames) was recorded at 5 frames s⁻¹ and is displayed at six-fold speed. *Scale bar* represents 10 μm.

Video 10

Actin filament gliding behavior of N'FLAG-tagged full-length Myosin Va from *Xenopus l.*

Atto488-labeled F-actin (green filaments) was infused into a flow cell containing surface-adhered N'FLAG-tagged full-length *Xenopus l.* Myosin Va. Assay was performed in 25 mM KCl and 2 mM ATP. Excitation wavelength was 488 nm and representative image sequences were false-colored. This movie (95 frames) was recorded at 1.4 frames s⁻¹ and is displayed at 3.6-fold speed. *Scale bar* represents 10 μm.

Video 11

Smooth actin filament gliding of N'FLAG-tagged full-length *Xenopus l.* Myosin Va – A closeup.

Here, a closeup (20 × 20 μm) of the image sequence from Video 10 is presented. This movie (95 frames) was recorded at 1.4 frames s⁻¹ and is displayed at 3.6-fold speed. *Scale bar* represents 5 μm.

Video 12

ATP-dependent movement of the full-length Myosin Va from *Xenopus l.*

Atto488-labeled F-actin (green filaments) was infused into a flow cell containing surface-adhered N'FLAG-tagged full-length *Xenopus l.* Myosin Va. Assay was performed in 25 mM KCl under zero-ATP conditions. Excitation wavelength was 488 nm and representative image sequences were false-colored. This movie (34 frames) was recorded at 1.3 frames s⁻¹ and is displayed at 3.8-fold speed. *Scale bar* represents 10 μm.

Video 13

Signs of Processivity: Single-point attachments for full-length *Xenopus l.* Myosin Va on F-actin.

Atto488-labeled F-actin (green filaments) was infused into a flow cell containing scarcely distributed surface-adhered N'FLAG-tagged full-length *Xenopus l.* Myosin Va molecules. Assay was performed in 25 mM KCl and 2 mM ATP. Excitation wavelength was 488 nm and representative image sequences were false-colored. This movie (100 frames) was recorded at 1.4 frames s⁻¹ and is displayed at 3.6-fold speed. *Scale bar* represents 10 μm.

Video 14

Single-molecule behavior of full-length *Xenopus l.* Myosin Va on F-actin.

Cy3-labeled N'FLAG-tagged full-length *Xenopus l.* Myosin Va (bright particles) was infused into a flow cell containing surface-attached Atto-488-labeled F-actin (fuzzy green filaments in background). Assay was performed in 25 mM KCl and 2 mM ATP. Excitation wavelength was 532 nm and representative image sequences were false-colored after channels were merged. This movie (42 frames) was recorded at 1 frame s⁻¹ and is displayed at five-fold speed. *Scale bar* represents 10 μm.

Video 15

Single-molecule behavior of full-length *Xenopus l.* Myosin Va on F-actin.

Here, a closeup (20 × 20 μm) of the image sequence from Video 14 is presented. This movie (42 frames) was recorded at 1 frames s⁻¹ and is displayed at five-fold speed. *Scale bar* represents 5 μm.

Video 16

Single-molecule behavior of full-length *Xenopus l.* Myosin Va on F-actin at high ionic strength.

Cy3-labeled N'FLAG-tagged full-length *Xenopus l.* Myosin Va (bright particles) was infused into a flow cell containing surface-attached Atto-488-labeled F-actin (fuzzy green filaments in background). Assay was performed in 150 mM KCl and 2 mM ATP. Excitation wavelength was 532 nm and representative image sequences were false-colored after channels were merged. This movie (22 frames) was recorded at 1 frame s⁻¹ and is displayed at five-fold speed. *Scale bar* represents 10 μm.

8 Literature

- 1 Haid, E., Lehmann, P. & Ziegenhorn, J. MOLAR ABSORPTIVITIES OF BETA-NADH AND BETA-NAD AT 260 NM. *Clinical Chemistry* **21**, 884-887 (1975).
- 2 Vale, R. D. The molecular motor toolbox for intracellular transport. *Cell* **112**, 467-480 (2003).
- 3 Desai, A. & Mitchison, T. Microtubule polymerization dynamics. *Annual Review of Cell and Developmental Biology* **13**, 83-117, doi:10.1146/annurev.cellbio.13.1.83 (1997).
- 4 Kreis, T. & Vale, R. (Oxford University Press, New York, 1999).
- 5 Haimo, L. T. & Rosenbaum, J. L. CILIA, FLAGELLA, AND MICROTUBULES. *Journal of Cell Biology* **91**, S125-S130, doi:10.1083/jcb.91.3.125s (1981).
- 6 Bardy, S. L., Ng, S. Y. M. & Jarrell, K. F. Prokaryotic motility structures. *Microbiology-Sgm* **149**, 295-304, doi:10.1099/mic.0.25948-0 (2003).
- 7 Mermall, V., Post, P. L. & Mooseker, M. S. Unconventional myosins in cell movement, membrane traffic, and signal transduction. *Science* **279**, 527-533 (1998).
- 8 Oliver, T. N., Berg, J. S. & Cheney, R. E. Tails of unconventional myosins. *Cell Mol Life Sci* **56**, 243-257 (1999).
- 9 Sellers, J. R. Myosins: a diverse superfamily. *Biochim Biophys Acta* **1496**, 3-22 (2000).
- 10 Odrionitz, F. & Kollmar, M. Drawing the tree of eukaryotic life based on the analysis of 2,269 manually annotated myosins from 328 species. *Genome Biology* **8**, doi:R196 10.1186/gb-2007-8-9-r196 (2007).
- 11 Reck-Peterson, S. L., Provance, D. W., Jr., Mooseker, M. S. & Mercer, J. A. Class V myosins. *Biochim Biophys Acta* **1496**, 36-51 (2000).
- 12 Berg, J., Powell, B. & Cheney, R. A millennial myosin census. *Molecular Biology of the Cell* **12**, 780-794 (2001).
- 13 Rodriguez, O. C. & Cheney, R. E. Human myosin-Vc is a novel class V myosin expressed in epithelial cells. *J Cell Sci* **115**, 991-1004 (2002).
- 14 Pastural, E. *et al.* Two genes are responsible for Griscelli syndrome at the same 15q21 locus. *Genomics* **63**, 299-306 (2000).
- 15 Menasche, G. *et al.* Griscelli syndrome restricted to hypopigmentation results from a melanophilin defect (GS3) or a MYO5A F-exon deletion (GS1). *J Clin Invest* **112**, 450-456 (2003).
- 16 Desnos, C. *et al.* Rab27A and its effector MyRIP link secretory granules to F-actin and control their motion towards release sites. *J Cell Biol* **163**, 559-570 (2003).
- 17 Seabra, M. C. & Coudrier, E. Rab GTPases and myosin motors in organelle motility. *Traffic* **5**, 393-399 (2004).
- 18 Wagner, W., Brenowitz, S. & Hammer, J. Myosin-Va transports the endoplasmic reticulum into the dendritic spines of Purkinje neurons. *Nature Cell Biology* **13**, 40-U101, doi:10.1038/ncb2132|10.1038/ncb2132 (2011).
- 19 Roland, J. T., Kenworthy, A. K., Peranen, J., Caplan, S. & Goldenring, J. R. Myosin Vb interacts with Rab8a on a tubular network containing EHD1 and EHD3. *Mol Biol Cell* **18**, 2828-2837 (2007).
- 20 Swiatecka-Urban, A. *et al.* Myosin Vb is required for trafficking of the cystic fibrosis transmembrane conductance regulator in Rab11a-specific apical

- recycling endosomes in polarized human airway epithelial cells. *J Biol Chem* **282**, 23725-23736 (2007).
- 21 Cheney, R. E. *et al.* Brain myosin-V is a two-headed unconventional myosin with motor activity. *Cell* **75**, 13-23 (1993).
- 22 Cope, M. J., Whisstock, J., Rayment, I. & Kendrick-Jones, J. Conservation within the myosin motor domain: implications for structure and function. *Structure* **4**, 969-987 (1996).
- 23 Goodson, H. V., Warrick, H. M. & Spudich, J. A. Specialized conservation of surface loops of myosin: evidence that loops are involved in determining functional characteristics. *J Mol Biol* **287**, 173-185 (1999).
- 24 Volkmann, N. *et al.* The structural basis of myosin V processive movement as revealed by electron cryomicroscopy. *Mol Cell* **19**, 595-605 (2005).
- 25 Walker, M. L. *et al.* Two-headed binding of a processive myosin to F-actin. *Nature* **405**, 804-807 (2000).
- 26 Mercer, J. A., Seperack, P. K., Strobel, M. C., Copeland, N. G. & Jenkins, N. A. Novel myosin heavy chain encoded by murine dilute coat colour locus. *Nature* **349**, 709-713 (1991).
- 27 Ikebe, M. Regulation of the function of mammalian myosin and its conformational change. *Biochem Biophys Res Commun* **369**, 157-164 (2008).
- 28 Sakamoto, T., Yildez, A., Selvin, P. R. & Sellers, J. R. Step-size is determined by neck length in myosin V. *Biochemistry* **44**, 16203-16210 (2005).
- 29 Hodi, Z. *et al.* Alternatively spliced exon B of myosin Va is essential for binding the tail-associated light chain shared by dynein. *Biochemistry* **45**, 12582-12595, doi:10.1021/bi060991e|10.1021/bi060991e (2006).
- 30 Wu, X., Kocher, B., Wei, Q. & Hammer, J. A., 3rd. Myosin Va associates with microtubule-rich domains in both interphase and dividing cells. *Cell Motil Cytoskeleton* **40**, 286-303 (1998).
- 31 Tsakraklides, V. *et al.* Subcellular localization of GFP-myosin-V in live mouse melanocytes. *J Cell Sci* **112 (Pt 17)**, 2853-2865 (1999).
- 32 De La Cruz, E. M., Wells, A. L., Rosenfeld, S. S., Ostap, E. M. & Sweeney, H. L. The kinetic mechanism of myosin V. *Proc Natl Acad Sci U S A* **96**, 13726-13731 (1999).
- 33 Sellers, J. & Veigel, C. Direct observation of the myosin-Va power stroke and its reversal. *Nature Structural & Molecular Biology* **17**, 590-U588, doi:10.1038/nsmb.1820 (2010).
- 34 Trybus, K. M. Myosin V from head to tail. *Cell Mol Life Sci* **65**, 1378-1389 (2008).
- 35 Yengo, C. M. & Sweeney, H. L. Functional role of loop 2 in myosin V. *Biochemistry* **43**, 2605-2612 (2004).
- 36 Goldstein, L. S. B. & Philp, A. V. The road less traveled: Emerging principles of kinesin motor utilization. *Annual Review of Cell and Developmental Biology* **15**, 141-183, doi:10.1146/annurev.cellbio.15.1.141 (1999).
- 37 Mehta, A. Myosin learns to walk. *Journal of Cell Science* **114**, 1981-1998 (2001).
- 38 Mehta, A. D. *et al.* Myosin-V is a processive actin-based motor. *Nature* **400**, 590-593 (1999).
- 39 Sakamoto, T., Amitani, I., Yokota, E. & Ando, T. Direct observation of processive movement by individual myosin V molecules. *Biochem Biophys Res Commun* **272**, 586-590 (2000).

- 40 Vale, R. D. Myosin V motor proteins: marching stepwise towards a
mechanism. *J Cell Biol* **163**, 445-450 (2003).
- 41 Hachikubo, Y., Ito, K. & Yamamoto, K. Roles of the hydrophobic triplet in the
motor domain of myosin in the interaction between myosin and actin. *J*
Biochem **134**, 165-171 (2003).
- 42 Veigel, C., Wang, F., Bartoo, M. L., Sellers, J. R. & Molloy, J. E. The gated
gait of the processive molecular motor, myosin V. *Nat Cell Biol* **4**, 59-65
(2002).
- 43 Kremmentsova, E. B., Hodges, A. R., Lu, H. & Trybus, K. M. Processivity of
chimeric class V myosins. *J Biol Chem* **281**, 6079-6086 (2006).
- 44 Hodges, A. R., Kremmentsova, E. B. & Trybus, K. M. Engineering the
processive run length of Myosin V. *J Biol Chem* **282**, 27192-27197 (2007).
- 45 Yildiz, A. *et al.* Myosin V walks hand-over-hand: single fluorophore imaging
with 1.5-nm localization. *Science* **300**, 2061-2065 (2003).
- 46 Yildiz, A. *et al.* Myosin VI steps via a hand-over-hand mechanism with its lever
arm undergoing fluctuations when attached to actin. *Journal of Biological*
Chemistry **279**, 37223-37226, doi:10.1074/jbc.C400252200 (2004).
- 47 Nelson, S. R., Ali, M. Y., Trybus, K. M. & Warshaw, D. M. Random Walk of
Processive, Quantum Dot-Labeled Myosin Va Molecules within the Actin
Cortex of COS-7 Cells. *Biophysical Journal* **97**, 509-518,
doi:10.1016/j.bpj.2009.04.052 (2009).
- 48 Pierobon, P. *et al.* Velocity, Processivity, and Individual Steps of Single
Myosin V Molecules in Live Cells. *Biophysical Journal* **96**, 4268-4275,
doi:10.1016/j.bpj.2009.02.045 (2009).
- 49 Gordon, A. M., Homsher, E. & Regnier, M. Regulation of contraction in striated
muscle. *Physiol. Rev.* **80**, 853-924 (2000).
- 50 Wang, F. *et al.* Regulated conformation of myosin V. *Journal of Biological*
Chemistry **279**, 2333-2336, doi:10.1074/jbc.C300488200 (2004).
- 51 Li, X. D., Mabuchi, K., Ikebe, R. & Ikebe, M. Ca²⁺-induced activation of
ATPase activity of myosin Va is accompanied with a large conformational
change. *Biochemical and Biophysical Research Communications* **315**, 538-
545, doi:10.1016/j.bbrc.2004.01.084 (2004).
- 52 Kremmentsov, D. N., Kremmentsova, E. B. & Trybus, K. M. Myosin V: regulation
by calcium, calmodulin, and the tail domain. *J Cell Biol* **164**, 877-886 (2004).
- 53 Sato, O., Li, X.-d. & Ikebe, M. Myosin Va becomes a low duty ratio motor in
the inhibited form. *Journal of Biological Chemistry* **282**, 13228-13239,
doi:10.1074/jbc.M610766200 (2007).
- 54 Wang, F. *et al.* Effect of ADP and ionic strength on the kinetic and motile
properties of recombinant mouse myosin V. *Journal of Biological Chemistry*
275, 4329-4335, doi:10.1074/jbc.275.6.4329 (2000).
- 55 Liu, J., Taylor, D. W., Kremmentsova, E. B., Trybus, K. M. & Taylor, K. A. Three-
dimensional structure of the myosin V inhibited state by cryoelectron
tomography. *Nature* **442**, 208-211 (2006).
- 56 Thirumurugan, K., Sakamoto, T., Hammer, J. A., 3rd, Sellers, J. R. & Knight,
P. J. The cargo-binding domain regulates structure and activity of myosin 5.
Nature **442**, 212-215 (2006).
- 57 Wu, X. S. *et al.* Identification of an organelle receptor for myosin-Va. *Nat Cell*
Biol **4**, 271-278 (2002).

- 58 Strom, M., Hume, A. N., Tarafder, A. K., Barkagianni, E. & Seabra, M. C. A
family of Rab27-binding proteins. Melanophilin links Rab27a and myosin Va
59 function in melanosome transport. *J Biol Chem* **277**, 25423-25430 (2002).
Fukuda, M., Kuroda, T. S. & Mikoshiba, K. Slac2-a/melanophilin, the missing
link between Rab27 and myosin Va: implications of a tripartite protein complex
60 for melanosome transport. *J Biol Chem* **277**, 12432-12436 (2002).
Kron, S. J. & Spudich, J. A. FLUORESCENT ACTIN-FILAMENTS MOVE ON
MYOSIN FIXED TO A GLASS-SURFACE. *Proceedings of the National
Academy of Sciences of the United States of America* **83**, 6272-6276,
doi:10.1073/pnas.83.17.6272 (1986).
61 Axelrod, D. Total internal reflection fluorescence microscopy. *Methods Cell
Biol* **30**, 245-270 (1989).
62 Lavker, R. M. & Kaidbey, K. H. Redistribution of melanosomal complexes
within keratinocytes following UV-A irradiation: a possible mechanism for
cutaneous darkening in man. *Arch Dermatol Res* **272**, 215-228 (1982).
63 Gross, S. P. *et al.* Interactions and regulation of molecular motors in *Xenopus*
melanophores. *J Cell Biol* **156**, 855-865 (2002).
64 Aspengren, S., Hedberg, D. & Wallin, M. Melanophores: a model system for
neuronal transport and exocytosis? *J Neurosci Res* **85**, 2591-2600 (2007).
65 Rogers, S. L., Tint, I. S., Fanapour, P. C. & Gelfand, V. I. Regulated
bidirectional motility of melanophore pigment granules along microtubules in
vitro. *Proc Natl Acad Sci U S A* **94**, 3720-3725 (1997).
66 Daniolos, A., Lerner, A. B. & Lerner, M. R. Action of light on frog pigment cells
in culture. *Pigment Cell Res* **3**, 38-43 (1990).
67 Nascimento, A. A., Roland, J. T. & Gelfand, V. I. Pigment cells: a model for the
study of organelle transport. *Annual review of cell and developmental biology*
19, 469-491, doi:10.1146/annurev.cellbio.19.111401.092937 (2003).
68 Tuma, M. C. & Gelfand, V. I. Molecular mechanisms of pigment transport in
melanophores. *Pigment Cell Res* **12**, 283-294 (1999).
69 Aspengren, S., Hedberg, D., Skold, H. N. & Wallin, M. New insights into
melanosome transport in vertebrate pigment cells. *International review of cell
and molecular biology* **272**, 245-302, doi:10.1016/S1937-6448(08)01606-7
(2009).
70 Raposo, G. & Marks, M. S. Melanosomes--dark organelles enlighten
endosomal membrane transport. *Nat Rev Mol Cell Biol* **8**, 786-797 (2007).
71 Levi, V., Serpinskaya, A. S., Gratton, E. & Gelfand, V. Organelle transport
along microtubules in *Xenopus* melanophores: evidence for cooperation
between multiple motors. *Biophys J* **90**, 318-327 (2006).
72 Wasmeier, C., Hume, A. N., Bolasco, G. & Seabra, M. C. Melanosomes at a
glance. *J Cell Sci* **121**, 3995-3999 (2008).
73 Rogers, S. L. & Gelfand, V. I. Myosin cooperates with microtubule motors
during organelle transport in melanophores. *Curr Biol* **8**, 161-164 (1998).
74 Rogers, S. L., Tint, I. S. & Gelfand, V. I. In vitro motility assay for melanophore
pigment organelles. *Methods Enzymol* **298**, 361-372 (1998).
75 Rodionov, V. I., Hope, A. J., Svitkina, T. M. & Borisy, G. G. Functional
coordination of microtubule-based and actin-based motility in melanophores.
Current biology : CB **8**, 165-168 (1998).
76 Wu, X., Bowers, B., Wei, Q., Kocher, B. & Hammer, J. A., 3rd. Myosin V
associates with melanosomes in mouse melanocytes: evidence that myosin V
is an organelle motor. *Journal of cell science* **110 (Pt 7)**, 847-859 (1997).

- 77 Langford, G. M. Actin- and microtubule-dependent organelle motors: interrelationships between the two motility systems. *Current opinion in cell biology* **7**, 82-88 (1995).
- 78 Gross, S. P. Hither and yon: a review of bi-directional microtubule-based transport. *Physical biology* **1**, R1-11, doi:10.1088/1478-3967/1/2/R01 (2004).
- 79 Welte, M. A. Bidirectional transport along microtubules. *Current biology : CB* **14**, R525-537, doi:10.1016/j.cub.2004.06.045 (2004).
- 80 Huang, J. D. *et al.* Direct interaction of microtubule- and actin-based transport motors. *Nature* **397**, 267-270, doi:10.1038/16722 (1999).
- 81 Rozdzial, M. M. & Haimo, L. T. Reactivated melanophore motility: differential regulation and nucleotide requirements of bidirectional pigment granule transport. *J Cell Biol* **103**, 2755-2764 (1986).
- 82 Sammak, P. J., Adams, S. R., Harootunian, A. T., Schliwa, M. & Tsien, R. Y. Intracellular cyclic AMP not calcium, determines the direction of vesicle movement in melanophores: direct measurement by fluorescence ratio imaging. *J Cell Biol* **117**, 57-72 (1992).
- 83 Aspengren, S., Skold, H. N., Quiroga, G., Martensson, L. & Wallin, M. Noradrenaline- and melatonin-mediated regulation of pigment aggregation in fish melanophores. *Pigment Cell Res* **16**, 59-64 (2003).
- 84 de Graan, P. N. & Eberle, A. N. Irreversible stimulation of *Xenopus* melanophores by photoaffinity labelling with p-azidophenylalanine-13- α -melanotropin. *FEBS Lett* **116**, 111-115 (1980).
- 85 Abe, K. *et al.* Role of cyclic AMP in mediating the effects of MSH, norepinephrine, and melatonin on frog skin color. *Endocrinology* **85**, 674-682 (1969).
- 86 Sugden, D. & Rowe, S. J. Protein kinase C activation antagonizes melatonin-induced pigment aggregation in *Xenopus laevis* melanophores. *J Cell Biol* **119**, 1515-1521 (1992).
- 87 Reese, E. L. & Haimo, L. T. Dynein, dynactin, and kinesin II's interaction with microtubules is regulated during bidirectional organelle transport. *J Cell Biol* **151**, 155-166 (2000).
- 88 Levi, V., Gelfand, V. I., Serpinskaya, A. S. & Gratton, E. Melanosomes transported by myosin-V in *Xenopus* melanophores perform slow 35 nm steps. *Biophys J* **90**, L07-09 (2006).
- 89 Nilsson, H. M., Svensson, S. P. & Sundqvist, T. L-NAME-induced dispersion of melanosomes in melanophores activates PKC, MEK and ERK1. *Pigment Cell Res* **14**, 450-455 (2001).
- 90 Deacon, S. W. *et al.* Dynactin is required for bidirectional organelle transport. *J Cell Biol* **160**, 297-301 (2003).
- 91 Nagashima, K. *et al.* Melanophilin directly links Rab27a and myosin Va through its distinct coiled-coil regions. *FEBS Lett* **517**, 233-238 (2002).
- 92 Wu, X., Wang, F., Rao, K., Sellers, J. R. & Hammer, J. A., 3rd. Rab27a is an essential component of melanosome receptor for myosin Va. *Mol Biol Cell* **13**, 1735-1749 (2002).
- 93 Kashina, A. S. *et al.* Protein kinase A, which regulates intracellular transport, forms complexes with molecular motors on organelles. *Curr Biol* **14**, 1877-1881 (2004).
- 94 Kashina, A. & Rodionov, V. Intracellular organelle transport: few motors, many signals. *Trends Cell Biol* **15**, 396-398 (2005).

- 95 Sheets, L., Ransom, D. G., Mellgren, E. M., Johnson, S. L. & Schnapp, B. J. Zebrafish melanophilin facilitates melanosome dispersion by regulating dynein. *Curr Biol* **17**, 1721-1734 (2007).
- 96 Nagano, F., Sasaki, T. & Takai, Y. Purification and properties of Rab3 GTPase-activating protein. *Methods Enzymol* **329**, 67-75 (2001).
- 97 Zerial, M. & McBride, H. Rab proteins as membrane organizers. *Nat Rev Mol Cell Biol* **2**, 107-117 (2001).
- 98 Evans, L. L., Hammer, J. & Bridgman, P. C. Subcellular localization of myosin V in nerve growth cones and outgrowth from dilute-lethal neurons. *J Cell Sci* **110 (Pt 4)**, 439-449 (1997).
- 99 Espreafico, E. M. *et al.* Localization of myosin-V in the centrosome. *Proc Natl Acad Sci U S A* **95**, 8636-8641 (1998).
- 100 Aspengren, S., Hedberg, D. & Wallin, M. Studies of pigment transfer between *Xenopus laevis* melanophores and fibroblasts in vitro and in vivo. *Pigment Cell Res* **19**, 136-145 (2006).
- 101 Aspengren, S., Wielbass, L. & Wallin, M. Effects of acrylamide, latrunculin, and nocodazole on intracellular transport and cytoskeletal organization in melanophores. *Cell Motil Cytoskeleton* **63**, 423-436 (2006).
- 102 Rodionov, V. I., Lim, S. S., Gelfand, V. I. & Borisy, G. G. Microtubule dynamics in fish melanophores. *J Cell Biol* **126**, 1455-1464 (1994).
- 103 Rogers, S. L. *et al.* Regulation of melanosome movement in the cell cycle by reversible association with myosin V. *J Cell Biol* **146**, 1265-1276 (1999).
- 104 Tuma, M. C., Zill, A., Le Bot, N., Vernos, I. & Gelfand, V. Heterotrimeric kinesin II is the microtubule motor protein responsible for pigment dispersion in *Xenopus* melanophores. *J Cell Biol* **143**, 1547-1558 (1998).
- 105 Langford, G. M. Myosin-V, a versatile motor for short-range vesicle transport. *Traffic* **3**, 859-865 (2002).
- 106 Wu, X. F., Bowers, B., Rao, K., Wei, Q. & Hammer, J. A. Visualization of melanosome dynamics within wild-type and dilute melanocytes suggests a paradigm for myosin V function in vivo. *Journal of Cell Biology* **143**, 1899-1918 (1998).
- 107 Ali, M. Y. *et al.* Myosin Va maneuvers through actin intersections and diffuses along microtubules. *Proc Natl Acad Sci U S A* **104**, 4332-4336 (2007).
- 108 Culver-Hanlon, T. L., Lex, S. A., Stephens, A. D., Quinyne, N. J. & King, S. J. A microtubule-binding domain in dynactin increases dynein processivity by skating along microtubules. *Nat Cell Biol* **8**, 264-270 (2006).
- 109 Matsumoto, K. *et al.* Assessment of atrial regional wall motion using strain Doppler imaging during biatrial pacing in the bradycardia-tachycardia syndrome. *Pacing Clin Electrophysiol* **29**, 220-225 (2006).
- 110 Ali, M. Y., Lu, H., Bookwalter, C. S., Warshaw, D. M. & Trybus, K. M. Myosin V and Kinesin act as tethers to enhance each others' processivity. *Proc Natl Acad Sci U S A* **105**, 4691-4696 (2008).
- 111 Joel, P. B., Sweeney, H. L. & Trybus, K. M. Addition of lysines to the 50/20 kDa junction of myosin strengthens weak binding to actin without affecting the maximum ATPase activity. *Biochemistry* **42**, 9160-9166 (2003).
- 112 Lorenz, M. & Holmes, K. C. The actin-myosin interface. *Proceedings of the National Academy of Sciences of the United States of America* **107**, 12529-12534, doi:10.1073/pnas.1003604107 (2010).

- 113 Lakamper, S. & Meyhofer, E. The E-hook of tubulin interacts with kinesin's
head to increase processivity and speed. *Biophysical Journal* **89**, 3223-3234,
doi:10.1529/biophysj.104.057505 (2005).
- 114 Thorn, K. S., Ubersax, J. A. & Vale, R. D. Engineering the processive run
length of the kinesin motor. *Journal of Cell Biology* **151**, 1093-1100 (2000).
- 115 Okada, Y. & Hirokawa, N. A processive single-headed motor: Kinesin
superfamily protein KIF1A. *Science* **283**, 1152-1157 (1999).
- 116 Helenius, J., Brouhard, G., Kalaidzidis, Y., Diez, S. & Howard, J. The
depolymerizing kinesin MCAK uses lattice diffusion to rapidly target
microtubule ends. *Nature* **441**, 115-119, doi:10.1038/nature04736 (2006).
- 117 Woehlke, G. *et al.* Microtubule interaction site of the kinesin motor. *Cell* **90**,
207-216 (1997).
- 118 Alonso, M. C., van Damme, J., Vandekerckhove, J. & Cross, R. A. Proteolytic
mapping of kinesin/ncd-microtubule interface: nucleotide-dependent
conformational changes in the loops L8 and L12. *Embo Journal* **17**, 945-951
(1998).
- 119 Okada, Y. & Hirokawa, N. Mechanism of the single-headed processivity:
Diffusional anchoring between the K-loop of kinesin and the C terminus of
tubulin. *Proceedings of the National Academy of Sciences of the United States
of America* **97**, 640-645 (2000).
- 120 Audebert, S. *et al.* DEVELOPMENTAL REGULATION OF
POLYGLUTAMYLATED ALPHA-TUBULIN AND BETA-TUBULIN IN MOUSE-
BRAIN NEURONS. *Journal of Cell Science* **107**, 2313-2322 (1994).
- 121 Karcher, R. L. *et al.* Cell cycle regulation of myosin-V by calcium/calmodulin-
dependent protein kinase II. *Science* **293**, 1317-1320 (2001).
- 122 Rosenberg, O. S., Deindl, S., Sung, R. J., Nairn, A. C. & Kuriyan, J. Structure
of the autoinhibited kinase domain of CaMKII and SAXS analysis of the
holoenzyme. *Cell* **123**, 849-860, doi:10.1016/j.cell.2005.10.029 (2005).
- 123 Chao, L. H. *et al.* Intersubunit capture of regulatory segments is a component
of cooperative CaMKII activation. *Nature Structural & Molecular Biology* **17**,
264-U223, doi:10.1038/nsmb.1751 (2010).
- 124 Chao, L. H. *et al.* A Mechanism for Tunable Autoinhibition in the Structure of a
Human Ca²⁺/Calmodulin-Dependent Kinase II Holoenzyme (vol 146, pg 327,
2011). *Cell* **147**, 704-704, doi:10.1016/j.cell.2011.10.013 (2011).
- 125 Basrur, V. *et al.* Proteomic analysis of early melanosomes: Identification of
novel melanosomal proteins. *Journal of Proteome Research* **2**, 69-79,
doi:10.1021/pr025562r (2003).
- 126 Chi, A. *et al.* Proteomic and bioinformatic characterization of the biogenesis
and function of melanosomes. *Journal of Proteome Research* **5**, 3135-3144,
doi:10.1021/pr060363j (2006).
- 127 Rickwood, D., Wilson, M. T. & Darley-Usmar, V. M. (IRL Press Oxford,
Oxford, UK, 1987).
- 128 Enriquez, J. A., Perez-Martos, A., Lopez-Perez, M. J. & Montoya, J. In
organello RNA synthesis system from mammalian liver and brain. *Methods in
enzymology* **264**, 50-57, doi:10.1016/s0076-6879(96)64008-7 (1996).
- 129 Fernandez-Vizarra, E., Lopez-Perez, M. J. & Enriquez, J. A. Isolation of
biogenetically competent mitochondria from mammalian tissues and cultured
cells. *Methods* **26**, 292-297, doi:Pii s1046-2023(02)00034-8
10.1016/s1046-2023(02)00034-8 (2002).

- 130 Frezza, C., Cipolat, S. & Scorrano, L. Organelle isolation: functional mitochondria from mouse liver, muscle and cultured fibroblasts. *Nature Protocols* **2**, 287-295, doi:10.1038/nprot.2006.478 (2007).
- 131 Schliwa, M. & Euteneuer, U. MICROTUBULE-INDEPENDENT COMPONENT MAY BE INVOLVED IN GRANULE TRANSPORT IN PIGMENT-CELLS. *Nature* **273**, 556-558, doi:10.1038/273556a0 (1978).
- 132 Schliwa, M., Weber, K. & Porter, K. R. LOCALIZATION AND ORGANIZATION OF ACTIN IN MELANOPHORES. *Journal of Cell Biology* **89**, 267-275, doi:10.1083/jcb.89.2.267 (1981).
- 133 Vaughn, J. L. & Fan, F. Differential requirements of two insect cell lines for growth in serum-free medium. *In Vitro Cellular & Developmental Biology-Animal* **33**, 479-482 (1997).
- 134 Smith, G. E. *et al.* MODIFICATION AND SECRETION OF HUMAN INTERLEUKIN-2 PRODUCED IN INSECT CELLS BY A BACULOVIRUS EXPRESSION VECTOR. *Proceedings of the National Academy of Sciences of the United States of America* **82**, 8404-8408, doi:10.1073/pnas.82.24.8404 (1985).
- 135 Vaughn, J. L., Goodwin, R. H., Tompkins, G. J. & McCawley, P. ESTABLISHMENT OF 2 CELL LINES FROM INSECT SPODOPTERA-FRUGIPERDA (LEPIDOPTERA-NOCTUIDAE). *In Vitro-Journal of the Tissue Culture Association* **13**, 213-217 (1977).
- 136 Philips, J. & Eberwine, J. H. Vol. 10 283-288 (Methods: A Companion to Methods in Enzymology, 1996).
- 137 Mullis, K. *et al.* SPECIFIC ENZYMATIC AMPLIFICATION OF DNA INVITRO - THE POLYMERASE CHAIN-REACTION. *Cold Spring Harbor Symposia on Quantitative Biology* **51**, 263-273 (1986).
- 138 Purcell, T., Sweeney, H. & Spudich, J. A force-dependent state controls the coordination of processive myosin V. *Proceedings of the National Academy of Sciences of the United States of America* **102**, 13873-13878, doi:10.1073/pnas.0506441102|10.1073/pnas.0506441102 (2005).
- 139 Engler, M. J. & Richardson, C. C. in *The Enzymes* Vol. 15B (ed P.D. (ed.) Boyer) 1-29 (Academic Press, New York, 1982).
- 140 Downard, K. Francis William Aston: the man behind the mass spectrograph. *European Journal of Mass Spectrometry* **13**, 177-190, doi:10.1255/ejms.878|10.1255/ejms.878 (2007).
- 141 BOYD, R. LINKED-SCAN TECHNIQUES FOR MS/MS USING TANDEM-IN-SPACE INSTRUMENTS. *Mass Spectrometry Reviews* **13**, 359-410, doi:10.1002/mas.1280130502 (1994).
- 142 HATEFI, Y. & HANSTEIN, W. SOLUBILIZATION OF PARTICULATE PROTEINS AND NONELECTROLYTES BY CHAOTROPIC AGENTS. *Proceedings of the National Academy of Sciences of the United States of America* **62**, 1129-&, doi:10.1073/pnas.62.4.1129 (1969).
- 143 COOPER, J. EFFECTS OF CYTOCHALASIN AND PHALLOIDIN ON ACTIN. *Journal of Cell Biology* **105**, 1473-1478, doi:10.1083/jcb.105.4.1473 (1987).
- 144 Xiao, H. *et al.* Insights into the mechanism of microtubule stabilization by Taxol. *Proceedings of the National Academy of Sciences of the United States of America* **103**, 10166-10173, doi:10.1073/pnas.0603704103|10.1073/pnas.0603704103 (2006).

- 145 Okada, Y. & Hirokawa, N. Mechanism of the single-headed processivity:
Diffusional anchoring between "K-loop" of kinesin and the C-terminal of
tubulin. *Molecular Biology of the Cell* **10**, 1366 (1999).
- 146 Hirokawa, N., Nitta, R. & Okada, Y. The mechanisms of kinesin motor motility:
lessons from the monomeric motor KIF1A. *Nature Reviews Molecular Cell
Biology* **10**, 877-884, doi:10.1038/nrm2807 (2009).
- 147 Cooper, J. R. & Wordeman, L. The diffusive interaction of microtubule binding
proteins. *Curr. Opin. Cell Biol.* **21**, 68-73, doi:10.1016/j.ceb.2009.01.005
(2009).
- 148 Lakamper, S. & Meyhofer, E. Back on track - On the role of the microtubule for
kinesin motility and cellular function. *Journal of Muscle Research and Cell
Motility* **27**, 161-171, doi:10.1007/s10974-005-9052-3|10.1007/s10974-005-
9052-3 (2006).
- 149 LUCKOW, V. & SUMMERS, M. TRENDS IN THE DEVELOPMENT OF
BACULOVIRUS EXPRESSION VECTORS. *Bio-Technology* **6**, 47-55,
doi:10.1038/nbt0188-47 (1988).
- 150 MILLER, L. BACULOVIRUSES AS GENE-EXPRESSION VECTORS. *Annual
Review of Microbiology* **42**, 177-199, doi:10.1146/annurev.micro.42.1.177
(1988).
- 151 Carbonell, L. F., Klowden, M. J. & Miller, L. K. Baculovirus-mediated
expression of bacterial genes in dipteran and mammalian cells. *J Virol* **56**,
153-160 (1985).
- 152 LUCKOW, V., LEE, S., BARRY, G. & OLINS, P. EFFICIENT GENERATION
OF INFECTIOUS RECOMBINANT BACULOVIRUSES BY SITE-SPECIFIC
TRANSPOSON-MEDIATED INSERTION OF FOREIGN GENES INTO A
BACULOVIRUS GENOME PROPAGATED IN ESCHERICHIA-COLI. *Journal
of Virology* **67**, 4566-4579 (1993).
- 153 WESTWOOD, J., JONES, I. & BISHOP, D. ANALYSES OF ALTERNATIVE
POLY(A) SIGNALS FOR USE IN BACULOVIRUS EXPRESSION VECTORS.
Virology **195**, 90-99, doi:10.1006/viro.1993.1349 (1993).
- 154 Meeusen, R. L. & Cande, W. Z. N-ethylmaleimide-modified heavy
meromyosin. A probe for actomyosin interactions. *J Cell Biol* **82**, 57-65 (1979).
- 155 Huang, T. G. & Hackney, D. D. Drosophila kinesin minimal motor domain
expressed in Escherichia coli. Purification and kinetic characterization. *J Biol
Chem* **269**, 16493-16501 (1994).
- 156 Adio, S. *et al.* Kinetic and mechanistic basis of the nonprocessive Kinesin-3
motor Nckin3. *J Biol Chem* **281**, 37782-37793, doi:M605061200 [pii]
10.1074/jbc.M605061200 (2006).
- 157 Nishikawa, M., Takagi, H., Shibata, T., Iwane, A. H. & Yanagida, T.
Fluctuation analysis of mechanochemical coupling depending on the type of
biomolecular motors. *Phys Rev Lett* **101**, 128103 (2008).
- 158 Churchman, L. S., Okten, Z., Rock, R. S., Dawson, J. F. & Spudich, J. A.
Single molecule high-resolution colocalization of Cy3 and Cy5 attached to
macromolecules measures intramolecular distances through time. *Proc Natl
Acad Sci U S A* **102**, 1419-1423 (2005).
- 159 Kudryashov, D. S., Phillips, M. & Reisler, E. Formation and destabilization of
actin filaments with tetramethylrhodamine-modified actin. *Biophysical Journal*
87, 1136-1145, doi:10.1529/biophysj.104.042242 (2004).

- 160 Tuszyński, J. A. *et al.* Molecular dynamics simulations of tubulin structure and
calculations of electrostatic properties of microtubules. *Mathematical and
Computer Modelling* **41**, 1055-1070, doi:10.1016/j.mcm.2005.05.002 (2005).
- 161 Minoura, I., Katayama, E., Sekimoto, K. & Muto, E. One-Dimensional
Brownian Motion of Charged Nanoparticles along Microtubules: A Model
System for Weak Binding Interactions. *Biophysical Journal* **98**, 1589-1597,
doi:10.1016/j.bpj.2009.12.4323 (2010).
- 162 Lu, H. L., Ali, M. Y., Bookwalter, C. S., Warshaw, D. M. & Trybus, K. M.
Diffusive Movement of Processive Kinesin-1 on Microtubules. *Traffic* **10**, 1429-
1438, doi:10.1111/j.1600-0854.2009.00964.x (2009).
- 163 Graneli, A., Yeykal, C. C., Robertson, R. B. & Greene, E. C. Long-distance
lateral diffusion of human Rad51 on double-stranded DNA. *Proceedings of the
National Academy of Sciences of the United States of America* **103**, 1221-
1226, doi:10.1073/pnas.0508366103 (2006).
- 164 Blainey, P. C., van Oijent, A. M., Banerjee, A., Verdine, G. L. & Xie, X. S. A
base-excision DNA-repair protein finds intrahelical lesion bases by fast sliding
in contact with DNA. *Proceedings of the National Academy of Sciences of the
United States of America* **103**, 5752-5757, doi:10.1073/pnas.0509723103
(2006).
- 165 Baker, N. A., Sept, D., Joseph, S., Holst, M. J. & McCammon, J. A.
Electrostatics of nanosystems: Application to microtubules and the ribosome.
*Proceedings of the National Academy of Sciences of the United States of
America* **98**, 10037-10041 (2001).
- 166 Trybus, K. M. *et al.* Effect of calcium on calmodulin bound to the IQ motifs of
myosin V. *J Biol Chem* **282**, 23316-23325 (2007).
- 167 Vale, R. D. & Milligan, R. A. The way things move: Looking under the hood of
molecular motor proteins. *Science* **288**, 88-95 (2000).
- 168 Erondü, N. E. & Kennedy, M. B. REGIONAL DISTRIBUTION OF TYPE-II CA-
2+ CALMODULIN-DEPENDENT PROTEIN-KINASE IN RAT-BRAIN. *Journal
of Neuroscience* **5**, 3270-3277 (1985).
- 169 Yamauchi, T. Neuronal Ca²⁺/calmodulin-dependent protein kinase II -
Discovery, progress in a quarter of a century, and perspective: Implication for
learning and memory. *Biological & Pharmaceutical Bulletin* **28**, 1342-1354
(2005).
- 170 Kameshita, I., Ishida, A., Okuno, S. & Fujisawa, H. Detection of protein
phosphatase activities in sodium dodecyl sulfate-polyacrylamide gel using
peptide substrates. *Analytical Biochemistry* **245**, 149-153,
doi:10.1006/abio.1996.9945 (1997).
- 171 Kolodziej, S., Hudmon, A., Waxham, M. & Stoops, J. Three-dimensional
reconstructions of calcium/calmodulin dependent (CaM) kinase II alpha and
truncated CaM kinase II alpha reveal a unique organization for its structural
core and functional domains. *Journal of Biological Chemistry* **275**, 14354-
14359, doi:10.1074/jbc.275.19.14354 (2000).
- 172 Barber, R., Harmer, D., Coleman, R. & Clark, B. GAPDH as a housekeeping
gene: analysis of GAPDH mRNA expression in a panel of 72 human tissues.
Physiological Genomics **21**, 389-395,
doi:10.1152/physiolgenomics.00025.2005|10.1152/physiolgenomics.00025.20
05 (2005).

- 173 Molyneaux, B. J., Mulcahey, M. K., Stafford, P. & Langford, G. M. Sequence
and phylogenetic analysis of squid myosin-V: A vesicle motor in nerve cells.
Cell Motility and the Cytoskeleton **46**, 108-115 (2000).
- 174 RUPPEL, K., UYEDA, T. & SPUDICH, J. ROLE OF HIGHLY CONSERVED
LYSINE-130 OF MYOSIN MOTOR DOMAIN - IN-VIVO AND IN-VITRO
CHARACTERIZATION OF SITE-SPECIFICALLY MUTATED MYOSIN.
Journal of Biological Chemistry **269**, 18773-18780 (1994).
- 175 Richards, T. & Cavalier-Smith, T. Myosin domain evolution and the primary
divergence of eukaryotes. *Nature* **436**, 1113-1118,
doi:10.1038/nature03949|10.1038/nature03949 (2005).
- 176 Hume, A. & Seabra, M. Melanosomes on the move: a model to understand
organelle dynamics. *Biochemical Society Transactions* **39**, 1191-1196,
doi:10.1042/BST0391191 (2011).
- 177 Homma, K., Saito, J., Ikebe, R. & Ikebe, M. Ca²⁺-dependent regulation of the
motor activity of myosin V. *Journal of Biological Chemistry* **275**, 34766-34771,
doi:10.1074/jbc.M003132200 (2000).
- 178 Trybus, K., Kremmentsova, E. & Freyzon, Y. Kinetic characterization of a
monomeric unconventional myosin V construct. *Journal of Biological
Chemistry* **274**, 27448-27456, doi:10.1074/jbc.274.39.27448 (1999).
- 179 Armstrong, J. *et al.* Full-length myosin Va exhibits altered gating during
processive movement on actin. *Proceedings of the National Academy of
Sciences of the United States of America* **109**, E218-E224,
doi:10.1073/pnas.1109709109 (2012).
- 180 Sellers, J. R. (Oxford University Press, New York, 1999).
- 181 Schroder, R. R. *et al.* Three-dimensional atomic model of F-actin decorated
with Dictyostelium myosin S1. *Nature* **364**, 171-174 (1993).
- 182 Kad, N. M., Trybus, K. M. & Warshaw, D. M. Load and Pi control flux through
the branched kinetic cycle of myosin V. *J Biol Chem* **283**, 17477-17484
(2008).
- 183 Joel, P., Trybus, K. & Sweeney, H. Two conserved lysines at the 50/20-kDa
junction of myosin are necessary for triggering actin activation. *Journal of
Biological Chemistry* **276**, 2998-3003, doi:10.1074/jbc.M006930200 (2001).
- 184 Onishi, H., Mikhailenko, S. & Morales, M. Toward understanding actin
activation of myosin ATPase: The role of myosin surface loops. *Proceedings
of the National Academy of Sciences of the United States of America* **103**,
6136-6141, doi:10.1073/pnas.0601595103|10.1073/pnas.0601595103 (2006).
- 185 Wells, A. *et al.* Myosin VI is an actin-based motor that moves backwards.
Nature **401**, 505-508 (1999).
- 186 Rosenfeld, S. S. & Sweeney, H. L. A model of myosin V processivity. *J Biol
Chem* **279**, 40100-40111 (2004).
- 187 Nyitrai, M. & Geeves, M. Adenosine diphosphate and strain sensitivity in
myosin motors. *Philosophical Transactions of the Royal Society of London
Series B-Biological Sciences* **359**, 1867-1877, doi:10.1098/rstb.2004.1560
(2004).
- 188 Veigel, C., Schmitz, S., Wang, F. & Sellers, J. R. Load-dependent kinetics of
myosin-V can explain its high processivity. *Nature Cell Biology* **7**, 861-869,
doi:10.1038/ncb1287 (2005).
- 189 Sweeney, H. L. & Houdusse, A. Structural and Functional Insights into the
Myosin Motor Mechanism. *Annual Review of Biophysics, Vol 39* **39**, 539-557,
doi:10.1146/annurev.biophys.050708.133751 (2010).

- 190 Selzer, T., Albeck, S. & Schreiber, G. Rational design of faster associating and
 tighter binding protein complexes. *Nature Structural Biology* **7**, 537-541
 (2000).
- 191 Zimmermann, D., Abdel Motal, B., Voith von Voithenberg, L., Schliwa, M. &
 Okten, Z. Diffusion of Myosin v on microtubules: a fine-tuned interaction for
 which e-hooks are dispensable. *PloS one* **6**, e25473 (2011).
- 192 Holmes, K., Schroder, R., Sweeney, H. & Houdusse, A. The structure of the
 rigor complex and its implications for the power stroke. *Philosophical
 Transactions of the Royal Society of London Series B-Biological Sciences*
359, 1819-1828, doi:10.1098/rstb.2004.1566 (2004).
- 193 Oda, T., Iwasa, M., Aihara, T., Maeda, Y. & Narita, A. The nature of the
 globular-to fibrous-actin transition. *Nature* **457**, 441-445,
 doi:10.1038/nature07685 (2009).
- 194 Milligan, R. A. Protein-protein interactions in the rigor actomyosin complex.
*Proceedings of the National Academy of Sciences of the United States of
 America* **93**, 21-26 (1996).
- 195 Bonafe, N. & Chaussepied, P. A SINGLE MYOSIN HEAD CAN BE CROSS-
 LINKED TO THE N-TERMINI OF 2 ADJACENT ACTIN MONOMERS.
Biophys. J. **68**, S35-S43 (1995).
- 196 Sutoh, K. IDENTIFICATION OF MYOSIN-BINDING SITES ON THE ACTIN
 SEQUENCE. *Biochemistry* **21**, 3654-3661, doi:10.1021/bi00258a020 (1982).
- 197 Rayment, I. *et al.* STRUCTURE OF THE ACTIN-MYOSIN COMPLEX AND
 ITS IMPLICATIONS FOR MUSCLE-CONTRACTION. *Science* **261**, 58-65,
 doi:10.1126/science.8316858 (1993).
- 198 Volkmann, N. *et al.* Evidence for cleft closure in actomyosin upon ADP
 release. *Nature Structural Biology* **7**, 1147-1155 (2000).
- 199 Ovechkina, Y., Wagenbach, M. & Wordeman, L. K-loop insertion restores
 microtubule depolymerizing activity of a "neckless" MCAK mutant. *Journal of
 Cell Biology* **159**, 557-562, doi:10.1083/jcb.200205089 (2002).
- 200 Gestaut, D. R. *et al.* Phosphoregulation and depolymerization-driven
 movement of the Dam1 complex do not require ring formation. *Nature Cell
 Biology* **10**, 407-U470, doi:10.1038/ncb1702 (2008).
- 201 Sindelar, C. V. & Downing, K. H. The beginning of kinesin's force-generating
 cycle visualized at 9-A resolution. *Journal of Cell Biology* **177**, 377-385,
 doi:10.1083/jcb.200612090 (2007).
- 202 Hirose, K., Akimaru, E., Akiba, T., Endow, S. A. & Amos, L. A. Large
 conformational changes in a kinesin motor catalyzed by interaction with
 microtubules. *Molecular Cell* **23**, 913-923, doi:10.1016/j.molcel.2006.07.020
 (2006).
- 203 Kikkawa, M. & Hirokawa, N. High-resolution cryo-EM maps show the
 nucleotide binding pocket of KIF1A in open and closed conformations. *Embo
 Journal* **25**, 4187-4194, doi:10.1038/sj.emboj.7601299 (2006).
- 204 Ogawa, T., Nitta, R., Okada, Y. & Hirokawa, N. A common mechanism for
 microtubule destabilizers - M type kinesins stabilize curling of the protofilament
 using the class-specific neck and loops. *Cell* **116**, 591-602,
 doi:10.1016/s0092-8674(04)00129-1 (2004).
- 205 Claesson, P. M., Kjellin, M., Rojas, O. J. & Stubenrauch, C. Short-range
 interactions between non-ionic surfactant layers. *Physical Chemistry Chemical
 Physics* **8**, 5501-5514, doi:10.1039/b610295f (2006).

- 206 Bishop, K. J. M., Wilmer, C. E., Soh, S. & Grzybowski, B. A. Nanoscale Forces
and Their Uses in Self-Assembly. *Small* **5**, 1600-1630,
doi:10.1002/smll.200900358 (2009).
- 207 Wang, Z. H. & Sheetz, M. P. One-dimensional diffusion on microtubules of
particles coated with cytoplasmic dynein an immunoglobulins. *Cell Structure
and Function* **24**, 373-383 (1999).
- 208 Brouhard, G. J. *et al.* XMAP215 is a processive microtubule polymerase. *Cell*
132, 79-88, doi:10.1016/j.cell.2007.11.043 (2008).
- 209 Powers, A. F. *et al.* The Ndc80 Kinetochore Complex Forms Load-Bearing
Attachments to Dynamic Microtubule Tips via Biased Diffusion. *Cell* **136**, 865-
875, doi:10.1016/j.cell.2008.12.045 (2009).
- 210 Konzack, S., Thies, E., Marx, A., Mandelkow, E.-M. & Mandelkow, E.
Swimming against the tide: Mobility of the microtubule-associated protein tau
in neurons. *Journal of Neuroscience* **27**, 9916-9927,
doi:10.1523/jneurosci.0927-07.2007 (2007).
- 211 Gorman, J. & Greene, E. C. Visualizing one-dimensional diffusion of proteins
along DNA. *Nature Structural & Molecular Biology* **15**, 768-774,
doi:10.1038/nsmb.1441 (2008).
- 212 Berg, O. G., Winter, R. B. & Vonhippel, P. H. DIFFUSION-DRIVEN
MECHANISMS OF PROTEIN TRANSLOCATION ON NUCLEIC-ACIDS .1.
MODELS AND THEORY. *Biochemistry* **20**, 6929-6948,
doi:10.1021/bi00527a028 (1981).
- 213 Winter, R. B., Berg, O. G. & Vonhippel, P. H. DIFFUSION-DRIVEN
MECHANISMS OF PROTEIN TRANSLOCATION ON NUCLEIC-ACIDS .3.
THE ESCHERICHIA-COLI-LAC REPRESSOR-OPERATOR INTERACTION -
KINETIC MEASUREMENTS AND CONCLUSIONS. *Biochemistry* **20**, 6961-
6977, doi:10.1021/bi00527a030 (1981).
- 214 Winter, R. B. & Vonhippel, P. H. DIFFUSION-DRIVEN MECHANISMS OF
PROTEIN TRANSLOCATION ON NUCLEIC-ACIDS .2. THE ESCHERICHIA-
COLI REPRESSOR-OPERATOR INTERACTION - EQUILIBRIUM
MEASUREMENTS. *Biochemistry* **20**, 6948-6960, doi:10.1021/bi00527a029
(1981).
- 215 Verhey, K. J. & Gaertig, J. The tubulin code. *Cell Cycle* **6**, 2152-2160 (2007).
- 216 Westermann, S. & Weber, K. Post-translational modifications regulate
microtubule function. *Nature Reviews Molecular Cell Biology* **4**, 938-947,
doi:10.1038/nrm1260 (2003).
- 217 Hammond, J. W., Cai, D. W. & Verhey, K. J. Tubulin modifications and their
cellular functions. *Curr. Opin. Cell Biol.* **20**, 71-76,
doi:10.1016/j.ceb.2007.11.010 (2008).
- 218 Cooper, J. R., Wagenbach, M., Asbury, C. L. & Wordeman, L. Catalysis of the
microtubule on-rate is the major parameter regulating the depolymerase
activity of MCAK. *Nature Structural & Molecular Biology* **17**, 77-U98,
doi:10.1038/nsmb.1728 (2010).
- 219 Bormuth, V., Varga, V., Howard, J. & Schaffer, E. Protein Friction Limits
Diffusive and Directed Movements of Kinesin Motors on Microtubules. *Science*
325, 870-873, doi:10.1126/science.1174923 (2009).
- 220 Hudmon, A. & Schulman, H. Neuronal Ca²⁺/calmodulin-dependent protein
kinase II: The role of structure and autoregulation in cellular function. *Annual
Review of Biochemistry* **71**, 473-510,
doi:10.1146/annurev.biochem.71.110601.135410 (2002).

- 221 Yamauchi, T. & Fujisawa, H. PURIFICATION AND CHARACTERIZATION OF THE BRAIN CALMODULIN-DEPENDENT PROTEIN-KINASE (KINASE-II), WHICH IS INVOLVED IN THE ACTIVATION OF TRYPTOPHAN 5-MONOOXYGENASE. *European Journal of Biochemistry* **132**, 15-21, doi:10.1111/j.1432-1033.1983.tb07319.x (1983).
- 222 Shoji, H., Sueyoshi, N., Ishida, A. & Kameshita, I. High level expression and preparation of autonomous Ca²⁺/calmodulin-dependent protein kinase II in *Escherichia coli*. *Journal of Biochemistry* **138**, 605-611, doi:10.1093/jb/mvi161 (2005).
- 223 Ohsako, S., Watanabe, A., Sekihara, S., Ikai, A. & Yamauchi, T. EXPRESSION OF A CATALYTICALLY ACTIVE POLYPEPTIDE OF CALMODULIN-DEPENDENT PROTEIN KINASE-II ALPHA-SUBUNIT IN *ESCHERICHIA-COLI*. *Biochemical and Biophysical Research Communications* **170**, 705-712, doi:10.1016/0006-291x(90)92148-s (1990).
- 224 BRICKEY, D., COLBRAN, R., FONG, Y. & SODERLING, T. EXPRESSION AND CHARACTERIZATION OF THE ALPHA-SUBUNIT OF CA-2+ CALMODULIN-DEPENDENT PROTEIN KINASE-II USING THE BACULOVIRUS EXPRESSION SYSTEM. *Biochemical and Biophysical Research Communications* **173**, 578-584, doi:10.1016/S0006-291X(05)80074-9 (1990).
- 225 Takao, K. *et al.* Visualization of synaptic Ca²⁺/calmodulin-dependent protein kinase II activity in living neurons. *Journal of Neuroscience* **25**, 3107-3112 (2005).
- 226 Fong, Y. L., Taylor, W. L., Means, A. R. & Soderling, T. R. STUDIES OF THE REGULATORY MECHANISM OF CA-2+-CALMODULIN-DEPENDENT PROTEIN KINASE-II - MUTATION OF THREONINE-286 TO ALANINE AND ASPARTATE. *Journal of Biological Chemistry* **264**, 16759-16763 (1989).
- 227 Hanson, P. I., Kapiloff, M. S., Lou, L. L., Rosenfeld, M. G. & Schulman, H. EXPRESSION OF A MULTIFUNCTIONAL CA-2+ CALMODULIN-DEPENDENT PROTEIN-KINASE AND MUTATIONAL ANALYSIS OF ITS AUTO-REGULATION. *Neuron* **3**, 59-70, doi:10.1016/0896-6273(89)90115-3 (1989).
- 228 Ohsako, S., Nakazawa, H., Sekihara, S., Ikai, A. & Yamauchi, T. ROLE OF THREONINE-286 AS AUTOPHOSPHORYLATION SITE FOR APPEARANCE OF CA²⁺-INDEPENDENT ACTIVITY OF CALMODULIN-DEPENDENT PROTEIN KINASE-II ALPHA-SUBUNIT. *Journal of Biochemistry* **109**, 137-143 (1991).
- 229 Yamagata, Y., Czernik, A. J. & Greengard, P. ACTIVE CATALYTIC FRAGMENT OF CA²⁺ CALMODULIN-DEPENDENT PROTEIN KINASE-II - PURIFICATION, CHARACTERIZATION, AND STRUCTURAL-ANALYSIS. *Journal of Biological Chemistry* **266**, 15391-15397 (1991).
- 230 Colbran, R. J., Fong, Y. L., Schworer, C. M. & Soderling, T. R. REGULATORY INTERACTIONS OF THE CALMODULIN-BINDING, INHIBITORY, AND AUTOPHOSPHORYLATION DOMAINS OF CA²⁺/CALMODULIN-DEPENDENT PROTEIN KINASE-II. *Journal of Biological Chemistry* **263**, 18145-18151 (1988).
- 231 Levine, H. & Sahyoun, N. E. CHARACTERIZATION OF A SOLUBLE MR-30000 CATALYTIC FRAGMENT OF THE NEURONAL CALMODULIN-DEPENDENT PROTEIN KINASE-II. *European Journal of Biochemistry* **168**, 481-486, doi:10.1111/j.1432-1033.1987.tb13442.x (1987).

- 232 Kwiatkowski, A. P. & King, M. M. AUTOPHOSPHORYLATION OF THE TYPE-II CALMODULIN-DEPENDENT PROTEIN-KINASE IS ESSENTIAL FOR FORMATION OF A PROTEOLYTIC FRAGMENT WITH CATALYTIC ACTIVITY - IMPLICATIONS FOR LONG-TERM SYNAPTIC POTENTIATION. *Biochemistry* **28**, 5380-5385, doi:10.1021/bi00439a010 (1989).
- 233 HANSON, P., MEYER, T., STRYER, L. & SCHULMAN, H. DUAL ROLE OF CALMODULIN IN AUTOPHOSPHORYLATION OF MULTIFUNCTIONAL CAM KINASE MAY UNDERLIE DECODING OF CALCIUM SIGNALS. *Neuron* **12**, 943-956, doi:10.1016/0896-6273(94)90306-9 (1994).
- 234 Zhang, J. *et al.* Mechanism of folding chamber closure in a group II chaperonin. *Nature* **463**, 379-U130, doi:10.1038/nature08701 (2010).
- 235 Zhang, X. & Zhou, Z. H. Limiting factors in atomic resolution cryo electron microscopy: No simple tricks. *Journal of Structural Biology* **175**, 253-263, doi:10.1016/j.jsb.2011.05.004 (2011).
- 236 Ludtke, S. J. *et al.* De novo backbone trace of GroEL from single particle electron cryomicroscopy. *Structure* **16**, 441-448, doi:10.1016/j.str.2008.02.007 (2008).
- 237 Cong, Y. *et al.* 4.0-angstrom resolution cryo-EM structure of the mammalian chaperonin TRiC/CCT reveals its unique subunit arrangement. *Proceedings of the National Academy of Sciences of the United States of America* **107**, 4967-4972, doi:10.1073/pnas.0913774107 (2010).
- 238 Morris, E. P. & Torok, K. Oligomeric structure of alpha-calmodulin-dependent protein kinase II. *Journal of Molecular Biology* **308**, 1-8, doi:10.1006/jmbi.2001.4584 (2001).
- 239 Woodgett, J. R., Cohen, P., Yamauchi, T. & Fujisawa, H. COMPARISON OF CALMODULIN-DEPENDENT GLYCOGEN-SYNTHASE KINASE FROM SKELETAL-MUSCLE AND CALMODULIN-DEPENDENT PROTEIN KINASE-II FROM BRAIN. *Febs Letters* **170**, 49-54, doi:10.1016/0014-5793(84)81366-6 (1984).
- 240 Hoelz, A., Nairn, A. C. & Kuriyan, J. Crystal structure of a tetradecameric assembly of the association domain of Ca(2+)/calmodulin-dependent kinase II. *Molecular Cell* **11**, 1241-1251, doi:10.1016/s1097-2765(03)00171-0 (2003).
- 241 Rellos, P. *et al.* Structure of the CaMKII delta/Calmodulin Complex Reveals the Molecular Mechanism of CaMKII Kinase Activation. *Plos Biology* **8**, doi:e1000426
10.1371/journal.pbio.1000426 (2010).
- 242 Saitoh, T. & Schwartz, J. H. PHOSPHORYLATION-DEPENDENT SUBCELLULAR TRANSLOCATION OF A CA-2+ CALMODULIN-DEPENDENT PROTEIN-KINASE PRODUCES AN AUTONOMOUS ENZYME IN APLYSIA NEURONS. *Journal of Cell Biology* **100**, 835-842, doi:10.1083/jcb.100.3.835 (1985).
- 243 Lai, Y., Nairn, A. C. & Greengard, P. AUTOPHOSPHORYLATION REVERSIBLY REGULATES THE CA2+/CALMODULIN-DEPENDENCE OF CA2+/CALMODULIN-DEPENDENT PROTEIN KINASE-II. *Proceedings of the National Academy of Sciences of the United States of America* **83**, 4253-4257, doi:10.1073/pnas.83.12.4253 (1986).
- 244 Miller, S. G. & Kennedy, M. B. REGULATION OF BRAIN TYPE-II CA-2+ CALMODULIN-DEPENDENT PROTEIN-KINASE BY AUTOPHOSPHORYLATION - A CA-2+-TRIGGERED MOLECULAR SWITCH. *Cell* **44**, 861-870, doi:10.1016/0092-8674(86)90008-5 (1986).

- 245 Warren, G. & Wickner, W. Organelle inheritance. *Cell* **84**, 395-400,
doi:10.1016/s0092-8674(00)81284-2 (1996).
- 246 Patel, R. *et al.* Calcium/calmodulin-dependent phosphorylation and activation
of human cdc25-c at the G(2)/M phase transition in HeLa cells. *Journal of*
247 *Biological Chemistry* **274**, 7958-7968, doi:10.1074/jbc.274.12.7958 (1999).
- Costa, M. C. R., Mani, F., Santoro, W., Espreafico, E. M. & Larson, R. E. Brain
myosin-V, a calmodulin-carrying myosin, binds to calmodulin-dependent
protein kinase II and activates its kinase activity. *Journal of Biological*
248 *Chemistry* **274**, 15811-15819, doi:10.1074/jbc.274.22.15811 (1999).
- Rodionov, V., Yi, J., Kashina, A., Oladipo, A. & Gross, S. P. Switching
between microtubule- and actin-based transport systems in melanophores is
controlled by cAMP levels. *Current Biology* **13**, 1837-1847,
doi:10.1016/j.cub.2003.10.027 (2003).
- 249 Kashina, A. S. *et al.* Protein kinase A, which regulates intracellular transport,
forms complexes with molecular motors on organelles. *Current Biology* **14**,
1877-1881, doi:10.1016/j.cub.2004.10.003 (2004).
- 250 Marks, M. S. & Seabra, M. C. The melanosome: Membrane dynamics in black
and white. *Nature Reviews Molecular Cell Biology* **2**, 738-748,
doi:10.1038/35096009 (2001).
- 251 Raposo, G. & Marks, M. S. The dark side of lysosome-related organelles:
Specialization of the endocytic pathway for melanosome biogenesis. *Traffic* **3**,
237-248, doi:10.1034/j.1600-0854.2002.030401.x (2002).
- 252 Marks, M. S. Darkness descends with two Rabs. *Journal of Cell Biology* **175**,
199-200, doi:10.1083/jcb.200608058 (2006).
- 253 Sugden, D., Davidson, K., Hough, K. A. & Teh, M. T. Melatonin, melatonin
receptors and melanophores: A moving story. *Pigment Cell Research* **17**, 454-
460, doi:10.1111/j.1600-0749.2004.00185.x (2004).
- 254 Coudrier, E. Myosins in melanocytes: to move or not to move? *Pigment Cell*
Research **20**, 153-160, doi:10.1111/j.1600-0749.2007.00376.x (2007).
- 255 Aebersold, R. & Mann, M. Mass spectrometry-based proteomics. *Nature* **422**,
198-207, doi:10.1038/nature01511 (2003).
- 256 Edelstein, C., Pfaffinger, D. & Scanu, A. M. ADVANTAGES AND
LIMITATIONS OF DENSITY GRADIENT ULTRACENTRIFUGATION IN THE
FRACTIONATION OF HUMAN-SERUM LIPOPROTEINS - ROLE OF SALTS
AND SUCROSE. *Journal of Lipid Research* **25**, 630-637 (1984).
- 257 Miltenyi, S., Muller, W., Weichel, W. & Radbruch, A. HIGH-GRADIENT
MAGNETIC CELL-SEPARATION WITH MACS. *Cytometry* **11**, 231-238,
doi:10.1002/cyto.990110203 (1990).
- 258 De Duve, C., Pressman, B. C., Gianetto, R., Wattiaux, R. & Appelmans, F.
Tissue fractionation studies.6. Intracellular distribution patterns of enzymes in
rat-liver tissue. *Biochem Jour* **60**, 604-617 (1955).
- 259 Timonen, T. & Saksela, E. ISOLATION OF HUMAN NK CELLS BY DENSITY
GRADIENT CENTRIFUGATION. *Journal of Immunological Methods* **36**, 285-
291, doi:10.1016/0022-1759(80)90133-7 (1980).
- 260 Kienberger, F., Kada, G., Mueller, H. & Hinterdorfer, P. Single molecule
studies of antibody-antigen interaction strength versus intra-molecular antigen
stability. *Journal of Molecular Biology* **347**, 597-606,
doi:10.1016/j.jmb.2005.01.042 (2005).
- 261 Kumagai, I. & Tsumoto, K. 1-6 (ENCYCLOPEDIA OF LIFE SCIENCES
Nature Publishing Group, 2001).

- 262 Hodges, A. R., Bookwalter, C. S., Kremontsova, E. B. & Trybus, K. M. A
Nonprocessive Class V Myosin Drives Cargo Processively When a Kinesin-
Related Protein Is a Passenger. *Current Biology* **19**, 2121-2125,
doi:10.1016/j.cub.2009.10.069 (2009).
- 263 Hammer, J. A. & Sellers, J. R. Walking to work: roles for class V myosins as
cargo transporters. *Nature Reviews Molecular Cell Biology* **13**, 13-26,
doi:10.1038/nrm3248 (2012).
- 264 Taylor, K. A. Regulation and recycling of myosin V. *Curr Opin Cell Biol* **19**, 67-
74 (2007).
- 265 Lindhout, D. A., Litowski, J. R., Mercier, P., Hodges, R. S. & Sykes, B. D.
NMR solution structure of a highly stable de novo heterodimeric coiled-coil.
Biopolymers **75**, 367-375, doi:10.1002/bip.20150 (2004).
- 266 Lu, H. L., Kremontsova, E. B. & Trybus, K. M. Regulation of myosin V
processivity by calcium at the single molecule level. *Journal of Biological
Chemistry* **281**, 31987-31994, doi:10.1074/jbc.M605181200 (2006).
- 267 Nascimento, A., Cheney, R., Tauhata, S., Larson, R. & Mooseker, M.
Enzymatic characterization and functional domain mapping of brain myosin-V.
Journal of Biological Chemistry **271**, 17561-17569 (1996).
- 268 Mason, J. M. & Arndt, K. M. Coiled coil domains: Stability, specificity, and
biological implications. *Chembiochem* **5**, 170-176,
doi:10.1002/cbic.200300781 (2004).
- 269 Casaletti, L., Tauhata, S. B., Moreira, J. E. & Larson, R. E. Myosin-Va
proteolysis by Ca²⁺/calpain in depolarized nerve endings from rat brain.
Biochem Biophys Res Commun **308**, 159-164 (2003).
- 270 Alavez, S. *et al.* Myosin Va is proteolysed in rat cerebellar granule neurons
after excitotoxic injury. *Neuroscience Letters* **367**, 404-409,
doi:10.1016/j.neulet.2004.06.043 (2004).
- 271 Belizario, J. E., Alves, J., Garay-Malpartida, M. & Occhiucci, J. M. Coupling
caspase cleavage and proteasomal degradation of proteins carrying PEST
motif. *Current Protein & Peptide Science* **9**, 210-220,
doi:10.2174/138920308784534023 (2008).
- 272 Rogers, S., Wells, R. & Rechsteiner, M. AMINO-ACID-SEQUENCES
COMMON TO RAPIDLY DEGRADED PROTEINS - THE PEST
HYPOTHESIS. *Science* **234**, 364-368, doi:10.1126/science.2876518 (1986).
- 273 Steen, H. & Mann, M. The ABC's (and XYZ's) of peptide sequencing. *Nature
Reviews Molecular Cell Biology* **5**, 699-711, doi:10.1038/nrm1468 (2004).
- 274 Sun, H. Q., Yamamoto, M., Mejillano, M. & Yin, H. L. Gelsolin, a
multifunctional actin regulatory protein. *Journal of Biological Chemistry* **274**,
33179-33182, doi:10.1074/jbc.274.47.33179 (1999).
- 275 Giffard, R. G., Weeds, A. G. & Spudich, J. A. CA-2+-DEPENDENT BINDING
OF SEVERIN TO ACTIN - A ONE-TO-ONE COMPLEX IS FORMED. *Journal
of Cell Biology* **98**, 1796-1803, doi:10.1083/jcb.98.5.1796 (1984).
- 276 Homma, K. & Ikebe, M. Ca²⁺ dependent regulation of the motor activity of
mammalian myosin V. *Molecular Biology of the Cell* **11**, 374A-374A (2000).
- 277 Li, X. D. *et al.* The globular tail domain puts on the brake to stop the ATPase
cycle of myosin Va. *Proc Natl Acad Sci U S A* **105**, 1140-1145 (2008).
- 278 Espindola, F. S. *et al.* The light chain composition of chicken brain myosin-Va:
Calmodulin, myosin-II essential light chains, and 8-kDa dynein light chain/PIN.
Cell Motility and the Cytoskeleton **47**, 269-281, doi:10.1002/1097-
0169(200012)47:4<269::aid-cm2>3.0.co;2-g (2000).

- 279 Li, X. D., Ikebe, R. & Ikebe, M. Activation of myosin Va function by
melanophilin, a specific docking partner of myosin Va. *Journal of Biological
Chemistry* **280**, 17815-17822, doi:10.1074/jbc.M413295200 (2005).
- 280 Coy, D. L., Hancock, W. O., Wagenbach, M. & Howard, J. Kinesin's tail
domain is an inhibitory regulator of the motor domain. *Nature Cell Biology* **1**,
288-292 (1999).
- 281 Brunnbauer, M. *et al.* Regulation of a heterodimeric kinesin-2 through an
unprocessive motor domain that is turned processive by its partner.
*Proceedings of the National Academy of Sciences of the United States of
America* **107**, 10460-10465, doi:10.1073/pnas.1005177107 (2010).
- 282 Coureux, P. D., Sweeney, H. L. & Houdusse, A. Three myosin V structures
delineate essential features of chemo-mechanical transduction. *Embo Journal*
23, 4527-4537, doi:10.1038/sj.emboj.7600458 (2004).
- 283 Houdusse, A. *et al.* Crystal structure of apo-calmodulin bound to the first two
IQ motifs of myosin V reveals essential recognition features. *Proc Natl Acad
Sci U S A* **103**, 19326-19331 (2006).
- 284 Coureux, P. D. *et al.* A structural state of the myosin V motor without bound
nucleotide. *Nature* **425**, 419-423, doi:10.1038/nature01927 (2003).
- 285 Pashkova, N., Jin, Y., Ramaswamy, S. & Weisman, L. S. Structural basis for
myosin V discrimination between distinct cargoes. *Embo Journal* **25**, 693-700,
doi:10.1038/sj.emboj.7600965 (2006).
- 286 Bittins, C. M., Eichler, T. W., Hammer, J. A. & Gerdes, H. H. Dominant-
Negative Myosin Va Impairs Retrograde but Not Anterograde Axonal
Transport of Large Dense Core Vesicles. *Cellular and Molecular Neurobiology*
30, 369-379, doi:10.1007/s10571-009-9459-2 (2010).
- 287 Park, M., Serpinskaya, A. S., Papalopulu, N. & Gelfand, V. I. Rab32 regulates
melanosome transport in *Xenopus melanophores* by protein kinase A
recruitment. *Current Biology* **17**, 2030-2034, doi:10.1016/j.cub.2007.10.051
(2007).
- 288 Larson, R. Myosin-V: A class of unconventional molecular motors. *Brazilian
Journal of Medical and Biological Research* **29**, 309-318 (1996).
- 289 Espreafico, E. M. *et al.* Primary structure and cellular localization of chicken
brain myosin-V (p190), an unconventional myosin with calmodulin light chains.
J Cell Biol **119**, 1541-1557 (1992).

9 Abbreviations

ABSA	Assay buffer with BSA
ADP	Adenosine 5'-diphosphate
Amp	Ampicillin
APS	Ammonium peroxodisulfate
ATP	Adenosine 5'-triphosphate
BBSA	Biotinylated bovine serum albumin
Bluo-Gal	Halogenated indolyl- β -galactosidase
bp	Base pair
BSA	Bovine serum albumin
c	Concentration
C-terminus (C')	Carboxy-terminus
CaM	Calmodulin
CaMK	Calcium-/Calmodulin-dependent Kinase
CCD	charge-coupled device
cDNA	Copy DNA
Da	Dalton
DC	Density gradient ultra-centrifugation
DMSO	Dimethylsulfoxide
DNA	Desoxyribonucleic acid
dNTP	Desoxynucleotide-5'-triphosphate
DTT	Dithiothreitol
EB	Elution buffer
EDTA	Ethylenediaminetetraacetic acid
EGTA	Ethylene-bis(oxyethylenenitrilo) tetraacetic acid
ELC	Essential light chain
F-actin	Filamentous actin
FACS	Fluorescent activated cell sorting
FBS	Fetal bovine serum
FL	Full-length

Abbreviations

FPLC	Fast performance liquid chromatography
G-actin	Globular actin
GCN4	General Control Nondepressible transcriptional activator gene 4
GTD	Globular tail domain
GTP	Guanosin 5'-triphosphate
HEPES	4-(2-Hydroxyethyl)piperazine-1-ethanesulfonic acid
HMM	Heavy-meromyosin
HMW	High molecular weight
IPTG	Isopropyl- β -D-thiogalactopyranoside
kbp	kilo base pair
LB	Luria Broth
LC-MS/MS	Liquid chromatography tandem mass spectrometry
LDH	Lactic Dehydrogenase
LMU	Ludwig-Maximilians-University Munich
MACS	Magnetic activation cell sorting
MALDI-TOF	Matrix-assisted laser desorption/ionization-Time of flight
MAPs	Microtubule associated proteins
min	minutes
mRNA	Messenger ribonucleic acid
MT	Microtubules
MWCO	Molecular weight cut-off
Myo V	Myosin V
N-terminus (N')	Amino-terminus
NADH	Nicotinamide-adenine-dinucleotide
OD	Optical density
PAGE	Polyacryl amide gel electrophoresis
PBS	Phosphate buffered saline
PCR	Polymerase chain reaction
PEP	Phospho(enol)pyruvic acid
P _i	Inorganic phosphate
PIPES	Piperazine-1,4-bis(2-ethanesulfonic) acid

Abbreviations

PK	Pyruvic Kinase
RACE	Rapid amplification of cDNA ends
rpm	Rounds per minute
RT	Room temperature
s	Seconds
S.D.	Standard deviation
S.E.M.	Standard error of the mean
S.O.C.	Super Optimal Catabolite
SDS	Sodium dodecyl sulfate
TAE	Tris-buffered acidic EDTA solution
Taq	<i>Thermus aquaticus</i>
TBS	Tris-buffered sodium
TE	Tris EDTA
TEMED	N, N, N', N'-Tetramethylethylenediamine
TIRF	Total internal reflection fluorescence
Tris Base	Tris (hydroxymethyl) aminomethan
TRITC	Tetramethylrhodamine isothiocyanate
TRP1	Tyrosinase-related protein 1
UV-Light	Ultra violet Light
WB	Wash buffer
x g	Gravitational force
ZfP	Zentrallabor für Proteinanalytik
ϵ	Molar absorptivity

Eidesstattliche Versicherung

Ich versichere hiermit an Eides Statt, dass die vorliegende Dissertation von mir selbstständig und ohne unerlaubte Hilfe angefertigt wurde. Ich habe weder anderweitig versucht eine Dissertation einzureichen oder eine Doktorprüfung abzulegen, noch habe ich diese Dissertation oder Teile derselben einer anderen Prüfungskommission vorgelegt.

München, den 27. Juli 2012

(Dennis Zimmermann)

Curriculum Vitae

■ **Personal and contact details**

Name	Dennis Alexander Zimmermann
Date of birth	5 December, 1982
Nationality	German
Contact	Einsteinstr. 28 D-82152 Martinsried Tel.: 0049-89-95422211 E-mail: dennis_zman@yahoo.de

■ **Educational history**

July 2008 - present

Ludwig-Maximilians-University, Munich, Germany
Anticipated degree Dr. rer. nat. (equivalent to PhD)

July 2008

Ludwig-Maximilians-University, Munich, Germany
Degree Diplom Biologist (equivalent to MSc)

June 2003

Feodor-Lynen-Gymnasium, Planegg, Germany
Degree Abitur (equivalent to A levels)

June 2000

Tourtellotte Memorial High School, Thompson (CT), U.S.A.
Degree High School Diploma (equivalent to A-Levels)

■ **Research experience**

July 2008 – Present

Institute for Cell Biology, Ludwig-Maximilians-University, Munich, Germany	
Project	The role of molecular motors in the spatiotemporal regulation of melanosome transport
Position	PhD Student
PI	Prof. Dr. M. Schliwa

September 2007 – June 2008

Institute for Cell Biology, Ludwig-Maximilians-University, Munich, Germany

Project Expression and characterization of Myosin V

Position Diploma Student

PI Prof. Dr. M. Schliwa

April 2007 – May 2007

Max-Planck-Institute for Biochemistry, Martinsried, Germany

Project Cloning of ILK, Qik and CHIP from mouse embryonic fibroblasts and subsequent characterization of those enzymes

Position Research Intern

PI Prof. Dr. R. Faessler

September 2006 – October 2006

Woods Hole Oceanographic Institute (WHOI), Woods Hole (MA), U.S.A.

Project Set-up of microarray targeting the developmental-dependent Cytochrome P450 gene expression in *Danio rerio*

Position Research Intern

PI J. Stegeman, PhD

■ Academic achievements

Publications (Peer-reviewed)

Zimmermann D, Abdel Motaal B, Voith von Voithenberg L, Schliwa M, Ökten Z (2011) Diffusion of Myosin V on Microtubules: A Fine-tuned Interaction for Which E-hooks Are Dispensable. PLoS ONE 6(9): e25473.

Publications (Non-peer-reviewed)

Zimmermann, D. (2011) *Germany: Experiencing a New Age of Research and Teaching*. ASCB Newsletter 34 (4): 15-17.

Conferences attended

The Chicago Cytoskeleton 2011

Chicago, U.S.A., 16 September 2011

How is Networking of the Cytoskeleton Achieved?

Talk

The 2011 Meeting of Nobel Laureates in Lindau

Lindau, Germany, 26 June – 1 July 2011

Two Transport Systems, One Goal: How is Networking of the Cytoskeleton Achieved?

Talk

Cellular Cytoskeletal Motor Proteins Meeting of the Biochemical Society 2011

Hinxton, U.K., 30 March – 1 April 2011

Myosin V scans along microtubules in an E-hook-independent fashion.

Poster Presentation

Annual ASCB Meeting 2010

Philadelphia, U.S.A., 11 – 15 December 2010

Diffusion of Myosin V along Microtubules: A Two-Step Process

Poster Presentation

The EMBO Meeting 2010

Barcelona, Spain, 4 – 7 September 2010

Myosin V on Microtubules: An Unexpected Interaction

Poster Presentation

Annual DGZ (German Society for Cell Biology) Meeting

Regensburg, Germany, 10 – 13 March 2010

The Attraction of Myosin V towards Microtubules

Poster Presentation

7th Annual ELSO Meeting

Nice, France, 30 August – 2 September 2008

Investigating Electrostatic Interaction with Microtubules

Poster Presentation

Scientific Prizes and Awards

ASCB Predoctoral Travel Award 2010

Award by American Society for Cell Biology (ASCB)

Philadelphia, U.S.A., December 2010

GlaxoSmithKline Travel Fellowship 2010

Funded by the GlaxoSmithKline Foundation

Barcelona, Spain, September 2010

■ **Work-related and extracurricular activities**

Memberships

2011 - present

Member of the Biochemical Society

2010 - present

Member of the American Society for Cell Biology (ASCB)

2010 - 2011

Elected spokesman of the Graduate School "Protein Dynamics in Health and Disease" as part of the Elite Network Bavaria (ENB)

2008 - present

Appointed member of the Graduate School "Protein Dynamics in Health and Disease" as part of the ENB

2005 - 2008

Elected member of the faculty student council at the Department for Biology (Ludwig-Maximilians-University)

Teaching

2008 – present

Supervision of Intern and Diploma/BSc/MSc students in the group of Prof. Dr. Schliwa/Dr. Ökten

2008 – 2011

Assessor at oral exams for MSc led by Prof. Dr. Schliwa

Voluntary Commitment

2008 – present

Organization of Nobel Laureate Seminars, Retreats, Regular Meetings, Workshops, Alumni Networking as member of the ENB Graduate Program

2008 – present

Organization of guest lecture by Prof. David Pellman (Harvard University, U.S.A.)

2004 – 2010

Area Representative of Bavaria for the exchange organization GIVE e.V. in Heidelberg, Germany

Hobbies

Running, Hiking, Tennis, Scuba Diving, Cooking

Acknowledgments

This thesis, and also my time as a PhD student was all about team-working. In that respect, I would like to express my deepest appreciation for all the people without whom this work would have never been possible.

I would like to thank Manfred Schliwa for letting me work as a PhD student under his supervision. He always kept the big picture in his mind and was especially helpful at times when I felt stuck with all those results that one day are supposed to become a paper and eventually a thesis.

A big Thank You goes to Zeynep Ökten, for her support, her trust in all my ideas and for encouraging me to think into all directions and to try out things that nobody had tried out before.

My dear lab-mates, you really rock! I will miss you, but I know that I will see you again soon! Either in Chicago or in Munich☺ Danke! Hvala! Cam on! Tesekkür ederim! Special thanks go to Hieu and Renate whose technical assistance was formidable.

I would like to thank Michael Schleicher, who has given me lots of great critical and constructive intellectual input. Also, for the great help all over the years, many thanks go to the whole Schleicher-lab.

I would like to thank Matthias Rief for his continuous support, and without whom many ideas would not have been able to be realized.

Many thanks to Günther Woehlke who let me use the TIRF microscope, always at my best convenience.

I want to thank Volodya Gelfand, who provided us with the *Xenopus* melanophores. But even more, I deeply appreciate his help in preparing the next steps in my future career as a postdoc.

I would like to thank Zdravko Kochovski and Vladan Lucic for the very fruitful collaboration on the CaMKII project, and for providing me with those nice cyro-EM 3D-reconstructions.

Thank you Michi and Nadine, for your support and friendship. I will miss you big time, but in Chicago there will always be a room reserved for you!

I would like to thank Steffi for her endless patience, her persistence and determination to cheer me up after all the drawbacks that one encounters. I love you and thank you for everything! Chicago, here I come☺

At last, I want to thank my Mom and Dad for their support and continuous encouragement! But above all, I would like to thank you for your trust and interest in what I have been doing, and in what I will be doing in the future! Ihr seid ganz super Eltern!